OUT-OF-PLANE BENDING OF MASONRY
BEHAVIOUR AND STRENGTH

PROEFSCHRIFT

ter verkrijging van de graad van doctor aan de Technische Universiteit Eindhoven, op gezag van de Rector Magnificus, prof.dr. M. Rem, voor een commissie aangewezen door het College voor Promoties in het openbaar te verdedigen op maandag 18 oktober 1999 om 16.00 uur door

Rob van der Pluijm
geboren te Almelo

Dit proefschrift is goedgekeurd door de promotoren:

prof.dr.ir. H.S.Rutten
en
prof.dr. N.G. Shrive

Copromotor:
dr.ir. C.J.W.P. Groot

ISBN 90-6814-099-X

Stellingen

Behorende bij het proefschrift
Out-of-Plane Bending of Masonry
Behaviour and Strength
van Rob van der Pluijm

1. Voor het bezwijken van metselwerk is het bestaan van een additioneel buigend moment in de lintvoeg in geval van wringing net zo belangrijk als het additionele wringende moment in de lintvoeg bij buiging om de verticale as.
2. Principieel kan het gedrag van op buiging belast metselwerk niet worden geformuleerd op grond van de plaattheorie: gestapelde lagen van vlakspanningstoestanden, gebaseerd op de stekelhypothese. Bij een dergelijke formulering kunnen de additionele momenten die wezenlijk zijn voor de krachtswerking in metselwerk en die ontstaan als gevolg van de interactie tussen stijve stenen en slappere voegen, niet worden beschreven.
3. Materiaaleigenschappen die in een model moeten worden gebruikt om een goede beschrijving van het werkelijke gedrag te verkrijgen, zijn niet alleen afhankelijk van het niveau van modelleren (micro-meso-macro) maar ook van de theorieën die worden gebruikt. Daarom bestaan 'echte' materiaaleigenschappen niet.
4. Het modelleren van het bezwijken van beton onder 2 of 3-assig trek op basis van de 1-assige treksterkte, zonder rekening te houden met de meer-assige spanningstoestand, is in principe onjuist.
5. De zogenaamde bond-wrenchproef is meer geschikt om de buigtreksterkte van metselwerk loodrecht op de lintvoeg te meten, dan de alom gebruikte 4-puntsbuigproef op kleine proefmuren.
6. Het complexe meso gedrag van de regelmatig gevormde onderdelen van metselwerk geeft aan dat het gedrag van beton op meso-niveau nog ingewikkelder is. In dit licht bezien, kan de modellering van beton met behulp van staafwerkmodellen primitief en fenomenologisch worden genoemd.
7. Voor het modelleren van metselwerk op meso-niveau is het voldoende om de krachtswerking in een kleine bouwsteen, bestaande uit twee kwart stenen, twee kwart stootvoegen en een lintvoeg, te beschrijven.
8. De 1-minuut proef die als praktische methode wordt gezien om zich te verzekeren van een goede hechting, biedt geen enkele garantie daarvoor. Omgekeerd sluit een negatief resultaat bij de 1-minuutpoef een voldoende hechting niet uit.
   N. Boterbloem, *Onderzoek naar invloedsfactoren op de hechting van mortels aan baksteen*, IKOB rapport nr. 93-1165, 1993
9. De eis van financiers dat fundamenteel wetenschappelijk onderzoek vrijwel direct utiliseerbaar moet zijn, is een aanmoediging voor korte termijn en trendgevoelig onderzoek dat weinig bijdraagt aan de wetenschappelijke ontwikkeling. Zo doende, spannen financiers het paard achter de wagen.
10. Op wetenschappelijk gronden kan geen verschil worden gemaakt tussen huisartsen die gespecialiseerd zijn in homeopathische geneeswijzen en middeleeuwse kwakzalvers.
11. Het risico dat wij wel van onze heilige koeien accepteren staat in schril contrast met het mogelijke risico dat wat wij niet van (vermeende) BSE koeien accepteren.
12. Er zijn twee zekerheden in dit leven: we zijn sterfelijk en wie een computer aanschaft weet zeker dat deze de volgende dag is verouderd. Gezien de ontwikkeling van de gerontologie is het niet ondenkbeeldig dat de eerste zekerheid ons in de toekomst wordt ontnomen. Dat geldt zeker niet voor de tweede.
13. Je moet wel erg goedgelovig zijn om te geloven dat je eigen geloof het enige ware geloof is.

Statements

1. The existence of additional bending moments in bed joints due to torsion is as important for failure of masonry as the additional torsion moments in bed joints in case of bending around the vertical axis.
2. In principle, the behaviour of masonry in bending cannot be formulated on the basis of conventional plate theory: piled thin layers in plane stress on the basis of the hypothesis of Bernoulli. With such a formulation, the additional moments essential of the force patterns in masonry, occurring from the interaction between stiff units and soft joints, cannot be described.
3. Material properties that have to be applied in a model to obtain an adequate description of the real behaviour, are not only dependent of the level of modelling but also on the theories applied. Therefore, 'true' material properties do not exist.
4. Modelling of failure of concrete in bi-axial or tri-axial tension on the basis of the uni-axial tensile strength, without taking the multi-axial stress state into account, is in principle not correct.
5. The bond wrench test is more suitable to establish the flexural strength of masonry with a crack parallel to the bed joint plane, than the widely used 4-point bending test with wallettes.
6. The complexity of the behaviour of masonry with its regularly shaped components, indicates that the behaviour of concrete at the meso level is even more complicated. In this perspective, the modelling of concrete with lattice models could be mentioned primitive and phenomenological.
7. For the modelling of masonry at the meso level, it is sufficient to take a basic module consisting of two quarter units, two quarter head joints and a bed joint into account.
8. The so-called one-minute test, which that is considered as a practical method to ensure adequate bond strength in the Netherlands, is useless. From the other side a negative result does not exclude adequate bonding.
   N. Boterbloem, *Onderzoek naar invloedsfactoren op de hechting van mortels aan baksteen*, IKOB rapport nr. 93-1165, 1993
9. The demand of sponsors of fundamental research that results should immediately be utilisable, is an encouragement for short-term en trendy research that does not support scientific developments. With this demand, sponsors put the cart before the horse.
10. On scientific grounds, no distinction can be made between a modern doctor who is specialised in homeopathic medicine and a mediaeval quack.
11. The hazards that we accept from our sacred cow (car) contrast sharply with the risks that we do not accept from (alleged) BSE cows.
12. There are two certainties in live: we die and when we buy a computer today, it is old fashioned tomorrow. Taking the developments in the gerontology into account, it is not unthinkably that the first certainty will be taken away form us. The second one will remain forever.
13. You have to be a naïve believer to believe that your own faith is the true faith.

DANKWOORD

Het onderzoek is uitgevoerd bij de vakgroep Constructief Ontwerpen van de faculteit Bouwkunde. Vanaf December 1994 tot en met 1998 heeft de Stichting Technische Wetenschappen (STW) het onderzoek gefinancierd onder projectnr. EBW.3367. Het proefschrift beschrijft ook delen van onderzoek die zijn uitgevoerd in het kader van het nationale industrie-brede onderzoeksprogramma Constructief metselwerk, begeleid door het Civiel Technisch Centrum Uitvoering Research en Regelgeving (CUR), dat oorspronkelijk was geïnitieerd door het Koninklijk Verbond van Nederlandse Baksteenfabrikanten (KNB) als het BRIK-project. Het KNB heeft separaat twee experimenten met grote metselwerkpanelen gefinancierd.

Het uitgevoerde onderzoek leunde voor een belangrijk deel op experimenten en derhalve op de medewerkers van het Pieter van Musschenbroek-laboratorium. Hoewel bij tijd en wijle het hele lab voor mij bezig is geweest, wil ik met name Martien Ceelen noemen waarmee ik het meest intensief heb samengwerkt. Ik zou bladzijden vol kunnen schrijven over de discussies die ik met hem over de sturing van experimenten heb gevoerd. Uiteindelijk kwam Martien altijd met een kastje voorzien van knopjes te voorschijn waardoor de proeven uitgevoerd konden worden zoals ik dat wilde.
De steun die ik van TNO heb gekregen doordat zij mij gedurende vrijwel de gehele onderzoeksperiode buiten de 'sterkte' hebben gehouden en de mogelijkheid om dit proefschrift te schrijven na mijn terugkeer bij TNO, mag niet onvermeld blijven.

Ondanks dat het wetenschappelijk onderzoek met betrekking tot metselwerk in Nederland weinig traditie kent, heeft Harry Rutten door zijn breed wetenschappelijk inzicht en ervaring mij meer dan voldoende ondersteuning kunnen geven. De vele discussies die wij hebben gehad zijn hiervan 'stille' getuigen. Op de achtergrond kon ik ook altijd terecht bij Dick Hordijk die met zijn grote experimentele ervaring altijd als kritische klankbord wilde dienen. Ad Vermeltfoort wil ik bedanken voor de steun, inhoudelijk discussies maar ook voor de vele uren kletspraat waarmee ik de onvermijdelijke frustraties die met onderzoek gepaard gaan, kon lozen. Het belangrijkste was en is onze vriendschap die we in de afgelopen jaren opgemetseld hebben.

Irene, Suzan en Bas, laat thuis komen, alleen eten, het was niet altijd even leuk. Irene, je geduld is vaak op de proef gesteld, het egoïsme dat het uitvoeren van onderzoek met zich mee brengt heb je altijd getolereerd. Ik ben dankbaar voor de ruimte die jullie mij hebben gegeven om mijn onderzoek te kunnen uitvoeren.

Experiment!
Make it your motto day and night.
Experiment,
And it will lead you to the light.
The apple on the top of the tree,
Is never too high to achieve,
So take an example from Eve...
Experiment!
Be curious,
Though interfering friends may frown.
Get furious,
At each attempt to hold you down.
If this advice you only employ,
The future can offer you infinite joy
And merriment..
Experiment
And you'll see!

Cole Porter

CONTENTS

1. INTRODUCTION

1.1 MOTIVATION

The interest of the author for masonry in bending has originates from an assessment of safety levels of structures in the Netherlands. The aim was to establish partial safety factors for different materials (steel, concrete, wood, masonry, etc) in an objective way. The results of this assessment are now incorporated in the Dutch standards. With the outcome of this probabilistic research it was very difficult to prove that masonry structures loaded by wind induced pressures had an acceptable probability of failure on the basis of the applied assessment techniques (Siemes[1985,[71]]). This outcome was in contrast with practice where, for example, the heavy winds on 25 January 1990 (Beaufort 11 (highest mean/h: 30 m/s, highest peak 44 m/s) did not cause noticeable damage to cavity walls in the Netherlands.
The fact that bond strength of masonry built in the 50-ties and 60-ties was often less than the assumed minimum value of 0.2 N/mm^2 in the study, due to abuse of air-entrainers, made the contrast between theory and practice even more intriguing. Two obvious conclusions with respect to the masonry cavity wall could be drawn:

1. the assumed wind pressures are too high, especially for low rise buildings where the majority of cavity walls is found;
2. the method used for the assessment of the load resistance of a cavity wall significantly deviates from the real behaviour of masonry

Design wind speeds for open terrain in the Netherlands are expected to be very realistic (Van Staalduinen[1990,[74]]). The mentioned wind speeds of 25 January 1990 correspond with pressures between 560 and 1210 N/m^2. The upper limit is high compared with the code pressure of 1090 N/m^2 for buildings up to a height of 11 m situated in open terrain of coastal areas. For the built-up area, local circumstances determine the actual speeds, and consequently, differences from place to place are great. For the build-up area, the design code takes wind speeds equal for 9 m height and lower. There will be circumstances where the assumed wind-speeds are too high, but the opposite case is likely also. It must be concluded that design wind speeds cannot be adopted in such a way that the observed problem vanishes.

Although a lot of work has been done in the field of masonry in bending (Baker[1981,[4]], Lawrence[1983,[28]], Haseltine et al.[1978,[21]], West et al.[1986,[85]] etc.) most of the work lacks a fundamental link between the material and the structural behaviour, especially with respect to cracking. Of course, this must be placed in the context of knowledge and research possibilities available. Baker for example, tried to establish rational design rules based on the strength of masonry in different directions, but was not able to handle cracking, resulting in an underestimation of the load bearing capacity of masonry panels.

Nowadays combined numerical and experimental research tools are available to gain insight in the fundamental behaviour of materials and structures, making possible a rationalisation of design rules. With the development of different methods to describe cracking in semi-brittle materials as concrete, rock and masonry (e.g. non-linear fracture mechanics and its implementation by means of smeared or discrete crack approach and plasticity models in continuum finite element (FE) models) and experimental techniques with which behaviour beyond the maximum load can be investigated, challenging possibilities have become available to bridge the gap as described above. Bridging this gap was the main motivation for this thesis.

1.2 AIM OF RESEARCH

The main subject of the thesis as addressed above: "to establish a fundamental link between the material and the structural behaviour" sounds nice but lacks a clear picture of what was intended. To be more specific, the main aim is to find a scientifically acceptable representation of the relation between the mechanical properties of masonry in bending at the meso and macro level. Meso properties are properties at the level of units and joints and are used in an approach were units and joints are modelled separately. At the macro level, masonry is considered to be a homogeneous (orthotropic) continuum. This definition of scale levels can be regarded to correspond with those distinguished by Wittman[1987,[86]] for concrete, who regarded concrete at the meso level as a composite of aggregates (units), pores and cracks in a hardened cement paste matrix (joints) and at the macro level as a homogeneous continuum.
The intended work to be done is to provide users and developers of (non-linear) finite element models with a basis on which they can utilise macro-properties of masonry in bending determined by a few mechanical properties commonly known in engineering of which bond strength is the most important one. The mechanical behaviour has not been related to the parameters influencing the physics of bond between units and mortar joints, but has been studied from the presumption that the behaviour is approximately the same for each level of bond (within the boundaries of its natural variation). In this way the research is restricted to cement based mortars used for the joints. More information on the underlying physics and parameters that govern bond can be found in e.g. Groot[1993,[20]], Schubert[1994,[69]] and Van der Pluijm[1996,[57]].

1.3 APPROACH & OUTLINE OF CONTENTS

As the focus is aimed on bending of masonry, cracking due to tensile and/or shear stresses is, in most cases, the major cause for failure. Cracking of masonry can take place at the following locations or a combination of these:

1. unit
2. mortar-joint
3. bond interface between mortar-joint and unit

In a meso model, these three components may be modelled. In this thesis, the bond interface is regarded as a layer with zero thickness where the mortar and unit are bonded together. Although there is evidence (see e.g. Groot[1993,[20]]), that a small layer of mortar near the unit exist of which the chemical composition differs from the rest of the mortar joint, modelling of such a layer is useless because it is not possible to apply mechanical properties to such a layer on the basis of the experimental techniques used.
A model where the bond-interface (for short interface) and mortar-joint (for short joint) are modelled together as a single entity can also be regarded as a meso model. In both cases it is necessary to describe cracking of the unit and joint+interface in one or another way.
With the choice to model masonry in bending at the meso level, the experimental data needed on this level is more or less fixed. Failure of units and joints under tension and shear must be described. Failure due to compression was not considered although in exceptional cases (arching) it may play a role. Also data at the macro level were gathered to be able to verify meso and macro models.

In the chapters 2, 3 and 4 the experimental work is described.
The experiments carried out solely for this study, involved two types of masonry:

A: clay brick masonry consisting of small wire cut bricks (wc-JO) and general purpose mortar designed in the laboratory and

B: calcium silicate masonry consisting of blocks (CS-block) with a factory-made thin layer mortar.

Masonry type A is often used for the outer cavity leaf and type B for the inner cavity leaf in the Netherlands. However also other material combinations were used. Those combinations were tested within the framework of 'the Dutch structural masonry research program'. This program, supported by nearly the whole Dutch masonry industry, started in 1989 as an initiative of the Royal Association of Dutch Clay Brick Manufacturers (KNB) and is supervised by the Centre for Civil Engineering Research and Codes (CUR).

In chapter 2, the behaviour of units and joint in tension is investiagted. The applied testing technique was already developed in concrete research. The available knowledge was used to build a testing arrangement in the Pieter van Musschenbroek laboratory of Eindhoven University of Technology, especially tuned for masonry. Uni-axial tensile tests were carried on parts of units and small masonry specimens. The mortar was not tested separately because the interaction between units and mortar makes it necessary to test the mortar in a joint. With the experimental results, the behaviour in tension of the masonry components could be established. The existing knowledge to describe the behaviour of quasi-brittle materials could be applied.

The behaviour of joints under combined normal and shear stress is explored in chapter 3. Two test arrangements developed by the author were used. One arrangement, developed at TNO within the framework of the Dutch national masonry research program, allowed for testing under compression and shear, while the arrangement developed in Eindhoven also allowed for combinations of tension and shear. On the basis of the obtained experimental results, a description of the behaviour of joints was given, including post peak behaviour and so-called dilatancy, a phenomenon that is essential to obtain a correct description of the behaviour of mortar joints under normal and shear stresses.

Bending tests at the macro-scale are being described in chapter 4. A well-known 4-point bending test technique was applied to test small masonry walls. The tests were carried out with different orientations between the bending axis and bed joint. Some of these test were carried out using deformation control and were also accompanied by deformation controlled tensile tests, making them very useful for numerical simulation because their modelling can be based on the knowledge gathered in chapter 2 and 3. For the same reason, two tests on large laterally loaded masonry panels (1.74×3.94 m^2) were carried out. Those tests are only briefly described.

Chapter 5 describes an extensive analysis of masonry in bending. Two linear elastic meso models for masonry in bending, an analytical and a FE model have been developed. The interaction between these two approaches proved to be beneficial. A detailed insight in the interaction between units and joints was obtained. Via an engineering approach, the analytical model was also used to predict the flexural strength of masonry under different conditions on the basis of a so-called Multiple Crack Pattern model.

In chapter 6 a numerical and an experimental study concerning bond tests are presented. The numerical study uses the non-linear material behaviour obtained in chapter 2. The flexural strength and its coefficient of variation were calculated numerically for different sized specimens with a three-dimensional FE model. A Monto Carlo approach, taking the tensile strength and mode I fracture energy stochastically into account was used. In the experimental part of the research, different bond test methods were compared with each other.

Chapter 7 presents a summary and some concluding remarks.

2. TENSION

This chapter describes the behaviour of masonry in tension. Tests, controlled by a monotonic increase of a deformation measured on the specimen itself, were carried out to establish the behaviour prior and beyond the maximum load.
Most of the tests described were uni-axial tensile tests, but also some bending tests were carried out.

The behaviour of units and mortar-joints under tension showed a great similarity to that of other softening materials like concrete. Experience in describing the non-linear behaviour of concrete under tension could be applied to the masonry components. The mode I fracture energy of units was of the same magnitude as that of concrete. The mode I fracture energy of mortar-joints and/or bond interface was approximately a factor ten smaller and showed a great scatter.

Keywords: **tension units, mortar-joints, bond interface, (post peak) behaviour, softening, mode I fracture energy, actual bonding area**

2.1 INTRODUCTION

The main goal of the experiments outlined in this chapter was the investigation of the behaviour of the masonry components under tension, enabling the modelling of masonry at the meso level.
If a tensile test of a quasi-brittle material like concrete, masonry-units or mortar-joints is controlled beyond the maximum load, a (schematic) diagram as presented in Figure 1 can be obtained.

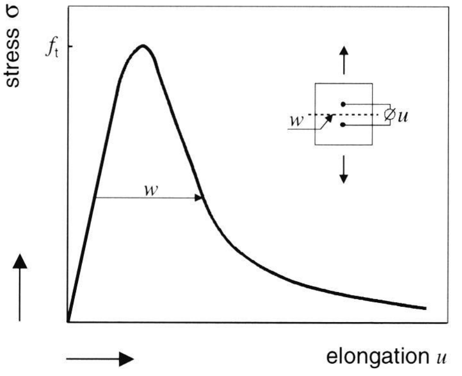

Figure 1 Schematic diagram of a deformation (u) controlled tensile test

With the designation 'quasi-brittle', behaviour is indicated where the transferred force not immediately drops back to zero, but gradually decreases. This kind of behaviour is often indicated with 'softening'. The behaviour prior to the maximum load is reasonably approached with linear behaviour. The post peak behaviour must be described in one or another way. Here, an approach that has been proven to be successful for plain concrete is followed: the fictitious crack model developed by Hillerborg et al.[1976,[23]]. This model assumes that in front of a visual crack, a process zone is present in which non-visible (='fictitious') cracking takes place (see Figure 2). In this zone stresses are still being transferred.

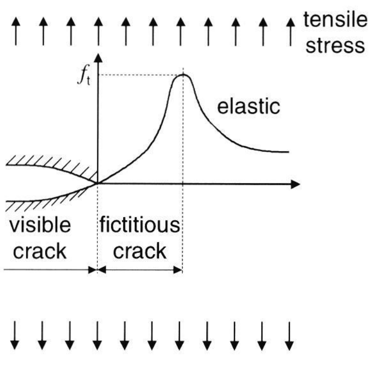

Figure 2 Fictitious crack model with the assumed stress distribution ahead of a visible crack according to Hillerborg et al.[1976, [23]]

On the micro level, cracks are growing in this zone making the material weaker or with other words: the material softens. Progressing micro cracking results in the softening behaviour in a deformation controlled tensile tests.

Hillerborg translates the measured diagram (σ-u) into a σ-ε diagram for the non-cracked part within the gauge length and a stress-crack width (σ-w) diagram for the crack (occurring in an infinitesimal small zone, as indicated in Figure 1).
From the first tests carried out by the author (Vermeltfoort et al.[1991,[79]]), it became clear that the σ-w diagram of masonry under tension (for both units and joints + interfaces) could be described with a formula developed by Hordijk and Reinhardt for plain concrete (Hordijk et al.[1990,[25]]):

$$\frac{\sigma}{f_t} = (1+(c_1\frac{w}{w_c})^3)\mathrm{e}^{-c_2\frac{w}{w_c}} - \frac{w}{w_c}(1+c_1^3)\mathrm{e}^{-c_2} \qquad (1)$$

c_1, c_2 : dimensionless constants, respectively 3.0 en 6.93;

w_c : theoretical crack width at which no stresses are being transferred any more:

$$w_c = 5.14\frac{G_{fI}}{f_t};$$

G_{fI} : mode I fracture energy (here defined with $\int \sigma\, du$, see Figure 1 (not to be confused with the energy release rate used in linear fracture mechanics).

With the shape of the descending branch defined by eq. (1), the three parameters c_1, c_2, and w_c must be known. For those parameters the same values as derived by Hordijk for plain concrete were adopted. Consequently only the tensile strength and the mode I fracture energy were needed to determine w_c and hence the post peak behaviour. The fracture energy is the amount of energy per unit of area needed to create a crack in which no tensile stresses can be transferred any more. Looking to the diagram of Figure 1 it can be seen that non-linearities due to micro cracking occur prior to the peak. For the determination of the fracture energy, it can be debated if the energy dissipated by the micro cracking prior to the peak has to be excluded or not. Similar remarks have been made by several authors e.g. Slangen[1993,[73]] and Hordijk[1992,[26]]. The same holds true for the energy absorbed in the tail of the diagram, because the measured force becomes unreliable when it approaches zero and a long tail can influence the amount of fracture energy considerably (Hordijk[1992, [26]]). The influence of the tail will be addressed in section 2.3.2. It is emphasised that the fracture energy is only used as a parameter for eq. (1).
When the behaviour of masonry components has to be established, the first thought goes to testing of the components on their own. Of course this is possible for units, but not for mortar joints, because their properties are influenced considerably by the interaction between mortar and unit during hardening (see e.g. Schubert[1988,[68]] and Vermeltfoort et al.[1991,[80]]). As a consequence, it is necessary to deduce the behaviour of the joint+interface from the behaviour of a masonry specimen. This problem will also be addressed in 2.3.2, where it will be argued that the way the behaviour of the

joint+interface is split up into that of joints and interfaces, is not very important from a modelling point of view.

In the concrete world debates are still going on in what kind of testing arrangement the fracture energy has to be established and even if it can be regarded as a material property. In Van Mier[1997,[43]] these issues are discussed into great detail. Here, the choice is made to use eq. (1) for modelling the descending branch because it gave a good approximation as will be shown later on. The influence of the test set-up will be briefly addressed in section 2.3.1.

2.2 MATERIALS AND SPECIMENS

Test carried out solely for this research, involved two types of masonry:

A: masonry consisting of wire cut bricks (wc-JO) with a general purpose mortar designed in the laboratory and

B: masonry consisting of calcium silicate blocks (CS-block) with a factory-made thin layer mortar.

Results obtained with other types of units and masonry were established within the framework of the Dutch structural masonry research program. Those results were obtained with clay bricks, calcium silicate bricks and blocks, and a normal density concrete brick, tested separately and in combination with different types of mortars.
A detailed overview of the materials used, can be found in Van der Pluijm[1997,[60]] for tests carried out up to 1995 and in Van der Pluijm[1998,[61]] for the tests carried out in the period 1996-1998.
In 1990, the first series of tensile tests were performed with yellow wire cut clay bricks (coded JO), red soft mud clay bricks (coded VE) and calcium silicate bricks (CS-brick90) tested separately and in combination with two mortar compositions: 1:2:9 and 1:½:4½ (cement:lime:sand ratio by volume). With these combinations a wide variety of different combinations of mortar and unit strengths was obtained.
In the series performed in 1993 tensile tests were carried out with parts of calcium silicate elements (CS-el) and concrete bricks (MBI) and a very strong wire cut clay brick, in combination with factory made general purpose mortars designed for that type of bricks. These tests included specimens with thin layer joints.
In tensile and flexural tests carried out in 1995, a new soft mud clay brick (coded RIJ) was used, because the previously used soft mud clay brick VE was no longer available on the market. Also the yellow wire cut clay brick JO, parts of calcium silicate blocks and the normal density concrete brick were used.

Tests carried out since 1995 were restricted to masonry types A and B and their main purpose was the establishment of values of parameters involved in modelling those types of masonry.
A description of the materials including normative references is presented in Appendix A 'Materials', including the pre-treatments of units and curing regimes that were followed throughout the years.

Specimens cut out of units and masonry specimens were used. Their dimensions and the way they were cut from units are shown in Figure 3.

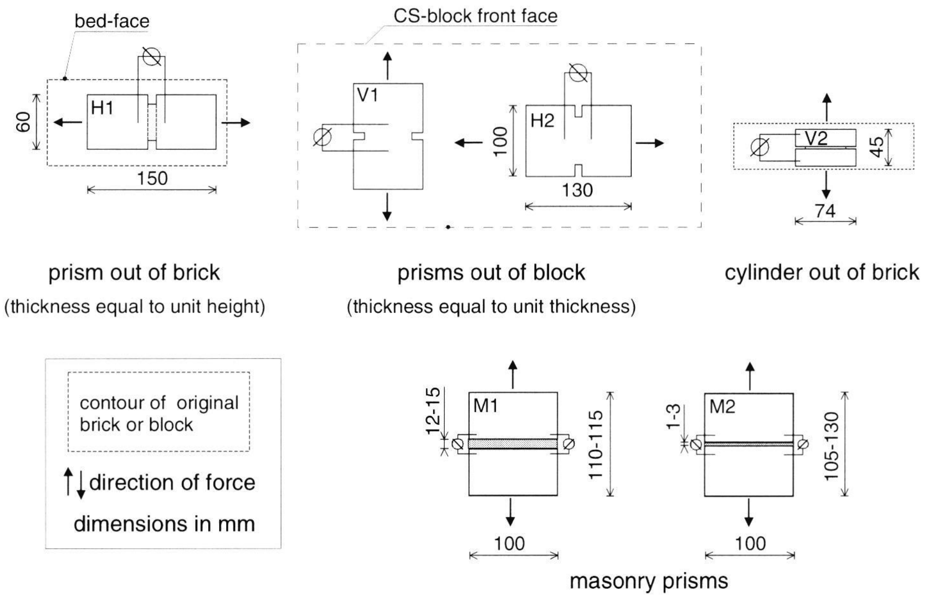

Figure 3 Tensile specimens

The exact dimensions of the masonry specimens depended on the brick type used. In 1990 the age at time of testing was at least three months. This long period was chosen to exclude changes in strength of the masonry specimens during testing, because testing would take a relatively long time. Later on, the bond strength development in the laboratory was measured and it was observed that the increase of strength after 28 days is very moderate (Vermeltfoort et al.[1995,[82]]) and it was decided that testing could start at 28 days.
Sawing bricks in half made the bats for the masonry specimens. When CS-blocks were used the 'bats' were sawn out of the blocks in such a way that the original bond surfaces were preserved for the joint of a specimen (see Figure 4).

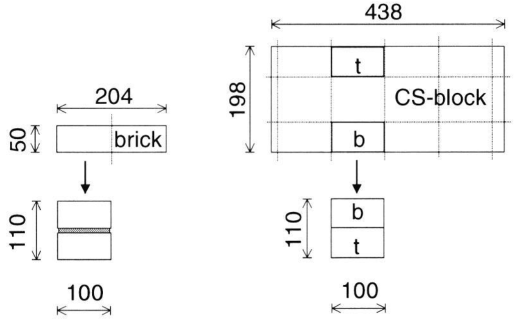

Figure 4 Sawing of bricks and blocks

2.3 TENSILE TESTS

2.3.1 TESTING ARRANGEMENT

For the series performed in 1990 and 1993 a testing arrangement in the Stevin laboratory of Delft University of Technology was used (see Figure 5).

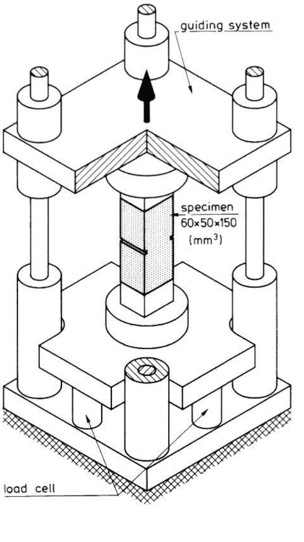

Figure 5 Tensile Testing Arrangement in the Stevin Laboratory (after Hordijk[1992,[26]])

For the series of 1995 and later an arrangement in the Pieter van Musschenbroek laboratory of Eindhoven University of Technology was developed (see Figure 6).

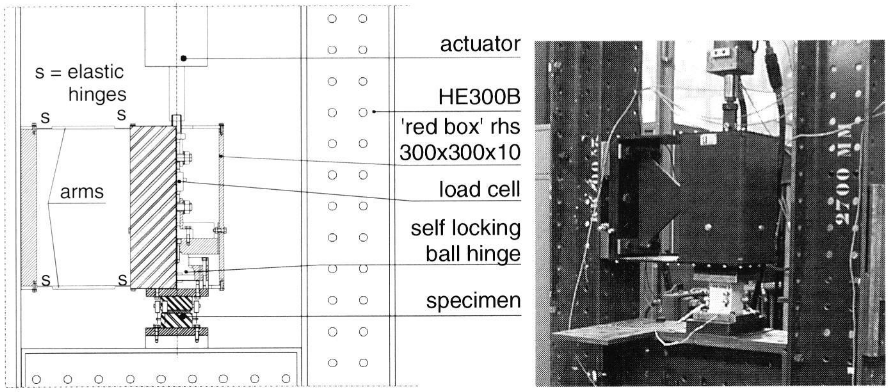

Figure 6 Tensile Testing Arrangement in the Pieter van Musschenbroek Laboratory

In both arrangements an as good as possible full restraints against rotation of the platens (fixed platens) between which a specimen is glued, are provided. In the case of concrete specimens, tested in this kind of arrangements, different cracks can start to grow at different sides of the specimen due to bending moments (Van Mier[1994,[41]]). The bending moments are the result of the fixed platens and eccentricities, originating either from the heterogeneity of the specimen or from growing (micro)-cracks. The different cracks can overlap ('bridge'), resulting in a specimen with more than one crack and consequently more energy absorption (=higher measured fracture energy) (see Figure 7).

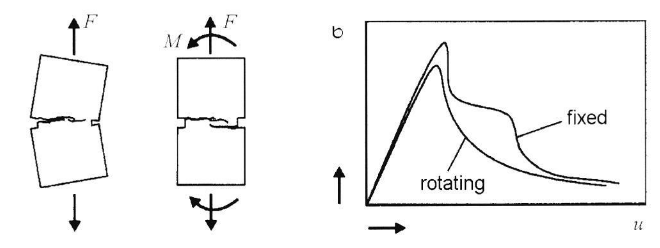

a) hinges b) fixed platens c) stress-crack width diagrams

Figure 7 Effect of boundary conditions on softening in the stress-crack width diagrams (after Van Mier[1997,[43]])

As a consequence, non-uniform crack-opening occurs, resulting in the typical S-shape of the descending branch in the stress-displacement diagram as shown in Figure 7 (see also Hordijk[1992,[26]]). According to Van Mier, the problem of bridging can be avoided by using hinges in stead of restraints. In a homogeneous specimen, either hinges or restraints at the boundaries lead to the same stress distribution up to the moment micro cracks start to develop. From that moment, however, hinges introduce high peak stresses

in the specimen and it is questionable if still a useable stress-crack width relation is obtained. At the meso level, modelling of tension behaviour implies averaging of local (micro) behaviour at which phenomena like bridging cannot be modelled. Furthermore, in the case of masonry, where the interface is in most cases the weakest link, bridging is very unlikely to occur. Of course, this is not true for the units themselves of which the behaviour resembles concrete very much.
Also the length of the specimen plays a role on the measured behaviour (Hordijk[1992,[26]], Van Mier et al.[1996,[43]]). Shorter specimens tend to give less brittle behaviour, but may result in lower strength values. Phenomena occurring are:

- the larger rotational stiffness of the specimen leads to a more uniform crack opening in shorter specimens;
- inhomogeneities will result in a less homogeneous stress distribution with shorter specimens.

To conclude the discussion about testing technique, on the one hand phenomena as bridging show that it is questionable whether the fracture energy is a true material parameter or not. On the other hand, it is questionable if it can ever be justified to speak about 'true' material properties at the modelling levels micro, meso and macro. All these levels imply averaging and simplification of behaviour at lower levels. The problem of the fracture energy being a 'true' material property seems of minor importance in case of which it is only used as a parameter in combination with eq. (1) to describe the descending branch. By comparing experimental and numerical results, Hordijk[1992,[26]] has validated that this approach can be used to model plain concrete as a softening material.

Furthermore, testing with hinges in case of masonry, where the actual bonding area between mortar and units can be significantly less than the cross sectional area of a specimen, is particularly complicated. Even with externally centrical loading of a specimen, a large eccentricity of the 'actual bonding area' may be present in the specimens, resulting in non-uniform internal stress distributions prior to the peak. The 'actual bonding area' will be discussed in depth in section 2.3.6.

In the arrangement of Delft the restraint of the platens is achieved by connecting the upper platen to a stiff guiding system in such a way that it can only move vertically, where in Eindhoven the upper platen is part of a parallelogram mechanism disabling rotation.

In the testing arrangement of the Stevin laboratory the load is measured under the bottom platen, so the friction between the guiding system and the upper platen has no influence on the measured force. In the test set-up of the Pieter van Musschenbroek laboratory the change of the spring-forces in the arms and the deadweight of the 'red box' (a red painted steel member with a rectangular hollow section 300×300×10 mm), have to be subtracted from the measured load. The deadweight (including the upper part of the specimen, was established with measurements taken when an open crack was formed. The change in spring force was determined using the internal linear variable differential transducer (LVDT) of the actuator in combination with the spring stiffness. In both arrangements LVDT's are glued on the specimens (see Figure 8). These LVDT's are used to control the increase of the deformation over a crack that will develop during the test. The gauge length must include a weak cross section of the specimen to fix the location of the crack. In case of a masonry specimen the joint is a naturally weak cross section. In case of testing units, the weak cross section is created by reducing a cross section within the gauge length by symmetric saw cuts (notches) at two or four sides of a specimen.
The gauge length used in the Stevin laboratory varied between 25 and 35 mm. The gauge length used in the Pieter van Musschenbroek laboratory was always 30 mm.

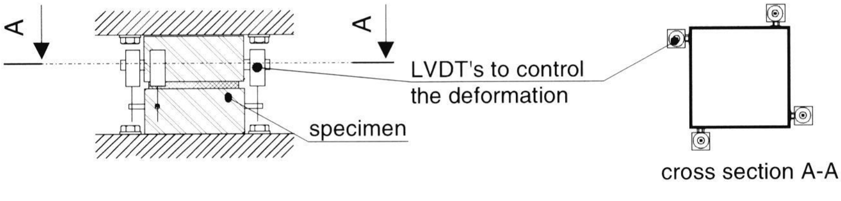

Figure 8 Location of LVDT's used to control the increase of deformation during a test

For a comprehensive analysis of the testing technique applied in the Stevin laboratory, the reader is referred to Hordijk[1992,[26]]. That analysis is mutatis mutandis valid for the Eindhoven arrangement.

2.3.2 Processing of test data

The quantities analysed were (see Figure 9):

- tensile strength;
- stiffness;
- mode I fracture energy related to equations describing the descending branch.

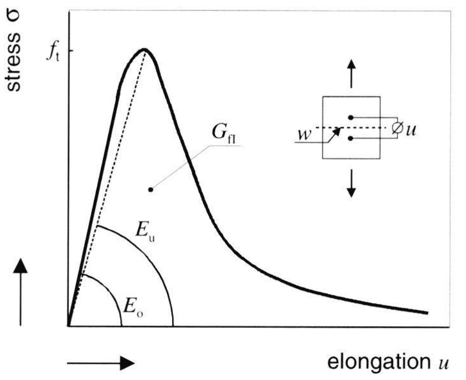

Figure 9 Schematic diagram of tensile test with quantities analysed

Before discussing the results for these quantities in the coming sections, the way they have been derived from the measurements will be explained.

In correspondence with the meso approach, the tensile strength f_t of a specimen was calculated from:

$$f_t = \frac{F_u}{A} \tag{2}$$

The scatter of the tensile (bond) strength directly follows from the scatter of the measured ultimate force.

The stiffness values of the units were determined with linear regression in the first, almost linear part of their σ-ε diagram. The values in tension were determined on prisms without notches. Due to their shape, notched specimens are not suitable to determine stiffness values. A non-uniform stress distribution occurs in specimens with notches due to the notches themselves and due to the changes of the cross sectional area within the load direction. Using the data from notched prisms, low values for the stiffness (20-40% lower values compared with those in Table 33) would have been obtained even when the reduced cross sectional area on the spot of the notches was used. This is the reason why no stiffness values are presented for the notched tensile unit specimens.

To be able to calculate the deformations of joint+interfaces in the masonry specimens, the measurements had to be corrected for the deformations in the parts of the units within the gauge length. Correction of the data for the deformations in these parts of the units was done using the stiffness of the units presented Table 33 (Appendix A 'Materials').

With the calculated deformations of the mortar-joints, stiffness values could be established. The calculation-process implies that a deviation between the actual unit stiffness and its assumed stiffness (mean of sample) influences the outcome for the mortar stiffness. So the scatter of the unit stiffness increases the scatter of the calculated joint stiffness. The modulus of elasticity of the mortar-joint was calculated assuming that the Poisson's ratios of both units and mortar were equal, because there are no reliable values available for mortar hardened between units. With this assumption it can be derived that (see also Figure 10):

$$E^{\mathrm{j}} = \frac{t^{\mathrm{j}} E^{\mathrm{j+u}} E^{\mathrm{u}}}{E^{\mathrm{u}}(t^{\mathrm{u}} + t^{\mathrm{j}}) - E^{\mathrm{j+u}} t^{\mathrm{u}}} \tag{3}$$

t^{j} : thickness of the joint;

t^{u} : thickness of parts of the units within the gauge length;

$E^{\mathrm{j+u}}$: modulus of elasticity of the specimen within the gauge length, following directly from the measurements.

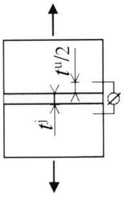

Figure 10 t^{j} *and* t^{u} in a masonry specimen

When the joint thickness is small and the stiffness of the specimen within the gauge length does not differ much from the unit stiffness, the outcome of the calculated stiffness of the mortar-joint becomes highly sensitive for the stiffness of the unit used and the thickness of the joint (the numerator in eq. (3) approaches zero).

In Figure 11 the influence of:

- relatively small changes of the value used for the stiffness of the unit,
- a small change of the measured deformation (via $E^{\mathrm{j+u}}$) and
- the joint thickness

on the calculated stiffness of the joint, is demonstrated.

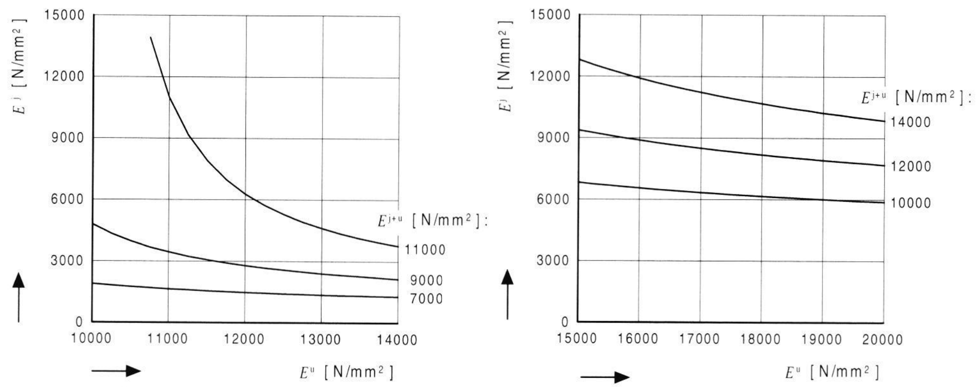

a) t^j = 1 mm; t^u = 29 mm   b) t^j = 12.5 mm; t^u = 17.5 mm

Figure 11 Average stiffness of thin layer mortar joint as a function of the unit stiffness E^u *and measured stiffness* E^{j+u}

The values presented in Figure 11a and b are respectively representative for CS-block masonry and wc-JO clay brick masonry. From Figure 11 it can be observed that the sensitivity is great for a small joint thickness but rapidly decreases when the joint thickness or the difference between E^{j+u} and E^{u} increases.

Consequently, the calculated stiffness of thin layer joints was unreliable in some cases. In these cases the stiffness of the specimen within the gauge length that can directly be derived from the measurements, has been presented. This modulus of elasticity is indicated as E^{j+u}.

Another factor that might influence the calculated stiffness of the joint is the effect of notches on the stiffness of the unit. In the masonry specimens, where the actual bonding area between mortar and units can be significantly less than the cross sectional area, the bonded area can be expected to function as a natural notch. Referring to the experience with the determination of the stiffness of notched unit specimens, this may lead to a lower average stiffness of the unit within the measurement length than used in the calculation procedure. This influence is difficult to assess and hence, left open in the calculations.

The initial stiffness E_0 and the secant modulus E_u of the masonry specimens and mortar-joints were calculated (see Figure 9). The initial stiffness was calculated with linear regression using a data-interval between 0 and a variable load level. The upper limit of the interval was established for each test by calculating the correlation coefficient r using load levels between $0.5 f_t$ and $0.9 f_t$ with increments of $0.05 f_t$. Finally the interval with the upper limit was selected for which the maximum value of r occurred.

After the peak, a distinction can be made between the behaviour of the mortar joint and the interface if cracking occurs in the interface. In those cases it is more or less natural to follow the approach of Hillerborg in splitting the deduced behaviour for the joint+interface in a σ-ε diagram for the joint and a σ-w diagram for the interface with its assumed zero thickness. However, in tests where cracking also occurred in the mortar itself or partly in the mortar and partly in the interface this is not obvious. Now the cracked zone could be modelled within the mortar joint. Looking to the consequence for modelling, however, it can easily be seen that according Hillerborg's approach, this mathematically leads to the same relations if the formation of a crack occurring in the interface or in the mortar shows the same behaviour. In tests where cracking occurred in the mortar itself no difference in behaviour could be observed with specimens of the same series where cracking only occurred in the interface. In those series, the tensile strength and fracture energy were of the same magnitude as in case of bond failure. Therefore, the behaviour of joint+interface could be split up between a σ-ε diagram and a σ-w diagram, irrespective of where cracking occurs from a modelling point of view. For this reason the mortar-joint and bond interface were denoted as joint+interface when no clear distinction is necessary.
As mentioned before, the descending branch of masonry under tension (both for units and bonding surface) could be described with eq. (1). An alternative formulation to model the descending branch on the basis of the fracture energy and the tensile strength has been used by Lourenço et.al.[1995,[36]]:

$$\frac{\sigma}{f_t} = e^{-\frac{f_t}{G_{fI}}w} \tag{4}$$

Both expressions give nearly the same result for the descending branch. Eq. (4) is less steep in the first part of the descending branch and does not approach the descending branch as well as eq. (1). Their applicability will be demonstrated later.
When an equation like eq. (1) or (4) is used to model the behaviour beyond the peak, it is necessary for the determination of the fracture energy that the experiments remain stable until a crack-width at which the transferred load has diminished. If the tail is 'incomplete', the amount of fracture energy that can be derived from the measurements is too small, and used in eq. (1) or (4), too brittle theoretical behaviour is the result. Contrary to this problem, Hordijk[1992,[26]] indicated that the theoretical behaviour according to eq. (1) becomes too tough when the tail in the experiment is very long. A long tail can increase the calculated fracture energy considerably. This problem did not occur in the tests on masonry.
The effect of 'the missing tail' was present in some tests. These missing tails may be caused by the occurrence of snap back behaviour due to non-uniform opening of the

crack as shown by Hordijk[1992,[26]]. For these tests, the measured amount of the fracture energy was corrected assuming that eq. (1) applies. By expressing the fracture energy measured up to w_{last} (in the descending branch) as a fraction of the total amount of fracture energy (both according to eq. (1)) and considering it as a function of σ_{last}/f_t, Figure 12 evolves.

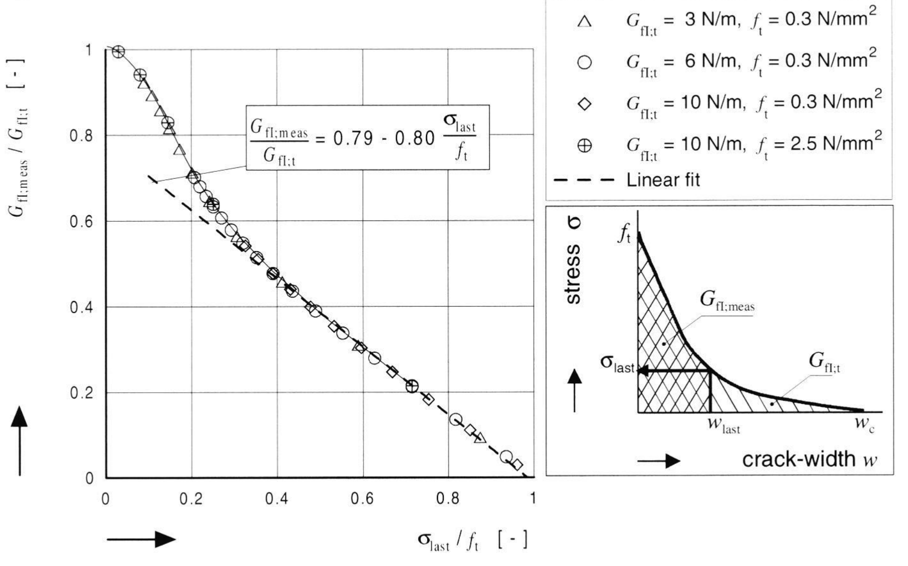

Figure 12 Ratio between the fracture energy measured up to a stress level σ_{last} and the total fracture energy ($G_{fl;meas}/G_{fl;t}$) using eq. (1)

From Figure 12 it can be observed that the theoretical relation between $G_{fl;meas}/G_{fl;t}$ and σ_{last}/f_t is independent of the actual values of G_{fl} and f_t. Furthermore, the ratio $G_{fl;meas}/G_{fl;t}$ is almost a linear function of σ_{last}/f_t in the interval [0.3; 1] for σ_{last}/f_t. The best fit through this part of the relation (indicated in Figure 12) has been used to correct the measured fracture energy if the stress level σ_{last} in the tail was greater than 0.2 f_t, ignoring the small deviation between the linear fit and the theoretical relation in the interval 0.2< σ_{last}/f_t <0.3. Also an upper limit for σ_{last} was applied. The measured amount of fracture energy deviates very much if σ_{last} approximates f_t, because the exact shape of the measured descending branch just after the top can be very irregular. Using a limited amount of data just after the top, led to a very unreliable prediction of the fracture energy to be used in eq. (1). Therefore, modification of the measured amount of fracture energy was checked by plotting the theoretical descending branch determined with the modified fracture energy in graphs of the test and comparing them with the measured data (Van der Pluijm[1998,[61]]). When it was obvious that no good description could be derived, the test result was not used as a valid outcome for the fracture energy.

In this way it seems that the validation of the usability of eq. (1) becomes a self-fulfilling prophecy, but it must be kept in mind that most of the values obtained from the experiments were not modified and in those cases eq. (1) gave a good approximation of the test results.

The fracture energy has already been defined with $\int \sigma \, du$, see Figure 1. As the shape of most of the descending branches can be described with eq. (1), the two parameters f_t and u_{last} (that were directly derived from the measured data) influenced the scatter of the fracture energy to a great extent. These two parameters both show independently of each other a large scatter and resulted in even a larger scatter of the fracture energy, also in comparison with the scatter of the tensile bond strength.

2.3.3 General observations

The results of all tensile tests can be found in Appendix B 'Experimental Results'. The average results per series are presented in Table 1 for the units and in Table 2 for the masonry specimens.

Table 1 Average results of tensile tests on parts of units

unit	specimen type	f_t [N/mm^2]	G_{fI} [N/m]
sm-VE	prism H1	2.47 (14%)	61 (24%)
	cylinder V2	1.50 (4%)	73 (3%)
wc-JO90	prism H1	2.36 (21%)	117 (-)
	cylinder V2	3.51 (3%)	128 (3%)
wc-JO96	prism H1	2.06 (16%)	101 (19%)
CS-brick90	prism H1	2.34 (10%)	67 (17%)
CS-element	prism H1	1.17 (49%)	47 (-)
CS-block96 HOR	prism H2	1.84 (15%)	71 (51%)
CS-block96 VER	prism V1	1.66 (13%)	58 (54%)

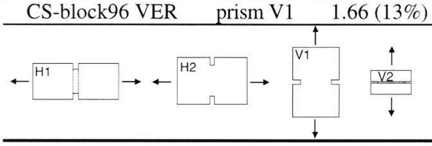

(see Figure 3)

In 1990, the clay bricks were tested parallel and perpendicular to the bed joint. The CS-brick90 was only tested in the direction parallel to the bed joint, because it is supposed that this unit-type behaves isotropic. In 1996, the CS-block96 was tested parallel and perpendicular to the bed joint. From the results in Table 1, it could be observed that:

- The wc-JO90 clay brick was stronger in the direction perpendicular to the bed joint (cylinder), while the sm-VE brick was stronger in the direction parallel to the bed joint (prism). This result can be explained by the difference in orientation of the layers in the clay bricks due to the fabrication process. The CV for the tensile strength of the cylindrical specimens was remarkably low.
- The CS-block96 showed a difference between the horizontal and vertical tensile strength, but the difference was not really significant with a probability of 30% (t-test).

Table 2 Average results of tensile tests on small masonry prisms (coefficient of variation % between brackets)

masonry		fabric. year	related chapter	E_o^j	E_u^j	f_{tb}	G_{fI}	$G_{fI;mod}$
unit	mortar			[N/mm^2]	[N/mm^2]	[N/mm^2]	[N/m]	[N/m]
sm-VE	1:2:9	1990	-	610 (12)	470 (12)	0.22 (60)	7.8 (65)	7.8 (65)
	1:½:4½	1990	-	670 (69)	320 (76)	0.13 (101)	4.2 (32)	4.2 (32)
	1:2:9	1990	-	2900 (13)	1410 (52)	0.30 (24)	11.5 (64)	11.5 (64)
wc-JO90	1:1:6	1995	-	2370 (55)	1220 (57)	0.40 (39)	5.6 (66)	5.6 (66)
	1:½:4½	1990	-	6000 (20)	3840 (37)	0.50 (29)	6.8 (51)	6.8 (51)
	1:2:9	1996	4, wallettes.	5653 (58)	4712 (59)	0.54 (33)	5.6 (53)	7.8 (51)
	1:2:12	1997	4, wallettes.	6198 (45)	3248 (68)	0.37 (22)	4.5 (37)	9.0 (28)
	1:2:9	1997	4, wallettes, 70°	2439 (118)	1516 (124)	0.15 (51)	0.9 (44)	2.0 (70)
wc-JO96	1:2:12	1997	3,shear	7991 (83)	3624 (56)	0.39 (44)	2.0 (52)	2.6 (34)
	1:1:6	1997	3,shear	5670 (37)	4330 (53)	0.43 (26)	3.3 (103)	5.1 (67)
	1:1:6	1998	4, panel I	3785 (63)	2420 (84)	0.24 (60)	1.7 (92)	2.6 (113)
	1:1:6	1998	4, panel II	1981 (126)	958 (106)	0.13 (66)	1.0 (71)	1.1 (79)
hswc-JOK	TLM	1993	-	4402 (16)	3140 (35)	2.24 (26)	17.1 (35)	17.1 (35)
CS-brick90	1:2:9	1990	-	5110 (17)	1490 (12)	0.32 (34)	*	*
	1:1:6	1190	-	2540 (19)	1790 (18)	0.33 (51)	*	*
CS-block95	TLM	1995	-	7990 (54) **	6040 (53) **	0.33 (27)	3.3 (41)	3.3 (41)
CS-block96	TLM	1996	4, wallettes.	6930 (49) **	7180 (46) **	0.50 (32)	10.1 (26)	10.1 (26)
		1997	3, shear	8469 (71) **	5689 (61) **	0.42 (34)	4.4 (53)	7.2 (51)
MBI	fmGPM	1993	-	8040 (26)	7470 (35)	0.73(19)	11.3 (-)	11.3 (-)

* uncontrolled failure

** presented value of E-modulus determined over whole gauge length (30 mm): E^{j+u}

In most of the masonry specimens a crack developed in the bond surface between mortar and unit. The bond surface after fracture of masonry with CS-units was remarkably smooth.

Differences between masonry series, in which the same material combinations were used, were mainly caused by differences in curing regimes and environmental conditions. Another important difference could be observed between combinations where the same mortar (from one batch) was applied between different units. The stiffness and bond strength of those combinations could differ considerably: up to a factor 5 for the bond strength and up to 10 for the stiffness of the joint. The interaction between the unit and the fresh mortar is the main cause for these differences (see

Groot[1993,[20]] for a detailed discussion on this interaction). A detailed discussion on the differences found, is given in Van der Pluijm[1997,[60]] for the tests up to 1995.

In general it can be observed that the coefficient of variation (CV) (given between brackets in Table 1 and Table 2) is large for all quantities, but it is emphasised that its reliability based on a few individual test results is very small. However, the CV of a few larger series was of the same magnitude as of the smaller series. It may be concluded that the CV's found in the small series are not much influenced by the sample size. In general CV's of 20% to 30% are typical for bond strength tests (De Vekey et.al.[1994,[12]]). Examples of stress-displacement curves obtained with specimens in the 1995 series wc-JO bricks with GPM 1:1:6, are presented in Figure 13.

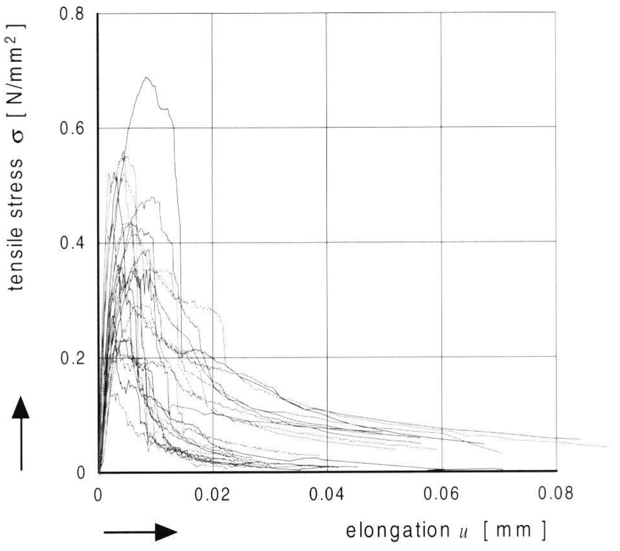

Figure 13 Stress-displacement curves of controlled tests in series with wc-JO bricks and 1:1:6 mortar

Although a diagram of one test can hardly be identified in Figure 13, all curves are presented together to give an impression of the scatter of the tensile bond strength and of the fracture energy (area under the curves).

To conclude the global discussion about differences between series, it should be noticed that the results of the tensile tests confirm the statement in section 1.1 that a lot of parameters determine the bond strength in masonry in an unknown manner. It is not (yet) possible to predict the bond strength from the basic materials and the processing conditions. Experience and suitability tests under realistic processing conditions will remain important to achieve a pre-set level of bond.

2.3.4 TENSILE STIFFNESS AND STRENGTH OF THE JOINT+INTERFACE

The method of determining the stiffness of the joints made it impossible to establish meaningful values of the stiffness of the thin layer mortar joints in the series with CS-blocks and thin layer mortar of each test. Using the average stiffness of the specimens of the CS-block95 +TLM series to establish the stiffness of the mortar-joint with eq. (3), led to the results presented in Table 3.

Table 3 Mean stiffness values E_o^j for TLM joints in CS-block95 +TLM series depending on the joint thickness with E^u = 12800 N/mm², t^u+t^j = 30 mm

joint thickness [mm]	E_o^j [N/mm²]	
	E^{j+u}=7990 N/mm²	E^{j+u}=6040 N/mm²
1	727	386
2	1372	749
3	1948	1090

The values for E^{j+u} in Table 3 were chosen on the basis of mean results of CS-block95 +TLM series and were taken equal to respectively E_o and E_u. From the results it can be observed that the relation between the (modelled) joint thickness and joint stiffness (in a numerical model) is important. It must be consistent with the data concerning t^u+t^j, E^u and $E^{j+u\,j}$. This can also be seen from eq. (3) rewritten as:

$$\frac{E^j}{t^j} = \frac{E^{j+u}E^u}{E^u(t^u+t^j)-E^{j+u}t^u} \approx \frac{E^{j+u}E^u}{t^u(E^u-E^{j+u})} \quad \text{if } t^j << t^u \qquad (5)$$

In 1991, Vermeltfoort carried out compression tests on specimens made simultaneously with the tensile specimens of 1991 (Vermeltfoort et al.[1991,[79]]). From the results in compression and tension a difference between the stiffness in compression and tension could be observed when the specimens were still showing linear behaviour. A possible cause will be discussed in 2.3.6 and extended in chapter 4 Bending behaviour on the macro scale.

In Figure 14 the modulus of elasticity E_o^j of the mortar-joint in clay brick masonry with GPM is plotted against the tensile bond strength.

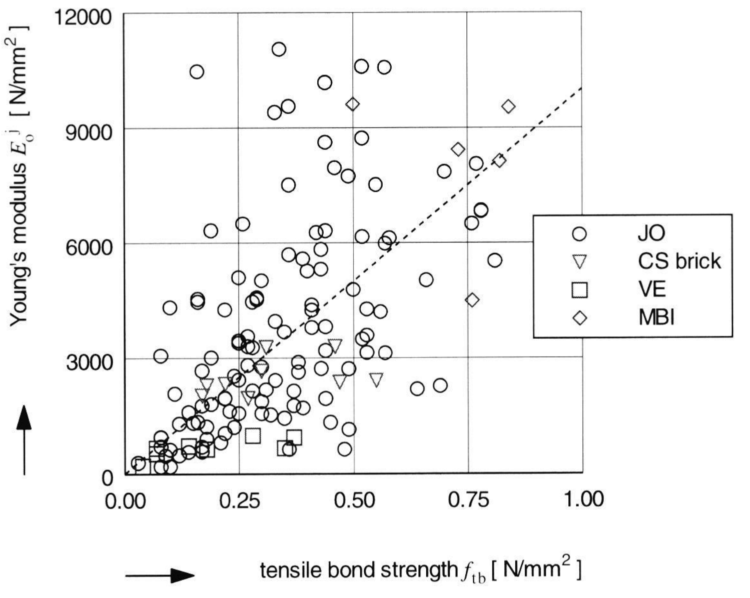

Figure 14 Tensile bond strength versus E_o^j of the mortar-joint of masonry with GPM

Although the linear regression line is plotted, no real correlation between f_{tb} and E_o^j can be observed. The correlation coefficient r of the plotted linear best fit ($E_o^j = 1000 \cdot f_{tb}$ N/mm^2, forced through the origin) equals 0.57, confirming the absence of correlation.

The results with sm-VE and CS-brick90 masonry may suggest that a scatter of the bond strength mainly causes the scatter and that the stiffness is more or less constant within a series. Considering all series with wc-JO masonry separately, this impression had to be rejected and the general impression that was obtained when all results were considered together, was confirmed.

Results of Lawrence[1983,[28]] confirms the absence of a relation between the tensile bond strength end stiffness. He showed that there was no useful relation between the flexural bond strength and stiffness based on 311 bending tests.

2.3.5 Mode I fracture energy and tension softening of the joint+interface

In Figure 15 the fracture energy is plotted against the tensile bond strength for all types of tested masonry, except hswc-JW + TLM. That series was excluded because of its clearly different behaviour, due to the specially developed TLM applied.

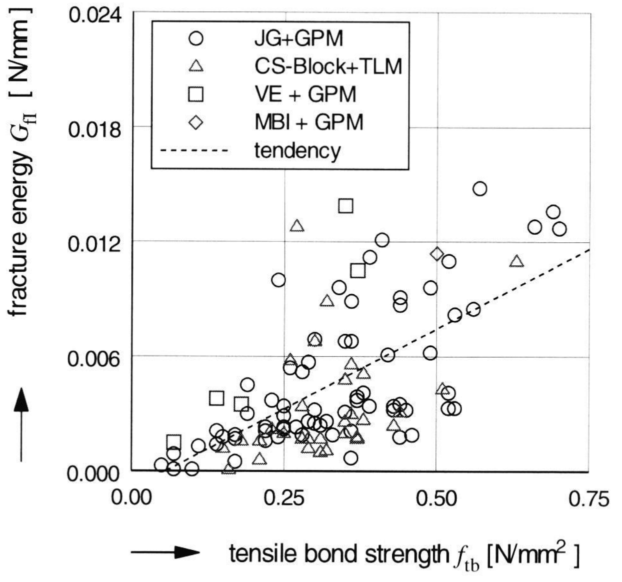

Figure 15 Tensile bond strength versus mode I fracture energy for all types of tested masonry except hswc-JW + TLM

It can be observed that there is no clear correlation between both quantities, but with increasing bond strength, the fracture energy also tends to increase. This is only logical when the definition of the fracture energy is taken into account. From its definition it is obvious that the fracture energy must be zero, when the tensile strength is zero and must be infinite, when the tensile strength is infinite. Despite of this expected coherence between the fracture energy and tensile strength, it is not found for concrete either. The amount of fracture energy is much more correlated with the kind of concrete (e.g. lightweight versus normal density concrete) than with its strength. However, such a correlation is difficult to extrapolate to masonry with its components, their interaction during hardening being a result of pre-treatments, handling and curing conditions.

If the shapes of the descending branches of the units and the masonry specimens resemble each other (which is more or less the case as they all could be approximated by eq. (1)), the brittleness of materials can be compared using the characteristic length l_{ch} defined by Petersson[1981,[46]]:

$$l_{ch} = \frac{G_{fI} \cdot E}{f_t^{\,2}} \tag{6}$$

With an increase of l_{ch}, the brittleness decreases. The average of all masonry prisms was 110 mm with a CV of 120% and of the units 230 mm with a CV of 55%. In terms of brittleness the joint+interface is twice as brittle as the units.

An example of the prediction of the descending branches with equations (1) and (4) is given in Figure 16.

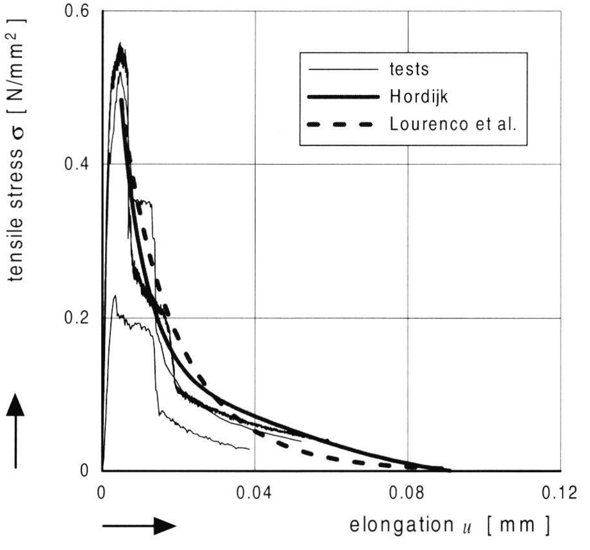

Figure 16 Stress-displacement curves of a sub-series of 1995 with wc-JO clay brick masonry (1:1:6 mortar), including the theoretical descending branches according to Hordijk-eq. (1) and Lourenço-eq.(4) based on average values of tensile strength and fracture energy of the sub-series

The typical plateau's in the descending branches followed by steep descents that can be observed in Figure 16, are caused by the non-uniform opening of the crack (see Hordijk[1992,[26]]). The non-uniform opening is demonstrated in Figure 17, showing the displacements measured with the 4 LVDT's at the corners of the specimen and their mean.

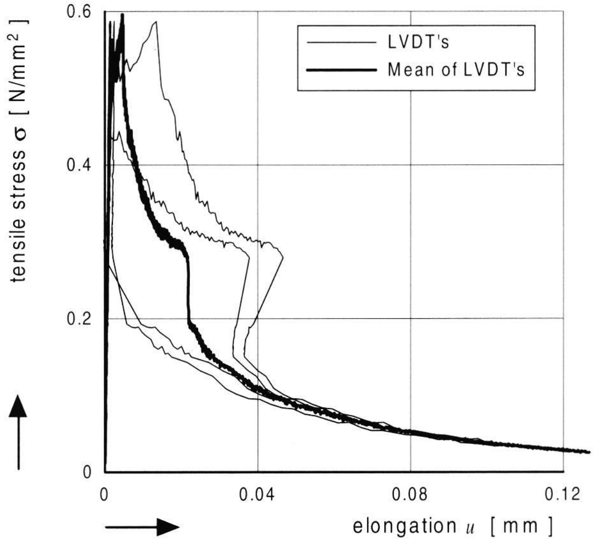

Figure 17 Example of differences between mean displacement and the displacements of the corners in a tensile test from the wc-JO+1:1:6 series

2.3.6 Actual bonding area

During the first series in 1990, it became clear by close observation of the cracked specimens, that the area over which joint and unit were bonded together was smaller than the cross-sectional area of the specimen. For each of the masonry specimens in that series the 'actual bonding area' was determined by visual inspection of the crack-surface. Of course, this is a very subjective method because a cracked surface is difficult to interpret, but at least an impression of the actual bonding area is received. This manner of determining the actual bonding area can be considered as an interpretation on the meso level.

According to Grandet et al.[1972,[19]] and Lawrence et al.[1987,[30]], bonding on the micro level is preliminary caused by mechanical interlocking of C-S-hydrates and/or $Ca(OH)_2$ crystals grown into the pores. They analysed bond interfaces with X-ray and scanning electron microscopy techniques and found no evidence of chemical reactions.

An example of the visual determination of the actual bond area is shown in Figure 18. The coefficients of variation of the tensile bond strength and the fracture energy reduced with respectively 34% and 18% for the series of 1990, when the actual bonding area was taken into account.

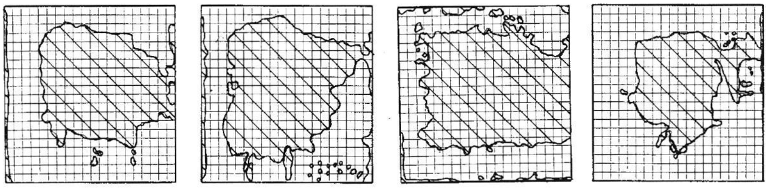

Figure 18 Actual bonding area of soft mud clay brick VE masonry specimens with1:2:9 mortar

These reductions show that use of the cross sectional area instead of the actual bond area, is one of the causes for the scatter of the bond strength and fracture energy. It may be expected that the unit itself (e.g. via pore diameters, available water in pores during the drying of the cement, roughness and even the shape of pores making possible more or less mechanical interlock) plays a role. Detailed analyses on the micro-level are necessary to reveal this kind of influences.
In many cases the actual bonding area was restricted to the central part of the specimen. Therefore it was supposed that the reduction of the bond surface is caused by the edges of the specimen. This may be the result of workmanship, setting of the mortar in its plastic phase and of shrinkage. In a normal wall, two of the four edges are not present. With the proposed influence of the edges, it is possible to estimate the fracture energy for a wall (see Figure 19). The average bond surface of the specimens was 35% of the cross-sectional area. If the actual bonding area is supposed to be square, it follows that the actual bonding area of a wall will be 59% of the cross-sectional area. So the bond surface of the wall is approximately 1.7 times greater than that of the tensile test specimens. The same holds true for the fracture energy and the tensile strength of the wall, both based on the cross-sectional area. It should be noted that a possible influence of head joints is totally neglected in this way.

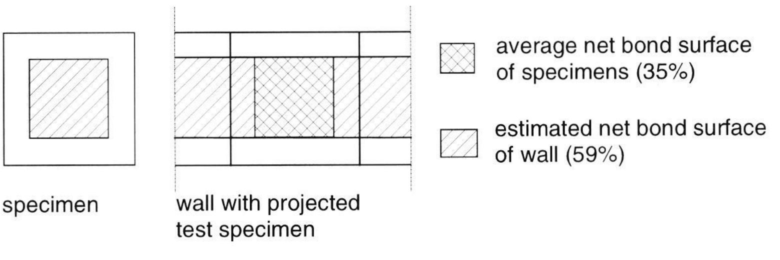

Figure 19 Estimation of the actual bonding area of a wall based on the average net bonding area of the test specimens.

The effect of a difference between the actual bonding area and the cross-sectional area of a specimen might play a role in the found difference in stiffness in tension and compression. Such differences can be explained if it is assumed that non-bonded contact areas exist, capable of transmitting compressive stresses.

It is obvious that the actual bonding area causes eccentricities in the tensile test. As already mentioned in section 2.3.1, eccentricities originating from the heterogeneity of the specimen, influence the behaviour of a specimen before and after the peak in contrast with eccentricities originating from cracking that influence the shape of the descending branch. The irregular shape of the actual bonding area is likely to be a cause of the scatter in pre- and post-peak masonry behaviour.

The effect of an actual bonding area that is smaller than the cross-sectional area of a specimen on the measured tensile bond strength was investigated numerically. A comprehensive description can be found in Van der Pluijm[1995,[53]].
Tensile tests with two boundary conditions are discussed here: hinges and fixed platens. Furthermore, the cross couplet test is considered (see Figure 20).

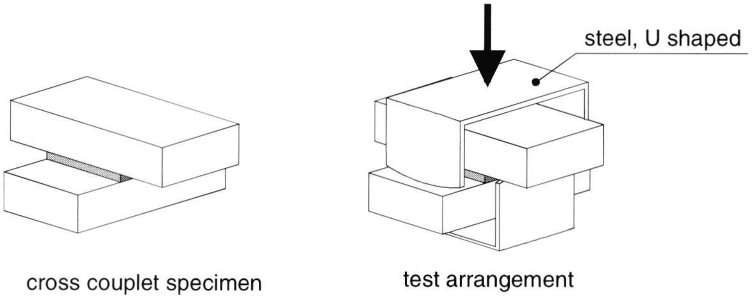

Figure 20 Cross couplet test prescribed by NEN 3835:1991

This test is prescribed by the Dutch mortar standard NE3835:1991 to check if minimum bond strength demands are fulfilled.

A specimen with an eccentric regular shaped bond surface was modelled two-dimensionally, using plane strain and interface elements. With the interface elements the 'real' interface between mortar and unit was modelled. The non-linear behaviour was attributed to these elements. All other parts were modelled linear elastically. A detail of the modelled joint between two bats is presented in Figure 21.
For each boundary condition 3 analyses were performed: one with average properties, one with a relatively low value for the fracture energy and one with a low value for the Young's modulus. In this way all parameters that influence the brittleness were taken into account (see eq. (6)).

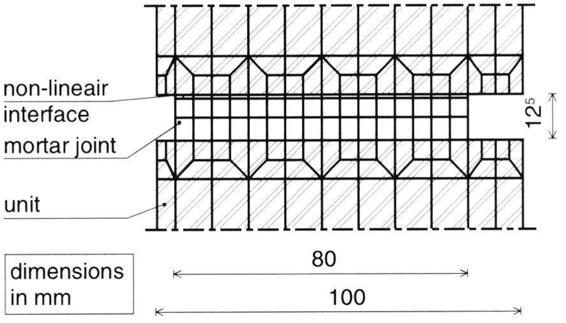

Figure 21 Part of the FE model: detail of the eccentric joint

In both models the two bats were glued between 20 mm thick steel platens. The bar between the upper platen of the model with hinges and 'the world' could only transfer axial forces. It was modelled in correspondence with a test arrangement used in the Pieter van Musschenbroek laboratory. All the calculations were carried out until the maximum load was reached and the load started to decrease. In this way, it was ensured that the real maximum load was recorded. The enlarged deformations at failure are presented in Figure 22.

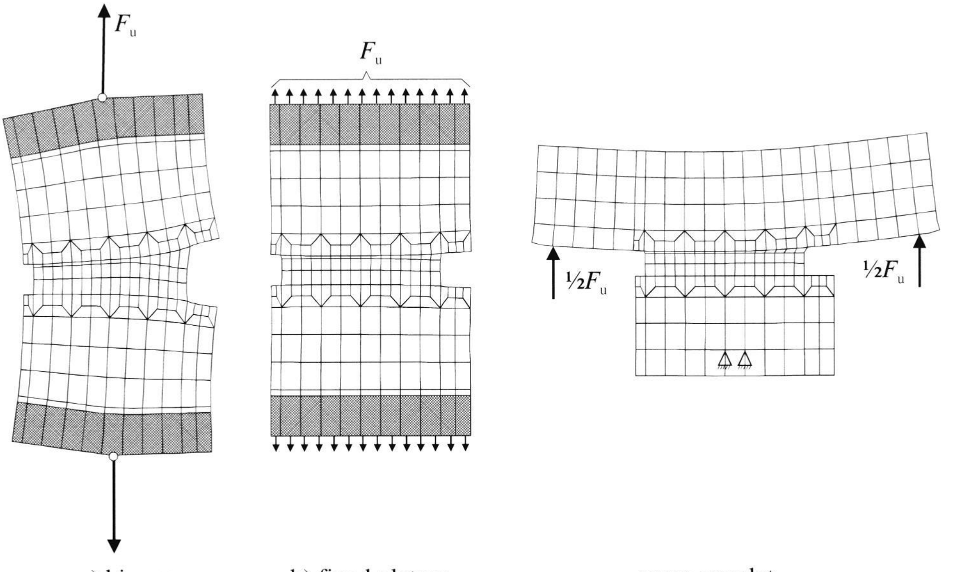

Figure 22 Deformations at peak-load (average properties)

The corresponding tensile and shear stress distributions in the interface are presented in Figure 23.

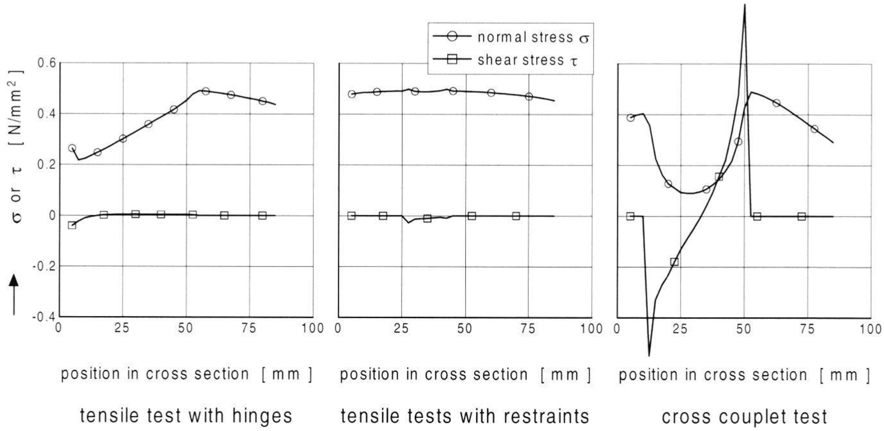

Figure 23 Tensile and shear stress distribution in the critical joint for the maximum achieved load (average properties)

From Figure 23, it can be observed that the tensile stress distribution is remarkably non-uniform for the cross couplet test and to a lesser degree also for tensile test with the hinges, resulting in a lower maximum load for those tests compared with the tensile test with restraints. The shear stress distribution is also shown because shear stresses influence the failure load. It can be observed that they will only play a role for the cross couplet test. This influence was not taken into account in the FE analysis. The influence of the shear stresses will be discussed in the next chapter. In Table 4 an overview of all calculation results is presented.

Table 4 Numerically 'measured' tensile bond strength f_{tb} (based on the gros cross sectional area) with a nominal bond strength of 0.4 N/mm^2 (0.5 N/mm^2 based on the actual bonding area)

Tensile test arrangement	average properties	E low	G_{fI} low
hinges	0.31	0.29	0.29
fixed	0.39	0.38	0.38
cross couplet	0.23	0.19	0.20

The results in Table 4 show that the numerically 'measured' bond strength with hinges was 23% to 27% lower than the input strength whereas the bond strength with restraints was 3 to 5 % lower. The cross couplet test resulted in a 42 to 52% lower 'measured' strength compared with the input strength. The peak load in the FE calculations of a tensile test with hinges is influenced considerably by an eccentric bond interface, which is not the case for the calculations with fixed platens. As has already been pointed out, a test arrangement with a full restraint can only be approximated and such an arrangement will perform not as well as the numerical simulation with perfect restraints. Therefore the measured strength will always be less than the material strength. In practice this difference cannot be quantified because the real eccentricity of the actual bonding area is an unknown parameter.

The bond interface in masonry specimen includes a 'natural' eccentricity. Therefore it is concluded that a test arrangement with fixed platens is the most suitable to measure the behaviour of masonry loaded in tension. The cross couplet test gave an unreliable value for the tensile bond strength. An experimental comparison of the tensile tests is presented in chapter 6.

2.4 Flexural Tests

2.4.1 Testing Arrangement

A 4-point bending test arrangement capable of testing relatively small masonry specimens was used. With this testing arrangement the fracture energy G_{fI} can be established, but it is not possible to establish the stress-crack width relation. The deflection of the specimen measured on the specimen itself, was used as the control parameter. Using this parameter it was possible to continue the test after the maximum load was reached and consequently G_{fI} could be established. In Figure 24, the test arrangement is presented in detail.

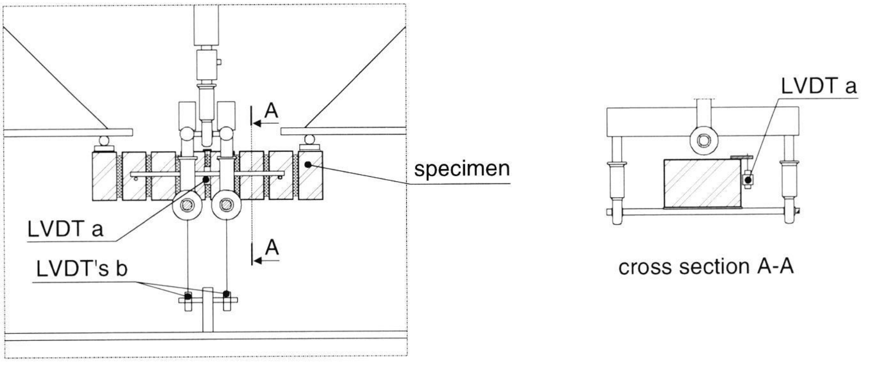

Figure 24 Detailed view of a specimen in the 4-point bending test arrangement

This testing arrangement was used, because it was expected that specimen types, for which it had not been possible to measure post peak behaviour in the tensile test set-up, could be controlled more easily. Although controlling the tests was difficult (steep descending branches), it was possible to establish values for the fracture energy of CS-brick90 masonry with 1:1:6 mortar. This was not achieved in the tensile test series of 1990 and 1993.

LVDT a in Figure 24 was used to control the deformation. It can be observed that the deflection used to control the test was only measured over a part of the span. Using the deflection over the whole span led to uncontrolled failure. LVDT's b were used to measure the distance covered by the load. Although nearly the same measurement could be performed with the internal LVDT of the actuator, LVDT's b were used because of their more accurate measurements. In some tests their signals were suddenly out of their measuring range, probably caused by small physical disturbances. In those cases the internal LVDT of the actuator was used to establish the amount of work done by the specimen. The reliability of those results is discussed in section 2.4.3.

2.4.2 SPECIMENS

The specimens used for the flexural test are presented in Figure 25. The exact dimensions of the stack-bonded prism depended on the brick type used. All stack-bonded prisms made with bricks were 6 layers high.

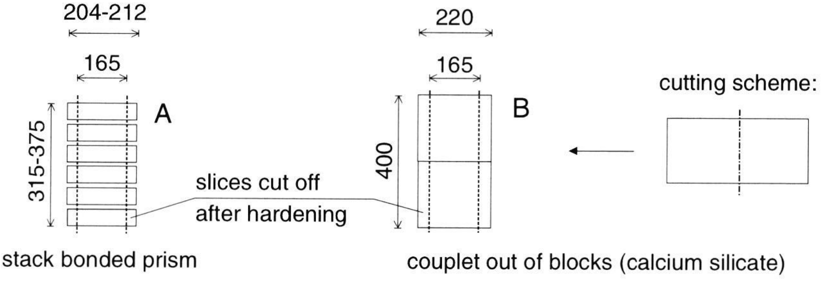

Figure 25 Flexural Specimens

After hardening slices were cut off the specimens to adjust their width to the testing arrangement.

2.4.3 RESULTS AND DISCUSSION

In Figure 26 an example of the measured data in a test is presented.

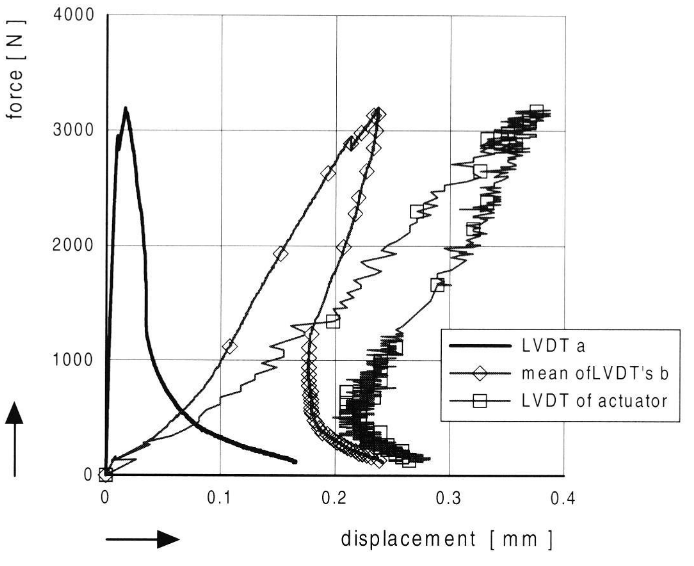

Figure 26 Example of measured date in the flexural test

It can be seen that LVDT a always gave an increasing deformation whereas the displacement measured with LVDT's b and the internal LVDT of the actuator showed snap back behaviour. Uncontrollable failure would have been the result, if the last two signals would have been used as parameters to control the test beyond the peak. It can also be observed that the area under the diagram of LVDT's b and the internal LVDT of the actuator are approximately the same. These areas are equal to the amount of work done.

The average results per series are presented in Table 5.

Table 5 Average results of deformation controlled flexural tests (1995) on small stack bonded prisms (coefficient of variation % between brackets)

masonry		f_{flb}	G_{fI}	$G_{fI;cyl.}$
unit	mortar	[N/mm^2]	[N/m]	[N/m]
sm-RIJ	1:1:6	0.19 (37)	9.1 (41)	8.7 (65)
wc-JO90	1:1:6	0.58 (34)	11.5 (103)	11.7 (77)
CS-brick90	1:1:6	0.23 (41)	3.8 (52)	4.2 (48)
CS-block	TLM	0.39 (35)	7.0 (52)	7.5 (47)

When the average flexural strengths of the series with wc-JO clay bricks with 1:1:6 mortar and CS-blocks with thin layer mortar are compared with the corresponding average tensile bond strength presented in Table 2 on page 22, it can be observed that the flexural strength is 1.5 respectively 1.2 times greater. This difference is well known (see e.g. Baker[1981,[4]], Beuker[1986,[8]], Van der Pluijm[1996[59]]). Generally a factor 1.5 is assumed.

The flexural bond strength f_{fl} was calculated by dividing the ultimate bending moment by the elastic section modulus of the failing cross-section. This way of calculating the flexural strength assumes a fictitious linear stress distribution at failure. The non-linear stress distribution in the cross section at ultimate load is schematically presented in Figure 27 with the bold solid line.

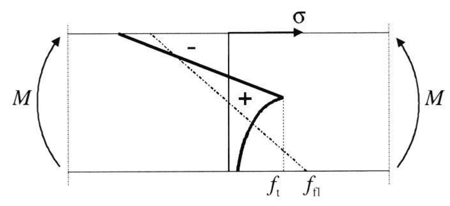

Figure 27 Non-linear stress distribution (solid line) due to bending and the fictitious elastic distribution (dashed line) at the maximum load level

These differences between the non-linear stress distribution in a bending test at failure and the assumed linear stress distribution, explain the difference between the tensile and flexural strength. Numerical assessments can be found in Van der Pluijm[1992,[47], 1995,[53]] and Lourenço[1997,[37]]. Because the non-linear redistribution of stresses, as sketched in Figure 27, is closely related to the height and shape of the cross section, stiffness, tensile strength and post peak behaviour, the flexural strength cannot be regarded as a material property, but must in principle be considered as a structural property. The factor 1.5 generally used, must therefore be seen as crude approximation.

2.5 COMPARISON BETWEEN THE FRACTURE ENERGY DETERMINED IN TENSION AND FLEXURE

The fracture energy of the wc-JO90 bricks + 1:1:6 and of CS-block95 + TLM series determined in the tensile and flexural tests can be compared, because the specimens for both test arrangements were made simultaneously with the same mortar batches. Comparing the values in Table 2 and Table 5, it can be observed that the fracture energy determined with the flexural tests is 2 times higher for the CS-block masonry and 3 times higher for the JO clay brick masonry in the flexural tests than in the tensile tests. This difference can partly be explained with the shape of the bonding surface. As has been shown, a ratio = 1.7 can be expected between the values of couplets and walls. From the bonding surface of the failed flexural specimens, it could be observed that this phenomenon played a role. Because two slices on the head sides of the flexural specimens were cut off, the bonding surface of the clay brick flexural specimens was practically the same as that suggested for a wall in Figure 19. An example is shown in Figure 28.

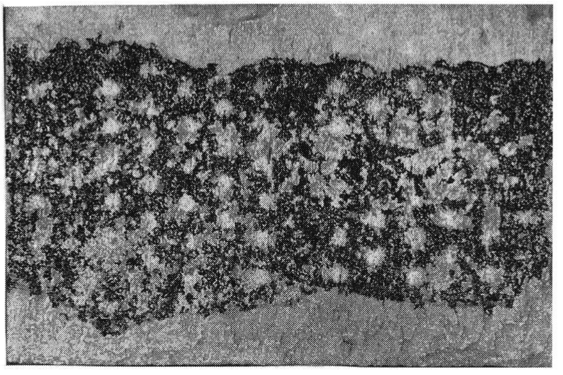

Figure 28 Example of the bonding surface of a cross section of a sm-RIJ specimen after failure (the dark area in the middle corresponds with the actual bonding area)

Although this phenomenon could also be observed for the bonding surfaces of calcium silicate specimens, it was less obvious there.
The determination of G_{fI} is sensitive for the length of the tail as shown by Hordijk[1992,[26]]. To assure an equal determination procedure for tensile and flexural specimens, Hordijk took the average maximum deformation in cracks of his tensile tests as the upper limit for the crack width in the middle of the flexural specimen when calculating the amount of work (see Figure 29).

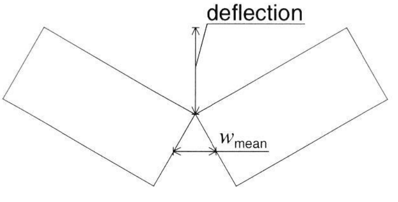

Figure 29 Determination of the mean crack width in a bending test as a result of the deflection, assuming rigid body movements of both parts of the specimen

Of course, assuming rigid non-deformed parts is only valid in the tail of a diagram where the bending deformations are nearly vanished. Using the upper limit of the crack width from the tensile tests, Hordijk found a good agreement between tensile and flexural tests. Analysing the tests here in the same way showed that the mean crack width in the bending tests at the end of the force-crack width diagram was somewhat

greater than the average crack width at the end of a tensile test. However, this phenomenon id not play a role in the differences found here.
An other cause for differences between the amounts of dissipated crack energy might be friction. When it is assumed that the friction coefficient in the outer bearings was 10% and the displacement of the bearings were calculated on the basis of Figure 29, the fracture energy would have been 7% less for the masonry with wc-JO90 bricks and 3% for the masonry with CS-block95.
It was concluded that the gap between the fracture energy determined in tension and in flexure could not totally be explained, but the actual bonding area played an important role.

2.6 Concluding Remarks

Although the amount of test data has been increased considerably within the scope of the research at hand, relations between quantities are still diffuse. The behaviour in tension is just as the bond strength, influenced by a great number of parameters that play a role prior to bricklaying and during hardening. The influence of each of them is difficult to understand and it is not clear whether all parameters are identified or not. Controlling all the parameters is impossible with the state-of-the art knowledge. A number of them are inherently connected to the units and mortar used, and these components can be combined in many ways. This will remain a natural and almost unmanageable theme. Nevertheless, it proved possible to model the non-linear behaviour of the mortar-joint + bond interface and units reasonably well.
It is advised that the sensitivity of calculation results is established for variation of stiffness, fracture energy and bond strength because of the ‘natural’ large scatter of bond properties of masonry. An example of such an analysis was presented section 2.3.6. Another example, taking the scatter via a stochastical approach into account, is presented in section 6.3.
The effect of the actual bonding area should be taken into account. Therefore, the experimental data obtained wih the experiments on small tensile specimen should be increased when applied in walls.

3. SHEAR BEHAVIOUR OF JOINTS

This chapter gives an overview of the behaviour of joints under combined shear and normal tension or compression. To establish the behaviour, test arrangements were developed in which so-called couplets were tested in a deformation-controlled manner. Different loading and control methods were used, but most tests were carried out under constant normal stress and increasing shear deformation measured over the joint. Unique tests under combined normal tension and shear were carried out, making possible the establishment of a complete failure envelope for the joint+interface.

Nearly all properties established to describe the shear behaviour of joint+interface proved to be dependent on the normal stress. These properties included shear strength, mode II fracture energy, cohesion softening and dilatancy. To describe cohesion softening, formulae originally developed for tension softening could be used. A formula describing dilatancy as function of the shear displacement is proposed.

Keywords: shear, bond interface, mortar-joints, (post peak) behaviour, failure envelope, mode II fracture energy, dilatancy behaviour

3.1 INTRODUCTION

In this chapter experiments to establish the strength and behaviour of bed joints + interfaces, loaded by a combined normal force perpendicular to the bed joint plane and shear force parallel to the bed joint plane, are presented and analysed. These two directions will be referred to as the normal and the shear direction. The tests were carried out to be able to describe the behaviour of the joint+interface at the meso level for reasons explained in section 1.2. To study the strength and behaviour of the joint+interface, two different test arrangements were used. One was developed at TNO within the framework of the Dutch structural masonry research program and it only allowed for shear tests under constant normal pre-compression. Tests carried out in this set-up formed the experimental basis for interface models that were developed by Lourenço[1996,[38]]. In a newly developed testing arrangement in the Pieter van

Musschenbroek laboratory of the Eindhoven University of Technology tests were carried out under programmable combinations of normal tension and shear.

It must be realised that other types of failure than shear failure of joint+interface can govern shear failure of masonry. The work of Mann and Müller[1977,[39]], Page[1982,[45]] and Ganz et al.[1988,[16]] must be mentioned in this context. Mann and Müller made a distinction between four different failure modes as a function of the normal stress σ, indicated in Figure 30.

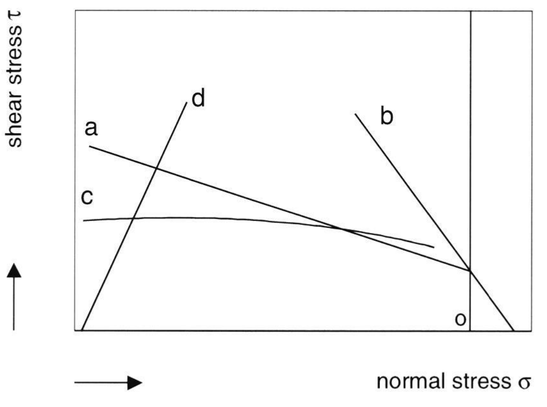

Figure 30 Failure modes for masonry loaded in shear according to Mann and Müller[1977,[39]]

These four failure modes are governed by:
a) bond failure of the interface (cohesion or shear bond strength);
b) tensile bond strength;
c) tensile strength of the units;
d) masonry compressive strength.

The distinction between failure modes a) and b) made by Mann and Müller is somewhat artificial, as they are both bond failures under different loading conditions.

The shear strength was analysed as a function the normal stress on the basis of Coulomb's friction failure criterion (already used by Mann and Müller[1977,[39]] for failure mode a). This 2-parameter criterion reads as follows:

$$\tau_u = c_0 - \tan\varphi \cdot \sigma \qquad (7)$$

τ_u : shear strength of a test;

c_0 : cohesion or shear bond strength, with other words the shear strength at $\sigma = 0$ (f_v in NEN 6790 / f_{vo} in EC6);

φ : angle of internal friction (not necessarily equal to the coefficient of dry friction μ);

From a shear test, carried out with normal pre-compression, a schematic diagram as presented in Figure 31 may be obtained.

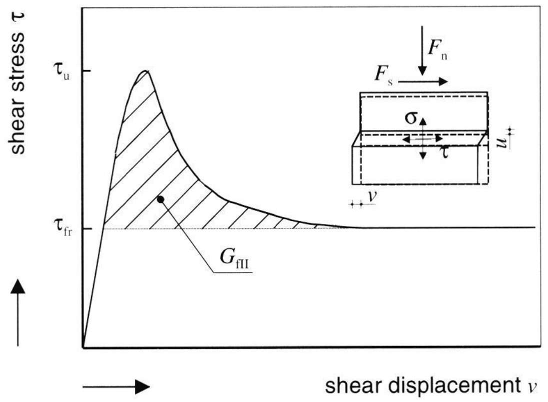

Figure 31 Schematic diagram of deformation (v) controlled shear test under constant normal compression

This behaviour shows a great similarity with the behaviour under tension (compare Figure 1 on page 8) except for the tail that does not fall back to zero, but becomes stable at a certain shear stress level. This level corresponds with the dry friction of two non-bonded surfaces. The descending branch between τ_u and τ_{fr} can be seen as softening of the cohesion. The mode II fracture energy G_{fII} was used by Lourenço[1996,[38]] to define the descending branch beyond the peak via softening of the cohesion in eq. (7) by replacing c_o with the following equation:

$$c_r = c_o e^{-\frac{c_o}{G_{fII}} v_{pl}} \tag{8}$$

c_r : residual cohesion;

c_o : initial cohesion;

G_{fII} : mode II fracture energy (see Figure 31);

v_{pl} : plastic shear displacement (defined in section 3.4).

Describing the residual cohesion with eq. (8) in eq. (7) while the shear stresses reduce to τ_{fr}, implies that a gap will arise when $\tan\varphi$ is not equal tot the friction coefficient. This can be observed in Figure 32 where Figure 31 is repeated for different normal compression stress levels.

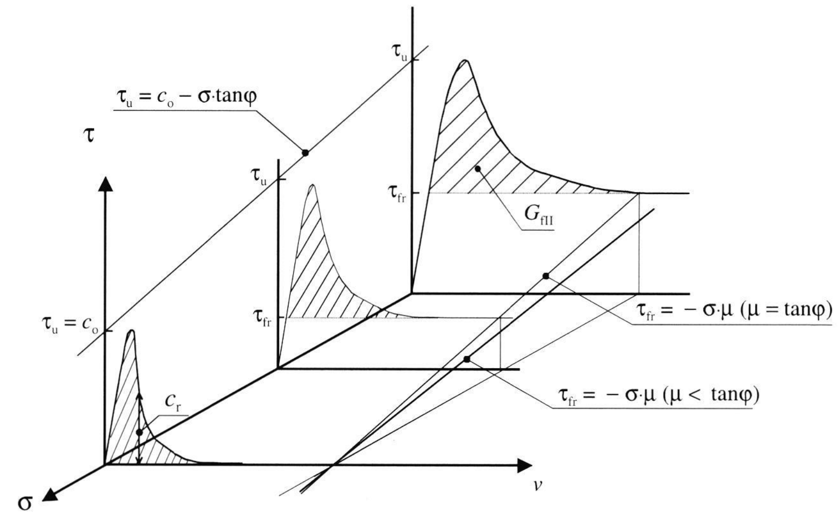

Figure 32 Schematic diagram of deformation (v) controlled shear tests under 3 different constant normal compression stress levels

To overcome this problem, Lourenço[1996,[38]] also implemented a linear softening of $\tan\varphi$ coupled to the cohesion.

Van Zijl[1996,[87]] explored the usability of eq. (1) by changing the mode I parameters in corresponding mode II parameters, resulting in the following formulae:

$$\frac{c_r}{c_o} = \left(1 + \left(c_1 \frac{v_{pl}}{v_{nonlin}}\right)^3\right) e^{-c_2 \frac{v_{pl}}{v_{nonlin}}} - \frac{v_{pl}}{v_{nonlin}} (1 + c_1^3) e^{-c_2} \tag{9}$$

v_{nonlin} : shear displacement over which the cohesion reduces to zero;
c_1, c_2 : constants, see eq. (1).
Both equations will be discussed in section 3.10.

An important phenomenon in a shear test as indicated in Figure 31, is the occurrence of a normal displacement u perpendicular to the imposed shear displacement v that occurs at and beyond the peak. This phenomenon is generally denoted with dilatancy, and the ratio between the normal and shear displacements as the tangent of the dilatancy angle. Physically, it is the result of a crack surface that is not perfectly smooth so shearing must go hand in hand with an uplift. Of course, the maximum uplift is limited and related to the roughness of the crack, and in case of bond failure the surface of the unit will be an important factor. An example of the importance of dilatancy in modelling the behaviour of masonry when bed joints are failing due to shear, is shown by Van Zijl et al.[1997,[88]] in Figure 33.

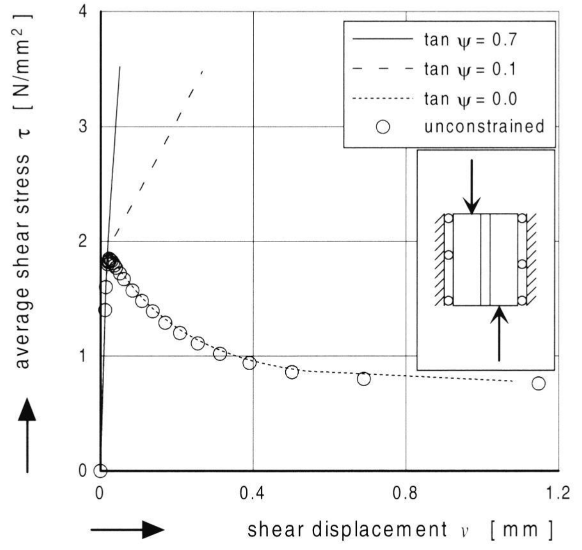

Figure 33 Influence of dilatancy angle (tan ψ) on the shear behaviour of confined masonry in numerical simulations (after Van Zijl et al.[1997,[88]])

In Figure 33 the results of shearing of two brick-type units and one joint (a couplet specimen) that are confined in the normal direction are presented. It can be seen that a constant value for the dilatancy angle greater than zero leads to infinite shear strength of a joint in case of perfectly constrained masonry in the normal direction, showing that a correct formulation of the dilatancy is imperative.

In the next section the test arrangements are presented. After that, the specimens are described and the way the test data was processed. In the sections thereafter results are presented and discussed.
A detailed description of shear tests can be found in Van der Pluijm[1992,[47]&1993,[49]] for tests carried out up to 1993 in the TNO test-arrangement and in Van der Pluijm[1998,[62]] for the tests carried out in 1998 in the arrangement of the Eindhoven University of Technology.

3.2 JOINT SHEAR TESTING ARRANGEMENTS

Introducing a pure shear stress distribution in a joint is nearly impossible. This problem was also looked at by Hofmann et al.[1990,[24]] who considered several test arrangements by means of linear FE calculations (see Figure 34).

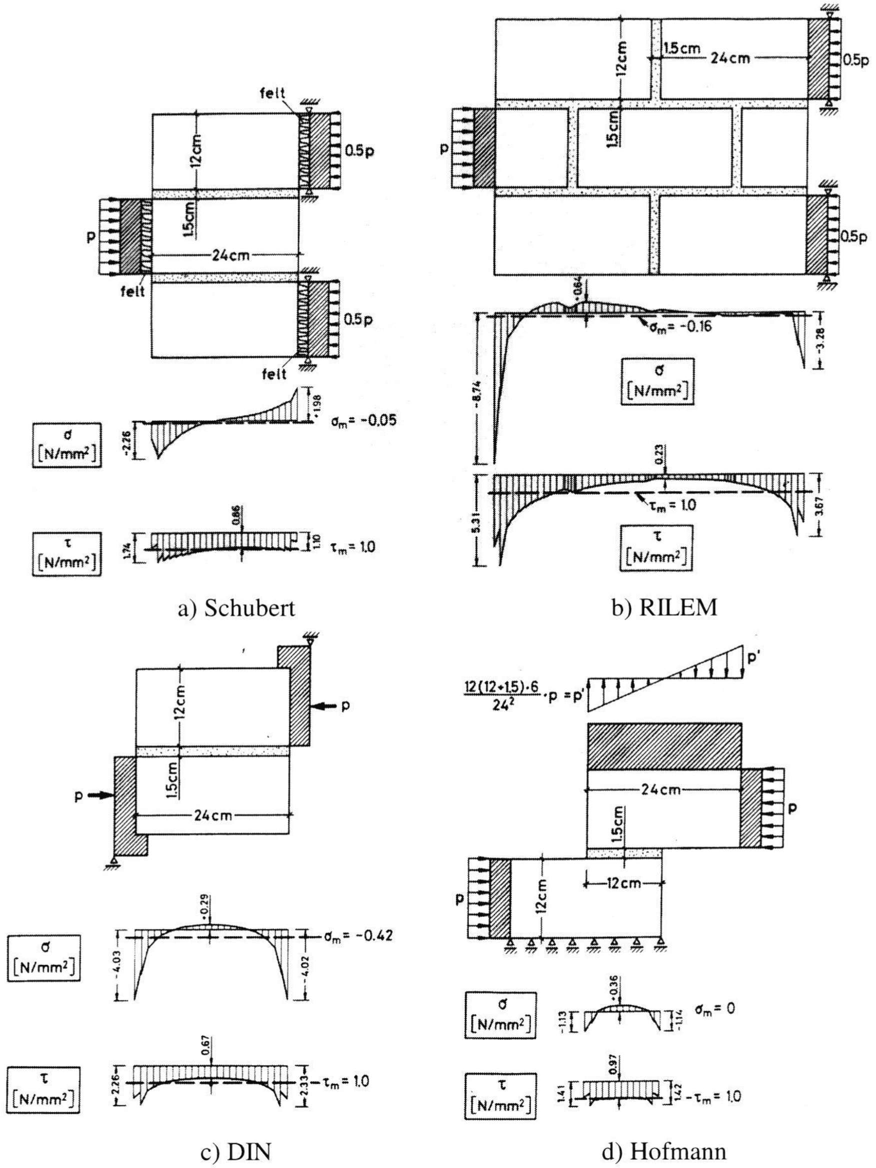

Figure 34 Stress distributions in joint shear testing arrangements (after Hofmann et al.[1990,[24]])

It can be observed that still large peak shear and/or normal stresses occur in all the arrangements. Although the arrangement of Hofmann (Figure 34d) shows a nearly perfect shear stress distribution, relatively high peak stresses perpendicular to the bed joint occur. Furthermore, the complicated loading arrangement and the specially shaped specimen do not make it very attractive. Within the framework of the Dutch structural masonry research program a new arrangement was developed at TNO and introduced in Van der Pluijm[1992,[47]]. The main part of the test rig is shown in Figure 35.

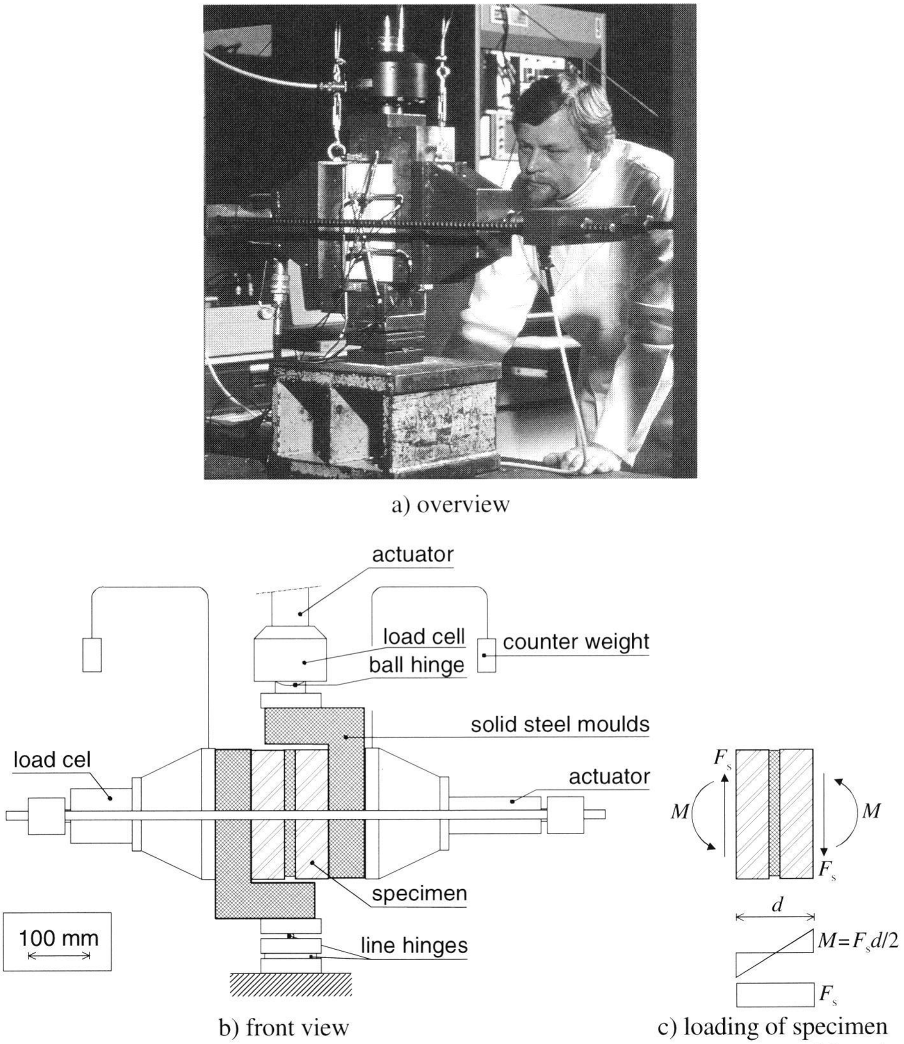

a) overview

b) front view

c) loading of specimen (without normal force)

Figure 35 TNO shear test arrangement (a, b) and loading on the specimen (c).

The basic idea of the test method is that moments and shear forces can lead to a pure shear load in the middle of the specimen if $M = F_s.d/2$. In the middle of the joint the bending moment is zero (see Figure 35c). By means of two L-shaped steel moulds an axial load is transformed into the desired moments M and shear forces F_s. This is an important difference with similar tests, where the load F_s is applied directly on a plane of the specimen perpendicular to the shear direction. With the test arrangement of Figure 35, the resulting shear stress distribution that is found with a linear FE-calculation and shown in Figure 36, was assumed to be satisfactory.

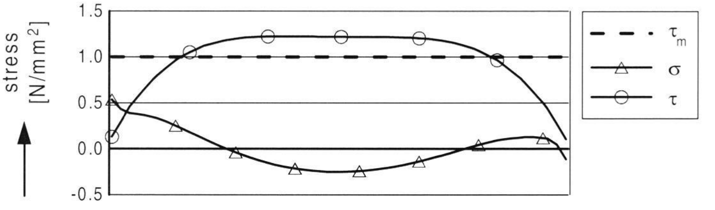

Figure 36 Shear (τ) and normal (σ) stress distribution in the joint of a specimen.

Still some normal stresses occur, but their magnitude is limited compared with the shear stresses. The magnitude of the normal stresses solely depends on the ratio between the stiffness of the specimen and the L-shaped steel moulds. The dimensions of the L-shaped moulds were arbitrarily chosen in such a way that the normal stresses at most 50% of the shear stresses for a stiffness of the units equal to 15000 N/mm^2.

The significance of linear elastic FE calculations concerning the stress distribution in a specimen as such, is limited. Although these assessments give a good impression in the linear phase, (micro) cracking may alter the stress distribution. This is especially true for the high peak stresses shown in Figure 34. So these arrangements may perform better than the linear elastic stress distribution suggests, especially when stress redistribution is possible after the first micro cracking has occurred. In section 3.7 this aspect is addressed further.

In the introduction of this chapter it was already said that the arrangement of Figure 35 does not allow for a combination of normal tension and shear. The idea of the TNO test-arrangement was further developed in the arrangement, schematically drawn in Figure 37. A couplet specimen is glued between the upper and bottom platen which both are connected to their own parallelogram-mechanism. The arrangement developed in the Pieter van Musschenbroek laboratory of Eindhoven University of Technology, makes it possible to move both platens independently of each other: the bottom platen in the shear direction and the upper platen in the normal direction. As the platens are kept parallel, they form restraints at both sides of the specimens. As a result, shear movement of the bottom platen leads to a pure shear force in the centre of the specimen comparable with the TNO-arrangement.

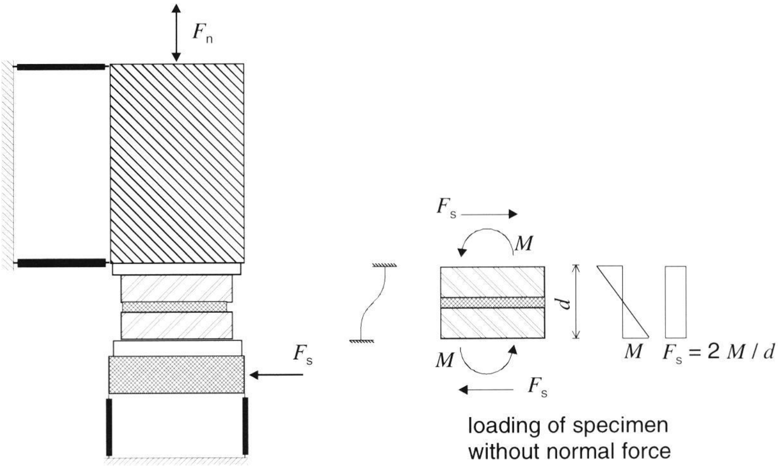

Figure 37 Schematic view of bi-axial arrangement in the Pieter van Musschenbroek laboratory

Some photos of the arrangement are presented in Figure 38.

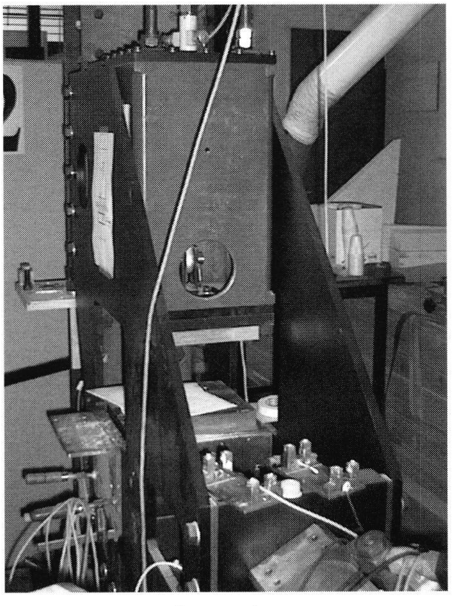

a) overview

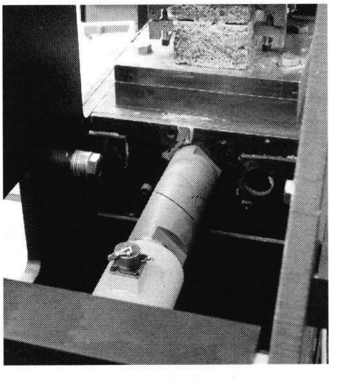

b) special rod

Figure 38 Photos of bi-axial test arrangement

A detailed drawing of the arrangement is presented in Figure 39.

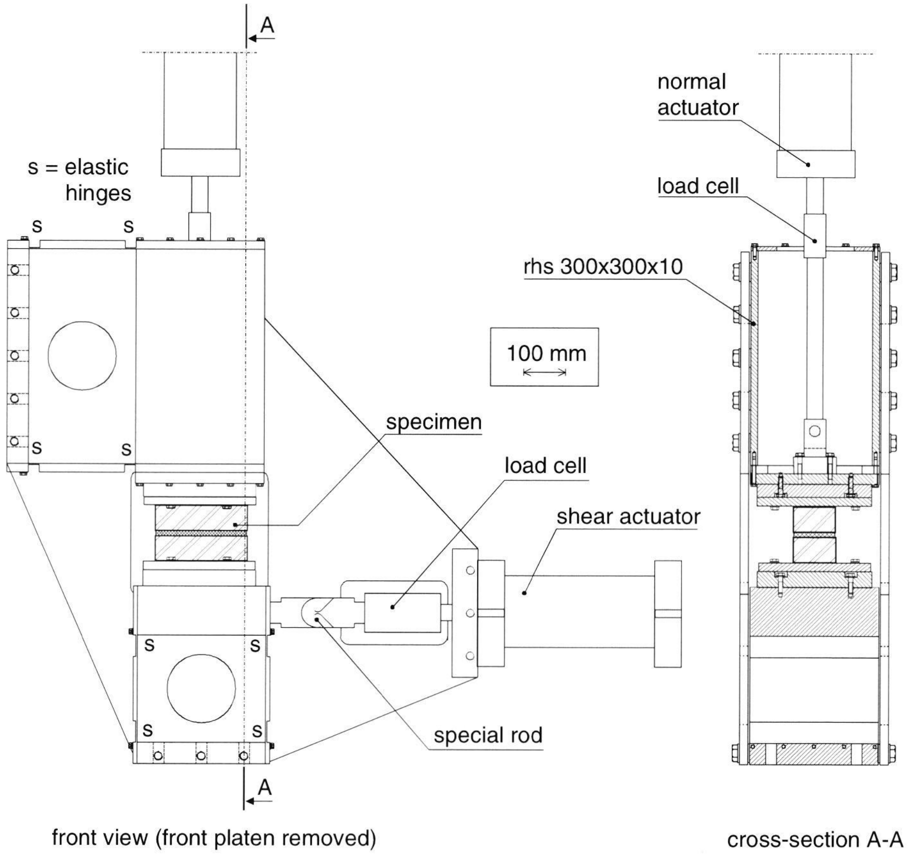

Figure 39 Bi-axial test arrangement (without surrounding HE300B frame)

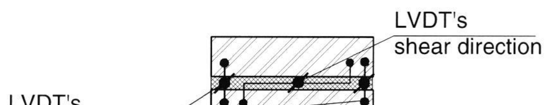

Figure 40 LVDT's on a specimen used to measure and/or control the displacements during a test

The displacements were measured on the front- and on the backside of a specimen. So four normal and two shear displacements were measured.
In Eindhoven, the LVDT's were first mounted in brass brackets and then attached to the specimen (see Figure 41a). To be sure that the LVDT's used to measure the normal displacements were lined up perpendicular to the shear movement, a special mounting procedure was followed. First the brass brackets (with LVDT's) were mounted to a steel

backup plate with little bolts (Figure 41b). To ensure exact positioning of the brackets relatively to each other, davel pins, mounted on the steel plate, fitted into holes of the brackets. As can be seen, the head of the LVDT for normal displacements rests against a little steel platen attached to the opposite bracket. The surface of this steel platen was polished flat and oriented exactly parallel to the shear LVDT.
The screws in the brackets that can be seen in Figure 41b were glued on the specimen while the brackets were mounted on the steel plate. After hardening of the glue, the steel platen is removed and exactly lined up LVDT's are obtained.
At TNO a similar procedure was followed.

a) brass brackets with LVDT's on specimen

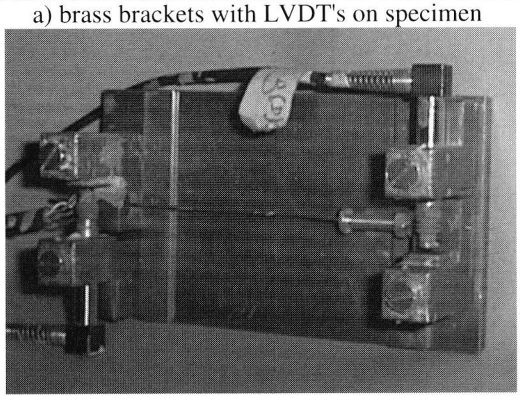

b) brass brackets mounted on backup plate

Figure 41 Detailed view of brass brackets and steel plate, used to mount the LVDT's onto the specimen in the arrangement of EUT

In the TNO arrangement, the shear displacement was controlled using the two LVDT's mounted in the shear direction on the specimen. The normal compression force was applied prior to testing and was kept constant by a pressure accumulator, so no electronic control equipment was necessary in the normal direction, despite of the displacements occurring in this direction. After the normal force was applied, the shear force was controlled by an imposed shear displacement via the shear LVDT's on the specimen.

In test arrangement in Eindhoven, the two actuators were controlled independently of each other. Each jack was controlled via a Schenck S59 Servo-controller by a parameter that followed a static or dynamic command value. The internal generator of the S59 produced command values in time. The parameter itself could be fed by two signals that could be mixed in any proportion using dedicated electronics. In Eindhoven four different control configurations were used. The first two hereunder, were mostly used.

- *Tests under constant normal compression and increasing shear*

In these tests, the normal force was applied first to the specimen and then kept constant. The shear force was controlled by an imposed shear displacement via the shear LVDT's on the specimen.

- *Tests under constant normal tension (inclusive zero tension) and increasing shear*

First, the normal force was applied to the specimen and then kept constant. The shear force was controlled using the response of the LVDT's in normal and in shear direction. Both signals were mixed equally in most tests, however in some tests only 80% of the shear signal was mixed with 100% of the signal in the normal direction. The reason for mixing the signals lies in the necessity of obtaining a signal that can always be increased to follow the command value. At the moment the peak is reached, the normal displacement starts to increase, so they slow down the shear movement at the right moment and make preservation of control over the peak possible. In some tests, beyond the peak, the mixing of the signals resulted in temporarily reversing the shear movement.

- *Tests under constant normal displacement and increasing shear*

Two tests were carried out with a constant normal displacement instead of normal force. In these tests the intended normal force was applied first. Next the control parameter was switched to the LVDT's in the normal direction and this displacement was kept constant. Thereafter, the shear displacement was increased and controlled via the LVDT's in the shear direction. Although one of the two tests started with normal tension, soon compression forces developed in normal direction as a result of the dilatancy (this is a conformation of effect of the dilatancy as was demonstrated theoretically by Van Zijl, see Figure 33). At the moment the compression force reached a level of approximately 25 kN, the control in this direction was switched back to force control and the force was kept constant during the remainder of the test. This was done to avoid damage to the 30 kN load cell used in the vertical direction.

- *Tests under constant shear force and increasing tension*

These tests were controlled in the same manner as the tests under constant normal compression. Now, the shear force was kept constant and in the normal direction the displacement was steadily increased, controlled by the LVDT's in this direction.

In the arrangement in Eindhoven, the process of gluing the specimen to the platens had to be carried out with great care. As the specimens and/or the platens of the test set-up are never exactly plan parallel, it was necessary to glue the specimen in the arrangement itself.

First a specimen was glued on a loose bottom platen. This made central positioning of the specimen on the platen easy. A clean upper platen was bolted to the upper part of the test set-up. Next the specimen with bottom platen was placed in position with glue on its top. Subsequently, the bolts of the bottom platen were screwed on before bringing the upper platen down with the servo controller in force mode. The applied force varied between 200 and 1000 N (max. 0.05 N/mm^2). It was essential to tighten the bolts of the bottom platen before the glue was hardened. If the glue was already hardened, forces might have been put on the specimen resulting in possible damage to the specimen prior to the test.

The glue (brand Plex 7742F + Pleximon 801 of Röhm GmbH) was a two-component thermosetting plastic that hardened in approximately 10 minutes. It showed to be a very good adhesive between steel and the masonry units. A disadvantage of this glue is that it shrunk during hardening. For this reason the upper platen in Eindhoven was placed on the specimen with force control. However if the top and bottom surface of a specimen did not run parallel enough (e.g. 2 mm difference over the specimen), eccentric normal forces were put on the specimen due to uneven shrinkage of the glue, that could led to bond failure of the specimen. The resulting cracks were never visible, but from a very low shear stiffness and strength of the specimen that occurred in some tests, it was obvious that cracking had occurred prior to testing.

In the TNO-arrangement, the specimens were glued between the L-shaped moulds using the same type of adhesive, but the arrangement allowed for non-parallelism.

More details about the TNO-arrangement can be found in Van der Pluijm[1992,[48]] and about the arrangement in the Pieter van Musschenbroek laboratory in Van der Pluijm[1998,[62]].

3.3 MATERIALS AND SPECIMENS

In 1992, tests were carried out in the TNO-arrangement with yellow wire cut clay bricks (coded wc-JO90), red soft mud clay bricks (coded VE) and calcium silicate bricks (CS-brick90) in combination with two mortar compositions: 1:2:9 and 1:½:4½ (cement:lime:sand ratio by volume).
In 1993, additional series were carried out in the TNO-arrangement with calcium silicate bricks (CS-brick93), parts of calcium silicate elements and concrete bricks and a very strong wire cut clay brick, in combination with factory made mortars designed for that type of bricks. These tests included specimens with thin layer joints.
The test series of 1992 and 1993 were carried out within the framework of the Dutch structural masonry research program.

In 1998, tests in the bi-axial test arrangement were carried out with masonry consisting of wired cut clay bricks (wc-JO96) with a GPM 1:1:6 designed in the laboratory and masonry consisting of calcium silicate blocks (CS-block96) with TLM.

A characterisation of the materials including normative references is presented in Appendix A 'Materials', including the pre-treatments of units and curing regimes that were followed throughout the years.

The masonry shear specimens were always couplets consisting of two (parts of) units and a mortar joint. They are shown in Figure 42.

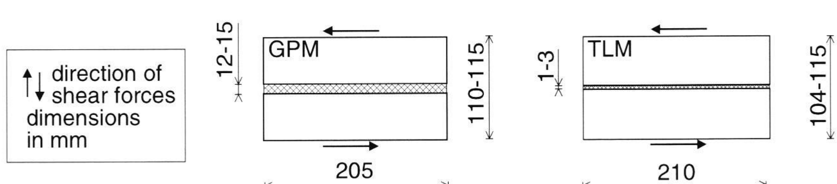

Figure 42 Shear masonry specimens made with GPM and TLM (exact dimensions depend upon unit size)

The exact dimensions of the masonry specimens depended on units used. In one series (hswc-JOK + TLM) notches were made in the joint to ensure failure in the interface or joint.

The age of the specimen at time of testing was between 117 and 138 days for the series of 1992, between 92 and 133 days for the wc-JO96 + 1:1:6 series and between 442 and 505 days for the CS-block96 + TLM series. The very long period between fabrication and testing of the specimens was caused by the considerable time needed to improve the bi-axial arrangement making controlled tests possible.
When CS-blocks were used, brick sized parts were sawn out of the blocks in such a way that the original bond surfaces were preserved for the joint of a specimen.
Accompanying tensile specimens were made simultaneously with the shear specimens from the same mortar batches. Their results were already presented in chapter 2.

3.4 PROCESSING OF TEST DATA

An overview of the quantities analysed of a single test, is presented in the schematic shear stress-displacement diagram in Figure 43.

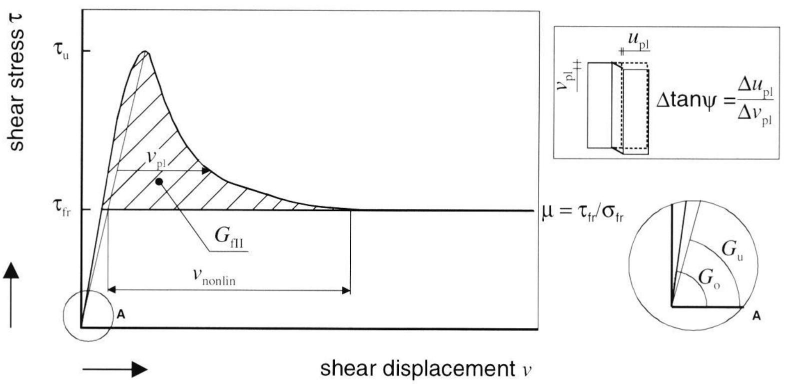

Figure 43 Schematic diagram of deformation (v) controlled shear test with quantities analysed

The initial shear stiffness G_o and the secant stiffness at peak load G_u were derived in the same manner as described in section 2.3.2 for the modulus of elasticity in tension. Additionally, values for Poisson's ratio of the units had to be known to calculate the shear stiffness of a unit on the basis of its modulus of elasticity. In all cases it was taken equal to 0.15 This value was based on compression tests carried out by Vermeltfoort[1991,[79]], using units from the same batches as used here, but not on the data Vermeltfoort presented. In his tests, Vermeltfoort found that at low stress levels lateral displacements were to small to measure. Because of the relatively low stress levels in the shear tests compared with the compression tests of Vermeltfoort, a low value for the Poisson's ratio was chosen.

Of course the same considerations as in section 2.3.2 concerning the subtraction of the deformations in the unit within the gauge length and the joint thickness, also played a role in determining the joint shear stiffness.

The shear and normal stress were simply derived by dividing the shear and normal force by the cross sectional area. The shear strength of a test was defined as the maximum measured load divided by the cross-sectional area of the specimen.
The shear strength was also analysed as a function the normal stress on the basis of Coulomb's friction failure criterion, eq. (7). If the Coulomb criterion is valid, the cohesion can be established by linear regression through the failure points of test (carried out with normal compression) in the σ-τ plane as the intersection with the τ-axis (indicated with c_o (lin. regr.)). The test-series carried out in the arrangement in the Pieter van Musschenbroek laboratory offered the opportunity to a direct determination of the cohesion calculated as the mean of the shear strength of tests carried out with zero pre-compression (indicated with c_o (σ=0)). For the series carried out in Eindhoven both methods for determining the cohesion were followed. The tensile bond strength was established with the tensile tests and compared with the shear bond strength.

The dry friction coefficient was only analysed for those tests carried out with constant normal pre-compression. It was calculated by dividing the mean shear stress with the mean normal stress in the last twenty measurements in the horizontal part of the tail of the diagram as presented in Figure 43. The CV of the twenty τ-values was typical 0.5% or less.

Deformations that occurred beyond the peak, additional to the elastic deformations, are indicated as plastic displacements with v_{pl} and u_{pl}. The exact definition of v_{pl} was given in Figure 43. The normal displacement perpendicular to the bed joint u_{pl} was defined in exactly the same way. These definitions closely correspond with the approach of Hillerborg as explained in chapter 2.
The dilatancy angle ψ defined by:

$$\Delta \tan \psi = \frac{\Delta u_{\text{pl}}}{\Delta v_{\text{pl}}} \qquad (10)$$

was analysed incrementally, designated by Δ for tests carried out with pre-compression. Under normal tension, the problem arose that it is no longer possible to attribute the normal displacement solely to the dilatancy caused by the shear movement. In that case the normal displacement is also a result of (micro)cracking in the direction of tension. Therefore the dilatancy cannot be determined for tests with pre-tension.

In Figure 33, we have seen that the calculated behaviour is very sensitive for the correct modelling of the dilatancy. From its physical background, as discussed in section 3.1, it can be expected that $\Delta\tan\psi$ will show some kind of softening behaviour.
Generally $\Delta\tan\psi$ was determined as the slope of the best fit through an interval with a fixed length.
For the series of 1992 and 1993 at least five successive measurements were used (the number of measurements were constant in time), with an arbitrary overlap of 33%. In the first part of the descending branch relatively few measurements were available in relation to the changes that occurred, resulting in a large variation of the successively calculated values for $\Delta\tan\psi$. Therefore the initial value of $\Delta\tan\psi$ was calculated as the slope of the measurements for which v_{pl} was not greater than 0.05 mm.
In the series of 1998 a different procedure was followed. The length of the interval was taken equal to 1/20 of the maximum plastic shear displacement in a test, because the maximum plastic shear displacement varied a lot. In addition, such an interval should contain at least 25 measurements to obtain a reliable slope ($\Delta\tan\psi$) through the data points. The intervals overlapped at least for 33%.

The mode II fracture energy is defined in Figure 43 as $G_{\text{fII}} = \int \tau \mathrm{d}v$ with the condition that $\tau > \tau_{\text{fr}}$ for tests under normal compression, inclusive zero normal compression, or $\tau > 0$ for tests under normal tension force. To be able to establish the fracture energy the friction level had to be established first.
As explained, it is not possible to attribute the normal displacement solely to the dilatancy for tests carried out with constant normal tension. Due to the interaction between tensile and shear micro-cracking, it was not possible to make a clear distinction between normal displacements due to dilatancy and due to cracking in the normal direction for tests carried out under combined tension and shear. This problem is addressed further in section 3.11.

3.5 General Observations

In a lot of shear tests carried out with normal compression, bond failure in the interface occurred. Bond failure combined with tensile failure of the units (near the heads of the units) was also an important mechanism. In the series of 1992-1993, pre-compression levels were as far as possible adapted to achieve bond or mortar failure. However also other failure modes occurred. The different failure modes are presented in Figure 44.

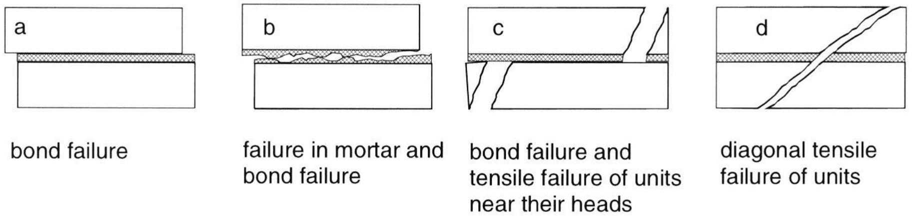

Figure 44 Failure mechanisms that may occur in a shear specimen

Tensile cracks in units (diagonally through the specimen, see Figure 44d) occurred sometimes, especially in the series with the sm-VE brick with GPM 1:½:4½ mortar carried out in 1992. In the sm-VE brick a shallow recess was present. It was believed that a compression strut was formed in the mortar towards the recess, resulting in a higher strength of the joint+interface. In some tests, corners of units cracked at the peak resulting in a reduced shear bond failure surface (see Figure 44c). A combined normal and shear stress state may result in principal tensile stresses that are greater than the tensile strength of the unit (see Figure 30 on page 40). Apart from the principal tensile stress occurring resulting from the applied average stresses σ and τ, additional tensile stresses occur due to:

- the bending moment that increases from the middle to its maximum value over the thickness of the unit and causes extra tensile stresses (see Figure 35b);
- the linear stress distribution in the test arrangement (see Figure 36).

The diagonal crack is caused by the principal tensile stress while the corner cracks originate from the additional tensile stresses. Of course the principal tensile stress also influences this type of cracking. The test results coming from specimens with diagonal cracks were considered as a lower bound for bond failure and used in analysing the strength. Including these results led to a more consistent image in relation to Coulomb's friction criterion. The tests where cracking of the unit near the headers of the units occurred, were analysed as if the units were not cracked. This type of cracking occurred in the wc-JO90 + 1:½:4½ series carried out in 1992, in the series CS-brick93 + fmGPM and in the series MBI93 + fmGPM both carried out in 1993. In 1993 test series were carried out with unit-mortar combinations in which the mortar was always factory made and suited for the brick type used. Those mortars included thin layer mortars. The combinations of 1993 were also tested in tension. Due to relatively high bond strength in some series, the tests were not as successful as the series of 1992. Only few controlled (in the sense that it was possible to continue the test deformation controlled until a constant shear stress level (dry friction) was reached) test results were obtained. The hswc-JOK + TLM series with a very high bond strength failed always uncontrolled. In most cases, however, it was possible to obtain measurements in the horizontal tail.

In the series of 1998 carried out in the Pieter van Musschenbroek laboratory, shear bond failure occurred in the wc-JO96 bricks + GPM series. In the CS-blocks + TLM series often (partly) failure in the mortar joint occurred.

An example of a test series with shear bond failure carried out under a combination of shear and normal compression is presented in Figure 45.

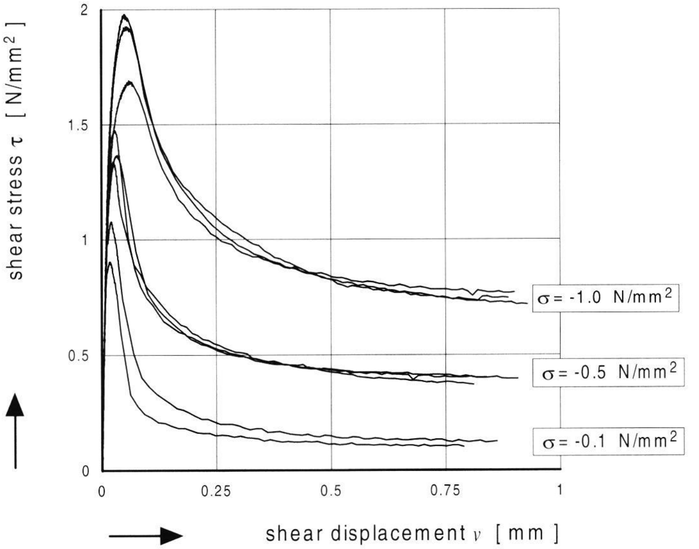

Figure 45 Example of τ-v diagrams of a test series under shear and compression (wc-JO90 + 1:2:9 mortar, 1992)

From Figure 45 some important phenomena can be observed.

- As expected, the strength and friction level were dependent on the compression stress level.
- The scatter of strength values obtained at the same level of pre-compression was small for the presented series. If the results of all test series are considered in this way, the average CV of the shear strength per pre-compression level was 12% and 25% per pre-tension level. The CV for the test with pre-compression is significantly less than with the tests with pre-tension. The CV of 25% is in line with CV's normally found for the tensile or flexural bond strength.
- The descending branch after the peak becomes less steep with increasing pre-compression. Consequently the fracture energy also increases with the level of pre-compression.

In the coming sections the results will be discussed in more detail.

3.6 SHEAR STIFFNESS

In chapter 2 it was discussed that the modulus of elasticity of the joint+interface was low compared to values obtained in compression tests. The shear moduli obtained in 1992 corresponded reasonably well with the stiffness values obtained in compression by Vermeltfoort[1992,[81]], although these values in compression and shear were obtained with different series of specimens making the comparison questionable. If non-bonded contact zones are responsible for the difference between tension and compression, it may be expected that these zones interact in shear tests carried out with pre-compression. Because of the agreement between the stiffness obtained in compression and in shear, it was concluded that these zones also played a role in the shear tests. Apart from the doubtful comparison, the magnitude of the shear moduli themselves indicates that they are significantly greater than the stiffness values obtained in tension. Results of the series of 1997 made a direct comparison between stiffness values obtained in tension and shear possible. A comparison could only be made for the clay brick masonry with GPM. The obtained results for the CS-block96 + TLM series were not reliable for reasons indicated in section 2.3.2.

Table 6 Comparison between average stiffness moduli obtained in shear and in tension

masonry	G_0^j [N/mm^2]	E_0^j [N/mm^2]
wc-JO96 + 1:1:6	4800	5670

If the Poisson's ratio of the mortar is taken equal to 0.2, the modulus of elasticity E_0^j corresponding with G_0^j = 4800 N/mm^2, equals 11520 N/mm^2. Comparing this value with the value following from the tensile test (5670 N/mm^2), confirms the hypothesis concerning non-bonded contact areas that interact in shear tests with pre-compression.

3.7 SHEAR STRENGTH

The obtained strength values depending on the normal pre-compression stress level are presented in Figure 46. Test results obtained under combined tension and shear will be discussed in the next section. In Figure 46, also the linear best fits per series through the points are presented. Because the number of tests per pre-compression level differed, first the mean value per pre-compression level was determined and subsequently the regression lines were determined with the mean values. The correlation coefficients r^2 of the regression lines varied between 0.91 and 1. These coefficients are higher than reported by Van der Pluijm[1993,[49]] for the series of 1992 and 1993 because in [49] the linear regression lines were determined using every single test result.

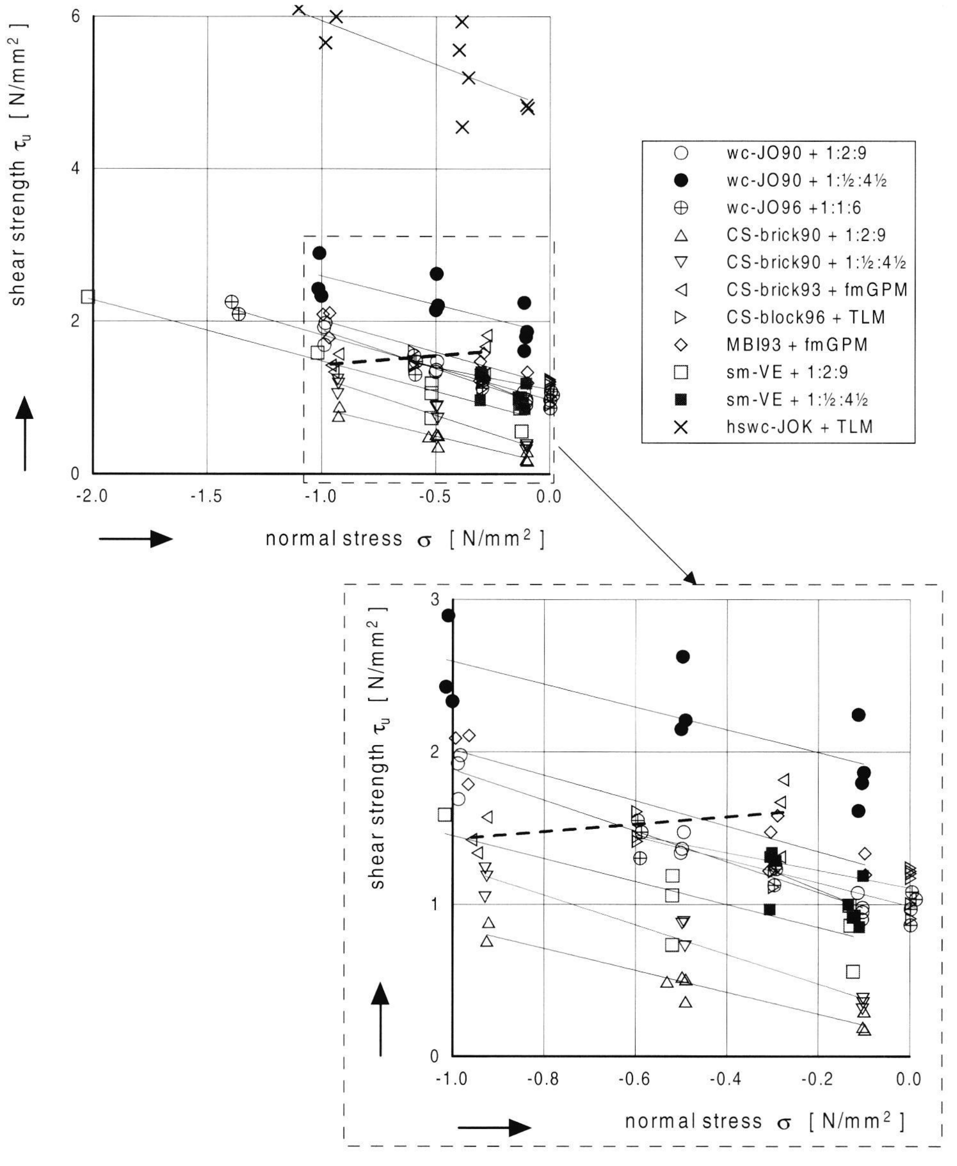

Figure 46 Shear bond strength depending on the normal compression stress (linear regression lines determined with mean values per pre-compression level)

With these linear best fits, the parameters for Coulomb's friction criterion (eq. (7)) were established. The difference with the parameters reported in [49] due to the changed procedure in determining the regression lines, was limited to 1-2%, but the magnitude of the correlation coefficients increased especially those values that were previously low. The obtained parameters are presented in Table 7.

Table 7 Average shear strength parameters and tensile bond strength

masonry unit	masonry mortar	fabric. year	$\tan\varphi$ [-]	c_0 (lin. regr.) [N/mm^2]	r^2 (best fit) [-]	c_0 ($\sigma = 0$) [N/mm^2]	f_{tb} [N/mm^2]
sm-VE	1:2:9	1992	0.81	0.68	0.98	-	0.10 (100) 1)
	1:½:4½		1.15	0.88	-	-	0.35 (48) 1)
wc-JO90	1:2:9		1.01	0.88	1.00	-	0.62 (28) 1)
	1:½:4½		0.73	1.86	0.93	-	1.43 (33) 1)
wc-JO96	1:1:6	1997	0.87	0.96	1.00	0.95	0.43 (26) 2)
hswc-JOK	TLM	1993	1.17	4.76	0.98	-	2.24 (26) 2)
CS-brick90	1:2:9	1992	0.73	0.14	0.99	-	0.02 (72) 1)
	1: ½:4½		0.97	0.28	0.98	-	0.06 (22) 1)
CS-brick93	fmGPM	1993	-	-	-	-	0.66 (48) 2)
CS-block96	TLM	1997	0.61	1.10	0.91	1.13	0.42 (34) 2)
MBI93	fmGPM	1993	0.84	1.17	1.00	-	0.73 (19) 2)

1 tensile test with hinges
2 deformation controlled tensile test

The angle of internal friction $\tan\varphi$ varied between 30° en 50°. The CS-brick93 + fmGPM series did not show an increase of strength with increasing normal pre-compression. This tendency is at variance with all other series. Although a clear cause for this deviation could not be found, cracking of the units near their heads occurred in all tests and might be a cause. Because both series with CS-brick90 and GPM in 1992 did show a normal increase of strength, it was assumed that the series of 1993 was not representative. For this reason a value for the cohesion c_0 is not given for this series in Table 7. It can be observed that two methods of determining the cohesion nearly gave identical results for the two series of 1997. It indicates that it is possible to obtain a good prediction of c_0 with linear regression through test results obtained at different levels of pre-compression.

The angle of internal friction of the CS-block96 + TLM series is relatively low. If the results at zero pre-compression would be ignored its value would increase to 0.94. In some tests at 'zero' pre-compression very small tensile stresses were present. However, their possible influence on the mean value at 'zero' pre-compression is pure speculative and was not observed for the wc-JO96 + 1:1:6 series.

3.8 FAILURE ENVELOPE

In this section the failure envelope of the interface / joint+interface under combined normal and shear force is discussed on the basis of the tests carried out in the arrangement in the Pieter van Musschenbroek laboratory. But first the ratio between the shear and tensile bond strength will be discussed for all series apart from the CS-brick93+fmGPM series.

To be able to compare the shear and tensile bond strength, all shear test series were accompanied by tensile tests on small masonry specimens made simultaneously with the specimen used in the shear tests. The tensile tests in 1992 were conducted force controlled because only the tensile bond strength had to be established. In 1992, the tensile specimens were glued between steel plates that were connected to a test-rig with hinges.

In Figure 47 the ratios between the cohesion and tensile bond strength are presented as a function of the tensile bond strength.

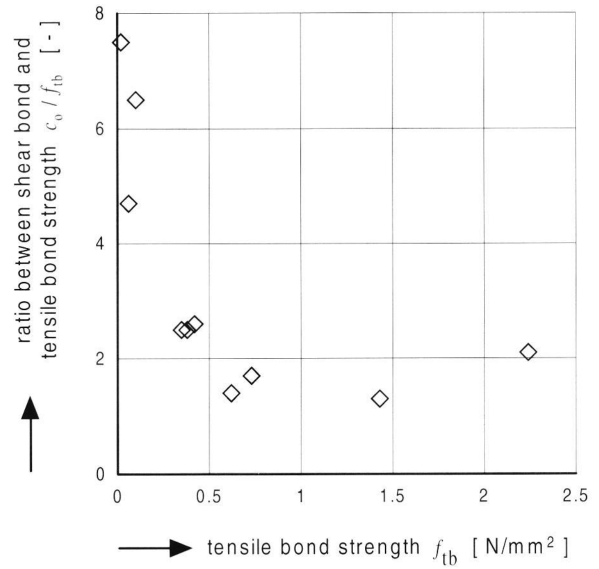

Figure 47 Ratio between the cohesion and tensile bond strength of joints as a function of the tensile bond strength

From Figure 47 and Table 7, it can be seen that the ratio between the cohesion c_0 and the tensile bond strength varies between 1.3 and 7.5. It can also be observed that the high ratios occur when the tensile bond strength is low. In general, two phenomena are expected to play a role viz.:

- the actual bonding surface is expected to be relatively small for low bond strength values which has a negative influence on the measured tensile strength, especially with hinges as boundary conditions (which is the case for the three high ratios exceeding a factor 4);

- the difference between the 'active' parts of the cross sections in the specimen in both type of tests, due the non-bonded contact zones that transfer load in shear tests with pre-compression, but not in the tensile tests.

In the series with the sm-VE brick the forming of a compression strut towards the recess might have played a role.
If the ratios exceeding a factor 4 are ignored, the average ratio equals 2.0 with a standard deviation of 0.55.

In Van der Pluijm[1994,[49]] an experimental assessment of the CEN triplet shear test (with modified load introduction according prEN 1052-3:1995) was carried out without pre-compression. In that research, the ratio between the shear and tensile bond strength was not greater than 0.7, which is low compared with the ratio's presented in Figure 47. This may indicate that peak stresses in the joint of the CEN-triplet test influence the result in a negative way. However, Van Zijl[1996,[88]] demonstrated with non-linear FE calculations, using material models based on the experimental results presented in this chapter, that the TNO-arrangement and the CEN-triplet test according to prEN 1052-3:1995 gave nearly the same result contrary to the experimental results. Discussing this contradiction with Van Zijl, he suggested that the effect of the actual bonding surface might play a role. In the theoretical assessment of the CEN-test the shear transfer is concentrated in the joint at the boundaries of the specimen. If in reality a non-bonded area is present there (and it is very likely that this is the case), it would influence the theoretical result in a negative way. In the latest version of the CEN triplet test, the experiments must be carried out with pre-compression. On the basis of the analyses of Van Zijl, it may be expected that this will improve the result of the CEN-triplet test.

In the following two figures, all points that can be obtained from the tensile and bi-axial tests of the wc-JO96 + 1:1:6 and CS-block96 + TLM series of 1997, are plotted in the σ-τ stress plane. Also mean values for groups of data that were tested with the same constant normal stress are drawn. In case of one group of data obtained with wc-JO96 masonry, the shear stress was constant.

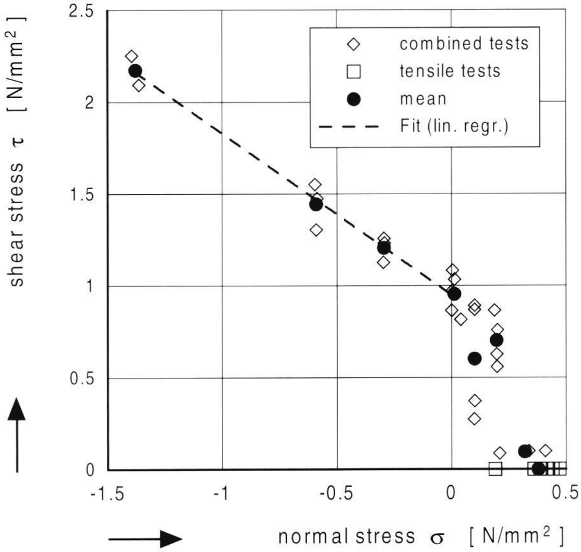

Figure 48 Failure stress points of the wc-JO96 + 1:1:6 series

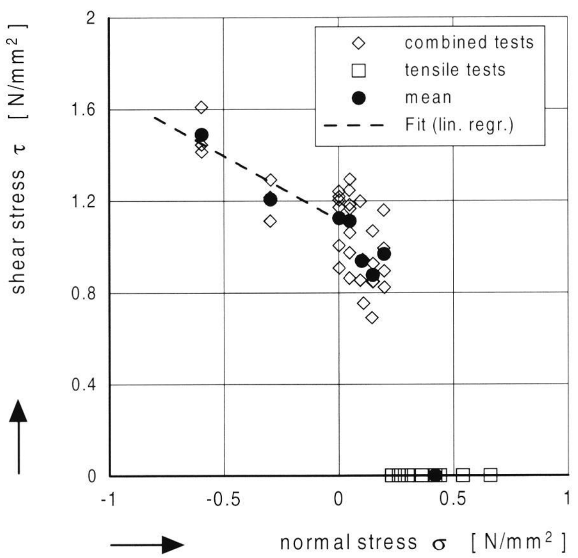

Figure 49 Failure stress points of the CS-block96 + TLM series

The already indicated usual large scatter for tests with normal tension is obvious. In the wc-JO96 + 1:1:6 series, the mean values show a strange 'dip' around $\sigma = 0.1$ N/mm^2.

This dip was caused by two very low values for the shear strength. A probable cause for these low values might be initial tensile stresses in the specimen caused by non-parallelism of the top and bottom side of the specimen in combination with shrinkage of the glue (for further information, see section 3.2). Looking back, it must be concluded that it would have been better if the specimens were ground flat an extra time, prior to gluing them in the test arrangement.

In Figure 50 results of both series are made dimensionless by dividing the normal stress by the tensile strength and the shear stress by the cohesion.

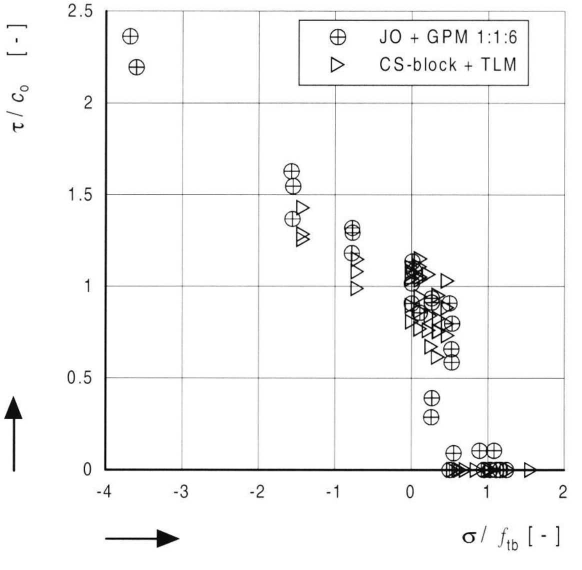

Figure 50 Relative failure stress points of the wc-JO96 + 1:1:6 and CS-block96 + TLM series

In Figure 51 only the mean values are plotted together with failure envelopes used by Rots et al.[1993,[67]] and Lourenço[1994,[35]].

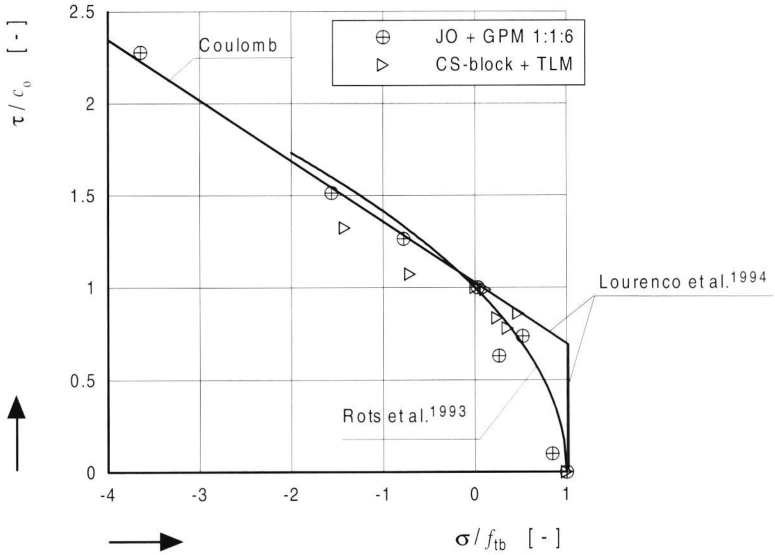

Figure 51 Groups of mean test data with failure envelopes according to Rots et al.[1993,[66]], and Lourenço et al.[1994,[35]]

Observing Figure 51, it may be concluded that the combination of Coulomb's friction with the parabolic fit through de cohesion c and the tensile bond strength f_{tb} is more suitable than Coulomb friction with a tension cut-off at f_{tb}. However, the present amount of test data is far too small to perform a reliable statistical analysis and reject one of the two failure envelopes.

A remark about the parabolic tension cut-off used in combination with Coulomb's friction has to be made: a smooth transition between both criteria is only obtained when:

$$c_o = 2 f_{tb} \tan \varphi \tag{11}$$

When this criteria is used in the context of a plastic formulation, a smooth transition is desirable because in incremental calculation procedures, a new plastic stress state can then be calculated unambiguously from the previous one (see e.g. Lourenço[1996,[38]]).

With $\tan\varphi = 0.75$, which is a reasonable lower bound, eq. (11) becomes:

$$c_o = 1.5 f_{tb} \tag{12}$$

This is somewhat conservative compared with the mean value of 2.0 for the ratio c_o/f_{tb} found in this section, but taking the standard deviation of the ratio c_o/f_{tb} (=0.55) into account, certainly useable.

3.9 DRY FRICTION COEFFICIENT

In Table 8, the mean friction coefficients per brick-mortar type combinations are presented. The choice for calculating the mean per brick-mortar type originated from the idea that in case of bond failure, the brick surface and the sand grading of the mortar mainly determine the structure of the crack surface and consequently the dry friction coefficient.

Table 8 Mean friction coefficient per brick + mortar type combination (CV between brackets)

masonry	μ [-]
sm-VE + GPM	0.98 (23)
wc-JO90 / wc-JO96 + GPM	0.82 (13)
hswc-JOK +TLM	0.84 (10)
CS-brick90 / CS-brick93 + GPM	0.75 (13)
CS-block96 + TLM	0.79 (7)
MBI93 + GPM	0.77 (36)

From Table 8 it can be observed that the sm-VE brick with GPM showed the highest friction coefficient. The recess in the bed face of this brick will have contributed to this result. Furthermore it can be seen that for both types of wired cut clay bricks nearly the same coefficient was determined. As can be expected, the smooth calcium silicate bricks and blocks and concrete bricks showed the lowest coefficient. The higher value for the CS-block96 + TLM series compared with the series with CS-bricks was caused by mortar failure instead of pure bond failure.

In Figure 52 the mean value of shear stress τ_{fr} in the tail of the shear stress-displacement diagram of tests carried out with pre-compression, is plotted against the corresponding mean normal compressive stress. Every marker is the result of one test.

Despite the variety of units and mortars used, the overall picture of test results is rather straightforwardly interpretable.
The dry friction coefficient that can be derived from the linear fit (forced through the origin) equals 0.73, which is rather low compared with the mean values per series as presented in Table 8. This is caused by the limited number of points in Figure 52 for $\sigma \leq -1$ N/mm^2, which influences the direction of the line relatively strong. Ignoring the results below $\sigma \leq -1$ N/mm^2 a friction coefficient of 0.8 is found. This line is also presented in Figure 52.

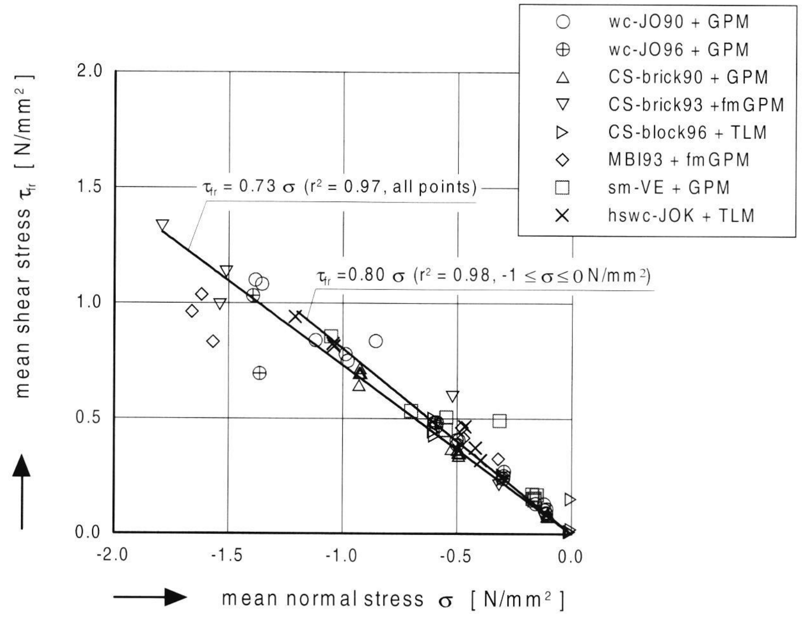

Figure 52 Mean shear and compression stress in the horizontal tail

Overlooking all results, it was concluded that the differences between the brick-mortar combinations used could be ignored and one value for the coefficient of friction μ may be used.

3.10 MODE II FRACTURE ENERGY AND COHESION SOFTENING

The values obtained for the mode II fracture energy are presented in Figure 53 up to Figure 55 for specimens made with clay bricks, CS-units and concrete bricks, as a function of the normal stress. The used data derived from the tests can be found in Appendix B 'Experimental Results', Table 46 up to Table 52.
In Figure 53 results of specimens made with sm-VE and wc-JO90 & 96 clay bricks are presented.

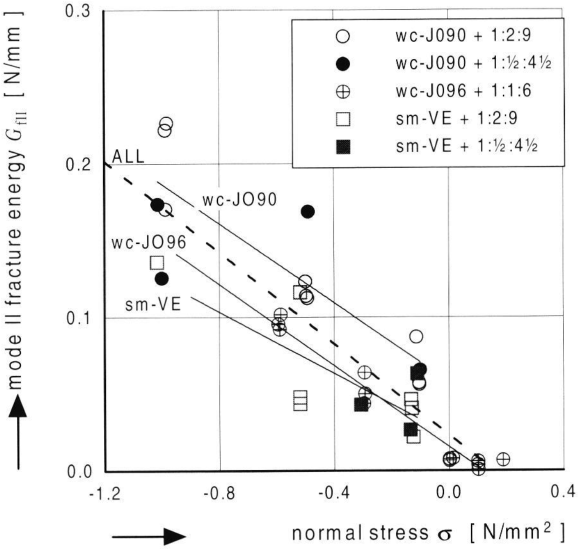

Figure 53 Mode II fracture energy of specimens made of clay bricks as a function of the normal stress (linear trend lines only drawn to show the general tendency)

The linear regression lines clearly show that the mode II fracture energy decreases with an increase of the normal stress. This trend was already observed on the basis of Figure 45. In the two series of 1992 (with sm-VE and wc-JO90) no distinction could be made between the two applied mortars in both series. The correlation coefficient of the regression lines of the series of 1992 were low ($r^2 < 0.74$) and consequently they can only be considered as an indication of the general tendency. However, the regression line of the wc-JO96 + 1:1:6 series (with relatively many tests) showed a reasonable value ($r^2 = 0.96$) for the correlation coefficient making the linear trend more reliable. The slope of the linear regression lines through the points belonging to each of the three series is more or less the same. If all results are used together to determine a trend for clay brick masonry, the dashed line in Figure 53 is obtained.

In Figure 54 result of specimens made with CS units are presented.

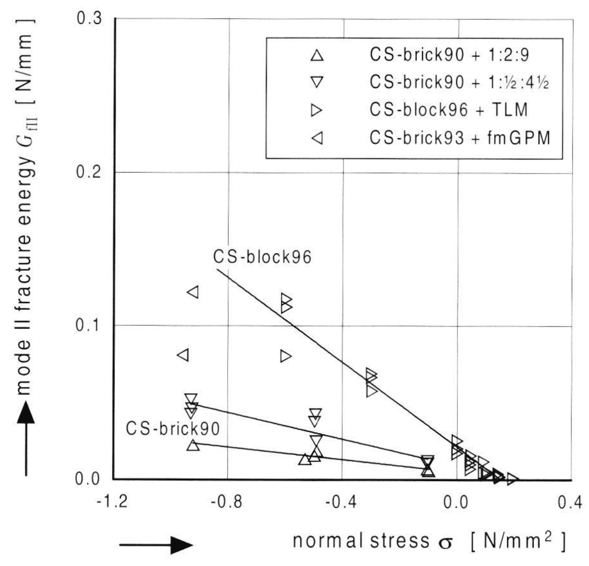

Figure 54 Mode II fracture energy of specimens made of CS-units as a function of the normal stress (linear trend lines only drawn to show the general tendency)

From Figure 54, it is obvious that the fracture energy of tests of 1992 (specimens made with CS-brick90) significantly differed from the fracture energy of the CS-block96 + TLM series. A meaningful distinction could also be made between the results of specimens made with the two different mortars (1:2:9 and 1:½:4½) in 1992. Therefore, linear regression lines are drawn for each mortar batch. A linear regression line is also drawn for the CS-block96 + TLM series. The correlation coefficient of the two regression lines of the CS-brick90 + 1:2:9 and CS-brick90 + 1: ½:4½ series was at least 0.86 and equalled 0.96 for the CS-block96 + TLM series. The distinction that could be made between the CS-brick90 + 1:2:9 and the CS-brick90 + 1:½:4½, indicate that the cohesion c_0 had an influence on the fracture energy of those series. Although the obtained data of the series of 1993 (CS-brick93 + fmGPM) are also plotted in Figure 54, they could not be analysed as a function of the normal stress. The location of the points of this series at a normal stress level of $\pm$0.9 N/mm^2 indicate that they do not correspond with one of the other series.

The results of the MBI93 + fmGPM series of 1993 presented in Figure 55, showed a relatively large scatter and the drawn linear regression line can only be seen as an indication of the trend.

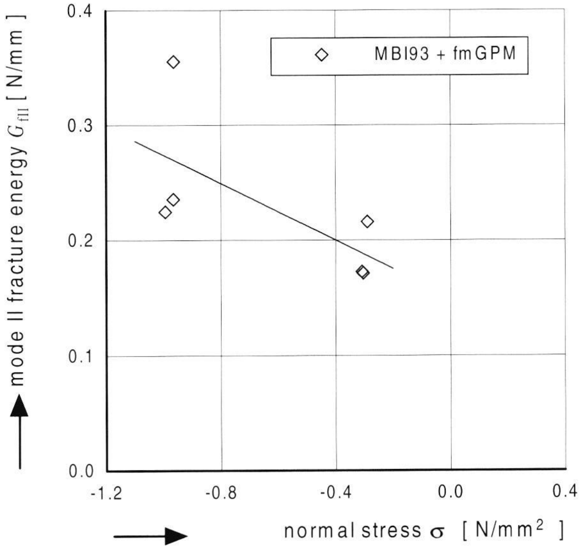

Figure 55 Mode II fracture energy of specimens made of concrete bricks (MBI93 + fmGPM series) as a function of the normal stress (linear trend line only drawn to show the general tendency)

Considering all series, it is obvious that the fracture energy becomes larger with increasing normal compressive stress. In the series where only one failure mechanism occurred, namely:

- bond failure in the wc-JO96 + 1:1:6 series and CS-brick90 + 1:2:9 / 1: ½:4½ series and
- combined bond + mortar failure in the CS-block96 + TLM series,

high correlation coefficients were obtained when a linear relation between the fracture energy and the normal stress was assumed. These series are pictured together in Figure 56, including the linear regression lines.

In the other series this was not the case. In those series often bond failure combined with tensile failure of the units near their head side occurred. Clearly, cracking of the units influenced the amount of absorbed energy and made the results more diffuse. It is believed that this phenomenon caused the relatively high values obtained in the MBI + fmGPM series compared with the tests on clay brick masonry. In the opinion of the author the high values should not be included in any model only used to describe bond failure.

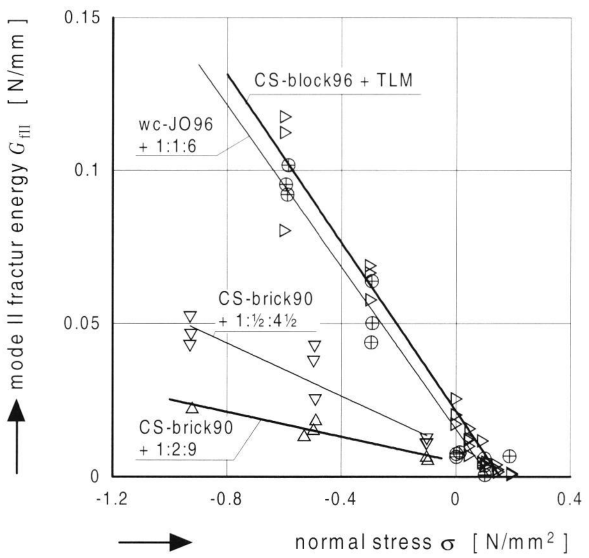

Figure 56 Mode II fracture energy of series in which one type of failure occurred as a function of the normal stress

It was concluded that mode II fracture energy of the joint+interface is linear dependent of the normal stress level.
The wc-JO96+1:1:6 and CS-block96 + TLM series that embraced tests with pre-tension as well as tests with pre-compression (see Figure 56), indicates that the linear dependency can be used up to the tensile (bond) strength. The increase of the fracture energy with decreasing normal stress can vary considerably, depending on the test-series.

When joints+interfaces or the interfaces themselves are considered separately in a masonry model the following recommendation is made about the magnitude of the mode II fracture energy.
Looking to the test data obtained in relation to the type of crack surface, the line obtained for CS-brick90 + 1:2:9 series can be considered as a lower bound, because the crack surface was very smooth and the out of plane tolerance of the bed face of the unit was very small ($\leq$ 0.1 mm). Furthermore the shear bond strength was also low in this series (0.14 N/mm^2). An upper bound is harder to give, as for example the hswc-JOK + TLM series with a very high shear bond strength (4.8 N/mm^2) did not give post peak results, and consequently, no values for the mode II fracture energy are available for this series, but they are expected to be high.

In the absence of test data, the line through the CS-block96 + TLM series can be considered as a 'conservative' upper bound for bond and/or mortar failure. The expression 'conservative' upper bound was chosen because it can be expected that the mode II fracture energy of brick mortar combinations can be higher, when mortars and/or curing conditions are used such high bond strength values are obtained.
The equations of the two regression lines are (G_{fII} in N/mm, σ in N/mm^2):

lower bound: $G_{fII} = -0.02\sigma + 0.005$ (13)

upper bound: $G_{fII} = -0.14\sigma + 0.02$ (14)

In Appendix B 'Experimental Results', Table 54, all equations of the linear regression lines for the fracture energy of the series tested are presented.

In analogy with the findings of Hordijk, it was explored whether a relation could be found between the mode II fracture energy, the initial cohesion and the distance v_{nonlin} (over which the cohesion reduces to zero). In Figure 57 v_{nonlin} is plotted against G_{fII}/c_o for all tests with pre-compression.

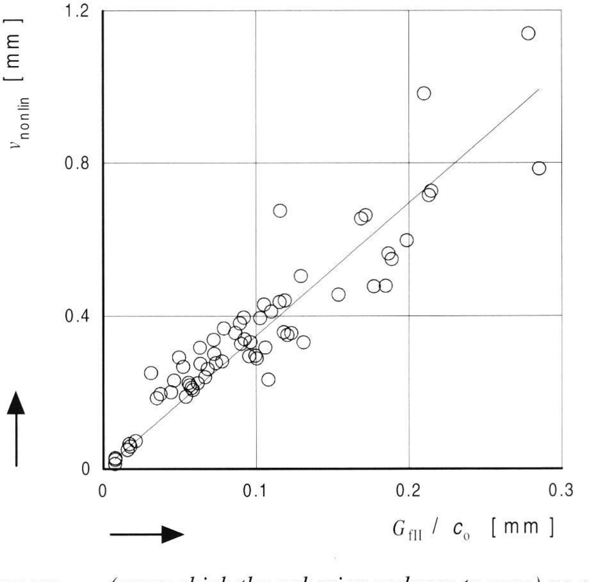

Figure 57 Distance v_{nonlin} (over which the cohesion reduces to zero) as a function of the ratio between mode II fracture energy and cohesion

Taking into account that data from all tests are plotted, it is remarkable that a clear linear trend can be observed. The correlation coefficient of the linear trend equalled 0.96. The formula for the linear regression line reads:

$$v_{\text{nonlin}} = 3.48 \frac{G_{\text{fII}}}{c_{\text{o}}} \tag{15}$$

In Figure 58, the applicability of both eq. (8) and (9) is demonstrated for test series of 1992 and 1998. Softening according to eq. (8) is denoted by exponential softening and according to eq. (9) by Hordijk softening. Bond failure occurred in all the test series presented. The mode II fracture energy of a series was derived on the basis of the linear regression lines (equations presented in Table 54 of Appendix B 'Experimental Results'). The distance v_{nonlin} was derived using eq. (15).

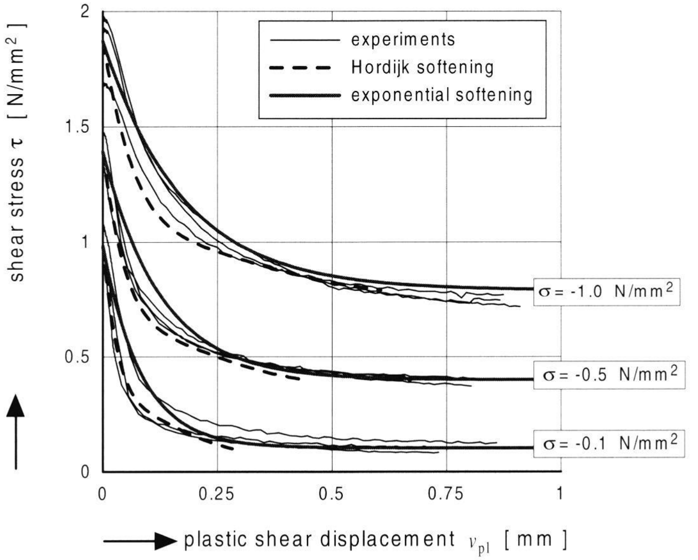

Figure 58 a) wc-JO90 + 1:2:9 series

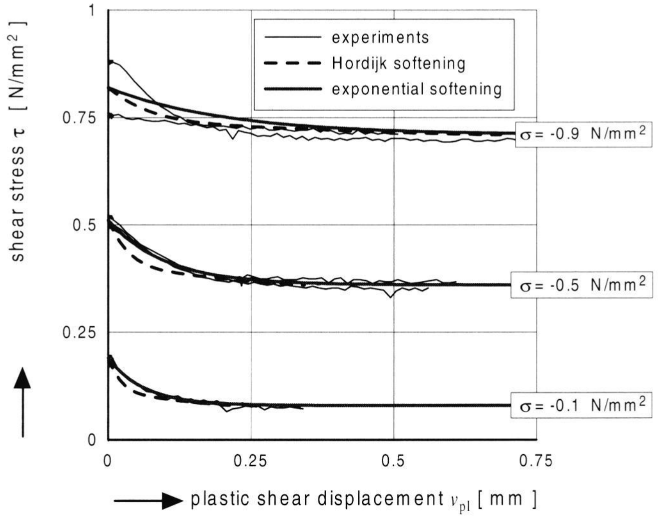

Figure 58 b) CS-brick90 + 1:2:9 series

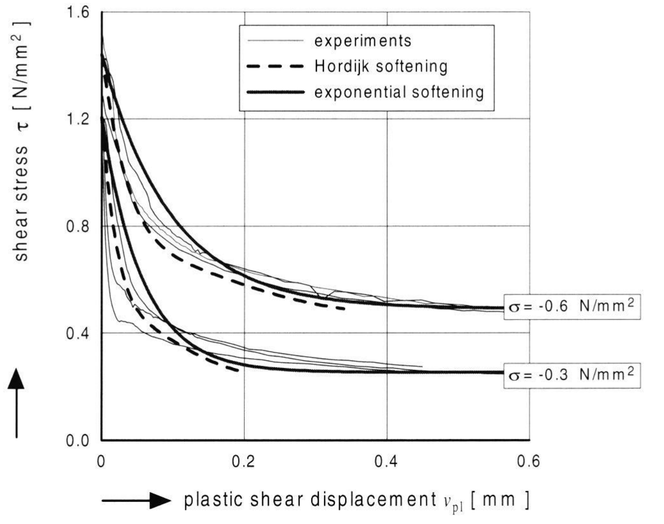

Figure 58 c) wc-JO96 + 1:1:6 series

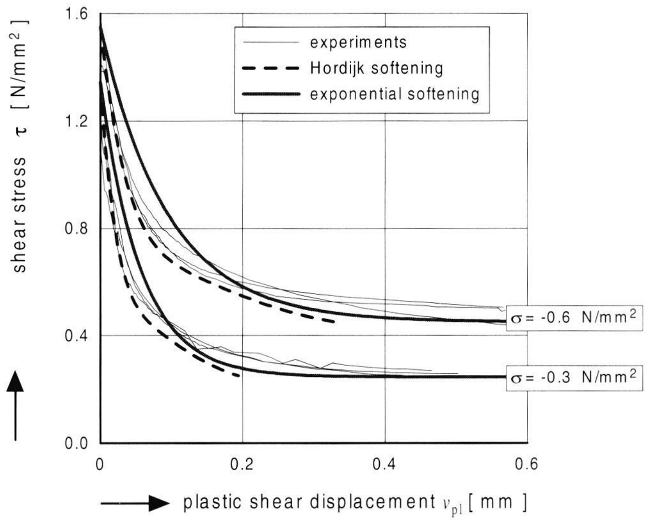

d) CS-block96 + TLM series

Figure 58 Application of eq. (8) (exponential softening) and eq. (9). (Hordijk softening) for the cohesion softening of shear tests.

In Figure 58 a to d, it can be observed that eq. (9) results in initially steeper descending branches. In Figure 58 a, c and it can be seen that eq. (9) is more appropriate especially for the first part of the descending branches. In Figure 58b it can be observed that eq. (8) is more appropriate, especially for the two lower pre-compression level.. The CS-brick90 + 1:2:9 series clearly showed less steep descending branches compared with the other series, making eq. (9) less suitable.

Using eq. (8) always results in a situation that the absorbed energy equals the 'input' value G_{fII}. Knowing this, it can be well observed in Figure 58 that this is not true for the energy dissipated according the Hordijk softening. This is caused by the use of eq. (15) instead of the original equation used in tension by Hordijk ($w_c = 5.14\frac{G_{fI}}{f_t}$). The parameters c_1 and c_2 should be changed to 'release' all the fracture energy when eq. (15) is used. However, it is doubtful if such a modification of eq. (9) would still result in the reasonably adequate description as it gives now. This possibility was not explored.

In general it can be stated that eq. (9) in combination with eq. (15) gives a better approximation of the first (and most important part) of the descending branch than exponential softening, even though the dissipated energy in the model is less than the 'input' value. However, Van Zijl[1996,[87]] showed that the application of eq. (8) in a numerical simulation of the TNO shear test arrangement gives a reasonable approximation of the experimental results. Lourenço[1996,[38]] showed that behaviour of shear walls (modelled on the meso level) can be approximated reasonably well using eq. (8).

3.11 DILATANCY

In Figure 59 an example of the measured dilatancy behaviour is presented for a test with pre-compression. The displacement u_{pl} perpendicular to the shear displacement that occurs beyond the peak in a τ-v diagram, is plotted against the plastic shear displacement v_{pl}. With the definition of the dilatancy in mind (tangent to the diagram in Figure 59, see eq. (10)), it can immediately be seen that the dilatancy decreases with increasing shear displacement.

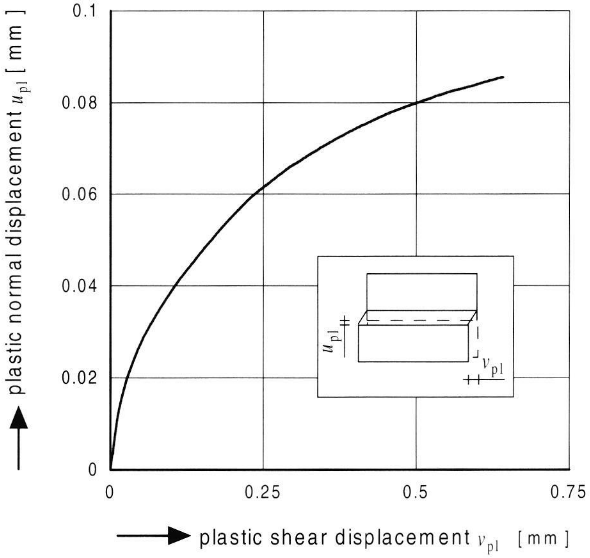

Figure 59 Example of the normal displacement u_{pl} as a function of the shear displacement v_{pl} beyond the peak of a test carried out with normal pre-compression

Before the dilatancy itself will be discussed, the plastic displacement u_{pl} and v_{pl} will be considered for the series carried out in the arrangement of the Pieter van Musschenbroek laboratory. With those series it was possible to gain insight in the difference between tests carried out with normal pre-compression and tests with normal pre-tension. In Figure 60 and Figure 61 the plastic normal displacements are plotted against the plastic shear displacements for both series.

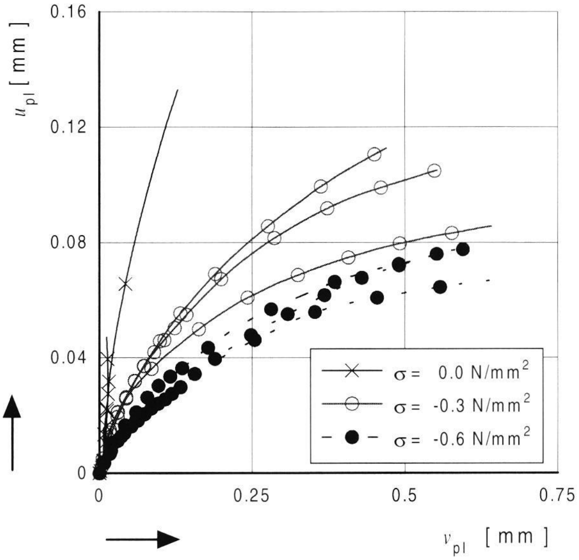

Figure 60 Normal displacement u_{pl} as a function of the shear displacement v_{pl} of the wc-JO96 bricks + 1:1:6 series

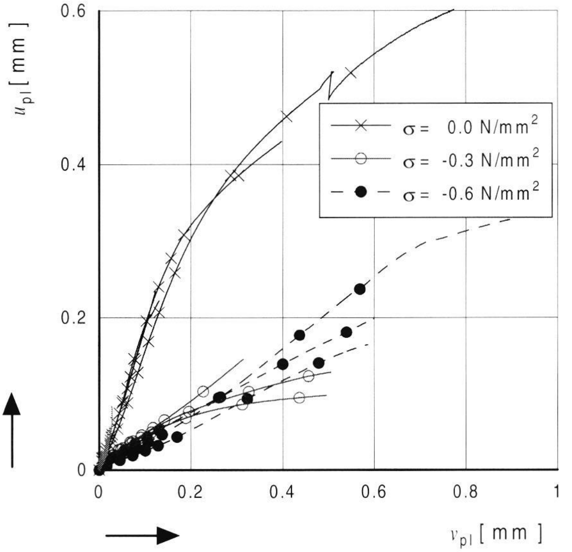

Figure 61 Normal displacement u_{pl} as a function of the shear displacement v_{pl} of the CS-block96 + TLM series

For both series, it can be observed that the initial slopes of the diagrams increase with increasing normal stress. In the series with wc-JO96 bricks + 1:1:6 GPM, the increase is more steady in contrast to the CS-block96 + TLM series. In the latter, the tests with a pre-compression of -0.3 N/mm^2 initially show a steeper slopes than the series with pre-compression of –0.6 N/mm^2, but after 0.2 mm slopes were equal or less than those of the tests with –0.6 N/mm^2 pre-compression.

A remarkable difference between both series is the magnitude of the normal displacements. The normal displacements in the CS-block96 + TLM series were much greater than those in the wc-JO96 + 1:1:6 series for all normal stress levels. The different failure modes that occurred in both series explain this difference:

- bond failure in the wc-JO96 bricks + GPM series and
- (partly) mortar failure in the CS-block96 + TLM series.

In Figure 44 on page 56, it could be observed that failure in the mortar would go hand in hand with larger normal displacements than with bond failure. An example of failure of the mortar in the CS-block96 + TLM series is presented in Figure 62.

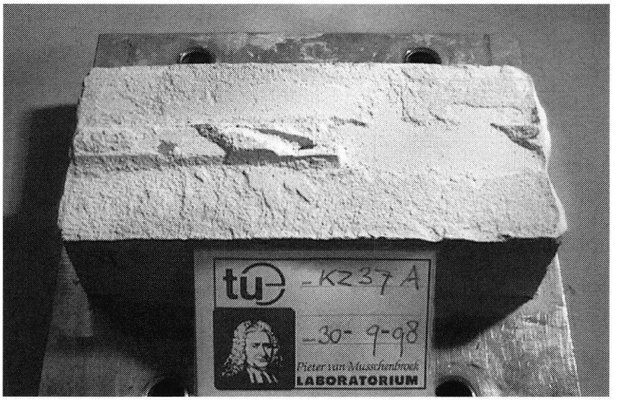

Figure 62 Example of shear failure in the mortar joint of a test of the in CS-block96 + TLM series

The diagrams with pre-tension in Figure 60 and Figure 61, although plotted, disappeared under the diagrams carried out with zero pre-compression. In Figure 63 and Figure 64 detailed views of the initial parts of the diagrams are presented for both series.

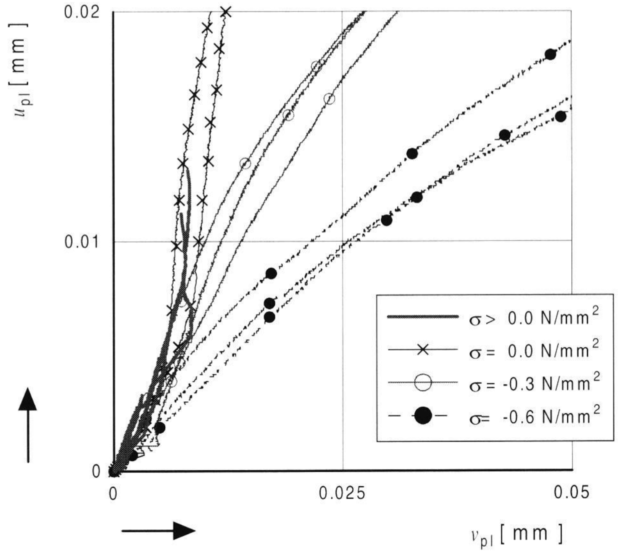

Figure 63 Detailed view of normal displacement u_{pl} versus the shear displacement v_{pl} of the wc-JO96 bricks + 1:1:6 series

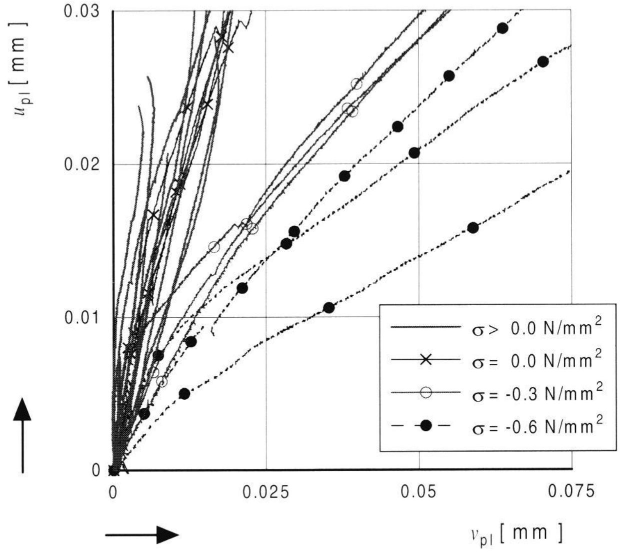

Figure 64 Detailed view of normal displacement u_{pl} versus the shear displacement v_{pl} of the CS-block96 + TLM series

In the series with wc-JO96 bricks + GPM only four complete diagrams of tests with pre-tension were available. Those diagrams corresponded very well with the tests with zero

pre-compression. In this series, all initial slopes of the diagrams of tests with $\sigma > -0.3$ N/mm^2 are more or less the same. In the CS-block96 + TLM series more diagrams were available resulting in a larger bandwidth, but in general the initial slope of the diagrams of tests with pre-tension correspond reasonably with the tests with zero pre-compression. In Figure 64, for the tests with pre-tension it can be observed that at a certain plastic shear displacement, the plastic normal displacement increases more than the plastic shear displacement, probably due to tensile micro cracking.
Looking at all graphs together, it could have been concluded that the tests with zero pre-compression were representative for the dilatancy of the tests carried out with pre-tension. Of course, this observation can be turned around. As a result the question arises whether the observed normal displacements at zero pre-compression are the result of dilatancy. The fact that the initial slopes of tests with pre-tension and zero pre-compression closely corresponded with each other, indicates that the behaviour at zero pre-compression is the result of tensile micro cracking. In this respect the following remark is being made.
Although the boundary condition in the tests with zero pre-compression was set at zero normal stress, tensile stresses can not be avoided during such a test.

- It must be kept in mind that the average stress is zero. This does not mean that no tensile stresses are present as, for example, is shown in Figure 36 on page 46.
- During a test, shear displacements will lead to normal expansion. Due to this expansion normal compression stresses tend to arise and are being compensated by a reaction of the control system that can go hand in hand with the occurrence of tensile stresses (with a short duration).

It was concluded that the normal displacements in the tests with zero pre-compression were already influenced by micro cracking in this direction. As a consequence, dilatancy should be modelled on the basis of tests with pre-compression. Considering the dilatancy in terms of $\Delta\tan\psi$ for the wc-JO96 + 1:1:6 supported this conclusion (see Figure 65).

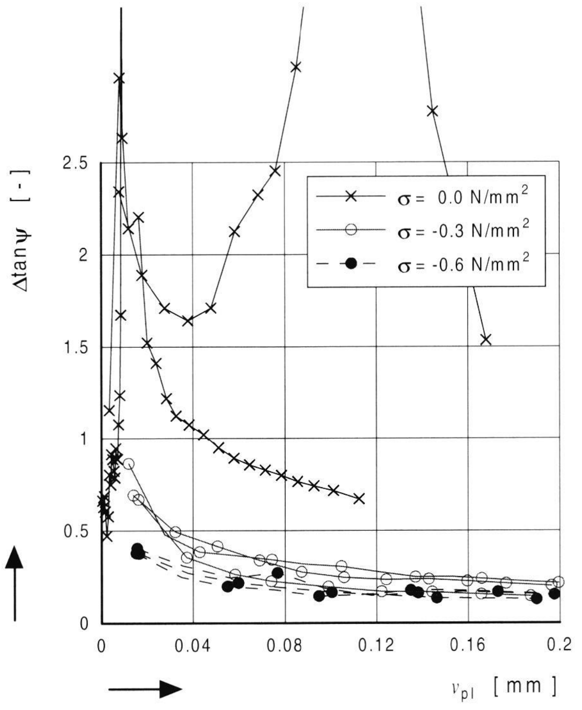

Figure 65 Dilatancy (Δtanψ) as a function of the plastic shear displacement v_{pl} *of the wc-JO96 + 1:1:6 series*

In Figure 65, a remarkable difference between tests without and with pre-compression can be observed. The diagrams of the tests with zero pre-compression are very fanciful which can be explained with tensile cracking, causing jumps in u_{pl} and consequently in Δtanψ.

In the remainder of this section only the dilatancy (Δtanψ) of all tests carried out with pre-compression is considered.

In Figure 66 up to Figure 70 Δtanψ is presented as a function of the plastic shear displacements per type of unit for the same reasons as explained in the previous section.

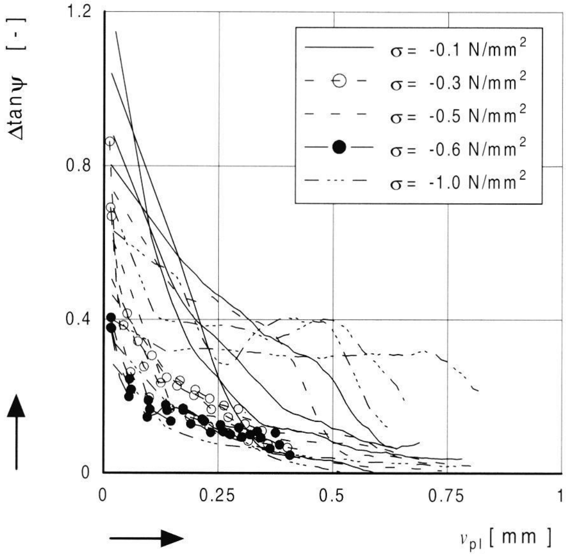

Figure 66 Dilatancy expressed in Δtanψ as a function of the shear displacement v_{pl} *of wc-JO90 and wc-JO96 bricks + GPM masonry*

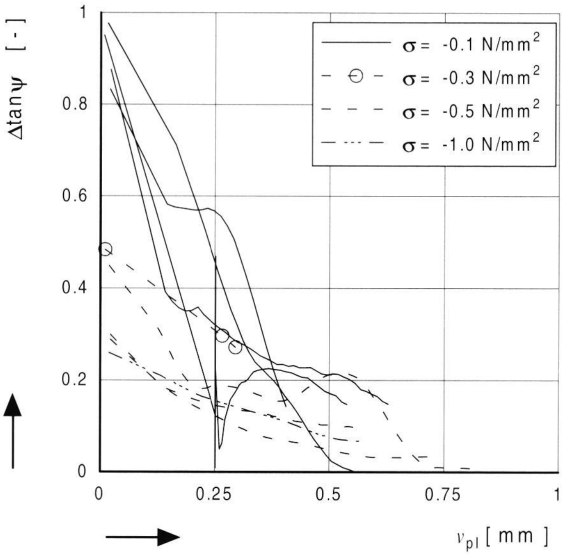

Figure 67 Dilatancy expressed in Δtanψ as a function of the shear displacement v_{pl} *of sm-VE bricks + GPM masonry*

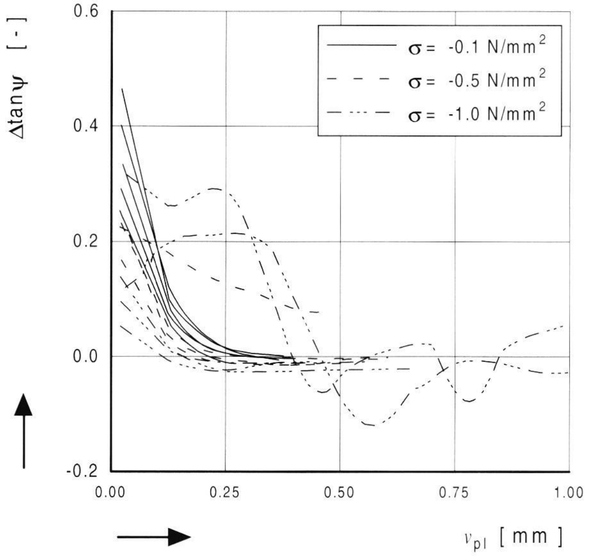

Figure 68 Dilatancy expressed in $\Delta tan\psi$ as a function of the shear displacement v_{pl} of CS-brick90 + GPM masonry

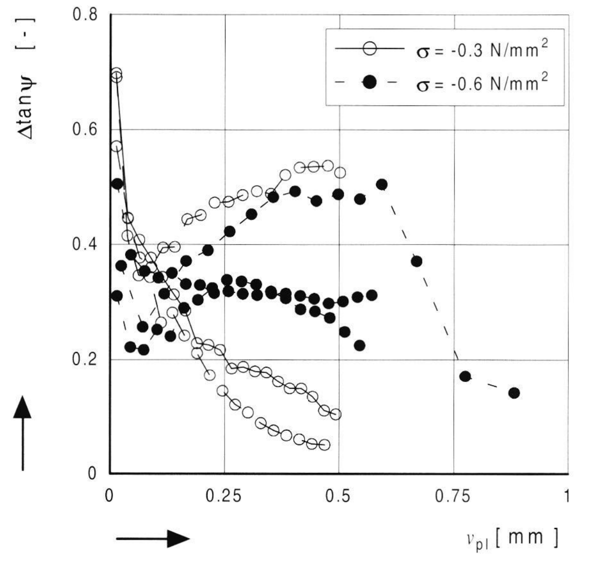

Figure 69 Dilatancy expressed in $\Delta tan\psi$ as a function of the shear displacement v_{pl} of CS-blocks96 + TLM masonry

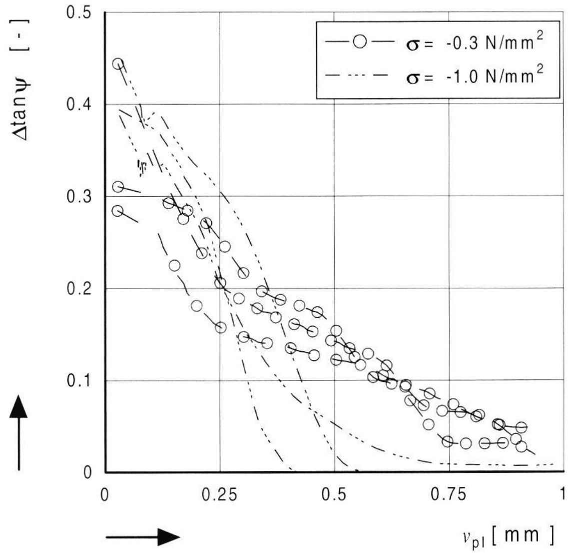

Figure 70 Dilatancy expressed in $\Delta tan\psi$ as a function of the shear displacement v_{pl} of concrete facing bricks MBI93 + GPM masonry

The following tendencies could be observed during analysis and from the diagrams shown above.

- The initial value of the dilatancy angle tends to decrease with increasing normal compressive stresses.
- Often, the dilatancy angle gradually reduces to zero with increasing shear displacement. However, also curves can be observed where the dilatancy angle remains more or less constant at a certain level before dropping back to zero, especially for normal stress levels of -0.5 N/mm^2 and -1.0 N/mm^2. This kind of behaviour can be associated with other types of failure than pure bond failure:
  - combined bond and mortar failure in the CS-block96 + TLM series;
  - combined bond and unit failure near the heads of the unit (see Figure 44c) in the MBI93 + fmGPM and Cebrick-93 + fmGPM series.

  A failure mechanism according to Figure 44c may go hand in hand with rotation of broke pieces of units, resulting in irregular dilatancy behaviour. Failure in the mortar also leads to irregular dilatancy.
- Of course the roughness of the crack surface determines the dilatancy behaviour. In section 3.5 the crack surfaces were discussed. In case of bond failure, the units themselves influence the roughness of the crack surfaces and consequently the dilatancy.

- The roughness of the crack surfaces of specimens made with both types of clay bricks (wc-JO and sm-VE) showed considerable resemblance, and consequently their dilatancy.
- The smooth cracks surface of the series with CS-brick90 + 1:½:4½ and 1:2:9 series resulted in a relatively low value of the initial value of the dilatancy and a quick reduction to zero.
- The crack surface of the specimens made with concrete bricks (MBI93) was rather smooth compared with the clay bricks, resulting in a lower initial value of the dilatancy angle. As explained, the dilatancy angle of this series showed an irregular and less steep decrease than with the clay bricks.
- The limited amount of data does not show an influence of the bond level on the dilatancy.

To find a general formula describing dilatancy, it was assumed that the roughness of the crack surface is rather independent of the strength. Furthermore, it could be observed that the point where $\Delta\tan\psi$ reduces to zero is not much influenced by the pre-compression level, especially when pure bond failure occurs (see Figure 66 and Figure 68). Therefore a two-parameter expression is proposed with the initial value for the dilatancy and a roughness distance r after which the dilatancy is reduced to zero:

$$\begin{aligned} &v_{\mathrm{pl}} \leq r: \ \Delta \tan \psi = \tan \psi_{\mathrm{o}} \{2(\frac{v_{\mathrm{pl}}}{r})^{1.5} - 3\frac{v_{\mathrm{pl}}}{r} + 1\} \\ &v_{\mathrm{pl}} > r: \ \Delta \tan \psi = 0 \end{aligned} \qquad (16)$$

$\tan\psi_o$: initial (maximum) value of the tangent of the dilatancy angle
r : roughness distance over which $\Delta\tan\psi$ reduces to zero.

The parameter $\tan\psi_o$ can be estimated on the basis of Figure 71. In Figure 71 $\tan\psi_o$ is presented per brick type as a function of the normal stress.

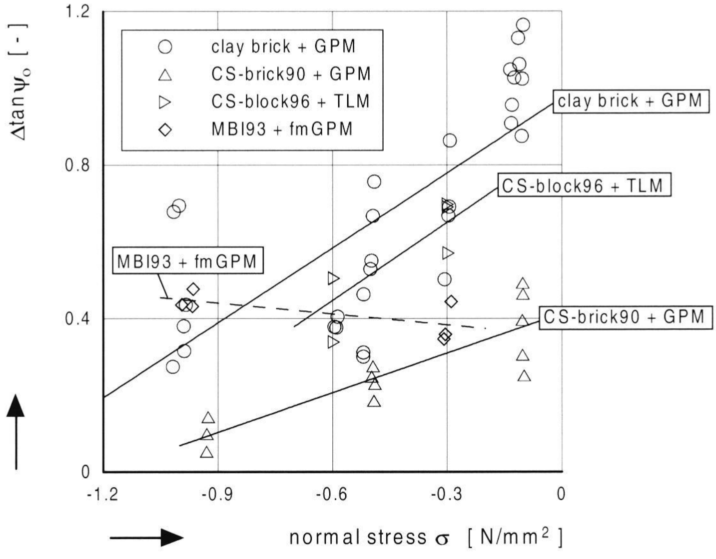

Figure 71 Influence of normal stress on tanψ_o per masonry type

Except for the MBI93 + fmGPM series, it can be observed that the initial value tanψ_o decreases with increasing normal compressive stress. The correlation coefficient of the linear regression lines were low, varying between 0.55 for clay brick + GPM up to 0.76 for CS-brick90 + GPM. The low correlation coefficients immediately indicate that the use of the linear trend lines to obtain values for tanψ_o, may result in large deviations compared with single test results.

A reason for the deviant behaviour of the MBI93 + fmGPM series was not clear, but tensile cracking of the units might have played a role.

The equations of the linear regression lines are given in Table 55 in Appendix B 'Experimental Results' on page 234.

Recommendations for parameters of eq. (16) to describe the dilatancy of the tested masonry series, are presented in Table 9.

Table 9 Suggested values of the parameters of eq. (16) to describe dilatancy softening; r on the basis of fitting, tanψ_o according to linear regression lines of Figure 71

	clay brick + GPM (bond failure)		CS-brick + GPM (bond failure)		CS-block + TLM (bond+mortar failure)		MBI93 + fmGPM (bond failure)	
σ [N/mm^2]	-0.1	-1.0	-0.1	-0.9	-0.3	-0.6	-0.3	-1.0
r [-]	0.75		0.3		0.75		0.75	
tanψ_o [-]	0.91	0.33	0.38	0.10	0.65	0.45	0.40	0.40

The recommendations are not intended to get an 'as good as' possible match with the obtained test data. The suggested values for *r* were not determined on the basis of some statistical method. The variation in the data is too large and too much influenced by various phenomena to make a robust approach possible. The most important consideration was (as already indicated in this section) that modelling of the dilatancy should be based on bond and/or mortar failure. It can be seen that for the rougher bond surfaces of the clay brick + GPM, *r* was taken equal to 0.75 and for the very smooth crack surface of the CS-bricks +GPM specimens equal to 0.3. The roughness of the partially mortar failure in the CS-block96 + TLM series made a higher value for *r* compared with CS-brick90 + GPM series necessary.
In Figure 72 up to Figure 75 an overview is given of the suggested theoretical behaviour against the background of the obtained test data.

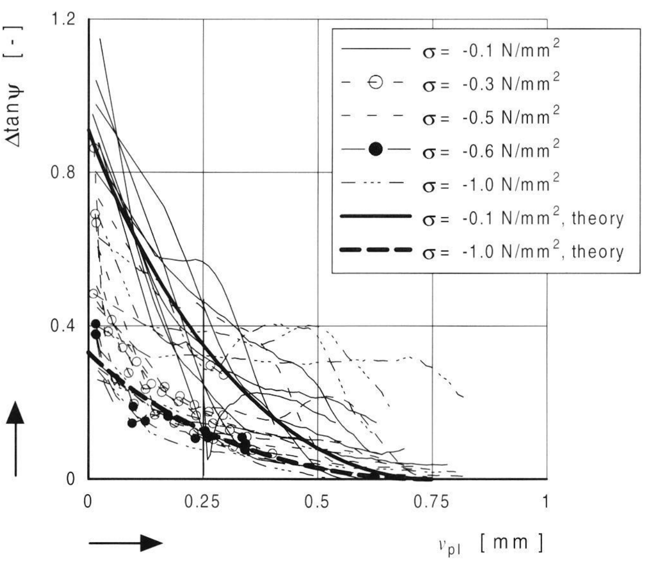

Figure 72 Suggested theoretical approach for the dilatancy behaviour of clay brick masonry with GPM

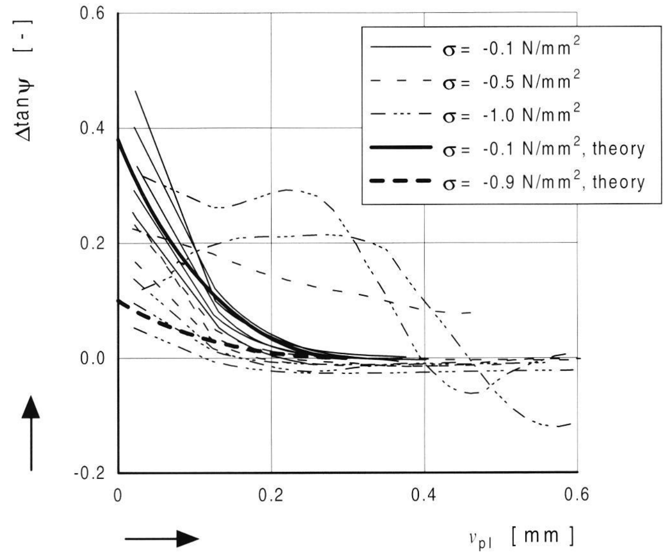

Figure 73 Suggested theoretical approach for the dilatancy behaviour of CS-brick90 + GPM masonry

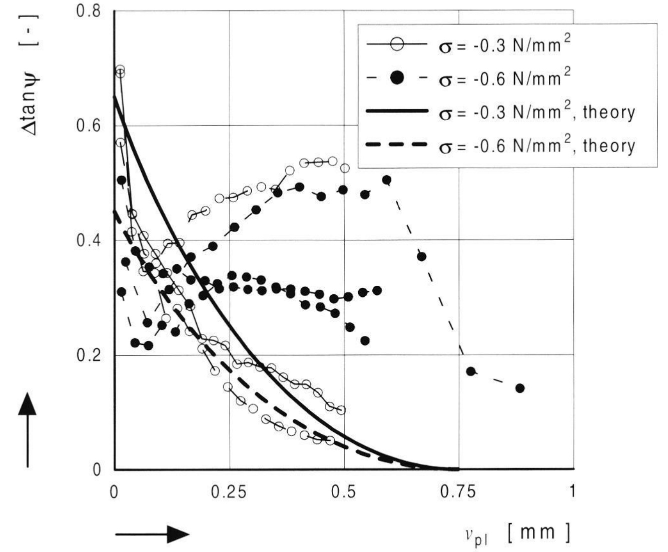

Figure 74 Suggested theoretical approach for the dilatancy behaviour of of CS-blocks96 + TLM masonry

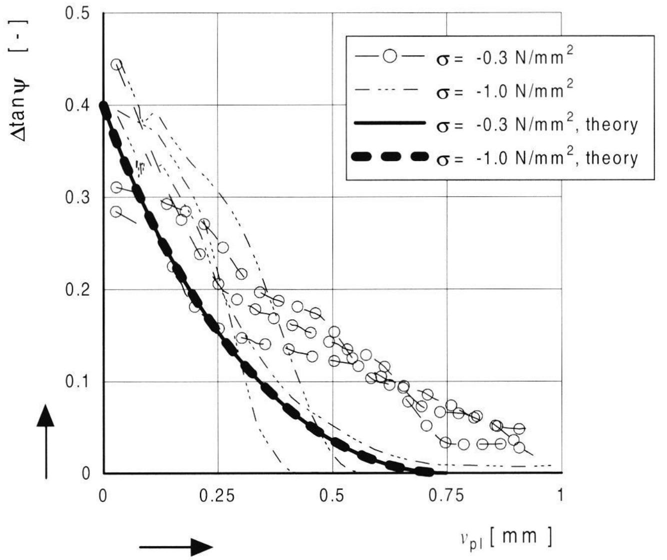

Figure 75 Suggested theoretical approach for the dilatancy behaviour of concrete facing bricks MBI93 + GPM masonry

Especially for the CS-block96 + TLM and MBI93 + fmGPM, it is clear that the irregular behaviour of the tests is ignored with the theoretical approach. The reason that only one curve (in fact two the same on top of each other) is presented for MBI93 + GPM masonry was the deviant values that were obtained for $\tan\psi_o$.

3.12 Concluding remarks

From the experiments, important tendencies concerning the failure envelope and post peak behaviour became clear.

Lourenço[1996, [38]] has developed a complete numerical implementation in the DIANA FE code of the shear behaviour of joint+interfaces, based on the experimental data obtained in 1992 and 1993. Although this implementation was a big step forward, it did not provide a solution for the dependency of the mode II fracture energy on the normal stress. Recently, Van Zijl[1999,[89]] has implemented a linear dependency of the mode II fracture energy on the normal stress, but this tool is not yet available in the distribution version of the DIANA-code. In combination with the upper and lower bound estimates of the dependency of the mode II fracture energy, deduced from the experimental results, this implementation will provide an advanced tool for modelling masonry on the meso level.

Continued research, especially with more brick-mortar combinations, is necessary in this field. Special attention has to be paid to obtain data sets with one type of failure because combined failure modes often lead to diffuse post-peak data. Notches in specimens might be a possibility to avoid cracks in units. It is also recommendable to carry out test series with a relatively low normal pre-compression level to gain more insight in the dilatancy.
Results obtained from the tests with normal pre-tension are suitable to verify numerical models, but have not been utilised in that way. However, this was beyond the scope of the research at hand.

4. BENDING BEHAVIOUR ON THE MACRO SCALE

This chapter primarily focuses on the bending behaviour of masonry until the maximum load capacity is reached. The main objective was the creation of consistent experimental data that could be related with the tensile and shear tests on the meso level, discussed in the two previous chapters. Small masonry walls (wallettes) were tested in a 4-point bending test arrangement. Although most tests were carried out until the maximum load was reached, the test results can be used to verify non-linear material models, because non-linear redistribution already occurs prior to the peak load. Some of the tests were carried out deformation controlled beyond the peak load, making them very suitable for verification of numerical non-linear material models used to model masonry. The angle between bed joint and bending axis was the most important parameter in the wallette tests.

It was shown that so-called bi-linear behaviour visible in the m-κ diagram of the specimen bent around an axis perpendicular to the bed plane (horizontal bending), was caused by cracking of the head joints. This type of behaviour found also for specimens bent in other directions, may also arise from (micro)-cracking due to complex stress combinations in the joints. The flexural strength in horizontal bending could be related to the flexural strength of the units.

Keywords: bi-linear behaviour, failure curvature, head joint, micro cracking, bending direction

4.1 INTRODUCTION

To study the behaviour of masonry in bending, experiments on small masonry walls (so called wallettes), bent in different directions, were carried out. The bending direction was defined with the angle θ between the bed joint and the bending axis, as shown in Figure 76.

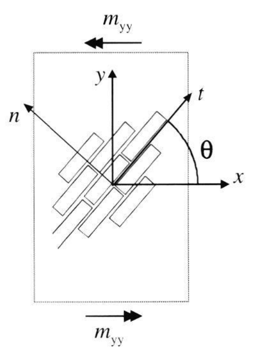

Figure 76 Definition of the angle θ between the moment-vector and the bed joints

Apart from studying the behaviour, another objective of the experiments was the creation of data sets consistent with the data obtained on the meso level with the tensile and shear tests discussed in the two previous chapters, enabling numerical verification of non-linear bending behaviour of masonry. Bending directions $\neq 0°$ always lead to complex stress distributions. This makes tests with bending directions $\neq 0°$ representative for more general loading conditions and suitable to verify models. However, experiments with bending angles different from 0° and 90° can only be scarcely found in literature. Furthermore, the data presented in literature mainly focus on the flexural strength. For this reason, data from literature cannot be used very well as they do not provide enough information and certainly not for non-linear numerical verifications.
The experimental work consisted of two separate programs with wallettes carried out in different periods and of two tests on laterally loaded simply supported large walls (referred to as panels). The main objective of the panel tests was the establishment of data suitable for numerical simulation. Panel tests have been carried out by many researchers (for an extensive overview see Jenkins and Potter[1996, [27]]), but the reported input data needed for numerical verification, is in most cases restricted to the flexural strength in the two orthogonal directions 0° and 90° making the tests from literature less suitable for numerical simulation.

Bending tests on wallettes with sizes of 0.15 to 1.5 m^2 are described. All wallette specimens were tested in 4-point bending test arrangements. In between the inner loads, the critical cross-section is tested in pure bending, which makes the 4-point bending arrangement ideal to establish the behaviour in flexure. The 4-point bending test arrangement is widely used and most masonry codes include a description of a 4-point bending test to establish the flexural strength of masonry.

The tests included the two types of masonry, clay brick and calcium silicate block masonry (see section 1.3), used throughout the research.
In the period 1992-1994, the clay brick masonry wallettes were tested with four different bending angles. For the calcium silicate block masonry three different angles were used. All those bending tests were carried out with deformation control of the actuator, resulting in uncontrolled failure at peak load, in the sense that it was not possible to continue the tests beyond the peak. For each type of masonry, the strength and behaviour in the different directions were compared with each other. The bending tests were accompanied by tensile tests with hinges in the period 1992-1994.
In the period 1996-1997, wallettes were used to investigate the difference between filled and unfilled head joints and to obtain torsion failure of bed joints. Most of the wallettes were bent in the 'horizontal' direction ($\theta = 90°$). Two wallettes with a low bond strength that were bent with $\theta = 70°$. The wallettes were bent deformation controlled. The bending tests of 1996-1997 were accompanied by deformation controlled tensile tests (their result were already used in chapter 2).

The directions 0° and 90° will be referred to as respectively 'vertical' and 'horizontal' bending. These terms originate from the spanning direction of masonry in walls e.g. in case of vertical spanning between floor slabs, the masonry is bent vertically (see Figure 77)

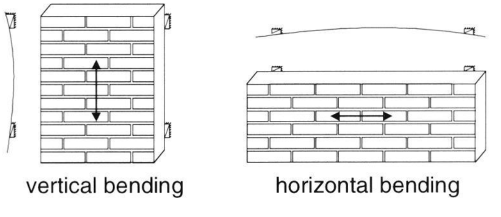

Figure 77 Definition of vertical and horizontal bending

In Table 10, an overview is given of the test series carried out in 1992-1994, including the number of specimens per series that were tested and analysed.
In Table 11, an overview is given of the test series carried out in 1996-1997, including the number of specimens per series.

Table 10 Test program of the 4 point bending tests carried out in 1992-1994

masonry		angle θ				
unit	mortar	0° (*VER*tical)	30°	45°	70°	90° (*HOR*izontal)
wc-JO90	1:½:4½	8	12	-	6	12
	1:1:6				6	
CS-block92	Calsifix	12	-	12	-	12

Table 11 Test program of the 4 point bending tests carried out in 1996-1997

masonry		test parameters				
		θ = 70°	θ = 90°			
unit	mortar	filled head joints	unfilled head joints	tongue removed filled head joints	tongue removed unfilled head joints	filled head joints
wc-JO96 + GPM	1:2:9	2	5	-	-	4
	1:2:12	-	5	-	-	-
CS-block96 + TLM	Calsifix	-	3	3	3	3

In the remainder of this chapter, the test series are referred to by the unit type, bending angle and the period in which they were tested, e.g. JO.30 series of 1992-1994. Detailed information about both series can be found in Van der Pluijm[1996,[56]] (1992-1994 series) and Van der Pluijm[1999,[64]] (1996-1997 series).

The two panel tests, loaded with air bags, were carried out with well-defined boundary conditions (see Figure 78).

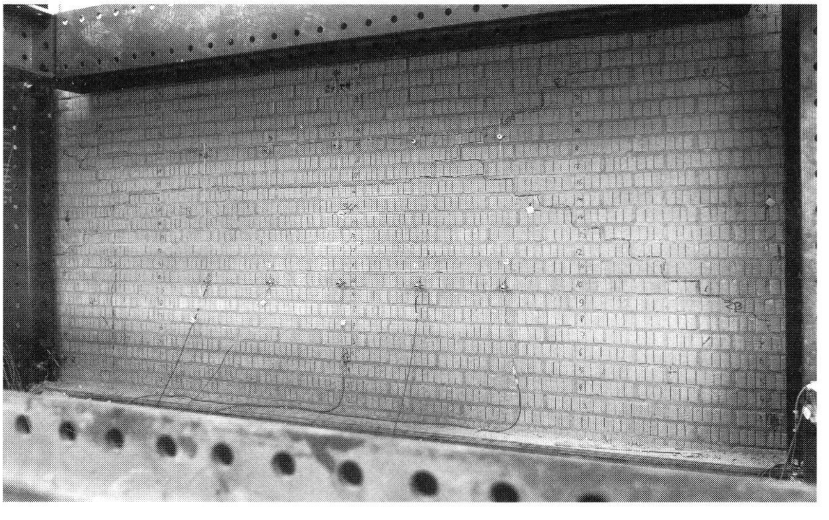

Figure 78 Laterally Loaded panel test arrangement with cracked specimen

The boundary conditions and dimensions of the panels ($1.74 \times 3.95\ m^2$) were chosen in such a way that redistribution of internal forces would occur after the occurrence of the first macro crack, making the test useful for verification of non-linear numerical models. The redistribution after cracking can be observed in Figure 79 from the deflection and from strain measurements in Figure 80.
To be able to model the tests in non-linear numerical models, accompanying deformation controlled tensile tests and bond wrench tests were carried out. The tensile and bond wrench specimens were made for each mortar batch used. For futher (comprehensive) information the reader is referred to Van der Pluijm[1999,[63]].

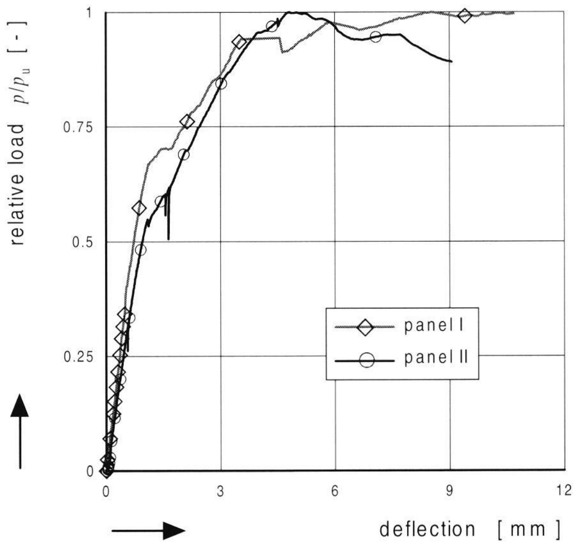

Figure 79 Relative load-deflection diagrams measured at the centre of both panels

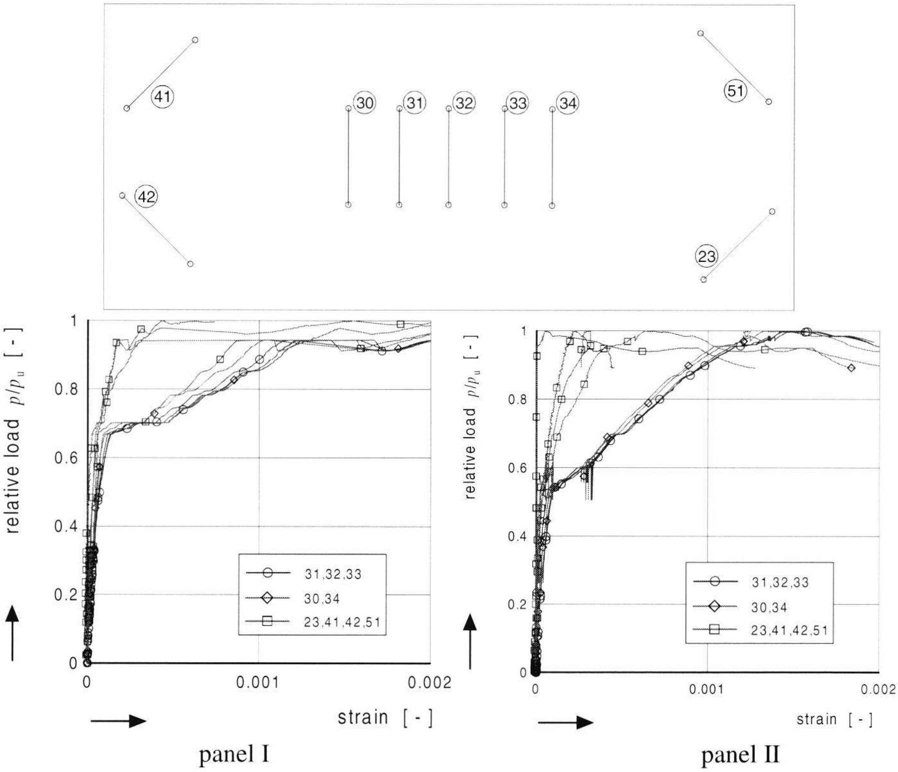

Figure 80 Strains and their locations measured on the tension side of the panels

4.2 SPECIMENS

The wallettes used are shown in Figure 82 and Figure 83. The definition of the bending direction was presented in Figure 76. The horizontal dash-dot lines in Figure 82 and Figure 83 refer to the load lines and supports of the test arrangement.

The wallettes of 1992-1994 were constructed in such a way that 3 to 5 potential fracture-lines parallel to the bending axes were present in the area where the bending moment is constant. An example of those anticipated potential cracks is presented in Figure 81 for a JO.70 specimen.

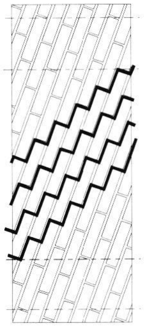

Figure 81 Example of four potential oblique cracks, anticipated in a JO.70 specimens

The thickness of all specimens was equal to the width of the units (≈100 mm). In the specimens for vertical bending a possible fracture-line normally coincides with a bed joint. In a specimen for horizontal bending a potential fracture-line coincides with a crack through the middle of two or three units and two or three head joints depending on the unit-type, or alternatively through head joints and bed joints. In the specimens for bending under 30° (JO) and 45° (CS) a fracture-line was supposed to coincide with a so-called oblique crack. An oblique crack runs alternately through bed joints and head joints. In those directions the oblique crack would coincide with the bending axis. The specimens in the JO.70 series were constructed in such a way that one out of four possible oblique cracks could occur between the load lines.

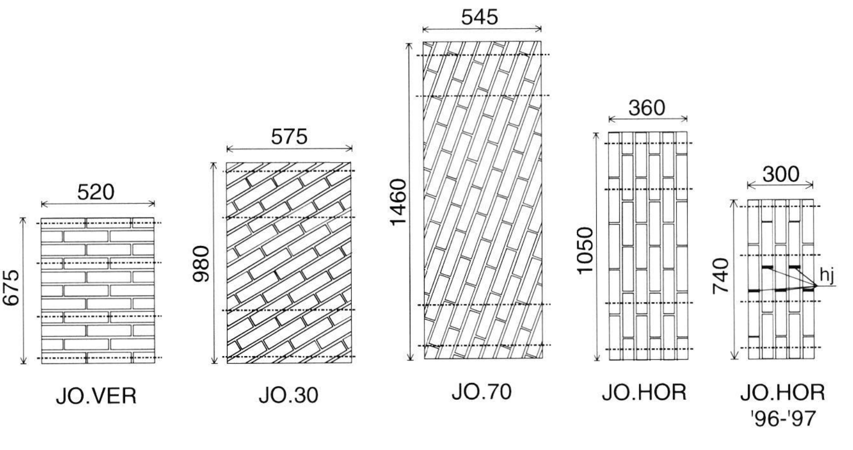

Figure 82 Wallettes of wc-JO90 & 96 + GPM series for bending in different directions (dimensions in mm)

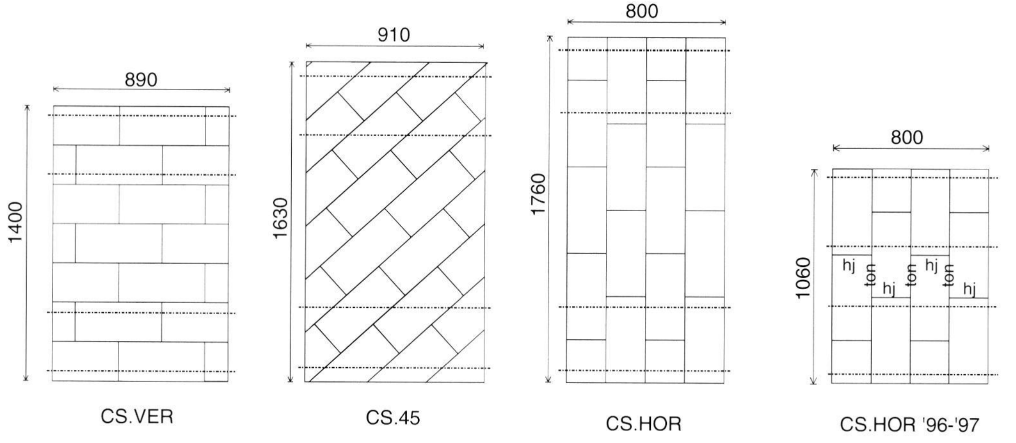

Figure 83 Wallettes of CS-block92 & 96 +TLM series for bending in different directions (dimensions in mm)

In the JO.HOR and CS.HOR specimens used in 1996-1997, the head joints marked with 'hj' in Figure 82 and Figure 83 were unfilled in the series indicated in Table 11. In the CS.HOR specimens, the tongues (marked with 'ton') were removed in two of the four sub-series.

The specimens with angles $\theta \neq 0°$ and $\theta \neq 90°$ were made on a frame made of HE300B profiles, in such a way that bed joints could be laid horizontally (see Figure 84).

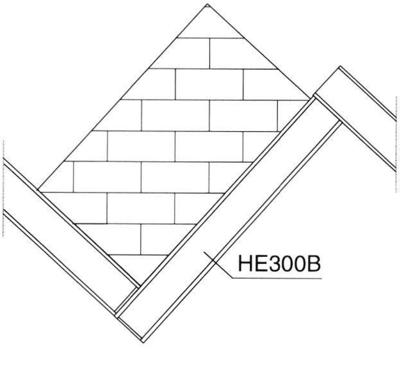

Figure 84 Fabrication of Specimens with $\theta = 45°$

Unit and mortar properties can be found in Appendix A 'Materials', in respectively Table 32 and Table 34. The specimens for the tensile tests consisted of two half bats on top of each other with a bed joint. They were made in the same way as presented in Figure 4 on page 12. At time of testing, the age of the specimens varied between 36 and 52 days.

4.3 Test arrangement

A four point bending test arrangement similar to NEN 6790 Appendix B[14], BS 5628: Part1: 1978 Appendix A.3[9] and prEN 1052-2[15], was used. Special attention was paid to the boundary conditions to avoid friction forces. The test arrangement presented in Figure 85, was stiffened compared with the one used in the period 1992-1994, mainly because the series of 1996-1997 were carried out deformation controlled.
In the testing arrangement, the specimens were placed vertically and loaded in such a way that the bending axis was always horizontal. At the base, the specimens were supported by a steel plate positioned on top of two flat ball bearings (developed by Van Hoof of the Pieter van Musschenbroek laboratory) and two ball hinges (see detail B in Figure 85). In this way horizontal friction forces are avoided and end rotations of a specimen does not lead to eccentricities of the vertical reaction force due to deadweight. The outer roller bearings were mounted to the test rig with springs and could easily move. However it must be realised that some friction forces always exist with steel roller bearings. The only way to avoid this type of friction, is the application of long pin-ended struts that connect the supporting beams with the surrounding frame. But such supports ask for horizontal testing instead of vertical, which make the handling of the specimens difficult, causes additional bending moments and shear stresses and introduces the possibility of spontaneous cracking due to deadweight. Steel wires suspended the inner loading beams and consequently friction forces could not develop. A flat steel plate 50×5 mm^2 and an intermediate layer of fibreboard was placed between all roller bearings and the specimen. The layer of fibreboard allowed for possible surface roughness of the specimen (see detail A in Figure 85).

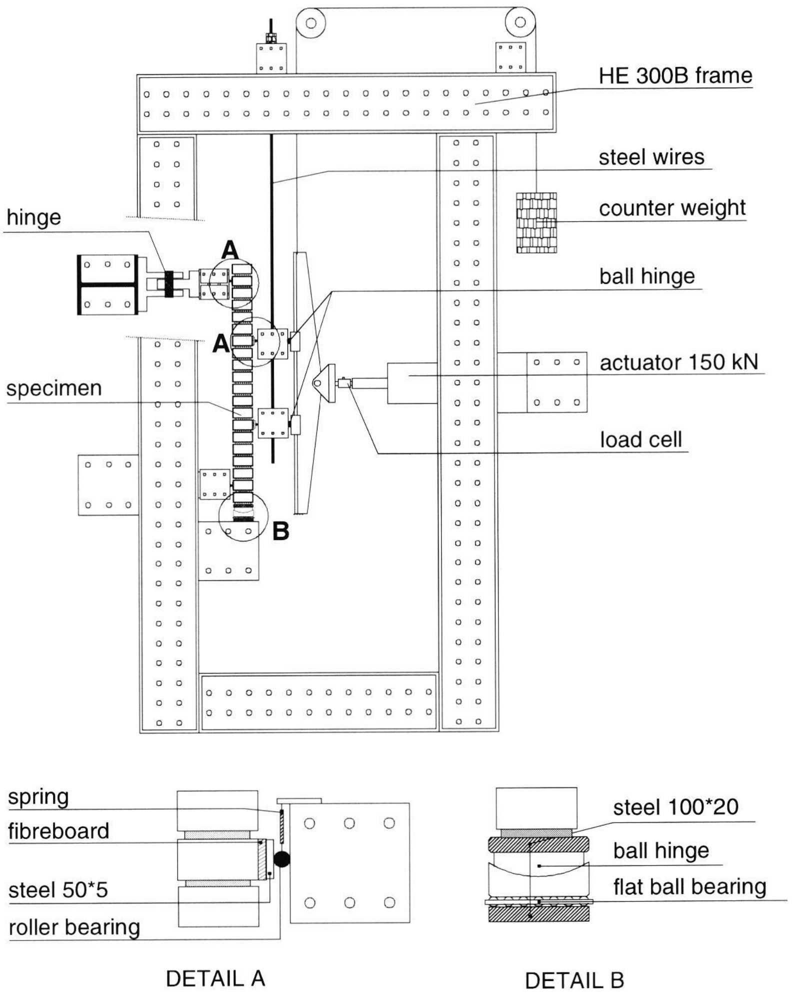

Figure 85a Drawing of 4-point bending test arrangement

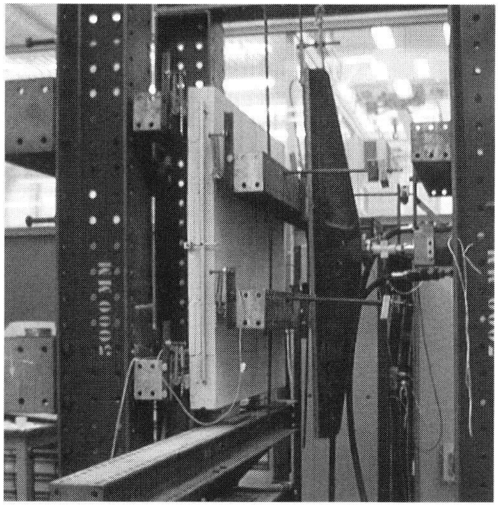

Figure 85b Foto of 4-Point bending test arrangement

The deformations of the supports are large compared to the deflection of the specimen due to the fibreboard used. Calculating the deflection from the difference between the displacement at mid span and at the outer supports produced no reliable results and made direct measurement on the specimen necessary. Deflections were measured directly on the specimen using a bridge that was connected to the specimen (see Figure 86).

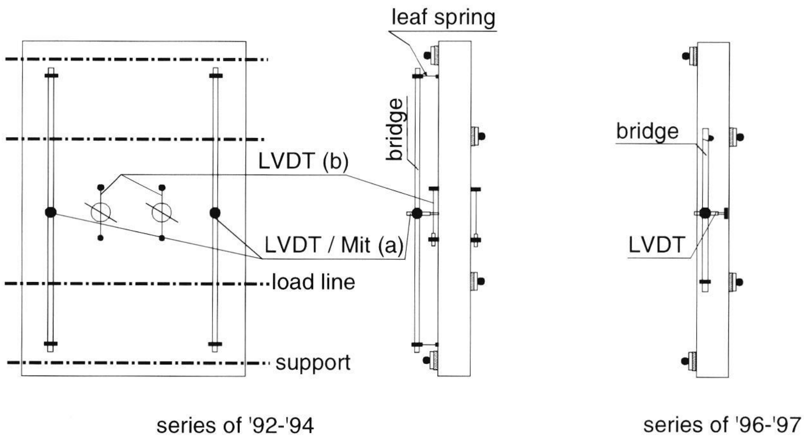

Figure 86 Measurement of deflections and deformations on wallette specimens

In 1992-1994, the deflections were at first measured with electronic Mitutoyo dial gauges with an accuracy of 1 μm. Because of friction between the dial gauge shaft and

the measuring rod, the readings obtained became suspect. The dial gauges, therefore, were replaced with LVDT's.
In the first two series carried out in 1992 (JO.VER en JO.HOR series), four extra deformations were measured at two points on either side of the specimen using LVDT's with a gauge length of 120 mm (LVDT b). The information thus obtained was used to calculate the strains in the outer fibres of the cross section.

From Figure 86 it can be observed that the length of the bridge was decreased for the deformation controlled wallette tests carried out in 1996-1997. On the one hand, this was necessary to obtain an always increasing signal that could be controlled. On the other hand it was also necessary because for some specimens the head joints were removed, but only in the constant moment zone. Measuring over a larger span would mix up two areas with different bending stiffnesses. The bridges were modified and mounted on the sides of the specimens.

Beside the wallette tests, accompanying tensile tests were carried out. The deformation controlled tensile test arrangement as described in section 2.3.1 was not yet available in the Pieter van Musschenbroek laboratory in the period 1992-1994. The tensile tests were carried out using a simple arrangement with hinges. The tensile test set arrangement is shown in Figure 87. The specimens were glued between steel platens and connected through hinges with a 100 kN Schenck test-rig. The merits and demerits of testing with hinges have already been discussed in section 2.3.1.

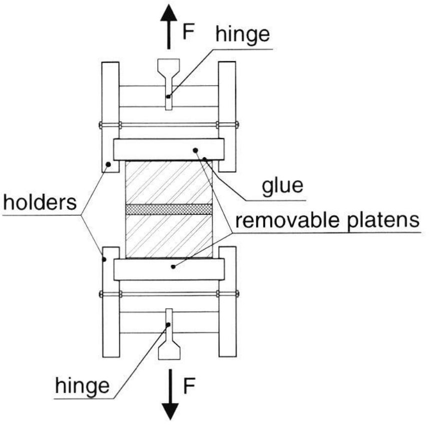

Figure 87 Tensile test set-up with hinges

After a test, the platens that could easily slide in and out their holders, were removed and a new specimen + platens was placed in the holders and tested. During the first series, the steel platens used were 10 mm thick. With these platens failure occurred in the glue. By increasing the thickness of the platen to 25 mm, this problem was solved. It was assumed that the deflection in the 10 mm thick platens resulted in peak stresses that caused the failure of the glue.

4.4 PROCESSING OF TEST DATA

In the series of '92-'94 and of '96-'97, the span of the bridges was less than the span of the specimen. Deflections and curvatures were calculated from the measured deflections assuming uniform stiffness in the specimens.
With this assumption, the stiffness of the specimen can be calculated from the measured deflections taking the bending-moment diagram and the position of the measurement into account. With the stiffness and load, the curvature can be calculated at any cross section. When joints and/or units are in a micro cracking stage, this assumption is no longer valid. The assumptions used led to an underestimation of the curvature in the cracked zone. Very detailed measurements would be necessary to determine possible non-homogeneous distributions of curvatures in the constant moment area. During the period that the bending tests were carried out, there was no practical method available for this kind of measurements. However, recently a commercial measurement system (ESPI) became available in the Pieter van Musschenbroek laboratory, that has the potential to measure deformations over an area with a very high accuracy using laser interferometry (for further information see e.g. Vermeltfoort[1997,[83]]).
Another aspect that plays a role in determining the stiffness from deflection measurements is the boundary condition. The wallettes cannot be seen as prismatic beams but will show some plate-action. The exact boundary conditions are not easy to determine. At the position of the supports and loading beams $\frac{\partial w}{\partial y} = 0$, when the stiffnesses of the supports and beams are infinite. In general this will never be the case and certainly not in the arrangement where fibreboard was applied. If it is assumed that the plate is bent to a cylindrical surface with generators parallel to the y-axis, then $\frac{\partial^2 w}{\partial y^2} = 0$ for the whole specimen.

When the deflection w is small compared with the plate thickness d, the well known relations between bending moments and deflection according to plate and beam theory are as follows.

- plate:

$$m_{xx} = -D\left(\frac{\partial^2 w}{\partial x^2} + \nu\frac{\partial^2 w}{\partial y^2}\right) \tag{17}$$

$$m_{yy} = -D\left(\frac{\partial^2 w}{\partial y^2} + \nu\frac{\partial^2 w}{\partial x^2}\right) \tag{18}$$

with

$$D = \frac{Ed^3}{12(1-\nu^2)} \tag{19}$$

- beam:

$$M = -EI\frac{\mathrm{d}^2 w}{\mathrm{d}x^2} \tag{20}$$

The deflection w is the same for both approaches. The stiffness, which is calculated, equals E according to beam theory and equals $E/(1-\nu^2)$ according to plate theory with the assumption $\frac{\partial^2 w}{\partial y^2} = 0$. If Poisson's ratio equals 0.2, the two approaches result in a difference of 4%.

The boundary condition at the boundaries parallel to the y-axis is $m_{xx} = 0$, but probably not at the centre of the specimen due to stiffness of the supports and loading beams. If it is assumed that $m_{xx} = 0$, the stiffness according to plate theory also equals E. The small difference that may occur due to real boundary conditions was ignored and simple beam theory was used to determine stiffness values. The following values were determined to characterise the behaviour.

- A secant stiffness value that represents the first linear branch of the m-κ diagram of the wallettes E_{1st}. It was practically the same as the tangent modulus at one third of the failure load.
- A value, up to which linear behaviour could be detected, expressed as a fraction of the failure load (r_{lin}). This fraction was determined by optimising the correlation coefficient of the linear regression line similar to the method described in section 2.3.2, page 18 for the determination of E_0 (for further information see Van der Pluijm[1996,[56]]).
- If appropriate, the secant stiffness value of a second linear branch in the m-κ diagram.

The four additional LVDT measurements taken in the first two series (JO.VER en JO.HOR series) were used to calculate the strains in the outer fibres of the cross section in the constant moment area. This enabled the detection of a possible shift of the neutral axis, but these measurements led to unreliable results and are not discussed here. A discussion can be found in Van der Pluijm[1996,[56]].

The flexural strength of the wallettes was derived by dividing the ultimate bending moment by the elastic section modulus (see section 2.4.3 for a discussion of this calculation method). The deadweight was not taken into account when calculating the flexural strength. The compressive stress in a crack depended on the size of the specimen and the position of the crack within the specimen. The possible influence of the deadweight was derived, based on the lowest crack that occurred in a series (giving the largest deadweight of the remainder of a specimen above the crack) and expressed as a percentage of the mean flexural strength.

4.5 BEHAVIOUR OF CLAY BRICK MASONRY SERIES

In Figure 88 a few characteristic moment-curvature (m-κ) diagrams are presented for the 4 different angles θ used in the 1992-1994 series.

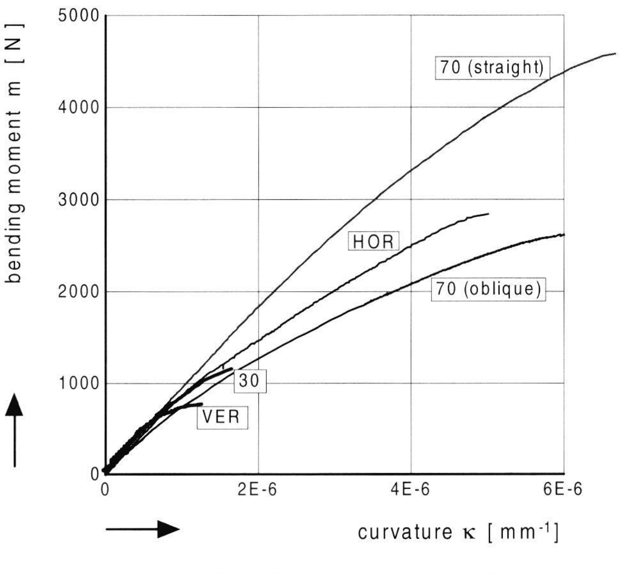

Figure 88 Examples of moment-curvature diagrams of wc-JO90 + GPM masonry of 1992-1994

In a lot of moment-curvature diagrams of specimens with $\theta \neq 0$, a sudden decrease in stiffness could be observed followed by a second linear branch before a gradual decrease of stiffness started to occur. This kind of behaviour was already noticed by Base et.al.[1973,[2]] and Lawrence[1983,[28]] and is denoted with 'bi-linear' behaviour. In Figure 89 the m-κ diagrams for the JO.VER and JO.HOR series of Figure 88 are shown again including two best fits for the JO.HOR diagram to illustrate this behaviour.

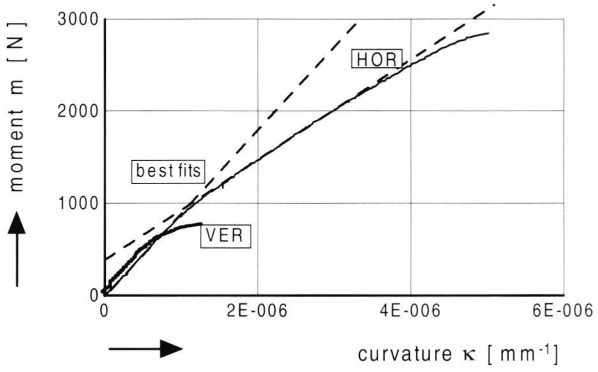

Figure 89 Examples of moment-curvature diagram of JO.VER and JO.HOR specimens including linear regression lines through linear parts of the curves (wc-JO90 + GPM masonry of 1992-1994)

In Table 12 and Table 13 average stiffness values and curvatures are presented.

Table 12 Average flexural stiffness values and curvatures of wc-JO90 + GPM series of 1992-1994

θ [°]	mortar	E_{1st} [N/mm^2]	r_{lin} [-]	$\kappa_{lin;yy}$ [10^{-6} mm^{-1}]	E_{2nd} [N/mm^2]	$\kappa_{u;yy}$ [10^{-6} mm^{-1}]
0 (VER)	1:½:4½	9460 (12)	0.71 (10)	0.51 (18)	-	1.51 (16)
30		11480 (5)	0.56 (21)	0.71 (27)	8751 (10)	2.05 (39)
70		11700 (12)	0.40 (20)	1.90 (21)	-	6.23 (10)
90 (HOR)		11090 (8)	0.31 (27)	0.97 (33)	7435 (7)	5.18 (11)
70	1:1:6	9410 (6)	0.22 (14)	1.00 (23)	-	7.42 (11)

Table 13 Average flexural stiffness values and curvatures of different wc-JO96 + GPM series of 1996-1997

θ [°]	head joints	mortar	E_{1st} [N/mm^2]	r_{lin} [-]	$\kappa_{lin;yy}$ [10^{-6} mm^{-1}]	E_{2nd} [N/mm^2]	$\kappa_{u;yy}$ [10^{-6} mm^{-1}]
90 (HOR)	filled	1:2:9	11980 (15)	0.32 (8)	0.92 (28)	6980 (23)	6.14 (14)
	unfilled	1:2:9	5830 (6)	0.30 (19)	1.56 (21)	-	7.01 (8)
		1:2:12	5460 (6)	0.41 (32)	2.13 (47)	-	6.29 (20)
70	filled	1:2:9	10090 (0)	0.49 (20)	0.70 (1)	-	2.08 (35)

In general the specimens in the JO.VER series showed a linear behaviour up to 70% of the failure load. Lawrence[1983,[28]] reported linear behaviour up to failure load for specimens bent in the 'VER'-direction. However, m-κ diagrams presented by Lawrence

show deviations from linear behaviour at 80 to 90% from the failure load. Beyond the 70% load level non-linear behaviour started to occur that was contributed to micro cracking in the ultimate fibres of the bed joints.
The curvature of the intercept between the two regression lines of all diagrams in the JO.HOR series lay between $1\cdot10^{-6}$ mm^{-1} and $1.5\cdot10^{-6}$ mm^{-1}. The mean curvature at failure in the JO.VER series was $1.6\cdot10^{-6}$ mm^{-1}. If it is assumed that the head joints and bed joints behave similarly, micro-cracking of the head joints should influence the behaviour of the JO.HOR specimens before the curvature of $1.6\cdot10^{-6}$ mm^{-1} is reached. It must be kept in mind that the wallettes were made as 'academic' masonry with properly filled head joints. On the basis of the experimental results, it was concluded that the second branch in the *m*-κ diagrams of the JO.HOR series could be explained by cracking of the head joints.
The second branch in the JO.30 series started approximately at a curvature of $1.7\cdot10^{-7}$ mm^{-1} (see Van der Pluijm[1996,[56]]). The corresponding curvatures in *n*- and *t*-direction are even smaller, so this behaviour could not be explained from cracking of the head joints. Non-linear behaviour as a result of partial cracking of the bed joint, where combined shear and torsional stresses act in the same direction, might have played a role.
In the JO.70 series of 1992-1994 (12 specimens) and of 1996-1997 (2 specimens) a gradual decrease in stiffness could be observed and bi-linear behaviour could not be detected. Deviations from linear behaviour of the JO.70 + 1:½:4½ series started to occur at ±40 % of the failure load. The mean magnitude of the curvature $\kappa_{lin;yy}$ at this point was $1.9\cdot10^{-6}$. Transformed curvatures around the *n*- and *t*-axis were respectively $\kappa_{lin;tt} = 1.7\cdot10^{-6}$ and $\kappa_{lin;nn} = 0.2\cdot10^{-6}$. Comparing the curvature $\kappa_{lin;tt}$ value with that of the JO.HOR series where non-linear behaviour started to occur ($1.0\cdot10^{-6}$), it was expected that non-linear behaviour would have been visible at a lower load level in the JO.70 + 1:½:4½ series. A reason for this deviant behaviour could have been a high tensile bond strength of this series. The accompanying tensile bond tests indicated a high bond strength, but their representativeness was disputable.
Further theoretical considerations concerning the influence of cracking of head joint and bed joint in the tested bending directions will be forwarded in section 5.60.

From the test results, it could be concluded that the stiffness in all directions was the same when the 1:½:4½ mortar was applied. The stiffness of the wc-JO90 brick itself is 16700 N/mm^2 (see Table 33). This indicates that the influence of the bed joint in flexure in the series JO.VER on the masonry stiffness is approximately the same as the influence of the head joints in flexure and the bed joints in torsion in the JO.HOR series.

However, the ratio between horizontal and vertical flexural stiffness of approximately 1 must not be seen as a generally valid value for brick masonry, which can be concluded from the rather scarcely ratios found in literature. Lawrence[1983,[28]] reported a factor 0.54 between horizontal and vertical stiffness (perforated bricks). Cajdert[1980,[11]] presented the stiffness as a function of the bending stress. For perforated clay brick masonry, he found ratios between the horizontal en vertical stiffness varying between 0.7 at very low stress levels up to 2 at the point where the vertically spanning specimens failed. Results of Cajdert must be the consequence of micro-cracking resulting in non-linear behaviour. Test results obtained by the author indicated a rather constant stiffness ratio until the JO.VER specimens started to behave non-linearly.

The series of 1996-1997 offered the opportunity to observe the influence of unfilled head joints. Unfilled head joint could be considered as completely cracked head joint, however the transfer of compressive stresses remains possible in cracked filled head joints. Therefore, it can be expected that the stiffness of the second branch of JO.HOR specimens with head joints is greater than the stiffness of JO.HOR specimens with unfilled joints.

From Table 12, the conclusion could be drawn that mortar quality influenced the stiffness of the JO.70 specimens in a clear way, because E_{1st} reduced by 20% with a change of mortar from 1:½:4½ to 1:1:6. However, between the tests series wc-JO96 + 1:2:9 mortar and with 1:2:12 mortar of 1996-1997 with unfilled head joints, no significant difference could be observed. In chapter 2, it was already recognised that the conditions under which the mortar can hydrate and bond develops, are more important for the properties of the hardened mortar in the joint than the mortar composition.

Vermeltfoort[1992,[81]] reported stiffness values varying between 10000 and 13200 N/mm^2 for masonry series made with wc-JO90 units from the same batch in combination with mortars 1:½:4½ tested in compression. Ignoring extreme values, the stiffness of masonry in tension, ranged between 5000 and 10000 N/mm^2. These values correspond with joint stiffnesses ranging between 2500 and 6000 N/mm^2 (see values for wc-JO90 + 1:½:4½ series in Table 38 on page 219).

The observed values in vertical flexure can be compared with values obtained in tension and compression. The stiffness value in vertical flexure, fitting in the range found in compression, seems to be rather high, if it is assumed that the behaviour in flexure is a mix of behaviour in compression and tension. It seems to be in contradiction with the findings concerning non-bonded areas as presented in section 2.3.6. The following aspects contribute to differences between tension, flexure and compression stiffness (keeping in mind that all observations concern the first, rather linear part of the load-displacement diagrams).

- In flexure and compression, the stiffness was determined for a relatively large piece of masonry, in contrast with the measurements in tension, where the gauge length was limited to one joint and two 'slices' of units resulting in a large contribution of the joint+interface. Calculating the stiffness of masonry under tension with the same ratio between joint and unit thickness within the gauge length as in flexure and compression, using eq. (3), page 17, a value ranging between 7800 and 12300 N/mm^2 in tension can be derived.
- The stress level, at which the initial stiffness in compression has been determined, was much higher, approximately 10-20 times higher. For lower stress levels a higher stiffness value will be found in compression although the effect will be limited.
- The loading rate in tension and flexure was higher than in compression.
- It can be expected that the two previous points, although not quantified, will lead to a higher stiffness in compression comparable with tension and flexure than reported by Vermeltfoort.

Taking the above points into account, it was concluded that the stiffness values found in (vertical) flexure corresponded well with the values found in compression and tension.

4.6 Behaviour of Calcium Silicate Masonry Series (CS-block)

In Figure 90 characteristic moment-curvature diagrams are shown for the three different angles θ used in the 1992-1994 series.

In Table 14 the average stiffness values for the CS series of 1992-1994 are shown and in Table 15 for the series of 1996-1997.

Table 14 Average flexural stiffness values and curvatures of the CS-block92 + TLM series of 1992-1994

θ [°]	E_{1st} [N/mm^2]	r_{lin} [-]	$\kappa_{lin;yy}$ [10^{-6} mm^{-1}]	E_{2nd} [N/mm^2]	$\kappa_{u;yy}$ [10^{-6} mm^{-1}]
0 (VER)	13920 (11)	0.88 (10)	0.66 (21)	-	0.85 (14)
45	11360 (14)	0.84 (15)	0.75 (30)	-	1.10 (38)
90 (HOR)	12990 (12)	0.52 (25)	1.07 (37)	7250 (27)	3.13 (10)

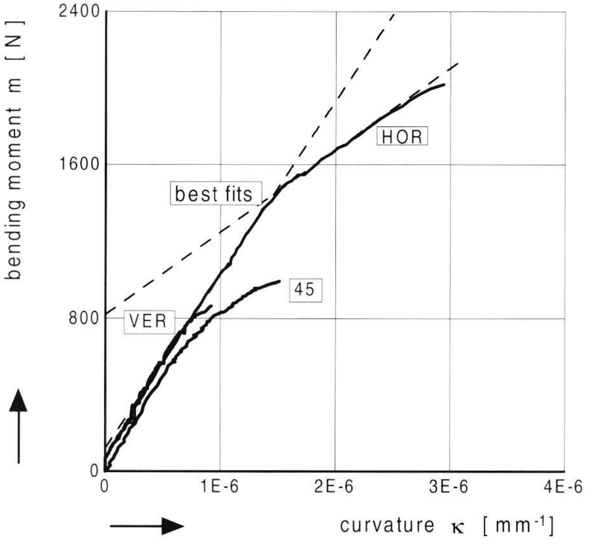

Figure 90 Examples of moment-curvature diagrams of the CS-block92 + TLM series of 1992-1994

Table 15 Average flexural stiffness values and curvatures of CS-block96 + TLM series of 1996-1997 ($\theta = 90°$)

head joint	tongue	E_{1st} [N/mm^2]	r_{lin} [-]	$\kappa_{lin;yy}$ [10^{-6} mm^{-1}]	E_{2nd} [N/mm^2]	$\kappa_{u;yy}$ [10^{-6} mm^{-1}]
filled	present	11900 (7)	0.28 (36)	0.55 (30)	9380 (7)	3.12 (11)
filled	removed	13420 (14)	0.27 (15)	0.57 (18)	11540 (20)	3.27 (5)
unfilled	present	6510 (12)	0.84 (1)	2.82 (3)	-	3.56 (5)
unfilled	removed	8170 (17)	0.78 (10)	2.20 (17)	-	3.05 (3)

Bi-linear behaviour was only present in the CS.HOR series. The average curvature at failure for the CS.VER specimens equalled $0.85 \cdot 10^{-6}$ mm^{-1}. In the CS.VER series non-linear behaviour starts to occur at 85% of the failure load. The point where the second branch started in the JO.HOR series varied between $0.5 \cdot 10^{-6}$ and $1.0 \cdot 10^{-6}$ mm^{-1}. For the calcium silicate block masonry, it was also concluded that cracking of the head joints caused the bi-linear behaviour in the CS.HOR series.

The stress states in head en bed joints were approximately equal in the CS.45 series, not only because of the equal orientation of head joint and bed joint, but also because of the geometry of the CS-block masonry. Therefore, cracking of head joint and bed joints should occur at approximately the same moment and could not cause bi-linear behaviour.

As expected, the calcium silicate masonry, having thin joints, homogeneous units and small ratios between joint thickness and unit height or width, behaved rather uniform. Rather unexpected was the higher stiffness of specimens with removed tongues, compared with specimens with tongues and grooves. The probability of the difference was at most 20% (t-test). Effects that might have played a role were the rough bond surface where the tongue was removed and improved hardening conditions of the mortar due to its larger volume in the groove.

4.7 FLEXURAL STRENGTH

4.7.1 INTRODUCTION

Comparing the strength values obtained in different directions implies comparison of results of specimens made with different mortar batches, on different days.
Consequently the conditions under which the series were made were different, although the series were made with the same pre-treatments and curing conditions in 1992-1994. Controlling the pre-treatments and curing conditions is not enough to obtain completely similar conditions, because other (non-controlled) factors play a role in the development of bond. As an example the JO.30 series can be mentioned. The average strength value originated from two sub-series, one made in a period of two days in December 1992 and the other made within two days in January 1993. Within a sub-series, specimens made on different days showed a different average strength but that difference did not appear to be statistically significant. However there was a significant difference (probability of 2%) between the strength of the sub-series specimens made in December and January. A similar situation could be observed in the CS.45 series.
This again shows the variability of bond strength. Consequently, it is difficult to make an objective comparison between series in which bond failure determines the strength. Although tensile bond tests were carried out parallel with most series in order to facilitate a comparison, the results of the tensile tests of the 1992-1994 series were not representative for the flexural bond strength of the wallettes and ignored here. Numerous reasons for this are discussed in Van der Pluijm[1996,[56]]. The series of 1996-1997 were accompanied by deformation controlled tensile tests. The average tensile bond strength of the tensile tests has already been presented in Table 2, chapter 2. Every single test result can be found in Table 38 in Appendix B 'Experimental Results'.
To make a comparison between the different series of 1992-1994 possible, it was assumed that their mechanical properties belonged to the same population, since per masonry type, the units came from one batch and the same pre-treatments and curing

regimes were applied. The fact that significant differences between sub-series were found is ignored. An example hereof are the results of the already mentioned JO.30 series that could be split into two sub-series with mean flexural strength of 0.80 and 0.66 N/mm^2 instead of the presented value equal of 0.73 N/mm^2 for the whole series.

An analysis of the strength, influenced by the orientation of the bending axis is presented in section 5.6 on the basis of a theoretical model. Here, a general discussion is presented. It is considered to be important to correlate the cracking patterns and the measured strengths.

4.7.2 FLEXURAL STRENGTH OF CLAY BRICK MASONRY

In Table 16 and Table 17 the mean results of the bending tests with clay brick masonry wallettes are collected.

Table 16 Average flexural strength of wc-JO90 + GPM series of 1992-1994

θ [°]	mortar	$f_{fl;yy}$ (M_u / W_{el}) [N/mm^2]	*Influence of dw.* $\sigma_{dw;max}$ / $f_{fl;yy}$ [%]
0 (VER)	1:½: 4½	0.45 (17)	1.7
30	1: ½:4½	0.73 (16)	1.2
70	1: ½:4½, 1:1:6	2.45 (7)	0.7
70 (oblique)	1: ½:4½	1.54 (-)	1.1
90 (HOR)	1:½: 4½	1.96 (13)	0.6

Table 17 Average flexural strength of wc-JO96 + GPM series of 1996-1997

θ [°]	head joint	mortar	$f_{fl;yy}$ (M_u / W_{el}) [N/mm^2]		*Influence of dw.* $\sigma_{dw;max}$ / $f_{fl;yy}$ [%]
70	filled	1:2:9	0.71 (18)		1.8
90 (HOR)	filled	1:2:9	1.68 (21)	1.56 (17) *)	0.5
	unfilled	1:2:9	1.46 (7)		0.5
	unfilled	1:2:12	1.37 (18)		0.5

*) mean of filled and unfilled series with 1:2:9 mortar

Apart from the flexural strength, the possible influence of the ignored deadweight is also presented. It can be observed that the influence of the deadweight is limited.

Depending on the tested angle, different cracking patterns were observed. In vertical bending (0^o), the crack followed a bed-joint. In horizontal bending the crack nearly always followed a straight line through the head joints and the middle of the units. The specimens in the series JO.30 were manufactured in such a way that an oblique pattern could be formed parallel to the bending axes. Nevertheless, in most cases the cracks followed one bed joint in a straight line. In two of the JO.30 specimens a so-called Z-crack appeared. This type of crack followed a bed joint and jumped over to another bed joint via a head joint somewhere in the middle of the crack (see Figure 91).

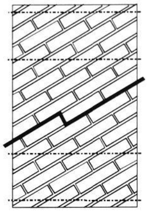

Figure 91 Z-crack in the JO.30 series

The strength of those specimens did not differ from the rest of the series.
In the JO.VER and JO.30 series, bond between units and mortar governed the strength.

From the theoretical model presented in chapter 5, it became clear that an oblique pattern with the wc-JO90 bricks (in fact nearly all masonry with the same geometrical dimensions) could occur at an angle of 70 degrees, when the bond strength is not too high compared to the tensile strength of the units.
In most JO.70 specimens, the crack was orientated in the direction of the bending axis, running through units and some head joints. Only in three JO.70 specimens (one in '92-'94 and two in '96-'97) an oblique crack occurred.

The number of units that were cracked or the greater length of the crack caused the higher strength of the JO.70 series compared with the JO.HOR series of 1992-1994. This can be seen in Figure 92.

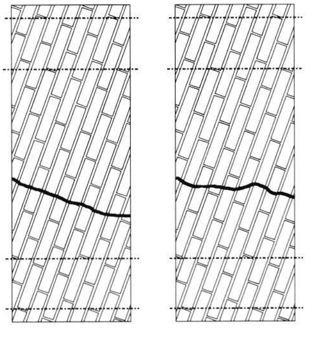

Figure 92 Two typical crack patterns in the JO.70 series of 1992-1994

For the JO.70 series of 1992-1994, the result of the test with the oblique crack is presented separately, because it significantly deviated from the other test results. The probability of the difference was 0.02 % (t-test). From the result it is apparent that a significant change in flexural strength for $\theta = 70°$ may occur with minor changes in other parameters. Within the series, a large difference in parameters between the specimen with the oblique crack and the other specimens is not likely. From a theoretical point of view some badly filled head joints may have caused the occurrence of the oblique crack. This point of view is explained in section 5.6.3.
The tensile bond strength of the JO.70 series of 1996-1997 was intentionally very low (0.15 N/mm^2, see Table 2, page 22) resulting in oblique cracks and the lowest average flexural strength in this direction.

The flexural strength of the JO.HOR series of 1992-1994 was governed by failure of the units.
The strength of the two different JO.HOR series of 1996-1997 with 1:2:9 mortar was somewhat influenced by presence/absence of head joints, but the difference was not significant (22% probability). Similar to the tests carried out in 1992-1994, the units governed failure. However a difference in crack patterns could be observed. In all specimens without head joints also one bed joint failed. This type of crack is referred to as mixed mode crack, because it can be regarded as the coincide of a straight crack through units and head joints and an oblique crack (see Figure 93).

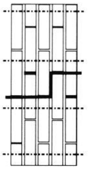

Figure 93 Mixed mode crack in a specimen of the JO.HOR series of 1996-1997 (wc-JO96+ 1:2:9 without head joints)

Causes for the lower strength of the JO.HOR series of 1996-1997 compared with that of 1992-1994 are:

- the difference in geometry of the specimen (see Figure 83). Only two failing units were present in 1996-1997 series in stead of three in the 1992-1994 series;
- the tensile strength of the wc-JO96 unit is 15 % less than the strength of the wc-JO90 unit (see Table 2, page 22).

If it is assumed that the flexural strength is directly proportional with the tensile strength of the units in the JO.HOR series, the first point can already explain the difference in

strength between the JO.HOR series +1:2:9 mortar of 1996-1997 and of 1992-1994. However the wc-JO96 units were less strong so the wallettes of 1996-1997 are 15% too strong, compared with those of 1992-1994. The fact that the fracture energy of both units was approximately equal and that the stiffness of the 1996-1997 unit was somewhat higher, might have resulted in less brittle behaviour and consequently a relatively high flexural strength of the wc-JO96 brick.
In the JO.HOR series of 1996-1997 with 1:2:12 mortar the units were no longer decisive for failure. The bond strength was low enough to cause 'oblique' cracks running through the bed joints and the (empty) head joints.

4.7.3 Flexural strength of calcium silicate block masonry

In Table 18 and Table 19 the mean flexural strength values of the calcium silicate block masonry with TLM are presented.

Table 18 Average flexural strength of CS-block92 + TLM series of 1992-1994

θ [°]	$f_{fl;yy}$ (M_u / W_{el}) [N/mm^2]	*Influence of dw.* $\sigma_{dw;max} / f_{fl;yy}$ [%]
0 (VER)	0.56 (13)	3.5
45	0.56 (25)	2.9
90 (HOR)	1.32 (9)	1.3

Table 19 Average flexural strength of CS-block96 + TLM series of 1996-1997 (θ = 90°)

head joint	tongue	$f_{fl;yy}$ (M_u / W_{el}) [N/mm^2]	*Influence of dw.* $\sigma_{dw;max} / f_{fl;yy}$ [%]
filled, unfilled	present, removed	1.21 (13)	1.1

The cracking patterns observed in the CS series are:

- a straight crack always following a bed-joint in the CS.VER and the CS.45 specimens;
- a straight crack running through head joints and units in CS.HOR specimens;
- a mixed mode crack running successively through a head joint, a unit, a head joint, a bed joint and a head joint in also in CS.HOR specimens;
- an oblique crack in one of the CS.45 specimens.

Bond failure governed both the CS.VER and CS.45 series. The relatively low strength of the CS.45 series compared with the CS.VER series will be discussed in section 5.6.3. In 50% of the CS.HOR specimens of 1992-1994 a mixed mode pattern (see Figure 94) occurred and in the other 50% a straight crack through units and head joints was visible after failure. Only in one CS.HOR specimen (with filled head joints and tongues and grooves present) of the 1996-1997 series a mixed mode crack occurred.

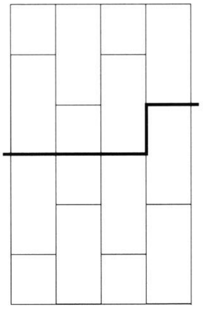

Figure 94 Mixed mode crack in the CS.HOR series

When the flexural strengths of these two patterns in the 1992-1994 series are compared, no significant difference could be detected. The average strength of the specimens with a mixed mode pattern equalled 1.35 N/mm^2 versus 1.29 N/mm^2 for the specimens with straight cracks.
Although different batches of units were used in the series of 1992-1994 and of 1996-1997, the strength in horizontal direction was nearly the same.

4.8 CONCLUDING REMARKS

Comparison of the results in the VER and HOR-series with clay brick and calcium silicate masonry has shown that cracking of the head joints caused the bi-linear behaviour.
The bi-linear behaviour found in other series may also arise from (micro)cracking due to complex stress combinations in the joints.

In oblique cracks, running alternately through head and bed joints, only occur when the bond strength is relatively low.
It is not possible to understand the flexural strength as a function of the angle between the bending axis and the bed joint directly from wallette tests very well. The cracks do not run parallel to the bending axis, and hence, complicated the stress distributions, making it impossible to interpret the strength from the test results directly.

5. MESO MODELS FOR MASONRY IN BENDING

To understand out-of-plane bending of masonry on the meso level, insight in the complex interaction between units and joints, caused by the difference in stiffness between units and joints, is necessary. On the basis of a qualitative analysis of the interaction, an analytical model has been developed. The model allows for the calculation of stresses in the joints and units for masonry subjected to bi-axial bending with torsion. A finite element (FE) model was used to verify the outcome of the analytical model.

Additional moments that occur in masonry due to stiffer units compared with joints, play an important role. Most important phenomena were the additional bending moments in the bed joint in case of torsion and the additional torsional moment in the bed joint in case of bending around the n-axis (horizontal bending).
Both the FE and analytical model gave insight in phenomena that occur in bending of masonry. The orthogonal stiffness moduli that were derived, corresponded well with experimental data. With a very simple approach, based on serial and parallel connections, the orthogonal stiffness moduli could also be determined.
A rational method used to establish the bending strength of masonry is presented. In this so called Multiple Crack Pattern (MCP) approach, different potential cracks were taken into account. A simple description was found in literature, that gave a reasonable match with the more rational MCP approach.

Keywords: meso level, finite element model, analytical model, orthotropic bending behaviour, Multiple Crack Pattern (MCP) approach

5.1 INTRODUCTION

In this chapter, meso models for masonry in bending are presented and discussed. The purpose of the models is the establishment of the behaviour of masonry at the macro level. The macro behaviour of the models is a result of the behaviour of the interacting components units and joints at the meso level. To deduce the macro behaviour, macro curvatures were imposed on the meso models at their boundaries. The macro curvatures were derived from thin plate theory that was assumed to be valid on the macro scale. At the meso level, all components were assumed to be isotropic. Due to the difference in stiffness between joints and units and their orthogonal layout, the macro behaviour is orthotropic. The relation between macro moments and macro curvatures (specified as tensors of the second degree, see SYMBOLS AND NOTATIONS on page 203) of an orthotropic material can be expressed as:

$$\begin{bmatrix} m_{tt} \\ m_{tn} \\ m_{nn} \end{bmatrix} = \begin{bmatrix} D_{11} & 0 & D_{13} \\ 0 & D_{22} & 0 \\ D_{31} & 0 & D_{33} \end{bmatrix} \cdot \begin{bmatrix} \kappa_{tt} \\ \kappa_{tn} \\ \kappa_{nn} \end{bmatrix} \tag{21a}$$

or for short as:

$$\vec{m} = \overline{D} \cdot \vec{\kappa} \tag{21b}$$

With the average bending moments of a meso model at its boundaries following from internal moments in different parts of the models, orthotropic flexural rigidities D_{ij} could be established.

As a consequence of the differences in stiffness between units and joints, a complex interaction occurs between units and joints, when masonry is bent. The differences in stiffness cause an unequal distribution of deformations over units and joints compared with the mean deformation of masonry as a whole in case of e.g. a constant bending moment. As a result, additional internal moments and forces exist, and consequently, the internal stresses in joints and units deviate from those normally found in a pure bending stress state of a plate.

A model has to be large enough be to be representative for all meso behaviour to occur. Limiting the size of the model, as far as possible, is important in the case of finite element models (FE models) because of limited computer resources. The displacements of meso (FE) models at their boundaries must link up with displacements of the orthotropic plate. In Figure 95 a piece of masonry is drawn. The dashed lines indicate symmetry planes for geometry and materials and also for the bending deformations.

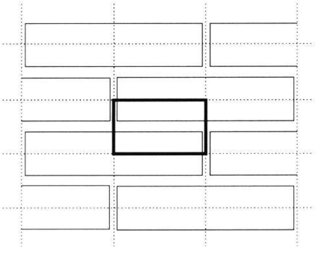

Figure 95 Face view of masonry in stretcher bond with a basic module in which all meso deformations occur.

The smallest part of masonry that fulfils those demands is indicated with a bold line in Figure 95 and will be denoted as the 'basic module'. In the indicated part of masonry, all deformations deviating from ordinary plate bending can occur, while at the boundaries the hypothesis of Bernoulli is fulfilled.

A FE model and an analytical model were developed for masonry in stretcher bond. With the FE model, it is in potential possible to explore the (non-linear) behaviour of any kind of masonry, taking the non-linear behaviour of units, joints and interfaces as presented in chapter 2 and 3 into account. Initially this was the main goal of the FE approach. The macro behaviour of the model (including the non-linear materials models via the materials models developed by Lourenço[1996,[38]] and implemented in the DIANA FE-code) could have been verified via the results of the experiments presented in chapter 4. However the non-linear calculations that were carried out suffered from numerical instabilities and with the chosen modelling it did not seems to be possible to obtain converged results. In Van der Pluijm[1999,[65]] the non-linear work carried out is discussed to some extent, as assistance to future researchers in this field.As a consequence, in this chapter only the modelling itself and linear elastic results are presented and discussed.

The analytical model is based on a relatively simple linear elastic approach. It can give insight in the effect of nearly every geometrical and stiffness property of the joints and units on the linear elastic macro properties of masonry without the need to use the laborious FE approach. To evaluate its value, the results of the analytical model were compared with those of the FE model. This was considered as a better check of the analytical model than comparing the analytical results with experimental results for the following reason. The analytical model needs input data on the meso level and this type of data is, at least for the joints, always a result of several assumptions to deduce meso stiffness values from experimental results (see e.g. section 2.3.2 on page 17). In the FE and analytical model, the meso properties can be taken exactly equal. Furthermore, both models assume ideal materials and perfect connections between components within the limitations of each model. Those idealisations make a comparison with experimental results less clear from a mathematical point of view because masonry is a far from ideal material, with voids, non-bonded contact zones etc.
The analytical model was also used to predict the flexural strength of masonry in various situations. The latter represents an 'engineer approach' and lacks a solid fundamental basis. Its usefulness will be discussed in section 5.6.

Before discussing the analytical model and the FE model, first a 'descriptive' analysis of bending of masonry is presented in which deviations from the average macro bending states are identified.

5.2 Descriptive analysis of bending of masonry

5.2.1 Introduction

In the analysis it was assumed that the units are stiffer than the joints. This assumption is nearly always made by practically the whole masonry (research) community, but this is not necessarily the case as has been indicated by Vermeltfoort[1998,[84]], who has shown that in ordinary masonry the joint stiffness can be approximately the same as the unit stiffness.
The analysis is divided into two pure bending states and a pure torsion (pure for masonry considered on the macro scale as a homogeneous composite):

1. bending around the axis perpendicular to the bed joint plane (horizontal bending)

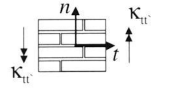

2. bending around the axis parallel to the bed joint plane (vertical bending);

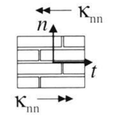

3. torsion

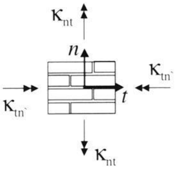

For a clear discussion of the internal distribution of moments, a right orientated orthogonal *t-n-z* co-ordinate system was defined. The *t*- and *n*-axis coincide with the mid-plane of the masonry. The *z*-axis runs perpendicular to the plane of the masonry. The *t*-axis coinciding with the direction of the bed joint, the *n*-axis running perpendicular to bed joint and the *z*-axis are drawn in Figure 96.

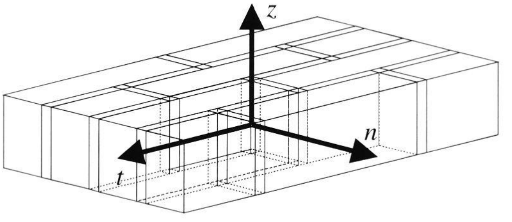

Figure 96 Definition of axes with respect to the bed joint direction and plane of masonry

In Figure 97 a piece of masonry in stretcher bond is presented, 'built' with the components that are considered in the analysis.

The cross joint is defined as the piece of the bed joint that is connected with a head joint. This definition clearly deviates from that given for the term 'cross joint' in BS6100:1992 part 5[10]. The length of the bed joint is equal to the lap of the units.

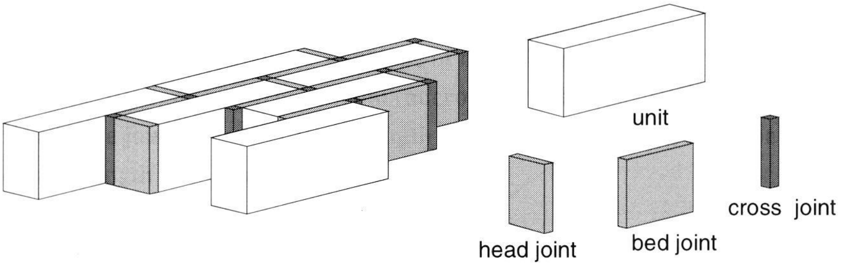

Figure 97 Overview of components considered in the analysis: unit, head joint, bed joint and cross joint

In the following three sections, a description of the three distinguished bending states is given. For each bending state, a constant curvature (for masonry considered on the macro level) was assumed.

5.2.2 Bending around the axis perpendicular to the bed joint plane (horizontal bending)

For masonry bent around the n-axis, deformations as presented in Figure 98 can be observed, if the units are considered to be infinitely stiff.

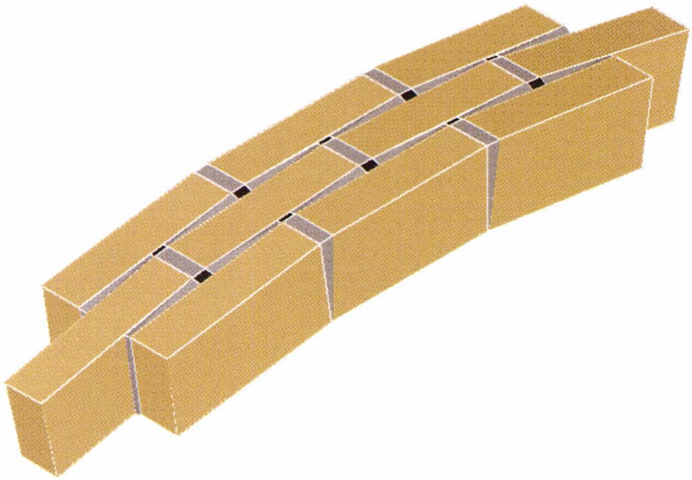

Figure 98 Deformed masonry bent around the n-axis (infinitely stiff units)

Units are not infinitely stiff and will also be bent, so in reality the deformations of joints, as shown in Figure 98, will be less pronounced.

The bed joints between overlapping units are distorted. This is a well known phenomenon, and widely recognised as an area where torsional failure may occur, resulting in a crack that runs alternately through head joints and bed joints. As a consequence of the resulting additional torsion moments $\hat{M}_{\mathrm{nt}}^{\mathrm{bj}}$ acting on the bed plane of the units, the bending moment $M_{\mathrm{tt}}^{\mathrm{u}}$ around the n-axis in the unit cannot be constant. In Figure 99 a half unit, seen from the face, is drawn with the moments acting on it.

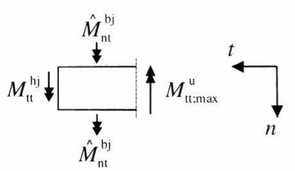

Figure 99 Equilibrium between additional torsional and bending moments acting on a half unit in masonry bent around the n-axis

The moment $M_{\mathrm{tt}}^{\mathrm{u}}$ will increase from a minimum value found in the connecting plane with the head joint to a maximum value in the middle of the unit.

The cross joints undergo a shear deformation between units and head joints. In Figure 100 a twisted bed joint and a shifted cross joint are presented in detail. If head joints are not present in the masonry, the cross joints still undergo a similar shift.

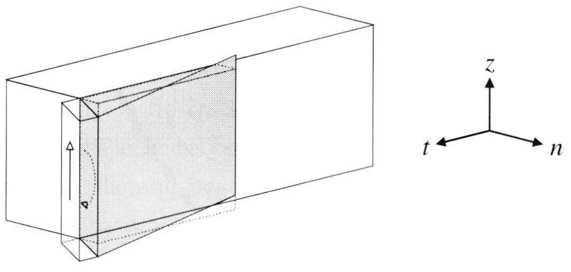

Figure 100 Detail of twisted bed joint and sheared cross joint due to a constant macro curvature κ_{tt}

The head joints or stiff units that exercise shear forces on the cross joints might cause the shear deformation of cross joints. It could also be assumed that torsion moments exercised by the bed joints on the cross joints 'create' the shear deformation. However, if there would be slits between cross joints and bed joints, the deformations of bed joints and cross joints would not change. Therefore, it is more obvious to assume that the shift of the cross joints is only caused by shear forces from the edges of the units (see Figure 101).

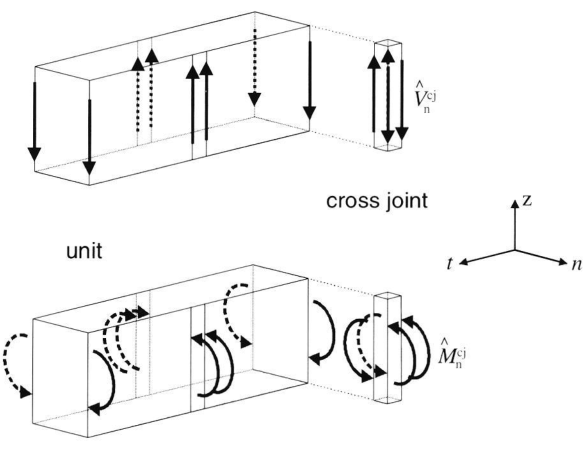

Figure 101 Concentrated shear forces and moments interacting between cross joints and units

This assumption implies that the shear deformation of a cross joint due to the difference between the vertical displacements of head joint and unit by which the cross joint is

enclosed, corresponds with the torsion deformation of the bed joint in the n-z plane. To obtain equilibrium of the cross joint, the shear forces must go hand in hand with bending moments as indicated in Figure 101.
The shear forces increase the curvature κ_{tt}^{u} of each unit in the same way and do not result in extra additional distortions of the bed joints.

It can be expected that the units impose their deformations on the bed joints and cross joints in the bonding area and that these joints are too thin to show important deviations from the imposed curvatures κ_{tt}^{u} by the units.
As already discussed the curvature κ_{tt}^{u} in the unit is not constant but increases from both ends towards the middle of the unit. This is the case in both units on either side of a bed joint, but in opposite direction. Therefore, the curvature κ_{tt}^{bj} cannot be constant over the thickness of the bed joint (in n-direction) but will show maxima on two diagonally opposite corners.

At one side a cross joint is connected to a head joint and at the opposite side to a unit. The bending curvature κ_{tt} in the head joint is greater than the bending curvature κ_{tt} in the middle of the unit. Because of the difference between the curvatures in the middle of the unit and head joint, the curvature κ_{tt} of the cross joint changes over its thickness in the direction of the n-axis. As a result the bending moment in the cross joint is not constant and a torsion moment must also be present in the cross joints.

If the units could deform as a beam, the bending moment m_{tt} in the units would also result in a lateral curvature $\kappa_{nn} = -\nu\kappa_{tt}$ according to linear elastic continuum mechanics. As a result of the non-constant bending moment $m_{tt,}$ a non-constant lateral curvature κ_{nn} of the units will develop to a certain extent because of the greater stiffness of the units compared with the joints. As a consequence, the bed joints will undergo additional deformations. In Figure 102, the additional deformation only as a result of the non-constant part of the lateral curvature is presented.

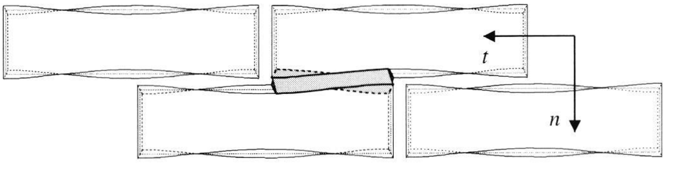

Figure 102 Face (tension side) view of deformation of units and one bed joint only as a result of the non-constant part of the lateral curvature κ_{nn} = -$\nu\kappa_{tt}$ of the units

From Figure 102 it can be observed that the bed joint undergoes an additional twist, resulting in additional torsion stresses.

5.2.3 BENDING AROUND THE AXIS PARALLEL TO THE BED JOINT PLANE (VERTICAL BENDING)

If the influence of the head joints is neglected, the analysis of the internal distributions of moments and curvatures would be very simple for a constant macro curvature κ_{nn}. The bending moments m_{nn} in units and bed joints would be equal and the difference in curvature between units and bed joints would follow directly from their difference in stiffness. However head joints are present, causing deviations from the sketched situation. It can be assumed that the curvature κ_{nn} of the head joints is the same as the curvature of the units between which they are located, but it can also be assumed that the curvature κ_{nn} of the cross joints is the same as the curvature of the bed joints between which they are located. Both assumptions lead to a singularity in the connecting plane between head joints and cross joints (see Figure 103a), because the bending moment m_{nn} in the head joint in the connecting plane with the cross joint would be less than the bending moment in the cross joint in the same connecting plane. In Figure 103b a possible distribution of deformations is drawn that gives a compatible connection between units and joints.

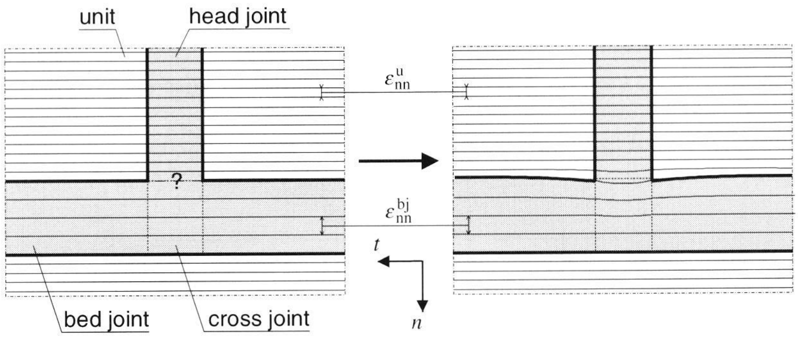

a) ε_{nn}-lines based on inconsistent assumptions b) estimate of real ε_{nn}-lines

Figure 103 Face view of a part of masonry bent around the t-axis with constant strain lines (distance between ε_{nn}-lines is a measure for the magnitude of ε_{nn})

The proposed distribution in Figure 103b shows that the part of the unit opposite to a head joint will not feel the influence of a head joint. In generally, it will depend on the geometry of the masonry and the differences in stiffness between joints and units. If an influence is felt, the bending moment in the units decreases towards the middle of the unit where the cross joints are located, leading to additional deformations similar to

those presented in Figure 102. It is expected, however, that this effect, if it is present at all, will be small.
In Figure 103b it can be observed that parts of a unit that are connected with head joints always will undergo a local increase of the curvature $\kappa^{\mathrm{u}}_{\mathrm{nn}}$, and consequently, local torsion moments $m^{\mathrm{u}}_{\mathrm{tn}}$ in the units must exist to ensure equilibrium with the locally non-constant part of $m^{\mathrm{u}}_{\mathrm{nn}}$ in the unit. Also local shear forces will be present there.

A 'pure' bending deformation around the t-axis implies that the curvature around the n-axis is zero, but only for masonry at the macro level. Because the units are stiffer than the joints, the units will be able to develop a lateral curvature $\kappa^{\mathrm{u}}_{\mathrm{tt}} \neq 0$. To obtain an overall $\kappa_{\mathrm{tt}} = 0$ for the masonry, the curvatures in the units must be compensated by opposite curvatures of the head joint. The curvature $\kappa^{\mathrm{u}}_{\mathrm{tt}} \neq 0$ involves all aspects mentioned in the previous section, although the magnitude of the corresponding moments may be expected to be much smaller than in this bending case.

5.2.4 Torsion

When masonry is twisted and the units are considered to be infinitely stiff, deformations as presented in Figure 104 can be observed.

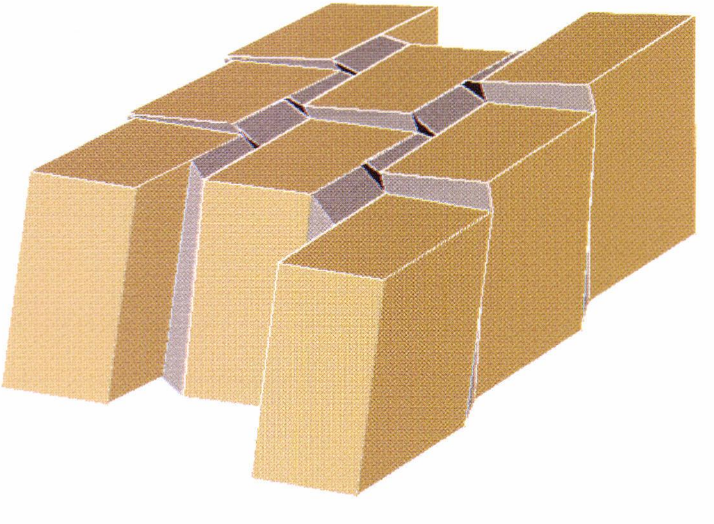

Figure 104 Deformed masonry twisted around n- and t-axis (infinitely stiff units)

Again, in reality, the deformations as shown in Figure 104 will be less pronounced.

The following observations can be made from Figure 104

- The head joints all are deformed in the same manner.
- The cross joints are twisted in an extreme way.
- The bed joints undergo an additional bending deformation.

First the additional bending moments in the bed joints are considered. The bending moments are caused by the different rotation of overlapping units in adjacent courses around the *t*-axis as already was observed in Figure 104. In Figure 105, 3 units from Figure 104 are drawn again with more space between them.

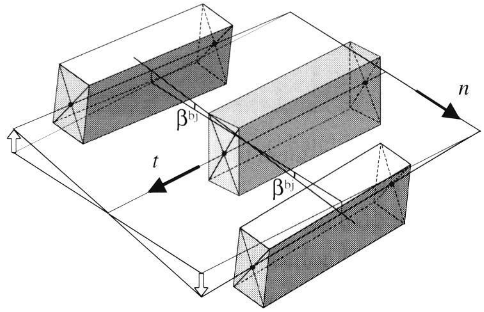

Figure 105 Rotation of overlapping units in adjacent courses in twisted masonry

The average rotation of a unit around the *t*-axis is determined by the location of its centre in *t*-direction. So, the two units with the equal position in *t*-direction rotate over the same angle β relatively to the unit between them. As a result the curvature of the bed joints is changed resulting in additional bending moments $\hat{M}_{\mathrm{nn}}^{\mathrm{bj}}$ acting on each unit, see Figure 106.

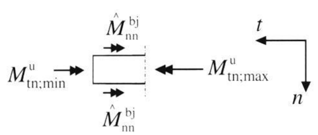

Figure 106 Equilibrium between additional bending $\hat{M}_{\mathrm{nn}}^{\mathrm{bj}}$ and torsion moments acting on a half unit in twisted masonry

As a result, the torsion moment in the unit is not constant, but increases from a minimum value found at the head of the unit to a maximum value in the middle of the unit.

This phenomenon can be compared with the additional torsional moment in the bed joints in case of bending around the *n*-axis. Now the uneven 'distribution of the torsion' over units and joints causes additional bending moments in the bed joints and non-constant torsion moments in the units.

In Figure 107, the additional bending of the two adjoining bed joints and the cross joint in between them are presented in detail.

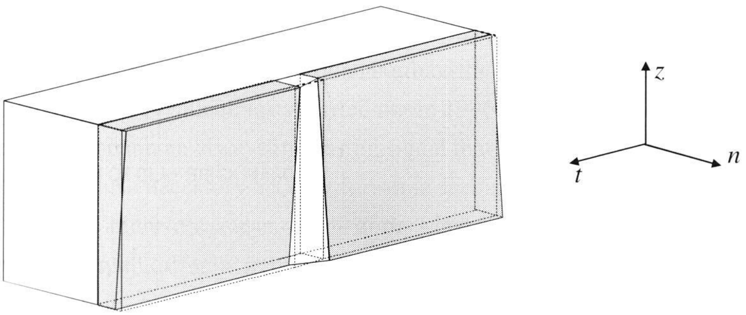

Figure 107 Additional torsion of cross joints due to the additional bending deformation of the bed joints

Similar to the shifted cross joint in case of bending around the n-axis, it can be argued that the head joints and opposite units may exercise respectively torsion moments and two opposite concentrated bending moments, or that the bed joints are applying additional torsion moment onto the cross joint. Similar remarks about the likelihood of the presence of additional torsion moments between cross joints and bed joints as in section 5.2.2 can be made.

The torsion of cross joints at the intersection with units is less than the torsion at the intersection with the head joint. So the torsion $\kappa_{\mathrm{nt}}^{\mathrm{cj}}$ changes over its thickness in the n-direction, and as a consequence, there must exist a non-constant additional bending moment including shear forces to ensure equilibrium of the cross joint.

5.3 ANALYTICAL MESO MODEL

5.3.1 INTRODUCTION

In the previous section, deviations from ordinary bending behaviour were identified. In this section 5.3, a relatively simple analytical model is presented taking the deviations to a certain extent into account. Mathematical details about the model can be found in Appendix C 'Meso models'.

The model assumes, as far as possible, constant internal forces and moments in the different parts. The model was not intended to obtain three-dimensional stress distributions within the components. As an example, the non-constant curvature κ_{tt}^{bj} over the thickness of the bed joint (in n-direction) mentioned on page 124 in section 5.2.2, was ignored in the model. Of course, it was not always possible to assume constant internal forces to obtain a reasonable model. An example is the increasing bending moment in the unit from its head towards its middle, as has been explained in section 5.2.2. Using average deformations within parts implied that especially the cross joint could not be modelled correctly at all. The large gradients of curvatures within and around the cross joints, shown in the previous section, make it difficult to model it analytically.
The question arises if it has any advantage to take the cross joint into account in the analytical model. Its contribution to the overall stiffness of the masonry is very limited. Another influence of the cross joint occurs when cracking or failure of the masonry is considered. Ignoring the cross joint and the additional forces it exercises on other parts, might increase the derived masonry strength. However, the strength of the cross joint is limited to the bond or mortar strength. We have seen that especially the corners of the cross joint are loaded by concentration of stresses. It can be expected that the cross joint itself has failed before it could have an influence on failure of the units, because of the difference in bond/mortar strength of the mortar and the tensile strength of the unit. As this is the case, the cross joint has to be excluded from the model to calculate a new stress state. In other cases, where the cross joint is not decisive for failure, its influence on the failure strength can be expected to be limited. It was concluded, that the influence of the cross joint was limited compared with the crude approximation of the distribution of internal forces in the analytical approach. Therefore, the cross joint was not taken into account in the analytical model. By comparing the outcome of the analytical and the FE model, the influence of this choice is reconsidered in section 5.5.1.

For each of the components (units, bed joints and head joints as defined in Figure 97) in the analytical model, equilibrium and compatibility were considered. This was done on the basis of assumed distributions of moments and deformations in each part. Moments and bending deformations within parts were, in most cases, related by the constitutive relations of thin plate theory.
The components were supposed to consist of homogeneous isotropic materials. Head joints and bed joints were considered as two separate materials, enabling the analysis of less stiffer head joints or even headless masonry.

When connecting parts, kinematic and static transitional conditions have to be taken into account. Because the constitutive relations of thin plate theory were used, it seems logical to use the same theory for the transitional conditions. It must be realised, however, that exactly at the intersecting planes between the different parts, local deviations from the assumed moments occur (see e.g. Figure 103).
The chosen approach led to a situation that the sum of curvatures in the different parts along their centre lines equals the macro curvature and that equilibrium and compatibility exist between units, head joints and bed joints but only on the average.
In the three following sections the model is explained on the basis of the three standard macro bending cases:

- horizontal bending;
- vertical bending;
- torsion.

In Figure 108 symbols for the geometrical dimensions of the masonry components are defined. The thickness of the units and joints perpendicular to plane of the wall equals d.

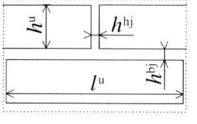

Figure 108 Overview of symbols for the geometrical dimensions of the masonry components

5.3.2 MODELLING OF HORIZONTAL BENDING AROUND THE *n*-AXIS

The additional torsion moments in the bed joint acting on the units are determined by the differential rotation $\psi^{bj} \cdot h^{bj}$ of two units enclosing a bed joint. To be able to calculate ψ^{bj}, it was assumed that the curvature κ_{tt}^{u} in the unit increases linearly from its minimum value in the connecting plane with the head joint towards its maximum in the middle of the unit (Van der Pluijm[1994,[52]]). Now, the curvature in the units is assumed constant in the area between the cross joints. Compared with Van der Pluijm[1994,[52]] this is a minor modification. In Figure 109 the assumptions concerning the curvature κ_{tt}^{u} in the masonry courses are shown as a function of t.

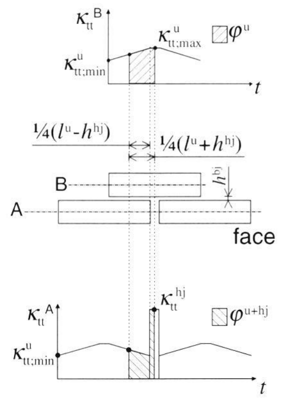

Figure 109 Curvatures κ_{tt} in units and head joints in t-direction

Although this distribution of curvatures was derived by the author independently, Lawrence[1983,[28]], already made similar assumptions, of which the author became aware by a more recent publication of Lawrence[1995,[33]]. In his analysis Lawrence ignored the influence of the lateral curvatures, contrary to the approach followed here.
The distortion of the bed joint must be compatible with the rotations of the units enclosing the bed joint (see Figure 109):

$$\varphi_{tt}^{u+hj} - \varphi_{tt}^{u} = \psi_{nt}^{bj} \tag{22}$$

With eq. (22) and the assumptions concerning the curvature κ_{tt}^{u} in the units according to Figure 109, it is possible to express ψ^{bj} explicitly into the plate bending curvatures of the components. For the constitutive relation between $\hat{M}_{nt}^{bj}$ and ψ^{bj} thin plate theory was used by assuming that $\hat{M}_{nt}^{bj}$ is equivalent to an equally distributed torsion moment $\hat{m}_{nt}^{bj} \cdot \frac{1}{2}(l^{u} - h^{hj})$ according to thin plate theory.

The curvature κ_{tt}^{u} in the unit is not constant but increases from both ends towards the middle of the unit. This is the case in both units on either side of a bed joint. In the mid-plane of the bed joint parallel to the t-z plane, the curvature κ_{tt}^{bj} is constant, when it is taken equal to the average of both unit curvatures enclosing it, on the basis of the assumed curvatures in both units according to Figure 109. The deviations of κ_{tt}^{bj} from the mean in the mid-plane are ignored in the model. So, the average curvature $\bar{\kappa}_{tt}^{bj}$ of the bed joints (with a length equal to ½(l^{u}-h^{hj}) equals:

$$\bar{\kappa}_{tt}^{bj} = \tfrac{1}{2}(\kappa_{tt;min}^{u} + \kappa_{tt;max}^{u}) \tag{23}$$

Equilibrium between head joints and head of the units demands:

$$m^{\mathrm{u}}_{\mathrm{tt;min}} = m^{\mathrm{hj}}_{\mathrm{tt}} \tag{24}$$

5.3.3 Modelling of vertical bending around the t-axis

It was assumed that the curvatures $\kappa^{\mathrm{bj}}_{\mathrm{nn}}$ and $\kappa^{\mathrm{u}}_{\mathrm{nn}}$ were constant. Furthermore, it was assumed that curvatures in the head joints are forced to follow those of the units, similar to the assumption for the bed joints in case of horizontal bending:

$$\kappa^{\mathrm{hj}}_{\mathrm{nn}} = \kappa^{\mathrm{u}}_{\mathrm{nn}} \tag{25}$$

Equilibrium between units and bed joint in the lap between units and joints demands:

$$m^{\mathrm{bj}}_{\mathrm{nn}} = m^{\mathrm{u}}_{\mathrm{nn}} \tag{26}$$

5.3.4 Modelling of torsion

The magnitude of the additional bending moments is determined by the differential rotation β^{bj} between to units overlapping each other in adjacent courses (see Figure 105).
Similar to assumptions made for the non-constant bending curvature $\kappa^{\mathrm{u}}_{\mathrm{tt}}$, the torsion $\kappa^{\mathrm{u}}_{\mathrm{tn}}$ of the unit in *t*-direction is supposed to increase linearly from a minimum value found at the head of the unit towards a maximum value found in the area at the middle of the unit between the cross joints. It was assumed that the torsion in head joints and units as a function of *t* had exactly the same course as that assumed for $\kappa^{\mathrm{u}}_{\mathrm{tt}}$ and $\kappa^{\mathrm{hj}}_{\mathrm{tt}}$ (see Figure 109 and Figure 105 where β^{bj} was defined), hence:

$$\varphi^{\mathrm{u+hj}}_{\mathrm{tn}} - \varphi^{\mathrm{u}}_{\mathrm{tn}} = \beta^{\mathrm{bj}} = \hat{\kappa}^{\mathrm{bj}}_{\mathrm{nn}} h^{\mathrm{bj}} \tag{27}$$

With eq. (27) and the assumptions concerning the additional torsion in the units in correspondence with Figure 109, it is possible to express $\hat{\kappa}^{\mathrm{bj}}_{\mathrm{nn}} h^{\mathrm{bj}}$ explicitly into the torsion of the components. The additional bending moment was simply calculated with the usual constitutive equation from thin plate theory.
The increase of the torsion $\kappa^{\mathrm{u}}_{\mathrm{tn}}$ of the unit was taken into account by assuming that the bending moments twist a unit like a beam. Therefore a constitutive relation according to membrane analogy was used for the non-constant part of the torsion moment in the unit (Timoshenko et al. [1970,[76]], art. 109). This way of modelling originated from the findings of the FE analyses. As a consequence round going shear stresses are present in the cross sections of the units perpendicular to the *t*-axis.

As a result of the non-constant $\kappa^{\mathrm{u}}_{\mathrm{tn}}$, the torsion $\kappa^{\mathrm{u}}_{\mathrm{nt}}$ varies in the same manner. The torsion in the bed joints and head joints was assumed to be constant.

To ensure equilibrium between the torsion moments in bed joint, head joint and unit, the torsion moments in the connecting planes were replaced by equivalent vertical forces equal to the torsion moments (Kirchhoff shear forces).

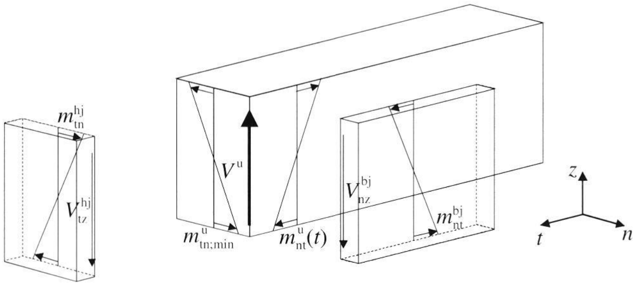

Figure 110 Equilibrium of shear moments via equivalent shear forces

Considering equilibrium between units bed joints and head joints at the corners of the units leads to:

$$V^{u} = V_{tn}^{hj} + V_{nt}^{bj} \tag{28}$$

At the corner $m_{nt}^{u}(t)$ equals $m_{tn;min}^{u}$, hence:

$$2m_{tn;min}^{u} = m_{tn}^{hj} + m_{nt}^{bj} \qquad (29)a$$

If no head joints are present, eq. (29)a becomes:

$$m_{tn;min}^{u} = m_{nt}^{bj} \qquad (29)b$$

5.3.5 COMPATIBILITY WITH THE MACRO DEFORMATIONS

Horizontal bending

Per course, the curvatures in units and head joints added together, must be compatible with the imposed masonry curvature (see Figure 111). For the rotations following from the curvatures along line p through units and head joints (see Figure 112) compatibility of the curvatures in units and head joints demands:

$$\varphi_{\mathrm{tt}} = \varphi_{\mathrm{tt}}^{\mathrm{u}} + \varphi_{\mathrm{tt}}^{\mathrm{hj}} \tag{30}$$

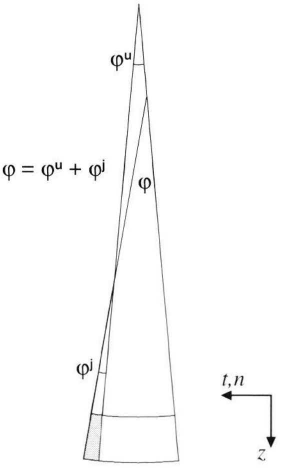

Figure 111 Compatibility of bending angles in units and joints with macro bending angle

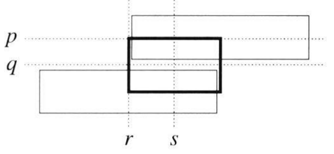

Figure 112 Lines where compatibility is ensured

This must be also valid along line q through the bed joint and the cross joint. If it is assumed that the curvature $\kappa_{\mathrm{tt}}^{\mathrm{cj}}$ in the (not modelled) cross joint is equal to the average of the curvatures in the head joint and the unit, such a demand is superfluous. Along line q, $\kappa_{\mathrm{tt}}^{\mathrm{bj}}$ and $\kappa_{\mathrm{tt}}^{\mathrm{cj}}$ can then be expressed in the curvatures $\kappa_{\mathrm{tt}}^{\mathrm{hj}}$ and $\kappa_{\mathrm{tt}}^{\mathrm{u}}(t)$, resulting in exactly the same compatibility equation as along line p.

Vertical bending

The curvature in the bed joint together with the curvature in the unit must be compatible with the imposed macro curvature so:

$$\varphi_{\mathrm{nn}} = \varphi_{\mathrm{nn}}^{\mathrm{u}} + \varphi_{\mathrm{nn}}^{\mathrm{bj}} \tag{31}$$

This must be valid along lines r and s. Because of the assumptions, expressed in eq. (25), and assuming that:

$$\kappa_{\mathrm{nn}}^{\mathrm{cj}} = \kappa_{\mathrm{nn}}^{\mathrm{bj}} \tag{32}$$

the compatibility along line r is implicitly fulfilled by eq. (31).

Torsion

In the two directions the curvature in both directions n and t must be compatible with the macro curvatures.

Along line p:

$$\varphi_{\mathrm{tn}} = \varphi_{\mathrm{tn}}^{\mathrm{u}} + \varphi_{\mathrm{tn}}^{\mathrm{hj}} \tag{33}$$

Along line *s*:

$$\varphi_{\mathrm{nt}} = \varphi_{\mathrm{nt}}^{\mathrm{u}} + \varphi_{\mathrm{nt}}^{\mathrm{bj}} \tag{34}$$

For the compatibility along lines *q* and *r* similar remarks as for horizontal and vertical bending can be made.

5.3.6 MACRO STIFFNESS OF THE ANALYTICAL MODEL

The equilibrium and compatibility equations of the previous sections result in total in nine 'end' equations presented in Appendix C 'Meso models'. By imposing each one of the macro curvatures κ_{tt}, κ_{nn} and κ_{tn} separately on the model, while the other two are zero, the rigidity moduli for the orthotropic plate can be derived by solving the nine equations. With the calculated curvatures of the components, and hence, the moments of the components for each of the three cases, the bending or torsion moments can be averaged at the boundaries, giving the average macro moments m_{tt}, m_{nn} and m_{tn}.
With the macro curvatures and macro moments both known, the orthotropic rigidity moduli can then be calculated.
In case of torsion, round going shear stresses in the middle of the unit due to the additional torsion moment are present (see Figure 113a).

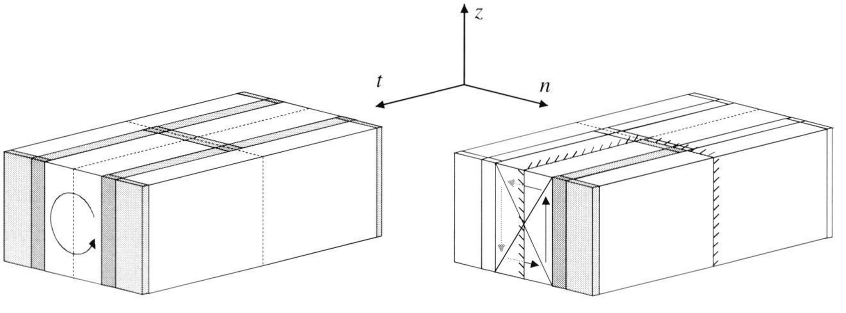

a) Additional torsion moment $\hat{M}_{\mathrm{tn}}^{\mathrm{u}}$ in the middle of the unit

b) remaining vertical shear force at the boundary of one basic module

Figure 113 Additional torsion moment at the boundaries of basic modules

If only one basic module would be considered to determine the macro moments, a remaining vertical shear force would exist on the boundaries perpendicular to the *t*-axis as can be observed in Figure 113b. This would make the determination of the macro moments m_{tn} at such a boundary apparently dependent on the position where the

moment is being calculated. This is not the case, when four basic modules together are taken into account in calculating the average macro moments.
In general the calculated moments m_{tn} and m_{nt} are not equal. The moments can be divided in even and uneven parts (see Figure 114).

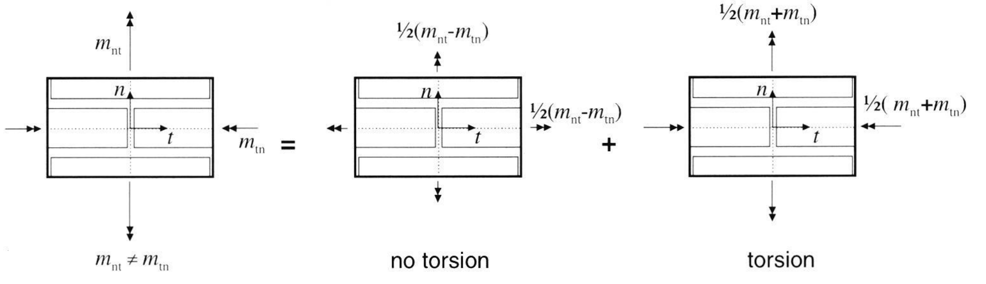

Figure 114 Division of torsional moments in even and uneven parts

Only the even parts cause plate torsion and were used to calculate the torsional rigidity D_{22}.

Before discussing results obtained with the analytical model, the FE model is introduced first in the next section and the macro behaviour of both the analytical and the FE model will be discussed and compared thereafter.

5.4 FE MESO MODEL

5.4.1 INTRODUCTION

In this section a three-dimensional (3D) FE meso model of the basic module (indicated in Figure 95 on page 118) is presented. In the model different material properties could be attributed to units, head joints, bed joints, cross joints and interfaces. At the boundaries of the model, macro curvatures were imposed by defining appropriate displacement fields for the nodes.
The linear elastic FE results were compared with those of the analytical approach.

5.4.2 3D FE MODEL

In the basic layout of the FE model is presented in Figure 115.

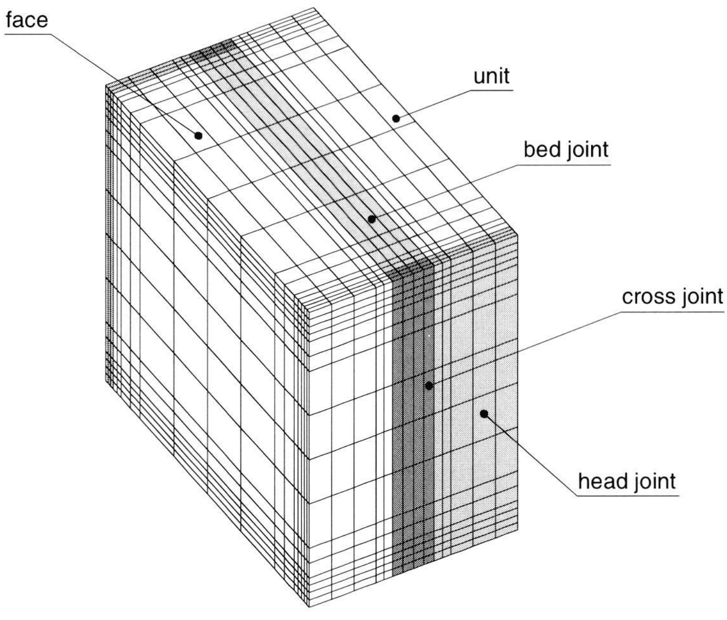

Figure 115 3D FE model of basic masonry module

An important difference with the analytical model is the incorporation of the cross joint and the fact that continuity of displacements and stresses over the intersecting planes between the components is fully ensured (within the limitations of the FE method). Furthermore, the internal deformations of the components do not have to fulfil the conditions according to thin plate theory, but they may deform three-dimensionally. Only on the outside of the basic module, the boundary conditions corresponding with the macro behaviour according to thin plate theory are imposed with displacement fields.

Different meshes were used, but they all had approximately the same structure. The units and joints were modelled with solid, brick type continuum elements. The interfaces between units and joints were modelled with 2D interface elements of a type corresponding with the solid elements. Application of interface elements is only useful for modelling non-linear material behaviour as derived in chapter 2 and 3, and therefore not discussed here further.

As shown in Figure 115, mesh refinements were applied towards the joints. The refinements towards the joints were applied because at the intersecting planes sudden jumps in stiffness occur, resulting in relatively large deformation gradients. Because the changes in deformations are the largest at the top (face side) and bottom, the mesh was also refined in z-direction near bottom and top.

5.4.3 KINEMATIC BOUNDARY CONDITIONS AND DEFORMATIONS

At the boundaries of the FE model, macro-curvatures were applied by defining appropriate displacement fields for the nodes. Those displacement fields will be discussed now for each of the three standard bending cases as introduced in the previous sections.

Horizontal bending (κ_{tt})

A constant curvature κ_{tt} was applied by prescribing the displacements in *t*-direction of the nodes in the *n-z* boundary planes and in *n*-direction of the nodes in the *t-z* boundary planes.

The displacement of the nodes in the *n-z* plane were calculated assuming that boundary planes remained plane. The displacements were proportional to the distance of the nodes to the mid-plane. The nodes were free to move in the *n-* and *z*-direction. Free movements in the *n-* and *z*-direction are essential to obtain unrestrained deformations within the masonry.

The *t-z* boundary planes were kept plane by prescribing a zero displacement in the *n*-direction for the nodes in those planes. The nodes were free to move within the planes. The boundary conditions can be observed in the different views of the deformed mesh as presented in Figure 116.

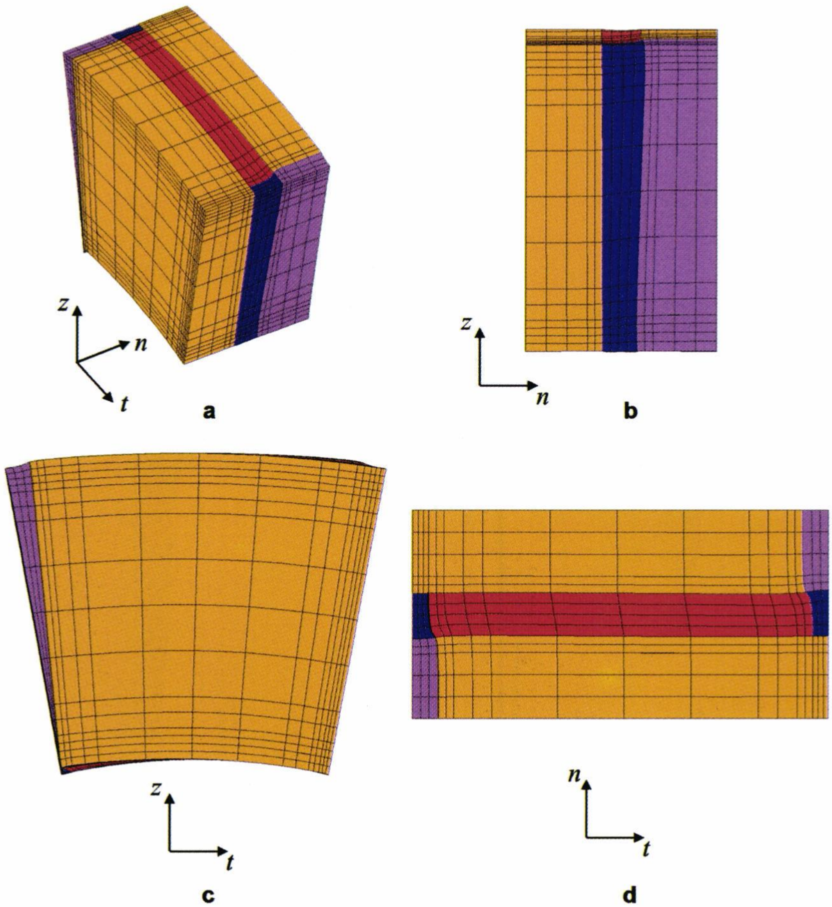

Figure 116 Deformations of mesh due to a curvature κ_{tt}
(E^u *= 10000 N/mm²,* E^j *=1000 N/mm²,* ν^u *=0.15,* ν^j *=0.25)*

In Figure 116b, it can be observed in the n-z plane what was described above as unrestrained deformations. The displacements of the nodes belonging to the head joint and cross joint clearly undergo displacements in n- and z-direction due to difference in stiffness between units and joints. In Figure 116c and d, the distortion of the bed joint can be observed. In Figure 116c, the unit on the back shows its right top and its left bottom due to the distortion of the bed joint. The difference in z-position of the two units near the cross joint causes the shearing of the cross joint. From Figure 116b and d, it can be observed that lateral curvatures influence the deformations of head and cross joint considerably. In Figure 116d, it can also be observed that the corners of the units are additionally bent in t- and n-direction. Furthermore, at the crossing between head joint and bed joint, the distortion of the bed joint vanishes where it goes over in the cross joint, but only at the side of the continuous unit and increases over the thickness of the bed joint towards the head of the other unit

Vertical bending (κ_{nn}).

The boundary conditions applied for vertical bending are of course the same as for horizontal bending, provided that conditions for the *t*-direction are changed in those for the *n*-direction, and vice versa. In Figure 117 different views of the deformed mesh are presented in which the boundary conditions can be observed.

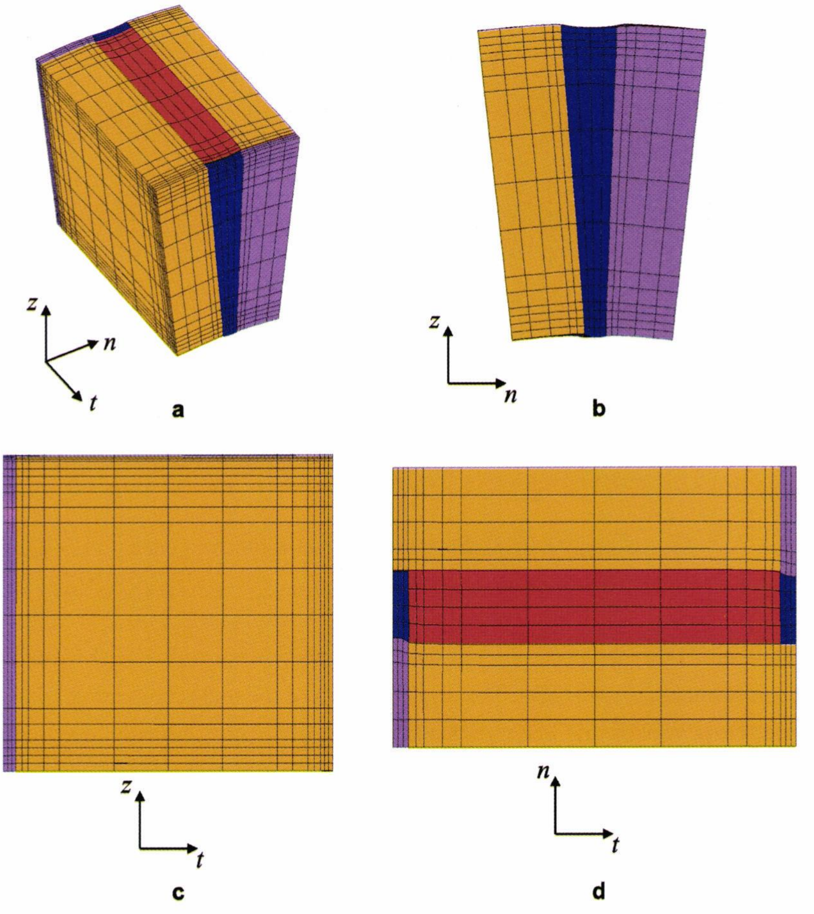

Figure 117 Deformations of mesh due to a curvature κ_{nn}
(E^{u} = 10000 N/mm², E^{j} =1000 N/mm², ν^{u} =0.15, ν^{j} =0.25)

Just as with bending around the n-axis it can observed that especially around the cross joints, the deformations show large gradients. In Figure 117b the effect of lateral deformations can be observed. On the tension side (top), the bed joint and cross joint show a declination and an inclination on the compression side.

Torsion (κ_{tn})

A constant torsion κ_{tn} was applied by prescribing the displacements in n-direction of the nodes in the boundary planes perpendicular to the t-axis and vice versa. However this is not enough to ensure continuity of stresses and deformations over the boundaries. The boundary conditions of opposite planes are antimetrical and shear forces may exist on the boundaries. Therefore, it was also necessary to prescribe the z-displacement of the nodes in the boundary planes. The vertical shear stresses in the unit due to torsional moments are examples of such stresses that are transferred over the boundaries of the FE model. The nodes of a boundary plane were free to move perpendicular to that plane. The displacements in horizontal and vertical direction of the nodes in the boundary planes were proportional with the distance of the boundary plane to the centre of the basic module and proportional with their vertical position, measured from the mid-plane.

In Figure 118, the boundary conditions can be observed in the different views of the deformed mesh. Especially in Figure 118b and c the imposed displacements can be observed very well. In Figure 118a and d, it can be observed that the boundary planes are not hyperbolic, but the normals remain straight and perpendicular to the mid-plane. To ensure the correctness of the imposed boundary conditions in this case, one FE calculation with a coarser mesh was carried out consisting of nine basic modules with exactly the same boundary conditions on the perimeter of the large mesh as for the FE model of one basic module. The stress state and deformations of the central basic module of the large model were checked against those of a single basic module. They were identical, and hence, it could be concluded that the applied boundary conditions were correct. A top view of the deformed mesh consisting of nine basic modules can be seen in Figure 119.

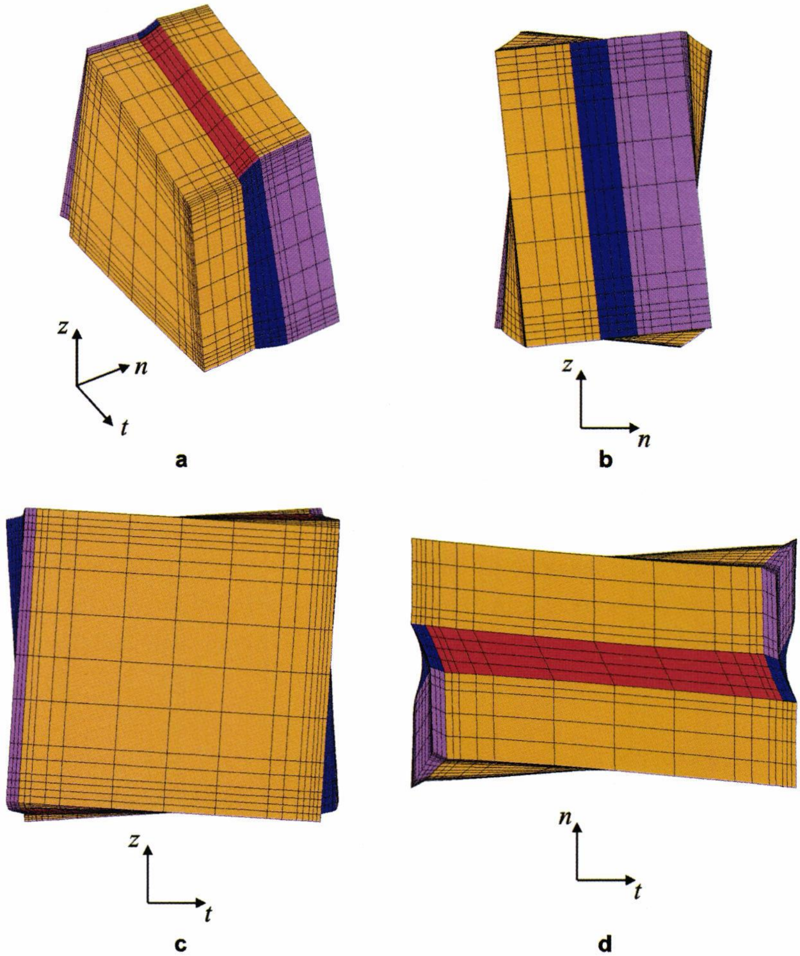

Figure 118 Deformations of mesh of the basic module due to a torsion κ_{nt}

($E^{u} = 10000\ N/mm^2$, $E^{j} = 1000\ N/mm^2$, $\nu^{u} = 0.15$, $\nu^{j} = 0.25$ *)*

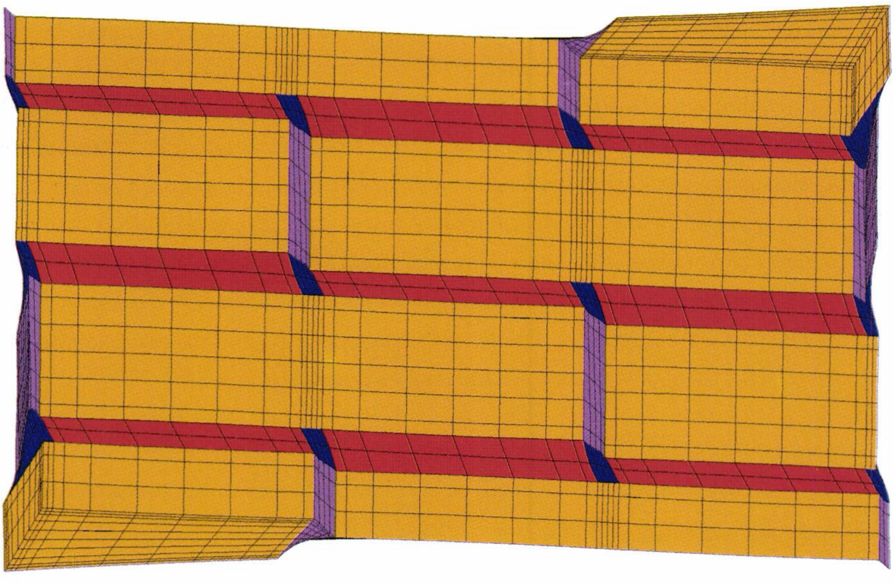

Figure 119 Deformations of nine basic modules due to a torsion κ_{tn} *(face view)*

$(E^u = 150000\ N/mm^2,\ E^j = 2000\ N/mm^2,\ \nu^u = 0.15,\ \nu^j = 0.25)$

In Figure 119 the additional bending deformation of the bed joint can be observed well because of the nearly infinite stiff units. Following one bed joint between two courses, it can be seen that the joint is alternately compressed and stretched on the face side due to bending.

5.4.4 BEHAVIOUR OF THE FE MODEL

In this section the stresses occurring in the FE model are discussed in a general way. All results shown were obtained with the model with the fine mesh presented in Figure 115 on page 137, consisting of 20 nodes brick solids with reduced Gauss integration. No interface elements were present. In all three principal bending cases, a constant curvature of $1 \cdot 10^{-6}$ 1/mm was applied. The material properties used are presented in Table 20.

Table 20 Material properties used in analyses of FE model behaviour

	head joint	bed joint	unit
E^i [N/mm^2]	1000	1000	10000
ν^i [-]	0.25	0.25	0.15

The applied factor 10 between the unit and joint stiffness is rather extreme, but useful to observe the effect of the difference in stiffness between units and joints.
The magnitude of the stresses in the model is not discussed in an absolute way. This is rather useless in a linear elastic approach with sometimes high peak stresses at corners of intersections that are on the one hand the result of the FE approach and on the other hand a result of the internal distribution of forces. In reality peak stresses result in (micro) cracking and will vanish. However, for a better understanding of the presented results, it is useful to know what the applied curvatures mean. On the macro scale, the applied curvatures correspond with average macro stresses in the extreme fibres ranging between 0.17 and 0.34 N/mm^2 for the applied material properties.

Horizontal bending (κ_{tt})
First, the main bending stresses will be considered. In Figure 120, the stresses σ_{tt} in the model are presented.

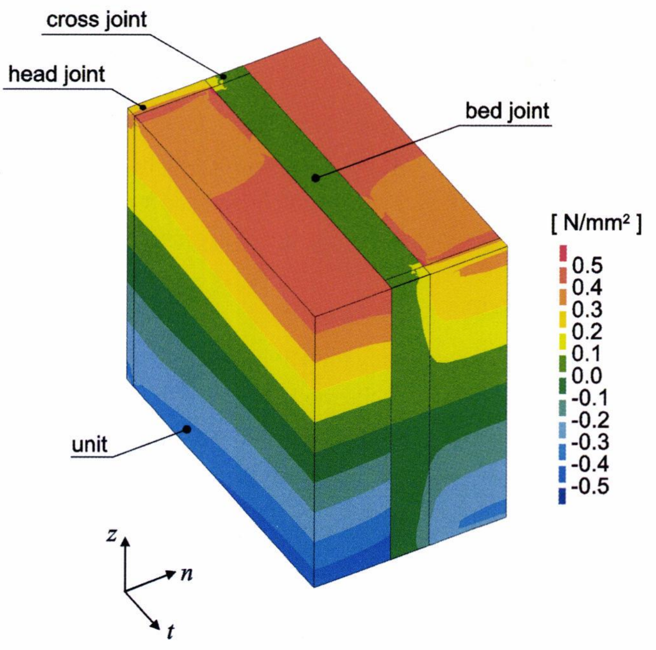

Figure 120 Bending stresses σ_{tt} in the FE model due to a curvature κ_{tt}

In Figure 120 it can be observed that bending stresses in the unit increases from the head joint towards the middle of the unit. Furthermore, the stresses σ_{tt}^{bj} in the bed joints are much smaller than the stresses σ_{tt}^{u} in the units, because the bending deformations in the bed joints are being 'dictated' by those of the units. In the *n-z* plane in Figure 120, the limited influence of the head joint on the stress level in the cross joint can be seen. This could already have been deduced from the deformations presented in Figure 116d on page 139.

In Figure 121 the shear stresses in the bed joint caused by its distortion are presented. In Figure 121a the vertical and in Figure 121b the horizontal shear stresses can be observed.

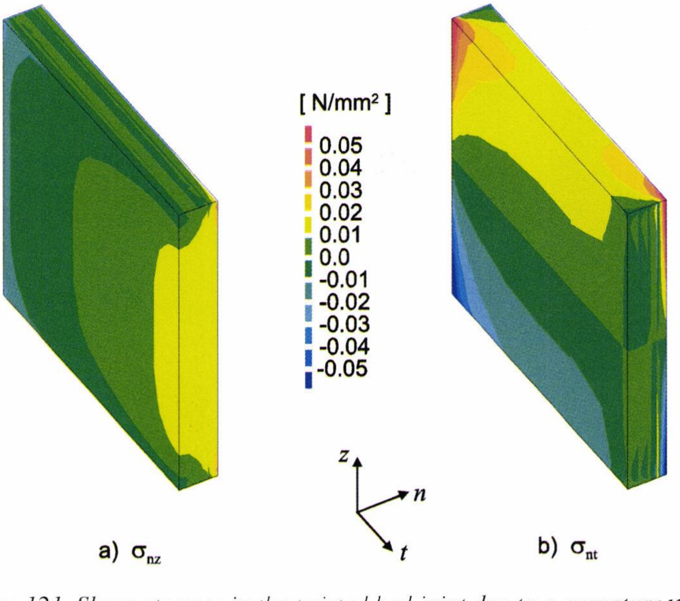

Figure 121 Shear stresses in the twisted bed joint due to a curvature κ_{tt}

Apart from the stress peaks in the corners of the bed joint in Figure 121b, the magnitude of the horizontal and vertical shear stress is approximately the same along the vertical and horizontal sides of the bed joints. Because of the large area over which the horizontal stresses are active, their contribution in the torsion moment of the bed joint is considerably greater than the contribution of the vertical stresses, making the modelling of the additional torsion moment in the bed joint according to thin plate theory in the analytical model plausible.

In the descriptive analysis attention has been paid to shift of the cross joint. From the FE analyses followed that the maximum shear stresses in the cross joint measured 14% of the bending stresses σ_{tt}^{cj} in the cross joint, so the influence of shear of the cross joint is limited. The additional bending stresses at the corners of the units were more important and over two times greater than the occurring shear stresses in the cross joint.

Vertical bending (κ_{nn})

The stresses occurring in units and joints did not show deviations from phenomena already discussed in the previous part of this chapter. Just as with bending in the horizontal direction, additional bending moments around the corners of the units are present causing stresses σ_{tt} measuring up to 30% of the bending stresses σ_{nn} . In Figure 122, the bending stresses in the joints are drawn.

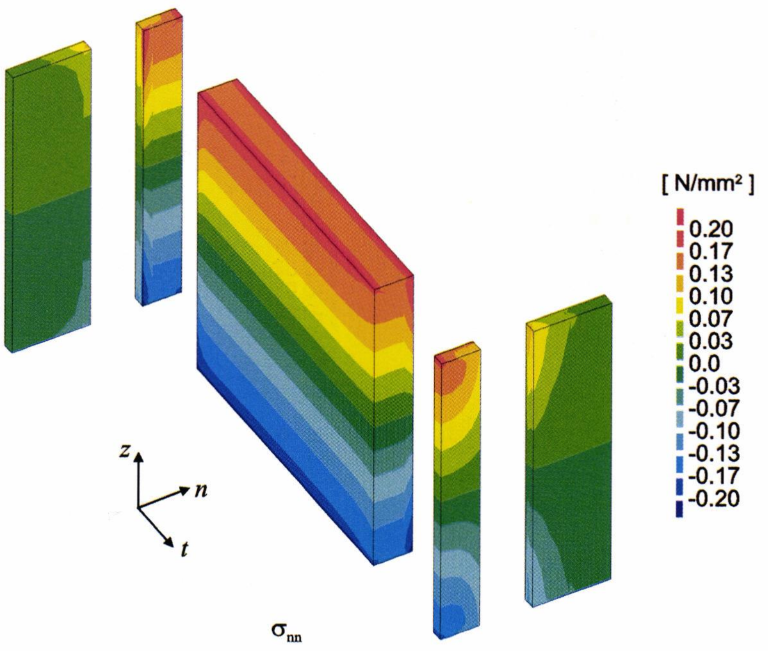

Figure 122 Bending stresses in the joints due to a curvature κ_{nn}

In Figure 122 it can be observed that the cross joint is bent approximately the same as the bed joint, but a limited influence of the head joint can be observed. Just as with the bed joint in case of horizontal bending, the deformation of the head joints, is now being dictated by the units resulting in very low bending stresses in the head joint.

Torsion

The focus is aimed at the non-constant torsional stresses in the unit, the bending stresses causing the distortion of the unit and the resulting vertical shear stresses on the boundaries of the basic module.

In Figure 123 the shear stresses σ_{tn}^{u} and σ_{tz}^{u} in the units are presented. The quarter unit on the left side of each couple of units shows its cross section in the middle. The head of the quarter unit on the right side can be seen where it is connected with a head joint.

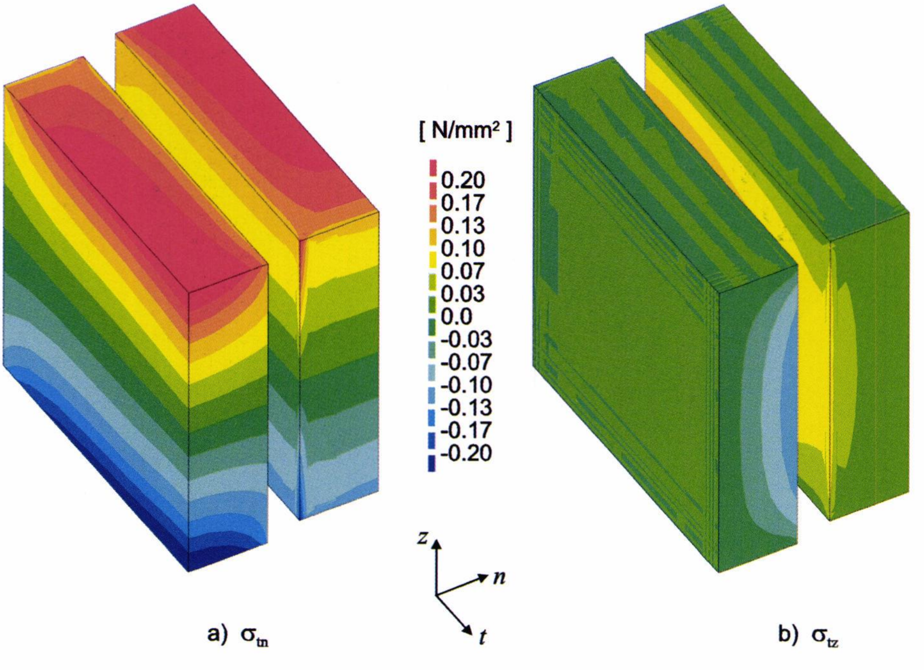

Figure 123 Shear stresses σ_{tn}^{u} and σ_{tz}^{u} in the units due to a curvature κ_{tn} (only the units of the mesh presented in Figure 115 are shown)

From Figure 123b it can be observed that the vertical shear stresses σ_{tz}^{u} increase considerably from the head (quarter unit on the right) towards to the middle of the unit (quarter unit on the left). The fact that vertical shear stresses (of the same magnitude as the horizontal shear stresses σ_{tn}^{u}) are present at in centre of the unit, indicated the distortion as a beam. The presence of the vertical shear at the head of the unit, indicate that the distortion, in the analytical model only taken into account for the units, is, to a certain extent, also present in whole courses consisting of units and head joints.
Compared with the shear stresses σ_{tn}^{u} (see Figure 123a, rightside unit), it can be seen

however that the contribution of the round going stresses in the torsion moment $m_{\mathrm{tn}}^{\mathrm{u}}$ at the head of the unit is limited.

The bending stresses $\sigma_{\mathrm{nn}}^{\mathrm{u}}$ and the vertical shear stresses $\sigma_{\mathrm{nz}}^{\mathrm{u}}$ in the unit are presented in Figure 124.

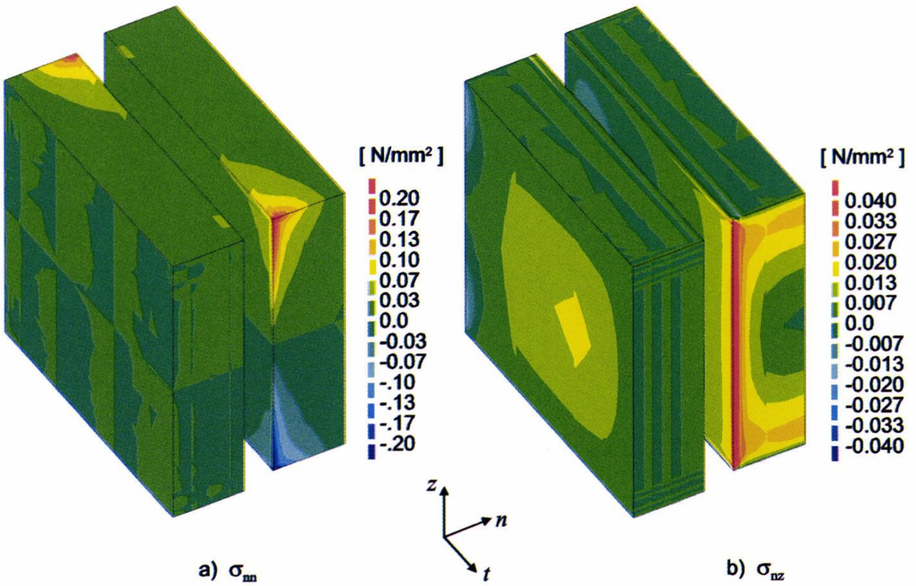

Figure 124 Bending stresses $\sigma_{\mathrm{nn}}^{\mathrm{u}}$ and accompanying shear stresses $\sigma_{\mathrm{nz}}^{\mathrm{u}}$ in the unit due to a curvature κ_{tn}

In the analytical model it was simply assumed that the additional bending moment in the bed joint was constant. In reality the bending stresses show large gradients as can be seen in Figure 124a. The bending stresses in the bed joint are very much the same as in the units, but at the corners of the units where large peaks occur not totally equal to those in the unit, due to the limitations of the FE method. The bending stresses quickly decrease in *t*-direction towards the middle of the unit but also towards the centre of the unit in *n*-direction. This change in *n*-direction goes hand in hand with the shear stresses $\sigma_{\mathrm{nz}}^{\mathrm{u}}$ in the units. In Figure 124b the result of vertical shift of the cross joint is visible as the concentrated introduction of shear stresses $\sigma_{\mathrm{nz}}^{\mathrm{u}}$ at the corners of the units visible as the vertical small red band at the corner of the unit in Figure 124b. The magnitude of the shear stresses is limited and hence their effect on the overall behaviour.

As a result of the interaction between units and joints, remaining vertical shear stresses are present at the boundaries of one basic module. The remaining vertical shear stresses at the boundaries of the FE model are presented in Figure 125.

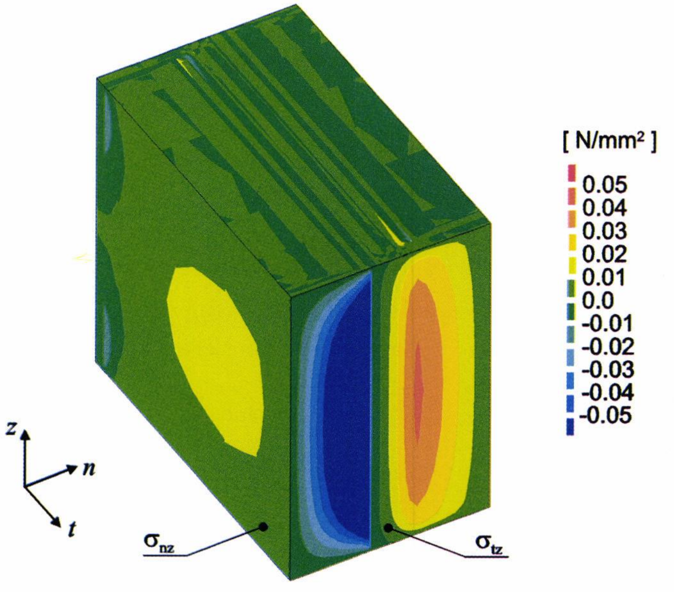

Figure 125 Remaining vertical shear stresses at the boundaries of the model due to a curvature κ_{tn}

The resulting shear forces at the boundary planes area are exactly equal on each plane and in equilibrium. As already has been pointed out in section 5.3.6, the resulting shear force on each boundary becomes zero when 4 basis modules together are considered.

With the FE approach stresses are calculated very precisely, but a remark has to be made about this 'accuracy'. Especially peak stresses at corners where jumps in stiffness are present must be regarded with great care. Numerical inaccuracies are large there. Masonry incorporates all kinds of micro cracks especially in the interfaces making the occurrence of the peak stresses at the corners unlikely. In realty the peaks are expected to vanish rapidly due to micro cracking.

5.4.5 MACRO STIFFNESS OF THE FE MODEL

Just as for the analytical model, macro stiffness values were established on the basis of average macro moments. The macro moments were derived from the support reactions of the nodes. Details can be found in Appendix C 'Meso models'. By averaging the two different torsional moments (see also Figure 114, page136), one value for the macro stiffness was obtained.

5.5 ORTHOTROPIC MACRO STIFFNESS OF MESO MODELS

5.5.1 COMPARISON BETWEEN THE ANALYTICAL MODEL AND THE FE MODEL

Results of the FE model discussed here were all obtained with the, in Figure 115 on page 137 presented fine mesh, consisting of 20 nodes brick solids with reduced Gauss integration. No interface elements were present. To be able to observe the effect of the two different torsional moments before they are being averaged, two torsional rigidities based on the values found for m_{tn} and m_{nt} respectively, are presented.

The geometry of the considered masonry in the comparison resembles that of the clay brick (wc-JO) masonry from chapter 4 and is presented in Figure 126.

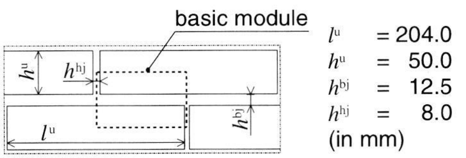

Figure 126 Geometry of units and joints of the considered masonry in the FE and analytical model

First, a trivial case is considered for the analytical model: equal moduli of elasticity and Poisson's ratios for units and joints.

Table 21 Isotropic stiffness of 'masonry' according to the FE and analytical model

	head joint	bed joint	unit	D_{ij} $[12/d^3 \cdot \text{N/mm}^2]$ Analytical	D_{ij} $[12/d^3 \cdot \text{N/mm}^2]$ FE
E^i [N/mm^2]	10000	10000	10000	$\begin{bmatrix} 10351 & 0 & 2083 \\ 0 & 8067/8023 & 0 \\ 2081 & 0 & 10417 \end{bmatrix}$	$\begin{bmatrix} 10417 & 0 & 2083 \\ 0 & 8333/8333 & 0 \\ 2083 & 0 & 10417 \end{bmatrix}$
ν^i [-]	0.20	0.20	0.20		

The two values that could be obtained for the torsional stiffness with the analytical approach are 'equal' in this case. The results closely approximate the stiffness values of thin plate theory. The deviations from the plate theory with expected values $12/d^3 D_{11;22}$ = 10417 N/mm^2, $12/d^3 D_{13;31}$ = 2083 N/mm^2 and the torsional stiffness $12/d^3 D_{22}$ = 8333 N/mm^2 are limited for the analytical approach and absent for the FE approach.

Secondly, masonry with an extreme difference between unit and joint properties is considered. For this case also FE results were derived.

Table 22 Orthotropic stiffness of masonry with an extreme difference between unit and joint stiffness according to the FE and the analytical model

	head joint	bed joint	unit	D_{ij} $[12/d^3 \cdot N/mm^2]$ Analytical	FE
E^i $[N/mm^2]$	1000	1000	10000	$\begin{bmatrix} 6600 & 0 & 551 \\ 0 & 4048/4392 & 0 \\ 549 & 0 & 3633 \end{bmatrix}$	$\begin{bmatrix} 6764 & 0 & 637 \\ 0 & 3440/2811 & 0 \\ 637 & 0 & 3852 \end{bmatrix}$
v^i $[-]$	0.25	0.25	0.15		

In Table 22, it can be observed that the difference between the analytical and the FE model is within 6% for the pure flexural rigidities D_{11} and D_{33}. The difference between the average torsional stiffness of the analytical model and FE model is -35%. In this case, the torsional stiffness is being overestimated with the analytical model.

The last case considered in the comparison, is the same masonry as before but without head joints.

Table 23 Orthotropic stiffness of headless masonry with an extreme difference between unit and bed joint properties, according to the FE and the analytical model.

	head joint	bed joint	unit	D_{ij} $[12/d^3 \cdot N/mm^2]$ Analytical	FE
E^i $[N/mm^2]$	-	1000	10000	$\begin{bmatrix} 3595 & 0 & 372 \\ 0 & 2425/2224 & 0 \\ 273 & 0 & 3602 \end{bmatrix}$	$\begin{bmatrix} 3916 & 0 & 472 \\ 0 & 2875/2545 & 0 \\ 472 & 0 & 3784 \end{bmatrix}$
v^i $[-]$	-	0.25	0.15		

It can be observed that the absence of the head joints has a large impact on the horizontal stiffness D_{11} that decreases to 54% of its original value of Table 22. The difference between the analytical and the FE model is now within 9% for the pure flexural rigidities D_{11} and D_{33}. The difference between the average torsional stiffness of the analytical model and FE model is 17 %.

It is obvious that the differences between the analytical and FE model for the torsion case cannot be simply ignored. The main cause for the difference in torsional stiffness is the assumption in the analytical model that the additional bending moment in the bed joint and unit is constant over the bed joint. In the FE model, the bending moments are only present near the head of the units (see Figure 124). As long as head joints are present, this deviation will play an important role, but at the moment the torsion can only be transferred via the bed joints, the bending moment in the bed joint is present over a larger area in the FE model and the models behave more alike.

From the fact that the behaviour of the cross joint in the FE model did not have an important impact on the stresses in the units and the reasonable resemblance between the analytical and the FE model it was concluded that cross joint may be ignored.

In general, it was concluded that the analytical model behaved satisfactorily compared with the FE model.

5.5.2 COMPARISON BETWEEN EXPERIMENTAL AND ANALYTICAL BEHAVIOUR

As already pointed out in the introduction of this chapter, comparing experimental and analytical (or FE) results includes the problem of deriving the material properties of the components. Tests on the units are available, but in principle, material properties of the joints must be derived from tests on masonry. When the same model is used for predicting the macro stiffness as for deriving the joint stiffness from the experimental results the prediction has little value. Therefore the comparison between the experimental and the analytical results is focussed on relations between material properties and variations of these, rather than on predicting accurate stiffness values.

The input values of the units for the analytical model are based on the stiffness values obtained for the units as presented in Table 33 in Appendix A 'Materials'. Stiffness values for joints were obtained on the basis of the tensile tests. The values used for the joint stiffness fall inside the range that could be obtained from the tensile tests, however for the wallette test series of 1992-1994 no directly related test data were available. Because the stiffness values of the wallettes of the series of 1992-1994 closely corresponded with those of 1996-1997, rounded average values of the tensile test series of 1996-1997 were used (see Table 38 and Table 39 in Appendix B 'Experimental Results').
The behaviour of the experiments has already been discussed in chapter 4 and is not further addressed here.

wc-JO clay brick masonry
The geometry of the masonry was presented in Figure 126 on page 150. In Table 24 the material properties used as input for the analytical model are presented together with average experimental results, based on Table 12 and Table 13 from page 106, and with the outcome of the analytical model. The influence of lateral (Poisson) deformations on

the flexural rigidities in the experiments was ignored for reasons motivated in section 4.4 (page 103).

Table 24 Comparison between average stiffness values from experiments and from the analytical model for wc-JO clay brick masonry

INPUT	E^{i} [N/mm^2]	ν^{i} [-]	RESULTS	experiments linear	experiments E_{2nd}	experiments headless	analytical model ordinary	analytical model headless
head joint	5500	0.2	E_{hor} [N/mm^2]	11650	7200	5650	13700	7900
bed joint	5500	0.2						
unit	16700	0.15	E_{ver} [N/mm^2]	11320	-	-	11770	-

The input values used (not obtained from some kind of fitting procedure) for the analytical model result in macro stiffness values that are in close correspondence with the experimental results. From the results in Table 24 it can be observed that the experiments (column with linear results) behaved more uniform than the model ('ordinary' column). The model is 16% stiffer in the horizontal direction than in the vertical direction. Less stiff head joints in the specimens than the perfectly assumed head joint in the model, could explain this difference. In Figure 127 the influence of a less stiffer head joint on the orthotropic macro flexural rigidities is presented. It can be observed that with a joint stiffness of 30% of the original value as used in Table 24, the horizontal and vertical macro stiffness are almost equal.

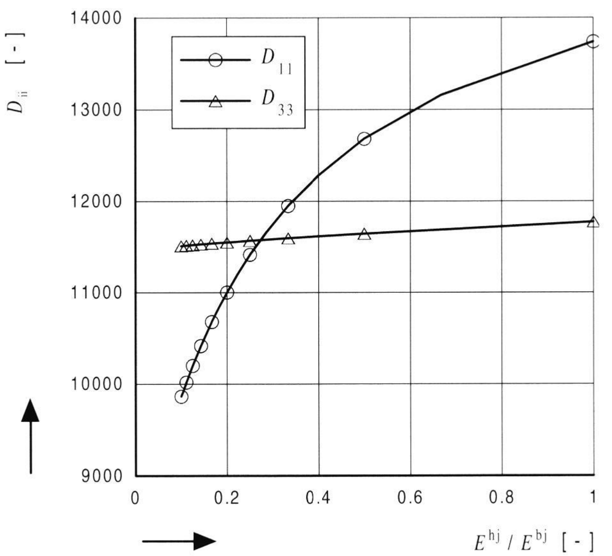

Figure 127 Influence of head joint stiffness on the orthotropic flexural rigidities for wc-Jo masonry (E^{u} = 16700 N/mm^2, E^{bj} = 5500 N/mm^2)

The bi-linear behaviour, observed in the horizontal direction, is another aspect for comparison. Because it was concluded that cracking of the head joints caused this effect, the bi-linear behaviour can also be compared with headless masonry according to the model. However,headless masonry will behave differently from masonry with cracked head joints, because in the experiments compression stresses and even some tensile stresses are still being transferred in the cracked head joints, leading to a stiffness in the second branch that is higher than the stiffness for headless masonry. From Table 24 it can be observed that the headless masonry is less stiff than the model and, as expected, less stiff than the second branch. The way the headless masonry was made, might have had also an influence on the (from the analytical point of view) too low horizontal stiffness of the masonry specimens. The head joints were made free from mortar with a jointing nail in such a way that the bed joints were discontinuous. As a result, cracks due to drying shrinkage may have been present in the bed joint, decreasing the actual bond area more than in ordinary bed joints, leading to an extra decrease in stiffness in the experiments.

CS-block masonry

The geometry of the modelled CS-block masonry is presented in Figure 128.

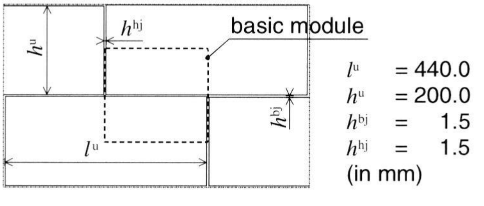

Figure 128 Geometry of units and joints of CS-block masonry

In Table 25, input values for the model and experimental and analytical results are collected. The experimental results originate from Table 14 and Table 15 on page 109.

Table 25 Comparison between average stiffness values from experiments and from the analytical model for CS-block masonry

INPUT	E^{i} [N/mm^2]	ν^{i} [-]	RESULTS	experiments linear	experiments E_{2nd}	experiments headless	analytical model ordinary	analytical model headless
head joint	500	0.2	E_{hor} [N/mm^2]	12500	7250	7340	12080	7660
bed joint	500	0.2						
unit	12800	0.15	E_{ver} [N/mm^2]	13900	-	-	11030	-

The same tendencies as with the wc-JO masonry can be observed, although some slight differences are present. Now the vertical stiffness in the experiment is even higher than input value for the unit stiffness, indicating a higher block stiffness in the experiments than assumed. This might also be a reason for the close correspondence between the model and experiments for headless masonry. The unexpected close correspondence between the stiffness of the second branch E_{2nd} and of the headless masonry specimens may be the effect of the fabrication process. The blocks were placed into the thin mortar bed and then slided towards the already placed block. The head joints were kept open by placing coins (Dfl 2½-coins) in between the blocks, removed later. Because the thin joints could not be cleaned (because of the profile on the blocks), some mortar dripped in from the top and some was piled up during sliding, making the joint not totally unfilled.

Considering all results obtained with the analytical model for wc-JO clay brick and CS-block masonry, it was concluded that the analytical model can well be used to predict the orthotropic bending stiffness values of the tested types of masonry, keeping in mind that the torsional stiffness is overestimated. Because the considered types of masonry had very different geometries and joint stiffnesses, it is expected that the model is also capable to predict the stiffness of other types of masonry. Of course, the problem of lack of data concerning the joint stiffness remains.

In Figure 129 the influence of different Young's moduli of the joints on the orthogonal stiffness ratio R_E between the horizontal stiffness (D_{11}) and vertical stiffness (D_{11}) of the wc-JO clay brick and CS-block masonry, is presented.

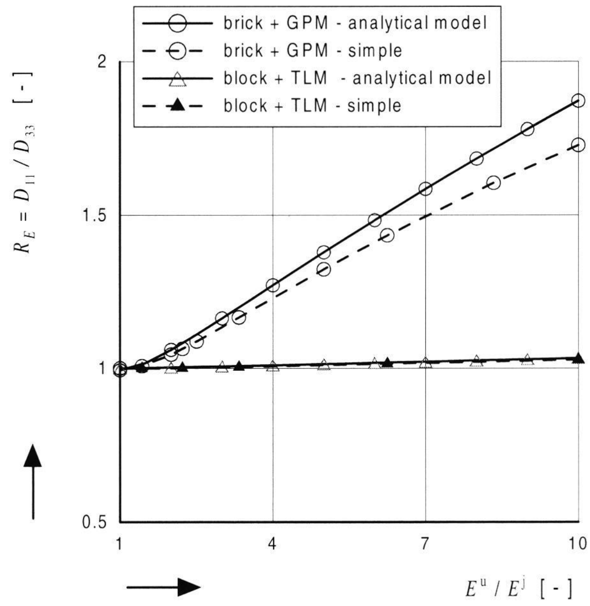

Figure 129 Influence of ratio between unit and joint stiffness on the orthogonal stiffness ratio R_E *between the horizontal and vertical stiffness*

Apart from the joint stiffness, the material properties used, were equal to those in Table 24 for wc-JO clay brick masonry and in Table 25 for CS-block masonry. It can be observed that the influence of the thin joint can be neglected in case of CS-block masonry. For the wc-JO clay brick masonry, an influence of the joint stiffness can be observed. Taking the experimentally stiffness values found for the joint stiffness of wc-JO clay brick masonry into account (see average values in Table 38 on page 219) and knowing that applied mortars varied between 1:½:4½ and 1:2:12, a ratio of 5 between unit and joint stiffness can be considered as a large value for Dutch materials (the sand and its grading is rather constant). This implies that the R_E will rarely be greater than 1.4. The magnitude of this ratio is to some extent confirmed by Sinha[1978,[72]] who reported a ratio of 1.4 based on experiments for clay brick masonry, while Henry[1981,[22]] states that a typical value is 1.25.

In Figure 129 also two lines, denoted with 'simple' for each type of masonry are included. Those lines are based on the same assumption as made for eq. (3), ignoring any influence of bending effects as discussed in 5.2 or lateral deformations. For the vertical stiffness (D_{33}) eq. (3) was used. This equation for serial connections can be rewritten as:

$$E_{\mathrm{serial}}^{\mathrm{j+u}} = \frac{E^{\mathrm{j}} E^{\mathrm{u}} (t^{\mathrm{u}} + t^{\mathrm{j}})}{E^{\mathrm{u}} t^{\mathrm{j}} + E^{\mathrm{j}} t^{\mathrm{u}}} \tag{35}$$

To calculate the horizontal stiffness (D_{11}), eq. (35) was used first to obtain the stiffness of a course consisting of units and head joints. Next it was assumed that these courses and the bed joint undergo the same deformation, so for parallel connection it can be derived that:

$$E_{\text{parallel}}^{\text{j+u}} = \frac{E_{\text{serial}}^{\text{u+hj}} t^{\text{bj}} + E^{\text{bj}} t^{\text{u}}}{t^{\text{bj}} + t^{\text{u}}} \tag{36}$$

From Figure 129, it can be observed that with this simple approach, the ratio R_E can be predicted reasonably well. Also the absolute stiffness values obtained with the analytical model and the simple method closely corresponded with each other for the considered wc-JO clay brick and CS-block masonry, as can be observed in Table 26.

Table 26 Comparison between stiffness values obtained with the analytical bending model and a simple approach based on serial and parallel connections

	JO-brick masonry		CS-block masonry	
	analytical	simple	analytical	simple
E_{hor} [N/mm^2]	13700	13500	12080	11730
E_{ver} [N/mm^2]	11770	11870	11030	10820

The close correspondence between the simple method and the analytical model already indicate that the influence of a variation of Poisson's ratio on the flexural rigidities is limited. In Figure 130 the limited influence of a variation of Poisson's ratio of the joints on the flexural rigidities can be observed.

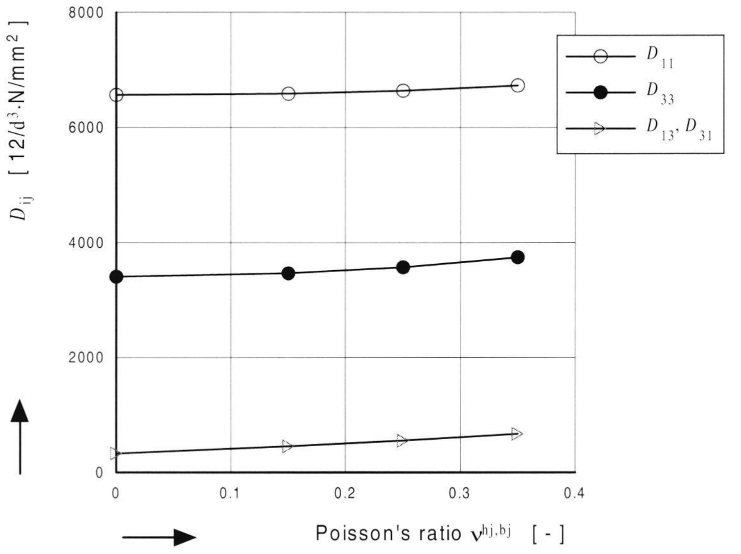

Figure 130 Influence of Poisson's ratio of the joints on the flexural rigidities (other parameters are given in Table 20)

The constant value $R_E = 2$ that the Dutch masonry standard NEN 6790:1997[14] prescribes for every type of masonry is too high in case of bending.
The simple approach can be also used for masonry in compression. There seems no reason that the simple approach would not be appropriate in compression, indicating that in general the ratio R_E is overestimated by NEN6790.

5.6 BENDING STRENGTH OF MASONRY BASED ON THE ANALYICAL MODEL

5.6.1 INTRODUCTION

As stated in the introduction of this chapter, the analytical model was also used to predict the flexural strength of masonry. Therefore different potential crack patterns, presented in Figure 131, were considered. This approach is denoted with the term Multiple Crack Pattern (MCP) approach.

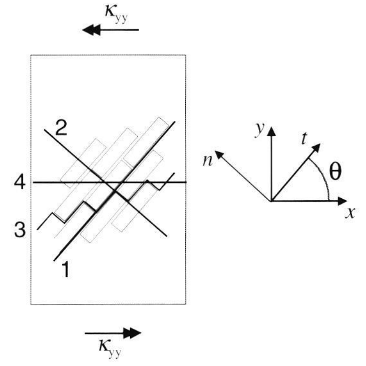

Figure 131 Overview of possible crack patterns in the MCP model

The four different cracks considered are:

1. straight crack through the bed joint;
2. straight crack through units and head joints;
3. crack running alternately through head and bed joints, denoted as oblique crack;
4. straight crack running parallel with the bending axis.

The fourth crack, generally running through units only (ignoring the crossing of the bed joint) has the highest capacity in ordinary clay brick masonry with relatively low bond strength compared with unit tensile strength. It forms an upper bound for the strength. That is why it is necessary to consider other potential weaker cracks not running parallel with the bending axis. The oblique crack pattern was also evaluated assuming that the head joints were already cracked. At the moment the strength of the oblique pattern with cracked head joints is larger than the oblique pattern without cracked head joints, the latter is no longer decisive for failure. The transfer of compression stresses in a cracked head joint was simulated by assuming that the head joint stiffness was reduced to 20% of the original value. In case of crack 2, it was always assumed that the head joints were cracked and had a reduced stiffness.

In the MCP approach, stresses that follow from imposed deformations are checked against the strength of the masonry components, using a failure criterion for each crack pattern. In this way the leading crack pattern, i.e. the flexural strength of masonry can be calculated based on the strength of the components. A distinction was made between the strength of the units and of the joints. In principle, it is possible to make a further distinction between the head and bed joints, but this was not done.

Several assumptions had to be made to obtain a realistic strength based on the linear elastic stress distribution of the analytical model and the adopted failure criterion. The approach followed is very similar to the way the flexural strength is generally calculated by dividing an ultimate bending moment by the elastic section modulus. These

assumptions are typical for an 'engineering approach' and it is recognised they lack a solid fundamental basis. Nevertheless it is believed that the MCP approach furnishes an improved insight in the way masonry fails in bending.
The flexural strength of masonry as function of the angle between the bending axis and the bed joint was investigated with the model. This is of particular interest if masonry panels are designed based on to the yield line analogy. The influence of several assumptions, as well as the influence of material properties, is discussed.

5.6.2 FAILURE CRITERION

On the basis of section 3.8 a parabolic failure criterion was used to check combinations of (σ, τ) for joints in the crack patterns. In Figure 132, the failure criterion is presented in a general way.

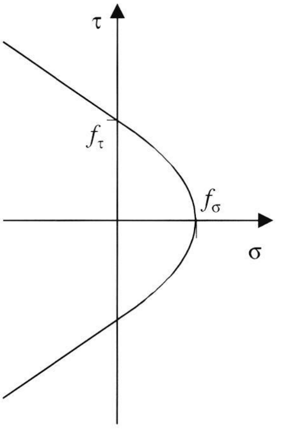

Figure 132 Parabolic failure criterion in the σ-τ plane

The parabolic failure criterion f_p reads:

$$f_p = \sigma + \frac{f_\sigma}{(f_\tau)^2}\tau^2 - f_\sigma \tag{37}$$

A joint fails when a stress combination (σ, τ) touches the parabolic criterion ($f_p = 0$). Because we are dealing with bending, the question arises which values must be used for f_σ and f_τ. The analytical model calculates a linear stress distribution in the masonry components, ignoring possibilities of redistribution of stresses due to cracking. In uni-axial bending around the *t*- or *n*-axis, this redistribution, with regard to the post peak behaviour is important, as discussed in section 2.4.3. The use of a linear elastic stress distribution in combination with a failure criterion, in general results in a lower bound of the strength, because the non-linear redistribution of stresses is ignored. However, by using respectively the flexural and torsional bond strength of a cross section for f_σ and f_τ respectively, the non-linear redistribution can be taken into account. Using the flexural and torsional bond strength of cross sections in the failure criterion, implies that a lower bound solution is not found any more.

The flexural strength may be derived directly from 4-point bending tests as discussed in chapter 4, but this is not the case for the torsional strength. A widely used experimental method is not available and experimental results on the torsional bond strength are very scarce. It was assumed that the factor 1.5 proposed in eq. (12) between c_o and f_{tb} could also be used to estimate the torsional bond strength of a cross section based on the flexural bond strength.

For reasons mentioned in the introduction of this chapter, it was not possible to derive this factor on the basis of non-linear calculations with the FE-model. There is some experimental evidence, however, that the assumption concerning the factor 1.5 is valid. In general, ratios varying between approximately 1.3-1.7 can be found between the tensile and flexural bond strength. Baker[1981,[4]] carried out a limited experimental comparison between the torsional and shear bond strength and found a ratio of 1.3 to 1.5 between both quantities, depending on the way he interpreted his results (elastic or plastic). Because the ratio between the flexural and tensile bond strength seems not to differ much from the ratio between the torsional and shear strength, the chosen factor 1.5 is more or less justified. With this ratio the failure criterion can be rewritten:

$$f_p = \sigma + \frac{1}{2.25 f_{fl}} \tau^2 - f_{fl} \tag{38}$$

The flexural and torsional bond strength were considered as material properties. Although this is not the case as pointed out in the beginning of this section and in section 2.4.3, this approach can be justified by the fact that all parameters that makes these strength properties structural, are the same in the considered cases.

For the strength of crack type 2 (see Figure 131) the flexural strength from wallettes bent around the n-axis with a crack running through units was used. In this case, the head joints were assumed to be cracked, as was shown in chapter 4. A unit was supposed to fail when the main tensile stress in the unit was greater than its flexural strength.

5.6.3 Strength of crack patterns

The strength of each of the four crack patterns was determined with the same approach. An imposed global deformation defined in a x-y-z co-ordinate system making an angle θ with the t-n-z co-ordinate system was transformed to the latter, using the well known relations for tensors of the second degree (similar to the circle of Mohr). With the aid of the analytical model deformations and stresses occurring in each component were then calculated. Next, the maximum stress combinations (σ_i, τ_i) for joints and principal tensile stresses in units were determined and checked against the failure criterion. For a possible further increase of the imposed deformation, multipliers λ_i were calculated on the basis of the distance between the stress points and the failure criterion for each component (see Figure 133).

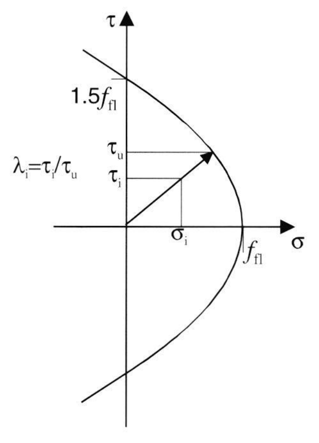

Figure 133 Determination of a multiplier λ_i for the critical stress combination (σ_i, τ_i) of a joint

The largest multiplier indicates which component fails and indicates the leading crack pattern in the case at hand. To be able to see what the strength of each crack pattern was, the bending moments acting in each crack were calculated and the resulting moments transformed to the original *x-y-z* co-ordinate system.

In Figure 134 the resulting bending moments in the oblique crack pattern are drawn. When a curvature κ_{yy} is imposed and κ_{xx} and κ_{xy} are zero, still moments m_{xx} and m_{xy} occur. These moments arise from the laterally restrained curvatures. But even when Poisson's ratios are zero, they still occur if $0° < \theta < 90°$. In that case, they are a result of the terms in the bending stiffness matrix that are zero in the *t*- and *n*-direction (see eq. (21) on page 118, but non zero in other directions.
To determine the flexural strength $f_{fl;yy}$ as a function of the angle θ, κ_{xx} and κ_{xy} were assumed to be zero. For each angle θ, the resulting moment m_{yy} was calculated from the moments in a considered crack, also taking the torsion moment m_{xy} along the vertical

boundary into account. The moment m_{yy} was divided by the elastic section modulus to obtain the strength $f_{fl;yy}$ of a crack pattern.

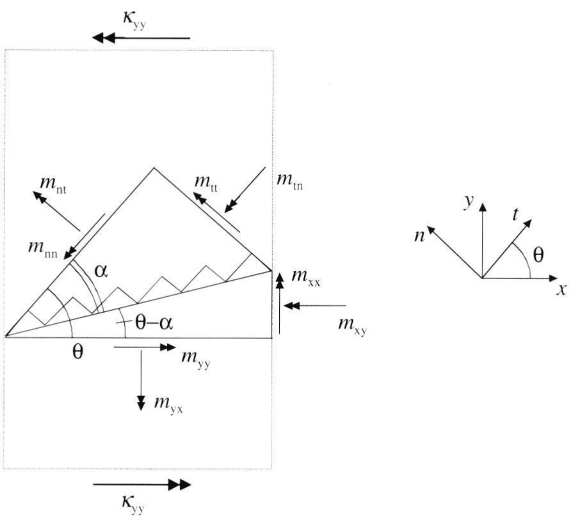

Figure 134 Moments in oblique crack

wc-JO clay brick masonry

The same geometry and stiffness values as before were used (see Table 24 on page 153). Deviations are explicitly mentioned. In all cases the values used for the flexural strength of units and joints are given.

The straight crack (number 4) parallel with the bending axes through units is not presented. Its capacity is at most f_{fl}^{u} (ignoring the influence of joints corssed in such a crack) and is used as the upper limit for the strength.

In the wallette tests of 1992-1994 of the wc-JO90 + GPM series, the flexural bond strength varied between 0.5 and 1.0 N/mm$^{2.}$ These values are based on wallette tests, but also on tensile tests carried out with the wallettes for directions of $\theta \neq 0$. The tensile tests were not representative on a one to one basis, as indicated in chapter 4, and were only used as an indication.

In Figure 135 the strength of crack patterns of wc-JO masonry with $f_{fl}^{u} = 4$ N/mm^2 and $f_{fl}^{j} = 1.0$ N/mm^2 is presented.

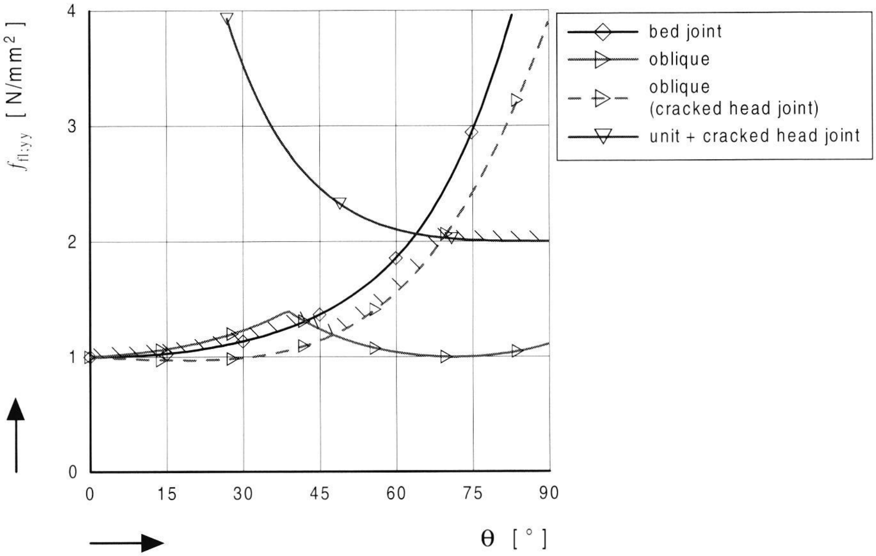

Figure 135 Flexural strength of crack-patterns of wc-JO masonry
(f_{fl}^{u} = 4 N/mm² and f_{fl}^{j} = 1.0 N/mm²)

Up to θ ≈ 42° the straight crack through the bed joint determines the ultimate load for both values of the flexural bond strength. Although the oblique crack without head joints gives a lower value, its value can only be used when they are higher than the values for the oblique pattern with head joints, because the head joints have to fail first. For θ > 42°, the oblique pattern determines the ultimate load until the crack through the units and head joints determines failure. The leading crack pattern for each θ is indicated with the hatching. In Figure 136, the influence of a lower flexural bond strength is presented. The other parameters were kept the same.

For the low flexural bond strength value, θ must be 90° before the crack through the units and head joints determines failure. Comparing Figure 135 and Figure 136, it can be observed that a larger flexural bond strength makes cracks running through units and head joint more likely to occur. That situation was representative for the JO.70 and JO.90 wallette series carried out in 1992-1994. The limited increase of strength up to θ = 40°, especially for the low flexural bond strength, makes it clear that the large difference in strength found between the JO.VER and JO.30 series (see Table 12 on page 106), must have been caused by a difference in bond strength and not by the different angles between bed joint and bending axis.

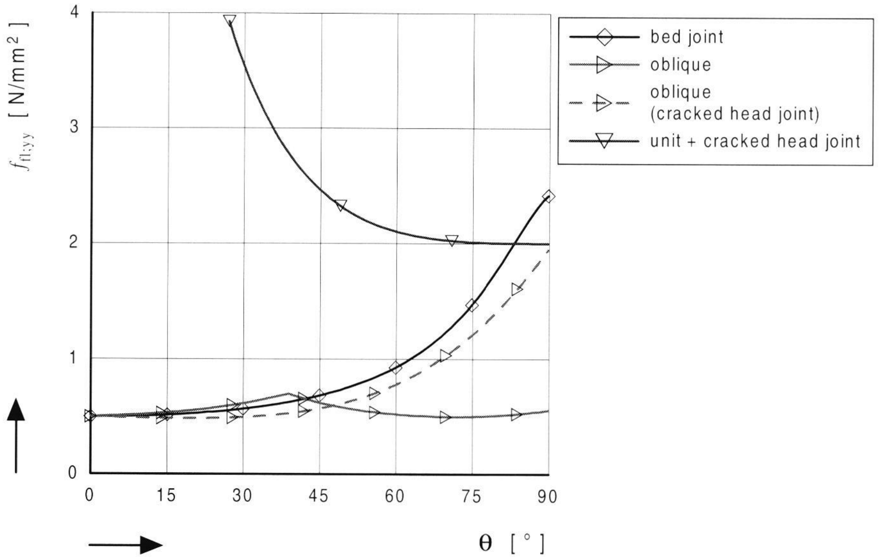

Figure 136 Flexural strength of crack-patterns of wc-JO masonry
(f_{fl}^{u} = 4 N/mm^2 and f_{fl}^{j} = 0.5 N/mm^2)

The nearly parallel curves for failure of the bed joint and for the oblique crack with cracked head joints with a limited difference in strength, indicate that both patterns may occur although the oblique crack is arithmetically less strong. The limited strength of the bed joint for large values of θ, not going to infinity like the strength of the crack through units and head joints for small values of θ, is caused by the lateral deformations imposed by the units. If the Poisson's ratios are equal to zero, the lateral curvatures are not present. This case is presented in Figure 137. It can also be regarded as a simulation of the boundary condition $m_{xx} = 0$.

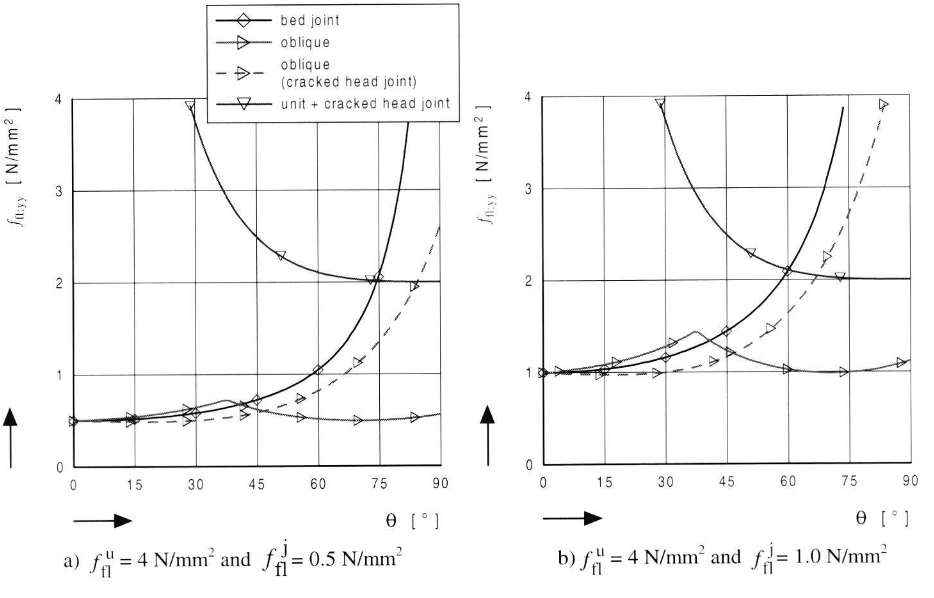

Figure 137 Flexural strength of crack-patterns of wc-JO masonry
$\nu^{u} = 0,\ \nu^{j} = 0$

The effect of Poisson's ratio being equal to zero, is obvious. The strength of the straight crack through the bed joint is increased considerably, but also of the oblique crack with cracked head joints. Especially in Figure 137b it can be observed that the occurrence of an oblique crack is approximately limited to $40° < \theta < 65°$.

The reduced stiffness of the head joint, that simulates load transfer in the cracked head joints, is an important parameter for the strength of the oblique crack with cracked head joints. The influence of an increase of this value from 20 (as used until now) to 40% of the original joint stiffness, is presented in Figure 138.

The difference in strength between the straight crack through the bed joint and the oblique crack with cracked head joints disappears in this case. This does not imply that the oblique crack cannot occur. For $40° < \theta < 65°$, the head joints of the oblique crack pattern will crack first. After that the possibility of a straight crack through the bed joint or an oblique crack is, according to the model, the same.

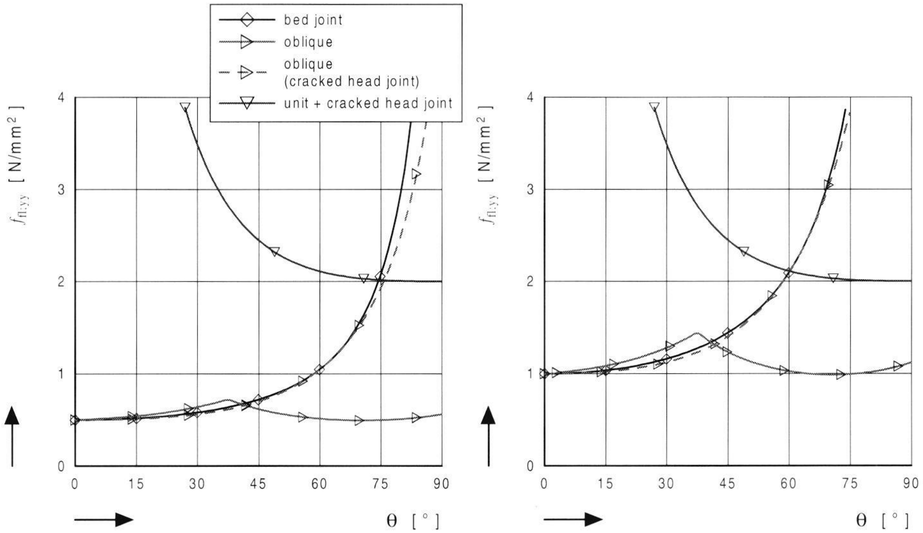

a) $f_{fl}^{u} = 4$ N/mm^2 and $f_{fl}^{j} = 0.5$ N/mm^2 b) $f_{fl}^{u} = 4$ N/mm^2 and $f_{fl}^{j} = 1.0$ N/mm^2

Figure 138 Flexural strength of crack-patterns of wc-JO masonry

$$v^{u} = 0,\ v^{j} = 0,\ E_{reduced}^{hj} = 40\%$$

In section 4.5 the behaviour of the wc-JO clay brick wallettes was discussed. In the JO.30 series ($\theta = 30°$) bi-linear behaviour was detected. This behaviour cannot be explained with the model and must probably be sought in a non-linear redistribution of stresses, and perhaps, a dilatancy effect in the cracking bed joint, but the author must admit that this is pure speculation. However from the model it is obvious that for $\theta > 40°$-$45°$ head joints will always be cracked and are a cause for bi-linear behaviour.

In one of the test of the JO.70 series of 1992-1994 an oblique crack occurred with a remarkably low strength compared with the other test of that series. Some badly filled head joints might have caused a less steep increase of the strength of the oblique crack in this case. After all, the sensitivity of the strength of this type of crack for the actual value of $E_{reduced}^{hj}$ is rather high according to the analytical model.

CS-block masonry

In Figure 139, the strength of the crack patterns, representative of the CS-block92+TLM series of 1992-1994, is presented. Now only the cases with Poisson's ratios equal to zero and the influence of a remaining stiffness of the cracked head joints are considered.

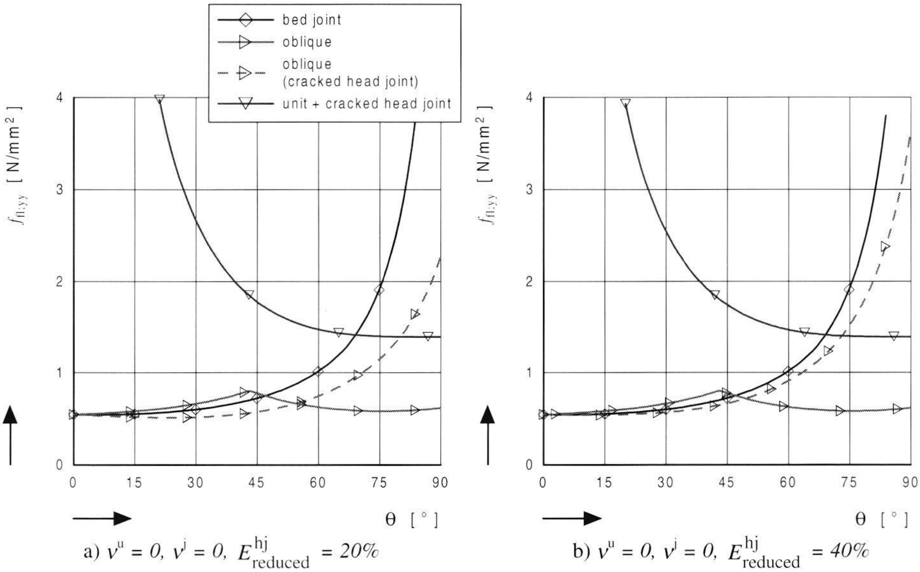

Figure 139 Flexural strength of crack-patterns of CS-block masonry
$f^u_{fl} = 4\ N/mm^2$ *and* $f^j_{fl} = 0.6\ N/mm^2$

From Figure 139 it can be observed that for $0° < \theta < 45°$ no significant increase of the strength occurs. This behaviour closely corresponded with the test results (see Table 18 on page 115). If the strength of an oblique crack and a straight crack through head and bed joints would have been the same for $\theta = 90°$, an explanation was found for the mixed mode type of failure (cracks running through head and bed joints and units) that occurred in the CS.90 series of 1992-1994 (see also Figure 94, page 116). The shape of tongues and grooves present in head and bed joints causing additional lateral stresses, might have caused a lower strength of the oblique pattern. Of course, this kind of phenomenon is not included in the model.

In Figure 140 the MCP approach is compared with other criteria found in literature.

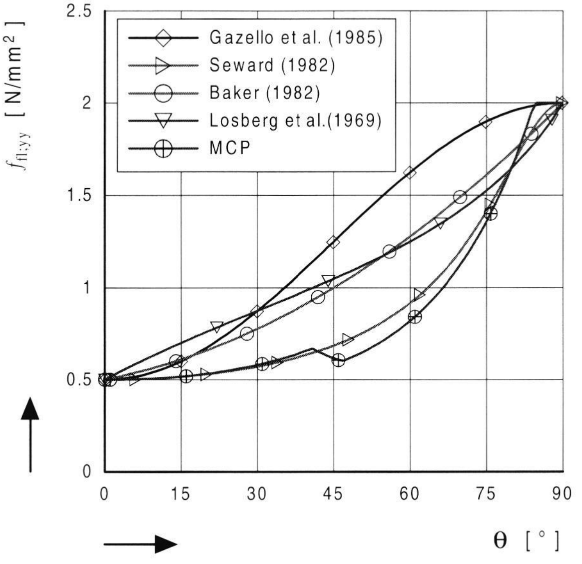

Figure 140 Flexural strength as a function of θ, comparison between different criteria from literature and the MCP approach with $f_{\mathrm{fl}}^{\mathrm{u}} = 4\ N/mm^2$, $f_{\mathrm{fl}}^{\mathrm{j}} = 0.5\ N/mm^2$, $\nu^{u} = 0$, $\nu^{j} = 0$, $E_{\mathrm{reduced}}^{\mathrm{hj}} = 20\%$

The criteria of Gazolla et al.[1985,[17]] and Baker[1982,[5]] are based on fits through experimental data of several researchers with relatively high CV's. Losberg and Johansen[1969,[34]] used a formula equal to the one used for the oblique crack in the MCP approach. However, they used the vertical flexural strength for the bending moment in the bed joints and the horizontal flexural strength for the bending moment in the head joint. So, Losberg and Johansen assumed that in both directions the ultimate strength is reached simultaneously.
Seward[1982, [70]] proposed an elliptical transition between the orthogonal strength values without a motivation. From Figure 140 it can be observed that all criteria found in literature seem to overestimate the strength, except the elliptical transition proposed by Seward, which seems to be a reasonable simplification of the MCP approach.

5.7 Concluding remarks

Additional moments in masonry that occur due to stiffer units compared with joints, play an important role. Most important phenomena are the additional bending moments in the bed joint in case of torsion and the additional torsional moments in the bed joint in case of bending around the n-axis (horizontal bending). Although the distortion of the bed joint in case of horizontal bending is widely recognised as an important phenomenon, this cannot be said of the additional bending of the bed joint in case of torsion.

It must be realised that both with the analytical and the FE model, a linear elastic stress distribution was derived based on perfect units and joints. In reality little cracks in units, mortar and especially in the interface between units and joints may reduce the peak stresses that were present in the FE model considerably. In the analytical model, these local effects are totally ignored. To be able to judge these effects a non-linear (FE) approach is necessary. Nevertheless both models improved the insight and understanding of the phenomena occurring in bending of masonry. The orthogonal stiffnessess derived corresponded well with experimental data. Based on serial and parallel connections, the orthogonal stiffness moduli could be derived even more simply.

The MCP approach used to establish the bending strength of masonry, is a rational method, giving insight in the bending strength of masonry. The model uses flexural strength values in the two orthogonal directions to predict the strength in other directions and may also be used for more complex load cases. The model, however, has its limitations because of the linear elastic approach. A future non-linear verification with a FE-model could provide a more fundamental basis of the MCP method. For the time being, the experimental results could already be explained reasonably well with the MCP approach.

6. FLEXURAL STRENGTH AND DESIGN

The determination of flexural bond strength related to design is considered. The influence of the test method and specimen size were investigated. A comparative research was carried out using five different test methods in combination with two types of masonry. In total 407 bond tests were performed, including tensile, 4-point bending and bond wrench tests.
The specimen size was not only taken into account in experiments, but also theoretically. In the theoretical research also the influence of the scatter of tensile bond strength and fracture energy upon the variation of the flexural strength of masonry was investigated numerically in a probabilistic manner taking the dimensions of the failing cross section into account.

The relatively simple bond wrench test can be used as a means to measure bond. Under laboratory conditions it gave the same or a lower CV as with 4-point bending tests on wallettes. The outcome of the bond wrench was equivalent to the flexural test on wallettes if the number of simultaneously loaded joints in the wallette test was taken into account.
The theoretical research indicated that with an increase of the failing cross section, the flexural strength decreases. This strength decrease could not be confirmed by the experimental results. An influence of the dimensions of the failing cross section upon the CV of the flexural strength was not found.

Keywords: **flexural bond strength, probability, distribution, numerical analysis, bond wrench test, 4-point bending test, tensile test, comparison**

6.1 INTRODUCTION

In chapter 2, it was shown that the flexural strength is a structural and not a material property. However the flexural strength will remain important in the practical design of laterally loaded masonry. If the flexural strength is based on experiments with the same materials and tested in the same assemblage as used in the design, the problem of being a structural property becomes purly theoretical. This explains more or less the broad acceptance of the 4-point bending tests on wallettes. These tests however, have a large disadvantage that they are too expensive and/or too laborious to be used as a suitability test on a project basis. The bond wrench test that is described in the Australian Masonry Code AS 3700-1988, annex A7[75] and in ASTM C 1072- 86[1] can be used with relatively small handsome specimens. However, it is still a debate in the masonry community if the bond wrench measures the flexural strength in a reliable manner. A bond test method must produce reliable information about bond and the CV of the test results must be within the range that is normally found with tests on masonry. De Vekey et al.[1994,[12]] have shown that the CV of bond wrench tests results was high for tests on site (50%), but reasonable (20-25%) for laboratory tests.

To investigate the utility of the bond wrench test, a comparative experimental research was carried out. The influence of the scatter of tensile bond strength and fracture energy upon the variation of the flexural strength of masonry was investigated in a probabilistic, numerical manner. In that research, the influence of the length of the failing bed joint was also taken into account with a three dimensional FE model, with randomly assigned values of the tensile strength and the fracture energy. This offered the opportunity to establish a relation between the strength and CV of small and larger cross sections loaded in bending.

6.2 Bond Test Methods

6.2.1 Introduction

In the comparative research 5 different test methods were used in combination with two, well know types of masonry:

- clay brick masonry with normal joint thickness (approx. 12 mm);
- calcium silicate masonry with thin layer joints (approx. 2 mm thickness).

The following test arrangements were used:

- tensile tests with restraints;
- tensile test with hinges;
- small 4-point bending tests on relatively small specimens;
- 4-point bending test on normal wallettes and double width wallettes;
- bond wrench tests.

On the one hand the tensile tests with restraints were used for comparison reasons but on the other hand they were intended to extent the amount of post peak data. The results of those tests were already taken into account in chapter 2. The tensile test with hinges was also chosen to experimentally explore the difference with the tensile tests with

restraints, given the outcome of the numerical assessment already discussed in section 2.3.6. Furthermore, its simplicity makes it useful for suitability/verification tests.
The numerical comparison of tests methods (Van der Pluijm[1995,[53]]) was the ground for ignoring the cross couplet test currently prescribed in de Dutch masonry standard NEN 6790:1993[[14]]. It became clear that its result is not representative for the tensile bond strength. The outcome is, among other things, too much dependent on the actual bond surface. The reason for including the 4-point bending tests on wallettes and the bond wrench test has already been motivated in section 6.1.
The small 4-point bending test was seen as an intermediate step between the wallette tests and the bond wrench test for which nearly the same specimen as in the small 4-point bending test was used. Moreover, the small 4-point test was also used as a means to establish the fracture energy (see section 2.4).
Before discussing the experiments themselves, the influence of another important aspect of wallette testing will be discussed.

6.2.2 Influence of number of joints

Apart from load introduction, specimen dimensions etc., the flexural tests used in the test program differ in the amount of joints that may fail. With the flexural strength, being a parameter with a high CV, this implies that the mean test result of e.g. wallettes tested in flexure with four joints in the constant moment area, is not equal to the mean of the population of joint strength values. In every test the weakest out of four joints determines the measured strength.
This phenomenon was studied by Lawrence[1991,[32]] and Baker et.al.[1976,[3]] by means of Monte Carlo simulations.
Baker et al. gave the ratio between the beam strength and bed joint strength of stack bonded piers as a function of the CV of the population of joint strength values. Baker et al. simulated beams tested in 4-point bending test arrangement with 4 joints in the constant bending moment area.
Lawrence gave nearly the same values for stack bonded piers with eight joints loaded in a third point bending test arrangement. He also presented some results for two brick wide beams (wallette) and used a weakest link assumption to calculate the failure load of a joint in the two brick wide beams based on the results of the stack-bonded pier. Failure of the weakest part was assumed to cause immediate failure of the whole joint. In section 6.3, it will be shown that the influence of the weakest link in one joint is limited when the non-linear redistribution is taken into account. Therefore, those results of Lawrence were ignored. Lawrence also used 'order statistics' (Mosteller et al.[1973,[44]]) from which relations between the strength of the whole population and the strength of a

sample can easily be derived. In Figure 141, the influence of the CV on the ratio between the specimen strength and the mean joint strength is presented.

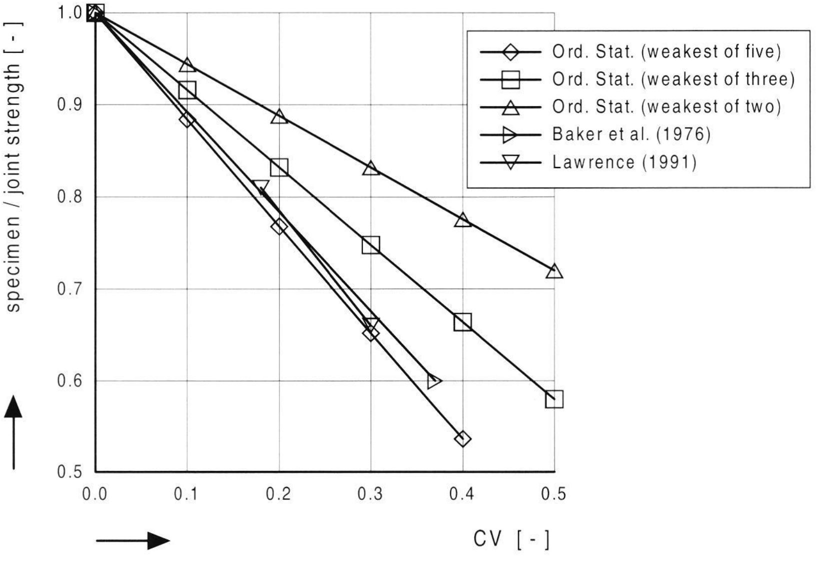

Figure 141 Overview of relations describing the influence of the CV on the ratio between the specimen and joint strength

It can be seen that the relations according to Lawrence, Baker et al. and order statistics (weakest of five) are approximately the same, although Baker et al. and Lawrence considered different test arrangements.
From these theoretical assessments, it can be expected that with a CV=25%, the mean strength of tests with 4 joints in flexure is approximately 70% of the mean joint strength of the population.

6.2.3 Test Methods

The tensile test with fully restrained platens was presented in Figure 6 of section 2.3.1 on page 13. The arrangement used for the tensile test with hinges has already been discussed and shown in Figure 87 on page 102. The small 4-point bending tests was shown in Figure 24 on page 33 and the arrangement for wallette testing in Figure 85 on page 101.

The bond wrench test set-up used, was introduced in Vermeltfoort et al.[1995,[82]] and is presented in Figure 142.

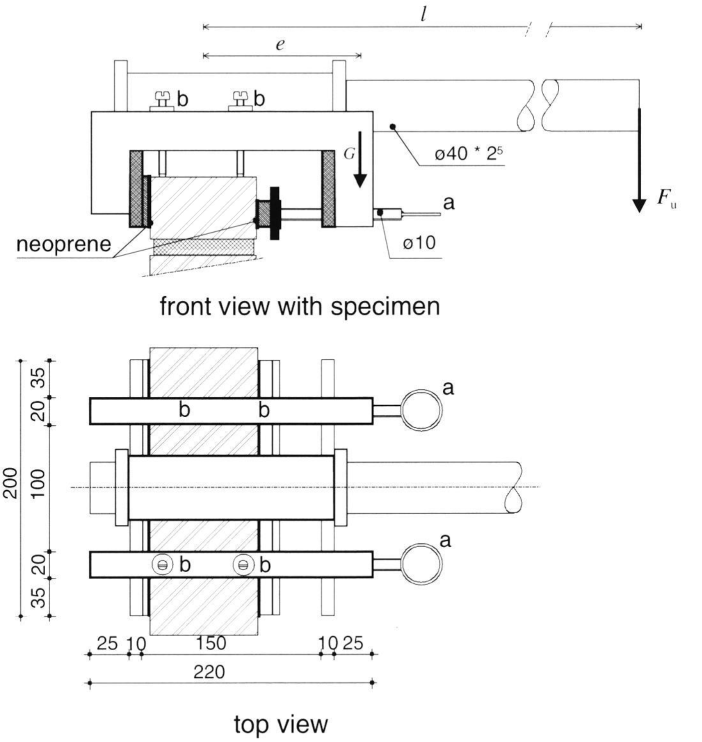

Figure 142 Bond wrench test set-up for couplets and piers

The bond wrench is a large clamp with a lever arm. The clamp is placed over the top-unit of a stack bonded prism, couplet or in case of in situ testing on a unit of which the head joints are removed. After fixing the clamp, the load F is increased until failure of the joint occurs. The flexural bond wrench strength is calculated from:

$$f_{\mathrm{fl;bw}} = \frac{F_{\mathrm{u}} \cdot l + G \cdot e}{W_{\mathrm{el}}} - \frac{F_{\mathrm{u}} + G}{A} \tag{39}$$

In Figure 143, the principal compressive stresses following from a non-linear FE analysis, are shown as well as the deformed FE model when the ultimate load was reached (for more details the reader is referred to Van der Pluijm[1995, [53]]).

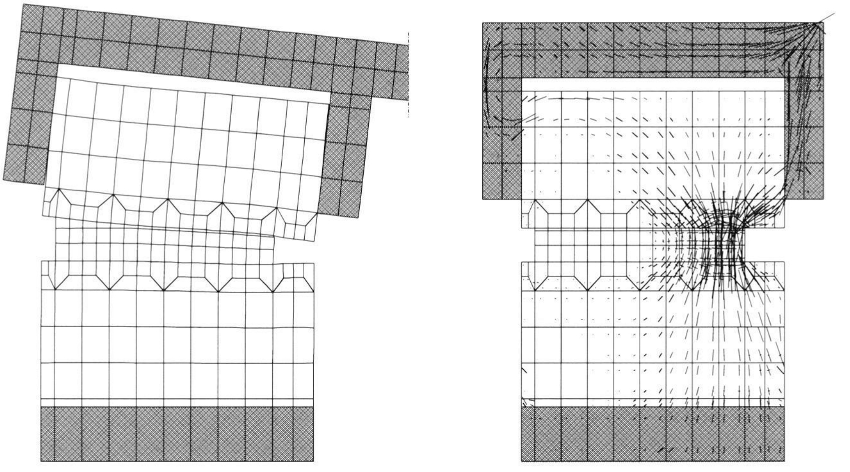

Figure 143 Principal compressive stresses and deformations in a specimen at ultimate load (Non-linear FEM calculation)

The numerical assessment showed that the bond wrench result was equivalent with the 4-point bending test when the lever arm was 1.0 m, having a tensile bond strength of 0.4 N/mm^2. Recently an additional calculation was made, showing that a lever arm of 0.5 m did not influence the outcome.

In the comparative research, the bond wrench specimens were calmped to a frame made of HE300B beams as shown in Figure 144.

The position of the specimen after testing a joint could be adjusted by means of a screw jack. The brick beneath the joint to be tested was clamped to the frame in the same way as the brick in the wrench.

In the performed tests, the load was always applied by means of a jack with a load cell via a steel wire and a pulley. The steel wire was connected to the lever arm with a screw eye. In this way a perfect vertical load could be applied. The maximum load was recorded.

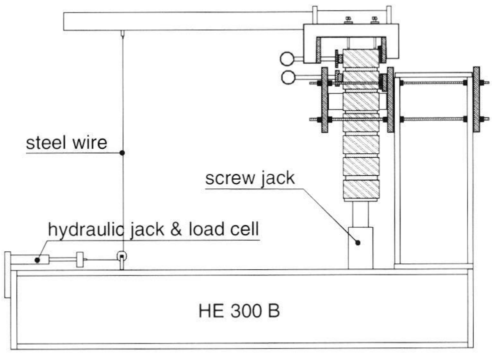

Figure 144 Frame for clamping prisms to be tested with bond wrench

6.2.4 Materials, specimens and test program

For the clay brick masonry, the wc-JO90 clay bricks were used and for the calcium silicate masonry CS-block95 units. The mortar for the calcium silicate units was a factory made, ready mixed thin layer mortar, brand Calsifix (summer quality). The 1:1:6 mortar for the clay brick masonry was composed in the Pieter van Musschenbroek laboratory. Details about units and mortars can be found in Appendix A 'Materials' in Table 32 and Table 34, respectively. Pre-treatments and curing conditions are given in Table 35.

Six different test series were made for each masonry type. The test program and the number of specimens are presented in Table 27.

Table 27 Overview of types and number of specimens used in the 5 test set-ups

	test arrangement					
	4-point bending		small 4-point bending	bond wrench	tensile, restraints	tensile, hinges
specimen type:	normal wallette	double width wallette	stack bonded prism / couplet		couplet	couplet
clay brick masonry	6	6	24	12 / 12 *)	36	36
Figure 145:	A	B	C	C / E	D	D
calcium silicate masonry	6	6	24	72	36	36
Figure 146:	A	B	C	D	E	E

*) In use with the bond wrench 60 / 59 test result were obtained from these specimens

Apart from ordinary wallettes, so-called 'double width' wallettes were used. These type of wallettes were made, because numerical research presented in Van Geel et al.[1994,[18]], indicated that an increased width could reduce the CV. The size of the ordinary wallettes fulfilled the demands of prEN 1052-2:1996.

The clay brick specimens and the calcium silicate specimens are presented in Figure 145 and Figure 146, respectively.

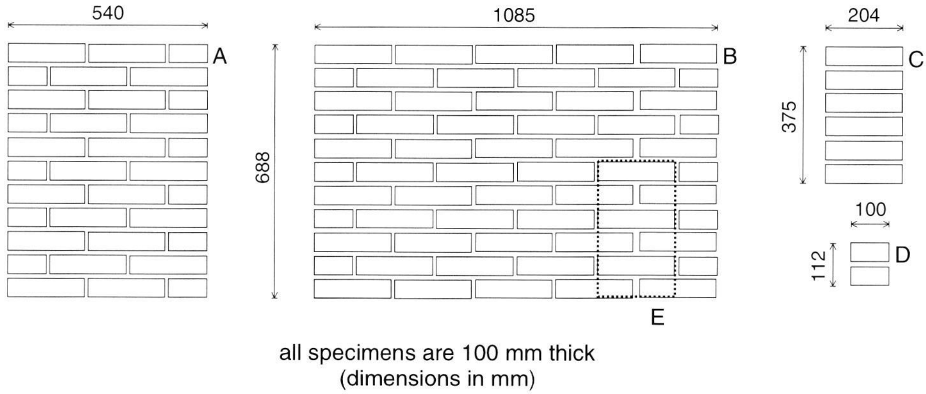

Figure 145 Overview of clay brick specimens: A) normal wallette, B) double width wallette, C) stack bonded pier for bond wrench and small 4-point bending test, D) couplets for tensile tests E) stack bonded pier sawn out of remainder of wallettes

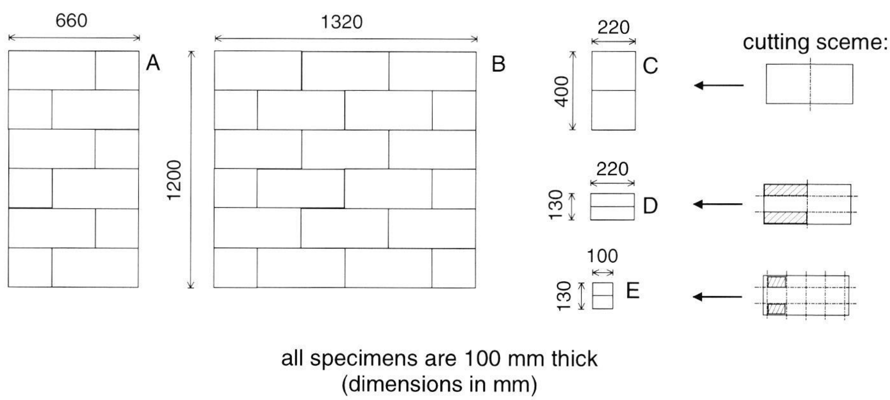

Figure 146 Overview of calcium silicate specimens: A) normal wallette, B) double width wallette, C) couplet for small 4-point bending test, D) couplet for bond wrench, E) couplet for tensile tests

In a comparative research it is most important that the specimens for the different test methods are made with the same mortar at the same time by the same mason in the same way. To reach this goal, the clay brick specimens were made in six sub-series in two days, because it was not possible to make the whole series in one batch. Each sub-series consisted of 1 normal wallette, 1 double width wallette, 4 stack bonded piers for the small 4-point bending test, 2 stack bonded piers for the bond wrench and 12 small couplets for the tensile tests (see Figure 147).

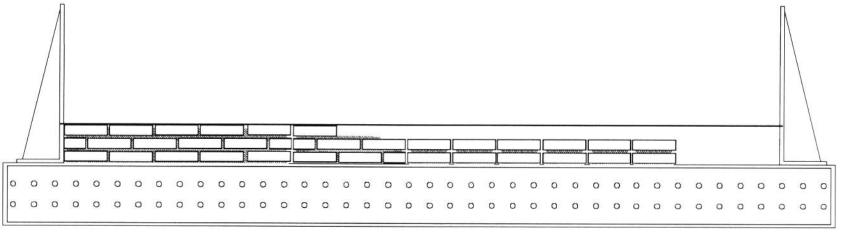

a) start

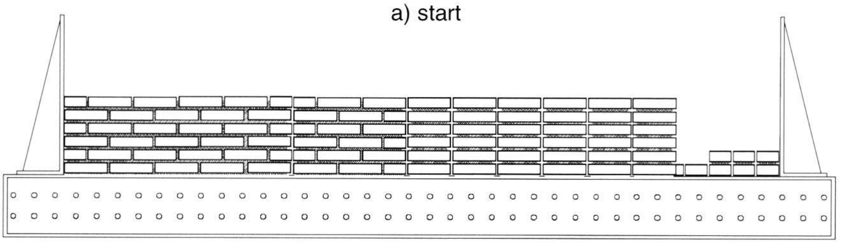

b) making of tensile specimen

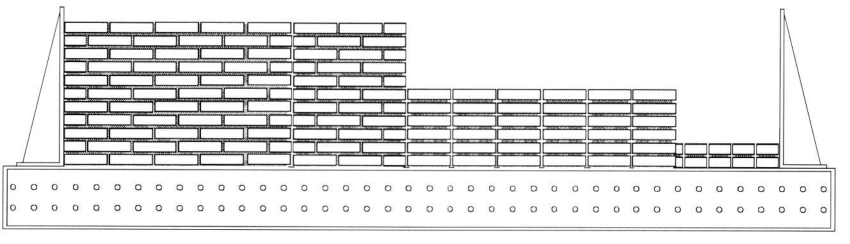

c) completed sub-series

Figure 147 Fabrication of specimen

The specimens of a sub-series were made with one mortar batch. The height of the courses was controlled with cord guiding. Joints were filled completely and a trowel was used to strike the joints flush. Courses of the wallettes and piers were made at the same time in a row on the same support, consequently the piers were completed when the wallettes were completed by half (Figure 147b). At that moment the couplets were made. The mason placed the top bats of the couplets in the same way as on a normal course. After finishing the couplets, the mason completed the wallettes (Figure 147c). The calcium silicate specimens were made in the same way, but no cord guiding was needed because the units are provided with tongues and grooves. The thin layer mortar was applied with a special tool developed by the Dutch calcium silicate industry (see Berkers[1995,[7]]). Now a subseries consisted of twice as much specimens as with the wc-

JO clay brick masonry mainly because the specimens could be built quicker. Furthermore the thin layer mortar can be used relatively long without loosing its workability.
Non of the specimens were pre-compressed in the curing period. In the experience of the author pre-compression does not influence the bonding of top layers.
The specimens for the small 4-point bending test were adjusted for the test set-up by reducing the width to approx. 160 mm.
Testing of the specimens started at an age of at least 48 days and was completed with a maximum age of 63 days. A starting age of at least 6 weeks was chosen to avoid changes in bond strength due to hardening effects during the testing period, because of the relatively long period needed to test a whole series. The specimens of a sub-series were, as much as possible, tested simultaneously.
After the clay brick wallettes were tested, specimens for bond wrench testing were sawn out of the remainders (Figure 145E). This was not done for the calcium silicate masonry wallettes because the remainders with the large blocks could not be used in the bond wrench test set-up. Due to capacity problems in the laboratory these specimens were tested at an age of 120±4 days.

6.2.5 Test Results

In all tests, failure occurred at the bond surface or partially at the bond surface and in the mortar. In the wallettes only joints in the contant moment area between the loading beams failed. In the clay brick stack bonded piers that were tested in the small 4-point bending test set-up, sometimes a joint between the loading beams and the supports failed. These results were also used. Mean results per mortar batch are presented in Table 60 and Table 61 in Appendix B 'Experimental Results'. The means of all results per test arrangement and per masonry type are presented in Table 28.
Looking at the values in Table 28, the following observations were made.

1. With the clay brick specimens, the tensile test with fully restrained platens gave higher results than the tensile test with hinges; the probability of the measured difference determined with the t-test equals 31%.
2. With the calcium silicate specimens, the tensile test with hinges gave higher results than the tensile test with fully restrained platens; now the probability of the measured difference is 0.02%.
3. The bond wrench tests on the clay brick piers gave almost the same results as the bond wrench tests on the piers out of the remainders of the wallettes.

Table 28 Mean strength values [N/mm^2] of clay brick and calcium silicate masonry for each test arrangement also relatively to the tensile tests with restraints

test arrangement		mean strength of clay brick masonry		mean strength of calcium silicate masonry	
		[N/mm^2]	relative [-]	[N/mm^2]	relative [-]
tensile	restraints	0.41(39)	1.00	0.33 (27	1.00
	hinges	0.38 (41)	0.94	0.41 (24)	1.24
small 4-point bending	stack bonded prism / couplet	0.60 (32)	1.49	0.40 (40)	1.22
4-point bending	normal wallettes	0.57 (29)	1.41	0.34 (31)	1.03
	double width wallettes	0.56 (27)	1.38	0.35 (13)	1.06
bond wrench	stack bonded prism / couplet	0.68 (29)	1.68	0.45 (18)	1.36
	wallettes	0.66 (31)	1.63	-	-

4. For both material combinations, the small 4-point bending test gave a 13% lower result than the bond wrench test. The probability of the difference between the means of the bond wrench and the small 4-point bending tests was 11% for the clay brick masonry and 18% for calcium silicate block masonry.
5. Wallette tests gave the lowest flexural strength results.
6. The ratio between overall mean wallette strength and the joint strength based on the bond wrench is 0.83 for the clay brick specimens and 0.77 for the calcium silicate specimens.
7. The normal and double width wallettes gave almost identical results for both clay brick and calcium silicate masonry. The results of both types of test can be considered as if they originated from one sample.
8. The ratio between the wallette tests and tensile tests with restraints were 1.6 and 1.4 for clay brick and calcium silicate masonry, respectively.
9. The CV of the bond wrench results was approximately the same as, or smaller than the CV of the wallette test results when both type of wallette tests are considered as one sample.

The tensile test with hinges gave a significantly higher mean strength than the tensile test with fully restrained platens for calcium silicate masonry. Looking to the results per mortar batch, two batches may have been switched, which would have resulted in nearly equal strength values for both types of tensile test arrangements.
If the actual bonding areas do not show an eccentricity, both types of tests will give nearly the same result as discussed in section 2.3.1. The difference between the results

obtained with clay brick masonry in both tensile test arrangements is too small to be attributed to a difference in test method.

The difference between the results obtained with the small 4-point bending test and with the bond wrench is statistically not significant but the probabilities (11 and 18%, see point 4 above) are small enough to become suspicious about the observed difference. An effect that might have played a role, is the observation that with 4 out of the 18 small 4-point bending tests on clay brick masonry, failure outside the constant moment area occurred and a second weaker joint in those specimen influenced the mean strength (see section 6.2.2). This effect, however, only explains 3% (estimated on the basis of Figure 141) of the 13% difference. The 'number of joints' effect did not play a role in series with calcium silicate block masonry.

For the clay brick masonry the difference between tensile tests and flexural tests was as expected. The same was true for the calcium silicate masonry.

Based on order statistics and a CV of 25% the expected ratios between the bond wrench and the wallette tests were (see Figure 141):

- 0.78 for the calcium silicate wallettes (3 joints in pure flexure) and
- 0.70 for clay brick wallettes (4 joints in pure flexure).

These theoretical ratios completely explained the ratios found between the bond wrench and the small 4-point bending test results and the wallette test results. The ratio of 0.87 that was found between the wallette test results and the bond wrench test results of the piers made out of the remainders of the wallettes, confirmed the correlation between bond wrench and wallette testing.

6.2.6 Concluding remarks

Although the tensile tests with hinges performed well in this research, it is not recommended as a suitability test. Especially for lower bond strength values it is expected to underestimate the bond strength.

The effect of measuring a lower mean flexural bond strength with wallette testing than an estimate of the mean strength of the population and consequently arriving at a lower characteristic strength used in design, is an important negative effect of this arrangement.

Comparing the results obtained with wallettes on the hand and those obtained with the small 4-point bending test and the bond wrench on the other hand, led to the conclusion that the presence of head joints (and consequently the bonding pattern) is not important for the flexural bond strength. Taking the theoretical considerations of chapter 5 into account there is little reason to expect that the presence of head joints could play a role visible within the scatter of the experimental results. Of course, the bonding pattern does play a role in the horizontal flexural strength.

6.3 TENSILE AND FLEXURAL BOND, STOCHASTICALLY RELATED

6.3.1 INTRODUCTION

The flexural bond strength parallel to bed joint, as a function of the length of the failing joint, was investigated numerically, taking into account the important parameters that determine the flexural strength: tensile bond strength, post peak behaviour, stiffness and their coefficients of variation (CV). The numerical results offered the opportunity to relate the flexural strength of small specimens and their CV's to that of larger ones.

In comparison with an experimental research, a numerical research offers the opportunity to apply exactly the same properties to 'specimens' and define exactly the same boundary conditions. Therefore, the results are not influenced by experimental errors (variations produced by disturbing factors both known and unknown).

Parts of masonry with varying length were modelled into a three-dimensional finite element (FE) model. The dimensions of the bond surface varied between 204×98 mm and 1224×98 mm (see Figure 148).

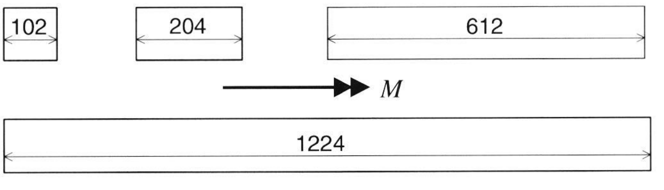

Figure 148 Overview of the dimensions of the modelled bond surface with the applied moment vector

Values for tensile bond strength and fracture energy were drawn out of distributions of probability and assigned to every part of the bond surface. The assignment of the randomly drawn values of the bond interface was performed in a special way that will be discussed later. With the assigned properties the ultimate bending moment M_u of the

FE model was determined and a value for the flexural strength was calculated with M_u/W_{el}. The assignment procedure and the calculation were repeated until a good impression of the mean strength and coefficient of variation (CV) could be derived. This Monte Carlo type of process was repeated for different assumptions concerning the bond strength, fracture energy and other properties. In total over 200 non-linear analyses were carried out for 16 different ways of submitting the random strength and fracture energy values using different kinds of correlation between parameters and different values for coefficients of variation.

A similar research was already presented by Van Geel et al.[1994,[18]], but at that time only the tensile bond strength was taken into account in a stochastical way.

6.3.2 FE MODEL

The three-dimensional FE models, developed within the DIANA finite element code, were exactly the same as used by Van Geel et al.[1994,[18]]. An example of a model with a length of 1224 mm is depicted in Figure 149. In the model, one bed joint is assumed to be decisive for failure and non-linear behaviour was modelled for this joint. The other joint and the units were assumed to behave linear elastic. A mesh refinement was applied near the fracture joint, allawing for a fine distribution of tensile bond strength values over the bond surface.
The units were modelled with solid brick type 20-nodes quadratic continuum elements. The interfaces between units and joints were modelled with 2D 16 nodes quadratic interface elements of a type corresponding with the solids. The influence of head joints was completely neglected in the FE model. Only in the decisive bed joint, non-linear material behaviour was modelled, representing the combined behaviour of the mortar (stiffness) and the brick-mortar bond interface (tensile bond strength and fracture energy). The load was introduced on one side of the model as a pure bending moment by means of a linearly altering surface load. From a preliminary study, it appeared that a model depth of two courses was necessary to guarantee a correct introduction of stresses (momentum) in the fracturing joint. The load was increased with a quadratic arc-length method with an automatically adjusted load increment. In combination with an automatic stop criterion for negative load increments, occurring after the peak has been reached, it was possible to complete every calculation without the need of monitoring the calculations.
The side opposite to the loaded plane was fully restrained in horizontal direction. The decisive joint is located at this side. This restrained side is a symmetry plane of the model.

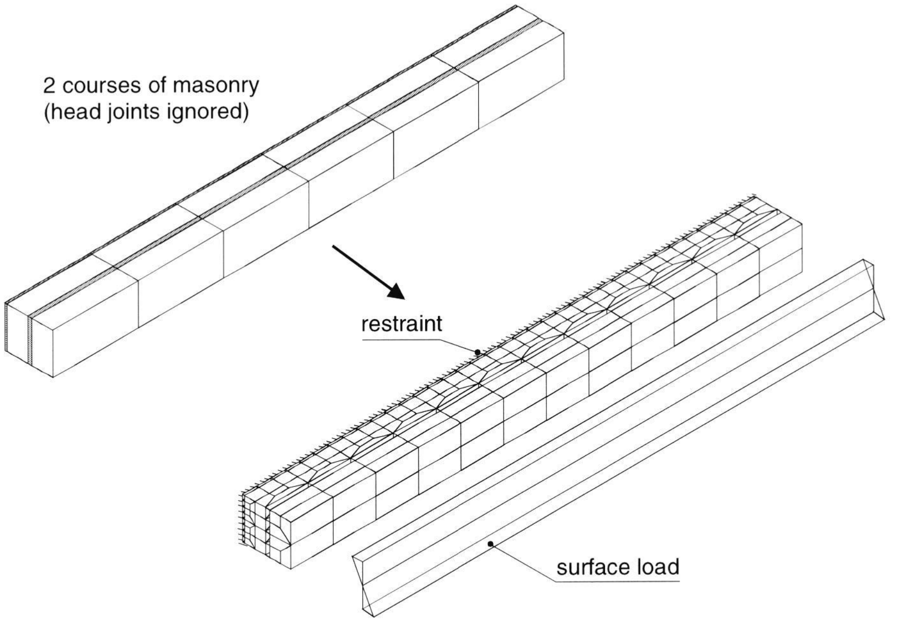

Figure 149 Example of one of the FE models with a length of 1224 mm (6 bricks)

As already indicated in Figure 148, models with a length of 204 mm, 612 mm en 1224 mm were used. To study the influence of different assumptions concerning e.g. the CV of the tensile bond strength, the model with a length of 612 mm was mainly used. As an alternative of applying a surface load, in some series an imposed deformation was used (see Figure 150).

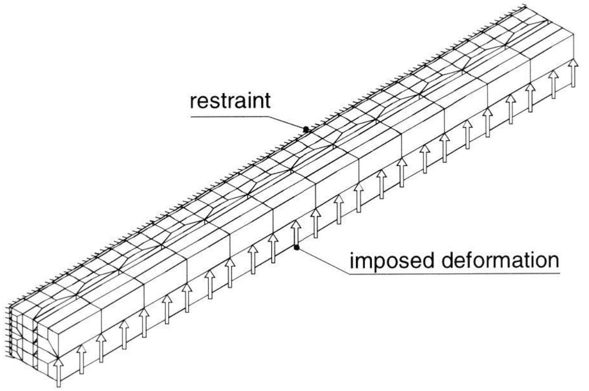

Figure 150 Loading of the FE-model via an imposed deformation

Material properties of brick, mortar and interface were based on the first wc-JO90+GPM series (Table 38), from which properties were chosen as presented in Table 29. Under tension, a lower Young's modulus was attributed to the mortar elements than under compression. This difference, observed in the experiments (see Vermeltfoort et al.[1991, [80]]), can be explained by contact areas within the mortar being able to transfer compressive stresses but unable to transfer tensile stresses. In Van der Pluijm[1992, [47]], it has been shown that this difference affects the ultimate bending moment only in a very limited way. Tension softening was modelled by means of eq. (1) (page 9). Because the decisive joint is located at the symmetry plane of the FE model, only half of the intended value for G_{fI} must be applied to obtain the correct stress-crack width diagram. These values are presented in the tables.

Table 29 Material properties in finite element analysis

elements for:	material property		value
bricks	E^u	[N/mm^2]	16700
	ν	[-]	0.20
all joints	E_c^j	[N/mm^2]	13000
	E_t^j	[N/mm^2]	4500
failing joint	f_{tb}	[N/mm^2]	variable
	G_{fI}	[N/mm]	variable

6.3.3 PROBABILITY DISTRIBUTIONS

The tensile bond strength and fracture energy were the stochastic variables. Based on many publications (see e.g. Baker[1981,[4]], Baker et al.[1985,[6]], Lawrence [1985,[29]], Lawrence and Cao[1988,[31]], Vermeltfoort et al.[1995,[82]]), the statistical distribution of the tensile bond strength was assumed to be normal. The amount of data available for the fracture energy is too little to determine its distribution. It was assumed to be normal or lognormal. The normal distribution for the fracture energy was replaced by a lognormal distribution when a small mean value led to drawing of negative values.
A pseudo random generator (Merchant[1981,[40]]) was used to produce uniformly distributed values between 0 and 1. These values were converted to a standard normal distribution using the central limit theorem and subsequently to the desired normal or lognormal distribution.

6.3.4 ASSIGNMENT OF VALUES

Besides the choice for mean values and standard deviations of the stochastic variables another important question arose: which of the several generated values is attributed to which interface (bed joint) element? It was assumed that the unit plays an important role in the scatter of bond and mortar properties e.g. due to scatter in suction rate of each unit. In first instance, half a unit was chosen as the representative area to assign one value. Series of calculations were also made with the whole unit as the representative area. The drawn value for the tensile bond strength of a representative areas was taken as the mean of a second distribution with a CV of 10%. Furthermore it was assumed that, due to the drying process of mortar resulting in shrinkage cracks, lower tensile bond strength values occur at the zones of a joint near the face of the masonry (top and bottom side of the FE model if Figure 149). Therefore, values drawn from the second distribution were ordered and the high values were randomly assigned to the elements in central zone (dark rectangular bars in Figure 151) and the remaining values randomly to the remaining elements in the outer zones (light cylindrical bars in Figure 151).

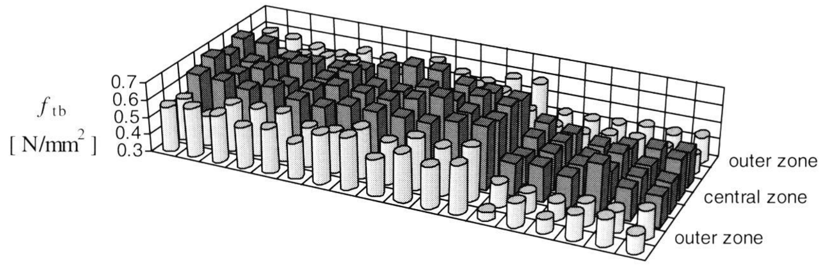

Figure 151 Example of generated tensile bond strength values of a calculation in series B (length = 612 mm) with a representative area equal to one unit, with low values submitted to the outer zones and high values to the central zone

For the fracture energy, one value per representative area was drawn. This resulted in many different combinations of the tensile bond strength and fracture energy values, which is in accordance with the experimental data.

6.3.5 Calculations

Before presenting the results of the calculations in a general way, an example is presented, so the aspects mentioned in the previous section will become more concrete. The input and output for a calculation series is presented in Table 30 and Figure 152.

Table 30 Input and output of a calculation series 7

	length = 612 mm		input-values	type of distribution	actual values
input	mean f_{tb}	[N/mm^2]	0.50	normal	0.486
	CV of f_{tb}	[%]	25.0		29.4
	mean G_{fI}	[N/m]	7.0	lognormal	6.62
	CV of G_{fI}	[%]	100.0		85.0
output	mean f_{fl}	[N/mm^2]	-		0.664
	CV of f_{fl}	[%]	-		8.1

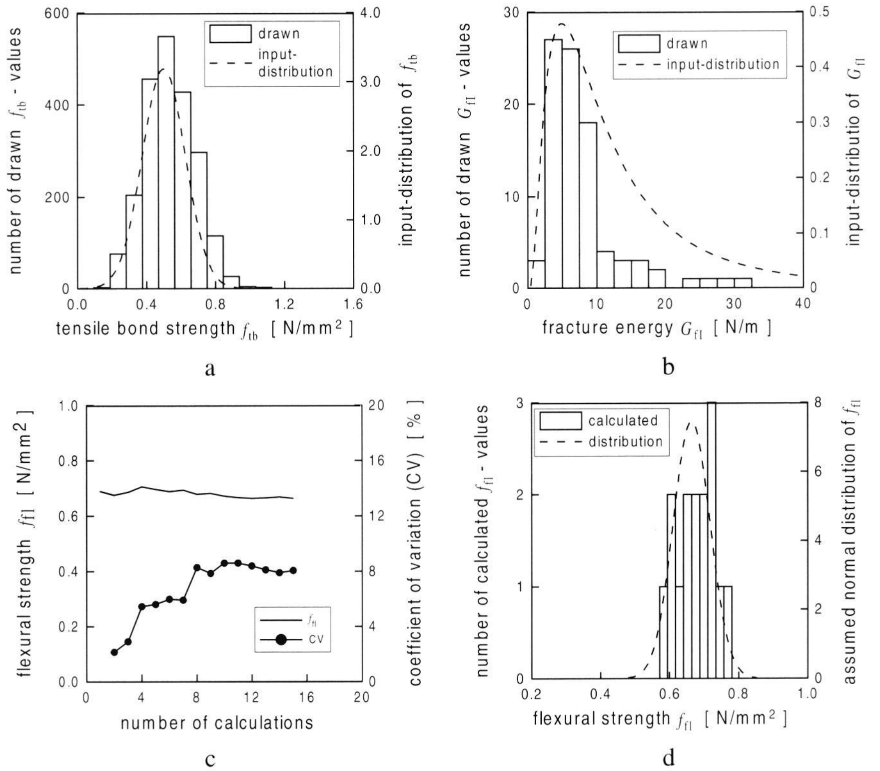

Figure 152 Input and results of a calculation series 7

For the drawing of values for the tensile bond strength a normal distribution with a mean value of 0.5 N/mm^2 and a CV of 25% was assumed. The drawn values were used as the mean for an area with a length of a half unit. Then, values for each element of this area were determined using that value with a CV of 10%. The input-distributions and the drawn values, are also presented in Figure 152a and b. The values drawn from this distribution that were assigned to the non-linear interface elements, resulted in a mean of 0.486 N/mm^2 and a CV of 29.4%. For the fracture energy a lognormal distribution with a mean value of 7 N/m and a CV of 100% was assumed. A normal distribution

would lead to drawing of negative values. The values drawn from the lognormal distribution with a mean of 7 N/m and a CV of 100% led to a mean of 6.62 N/m and a CV of 85% of the drawn values, assigned to all elements in the ½ unit area.
After 15 calculations the mean flexural strength was 0.664 N/m^2 with a CV of 8%. A histogram of these results is presented in Figure 152d. In Figure 152c the mean and CV are presented as a function of the number of calculations. From this kind of diagrams, it was concluded that the number of calculations was sufficient to get a reliable impression of the mean and the CV of a series of calculations.

6.3.6 DISCUSSION OF RESULTS

A summary of the results of the series of interest is presented in Table 31.

Table 31 Overview of calculated series

series	model-length	tensile bond strength f_{tb} [N/mm^2]				fracture energy G_{fI} [N/m]				flexural strength f_{fl} [N/mm^2]	
		mean	CV[%]	distr.	Area*)	mean	CV[%]	distr.	Area 5)	mean	CV[%]
1	612	0.492	25.1	N	½	7.00	-	-	-	0.70	3.8
5	612	0.489	25.8	N	½	9.19	64.8	N	½	0.70	11.0
6 1)	612	0.489	25.8	N	½	9.19	64.8	N	½	0.71	10.7
7	612	0.486	29.4	N	½	6.62	84.9	LN	½	0.66	8.1
8	612	0.491	28.8	N	½	6.74	35.0	LN	½	0.70	6.3
9 2)	612	0.491	37.4	N	½	6.19	84.8	LN	½	0.64	8.3
A	612	0.245	28.1	LN	½	6.56	87.3	LN	½	0.42	7.6
B	612	0.508	24.1	N	1	7.58	94.3	LN	½	0.67	12.9
C	1224	0.489	26.5	N	1	6.95	95.5	LN	½	0.61	16.1
D	204	0.544	23.5	N	1	7.28	91.1	LN	½	0.77	16.1
B' 3)	612	0.508	24.1	N	1	7.58	94.3	LN	½	0.71	10.4
C' 4)	1224	0.489	26.5	N	1	6.95	95.5	LN	½	0.68	9.1

1): $E_t^j \sim f_{tb}$
2): increased value of CV in representative area
3): as B, deformation controlled
4): as C, deformation controlled
5): the representative area for submitting bond strength values ½: 102×98 mm^2; 1: 204×98 mm^2

In series 1 only the tensile bond strength was treated stochastically. This resulted in a CV of the flexural bond strength that reduced to 0 with an increasing length of the crack. This series represents the work presented in Van Geel et al.[1994,[18]]. In series 5 the fracture energy is treated stochastically by using a normal distribution. One value per ½ brick length area was used. This results in a large increase of CV of the flexural strength from 3.8 to 11 %. However, the normal distribution led to drawing of negative values that were not used, resulting in a mean of the fracture energy that was higher than the intended value of 7 N/m. This was corrected in series 7 leading to a lower mean and CV of the flexural strength.

The data from the tensile tests showed a weak correlation between the stiffness of the joint and the tensile bond strength f_{tb} (see Figure 14 on page 25). This correlation was used in series 6. The influence of this correlation by applying a linear relation between them, was negligible compared with series 5,. In series 8 the assumed CV of the fracture energy was reduced to 40% instead of 100% in the previous series. As expected the results of this series fitted between those of series 1 (CV of G_{fI} is 0 %) and the series with the high values for the CV of the fracture energy. In series 9 the CV of 10% that was used for submitting tensile bond strength values to the finite elements of the ½ brick area was increased to 25%. Other assumptions were the same as for series 7. The differences between series 7 and 9 were negligible.
In series A, the mean tensile bond strength was lowered to 0.25 N/mm^2 compared with series 7. The CV of the flexural bond strength hardly changed, but the ratio between the tensile bond strength and the flexural strength increased from 1.4 to 1.7. This is understandable as the mean fracture energy was the same for both series, resulting in a more ductile behaviour of series A. This effect clearly show that the flexural strength is not a material property but a structural one.
In series B the representative area for submitting tensile bond strength values to the elements was increased to 1 brick compared with series 7. As a result the mean flexural strength hardly changed, but the CV of the flexural strength increased from 8 to 13%. Assumptions for the material-properties in series C and D are the same as in series B, but the model length was different. It could be observed that with an increasing length the mean flexural strength decreases. The influence on the CV of the flexural strength is not really unambiguous as can be observed in Table 32, but it might be concluded that the CV of the flexural strength is not influenced by an increase of the length of the model for series B, C and D.
Series B and C were repeated using a deformation controlled load (series B' and C'). This resulted in an increase of the mean flexural strength and a decrease of the CV of flexural strength. The ratio between the mean flexural strength and the mean tensile bond strength is presented in Figure 153 for the series B,C, D and C', D'.

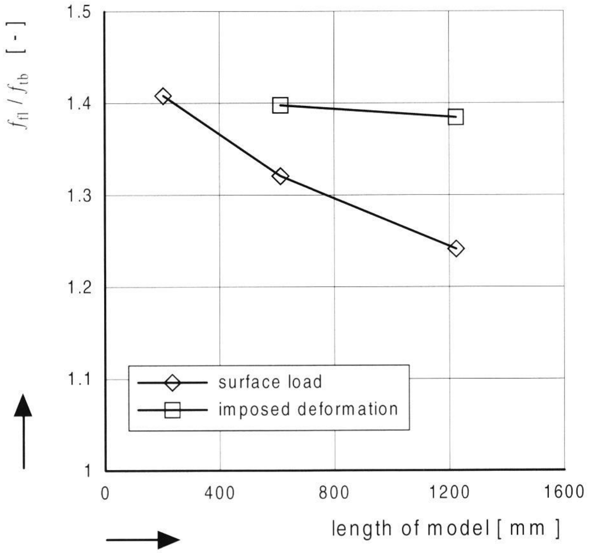

Figure 153 The ratio between the flexural and tensile bond strength as a function of the length of the model for series B, C, D and B', C'

A decrease of this ratio could be observed with increasing model length. This effect can be seen as a 'weakest link' effect. In case of a deformation-controlled load, the decrease was small.
A 2½ brick wide (≈ 540 mm) should give a 6% lower strength than a 1 brick wide (≈ 205 mm) specimen in case of surface loading according to Figure 153. With imposed deformations the difference is not more than 1%.

6.3.7 CONCLUDING REMARKS

In generally 20 calculations per series were necessary, to obtain a reliable impression of the CV of the flexural strength. To get results with a CV of the flexural strength that becomes realistic, a CV of 100% for the fracture energy was necessary in combination with a representative area equal to one brick.

By considering the tensile bond strength and the fracture energy stochastically in combination with a representative area of 1 brick, no influence of the length of the model on the CV of the flexural strength could be found.
As the length of the model increased, the chance of the occurrence of low strength values increases. This 'weakest link influence' is limited because partial cracked areas still have moment capacity allowing for redistribution of loads. This is also the main reason for the influence of the type of loading.

Using a deformation controlled load, the flexural strength is higher and only decreases in a limited way with an increase of the model length. Now an interesting question arises: which load application is representative for a crack that occurs in practise. Of course, a clear answer is not available. In narrow walls the surface load might be representative and for large panels the deformation controlled case, as the cracking part of the masonry is restrained by uncracked parts around it.

6.4 CONCLUDING REMARKS

The bond wrench can be used as a means to predict bond. Under laboratory conditions it gave the same or a lower CV as the wallette test. Taking the number of joints in the wallette test into account, the outcome of the bond wrench and wallette tests was equal. It was concluded that the bond wrench could be used to determine the flexural strength parallel to the bed joint as reliable as the flexural test on wallettes.

By considering the tensile bond strength and the fracture energy stochastically in combination with a representative area of 1 brick, no influence of the length of the model on the CV of the flexural strength could be found. This is in correspondence with experimental results in the previous section, where no influence of the specimen width on the CV was found. Therefore, the characteristic strength of masonry cannot be chosen larger than the characteristic flexural strength of relatively small specimens.

In section 6.2, an influence between specimens with a width of 1 brick (bond wrench tests) and wallettes (4-point bending test) was found, but that difference could be explained by the difference in number of loaded joints on the basis of Figure 141. The theoretical effect of the decrease of the ratio between flexural and tensile bond strength found in section 6.3.6, could not be observed in the experimental result due to scatter.

7. SUMMARY

The bending behaviour of masonry is governed by a complex interaction between masonry units and joints. The understanding if this interaction was the main subject of this dissertation. The problem was explored at the meso level. At this level joints and units were modelled as homogeneous isotropic materials, each with their own material properties.

Chapter 2 describes the behaviour of units, joints and interfaces under tension established in experiments. The applied experimental technique and method of analysis were already available. Non-linear fracture mechanics developed for quasi-brittle materials could be applied to describe the behaviour of the masonry components.
Chapter 3 explains the shear behaviour and failure of masonry in the bond interface between units and joints and/or in the mortar itself. Two newly developed test arrangements were used to establish the pre- and post-peak behaviour of joints and interface under load combinations of shear and normal (perpendicular to the bed joint) compression or shear and normal tension. From literature, it was already known that in combination with normal compressive stresses, the shear strength could be described with Coulomb's friction criterion. This was confirmed by the experimental data. The research went a step further with the establishment of the influence of normal tensile stresses on the shear strength. Furthermore, the post peak behaviour was described. The softening behaviour under shear after the peak showed a close correspondence with the post peak behaviour under tension and similar formulations as used in tension could be applied. Important distinctions with tension are the influence of the normal stresses perpendicular to the bed joint and the uplift perpendicular to the bed joint plane as a result of shearing along the bed plane (so-called dilatancy). Formulations to describe these phenomena have been proposed in this work.
Bending tests on masonry walls are presented in chapter 4. The tests primarily focussed on the influence of the angle between the bed joint and the bending axis. Although all tests were carried out in an uni-axially, stresses occurring in masonry tested with angles between bed joint and bending axis other than 0°and 90° are also representative for bi-axial bending. The stiffness, strength and behaviour were analysed.
Together with the test data obtained in chapter 2 and 3, the results of the bending tests form a unique set of data, enabling researchers to model and verify masonry in bending at the meso level non-linearly.
The bending behaviour of masonry at the meso level was analysed in chapter 5. A description was given of phenomena that occur at the meso level on the basis of three

distinguished bending states: horizontal bending, vertical bending and torsion. Similar to the 'additional' torsion in the bed joint in case of horizontal bending, 'additional' bending of the bed joints in case of torsion was identified as an important phenomenon. An analytical model and a finite element (FE) model were developed to establish the behaviour linear elastically. The models were restricted to a small basic modile in which all meso deformations can occur. The orthogonal stiffnesses (parallel and perpendicular to the bed joint) derived with these models, corresponded well with experimental data. Based on serial and parallel connections, the orthogonal stiffness moduli could be derived even more simply. A rational approach based on the analytical model, taking into account different cracks that may occur (Multiple Crack Pattern or MCP approach), gave insight in the bending strength of masonry. The model uses flexural strength values in the two orthogonal directions to predict the strength in an arbitrary direction. The model can also be applied to calculate the strength in a bi-axial bending state.
Chapter 6 deals with the measurement of the flexural bond strength. With non-linear numerical research based on the data obtained in chapter 2, the influence of the scatter of data obtained with small 'specimens', on the strength of larger specimens was explored in a probabilistic way. Via a comparative experimental research it was shown that the bond wrench test method can be used to measure the flexural strength parallel to the bed joint, as reliable as the flexural test on wallettes. An important advantage of the bond wrench test compared with 4-point bending tests on wallettes, is its representativeness for the average flexural strength of the population.

In chapter 1, it was stated that the research was initiated "to find a scientific acceptable representation of the relation between the mechanical properties of masonry in bending at the meso and macro level" and that the intended work to be done is "to provide users and developers of (non-linear) finite element models with a basis on which they can utilise macro-properties of masonry in bending determined by a few mechanical properties commonly known in engineering". Although, it is in principle possible to model masonry in bending at the meso level in a completely non-linear way with the experimental data and theoretical formulations provided, the modelling of the non-linear macro behaviour has not been accomplished on the basis of the followed bottom-up approach via the proposed FE model. For this, a future research effort is needed. Engineering models only needing the flexural strength can use the MCP-approach to establish the flexural strength in different directions. The model, however, has its limitations because of the linear elastic approach. A future non-linear verification with a FE-model should provide a more fundamental basis of the MCP method.

REFERENCES

[1] American Society for Testing and Materials (1986), *Standard method for Measurement of Masonry Flexural Bond Strength* C1072-86

[2] Base, G.D.; Baker, L.R. (1973), *Fundamental properties of structural brickwork*, Journal of the Australian Ceramic Society, Vol.9, No. 1,

[3] Baker, L.R.; G.L Franken (1976), *Variability aspects of the flexural strength of masonry*, Proceedings of the 4th International Brick/Block Masonry Conference, Brugge, Belgium, No. 2b4

[4] Baker, L.R. (1981), *The flexural action of masonry structures under lateral load*, PhD-Thesis, Deakin University, Geelong, Victoria, Australia

[5] Baker, L.R., (1982), *A principal stress failure criterion for brickwork in biaxial bending*, Proceedings of the 6th International Brick/Block Masonry Conference, Rome, Italy,

[6] Baker, L.R.; Gairns, D.A.; Lawrence, S.J., (1985) *Flexural behaviour of masonry panels - a state of the art*, Proceedings of the 7th International Brick/Block Masonry Conference, Melbourne, Australia, pp. 27-55.

[7] Berkers, W.G.J. (1995), *Building with calcium silicate elements*, Proceedings of the 4th International Masonry Conference / the British Masonry Society, Masonry (7), London, October, pp. 176-179

[8] Beuker, A.J. (1986), *Review of the flexural strength of masonry, practical conclusions*, Adviesbureau ir. G.J. Hageman B.V., Technical report 1654-0-3 (in Dutch)

[9] British Standards Institution BSI (1978), BS 5628 part 1:1978 *Code of practice for use of masonry, Part 1, Structural use of unreinforced masonry*, London

[10] British Standards Institution BSI (1992), BS 6100 part 5:1992 "Glossary of Building and civil engineering terms, part 5. Masonry", London

[11] Cajdert, A. (1980), *Laterally loaded masonry walls*, PhD-Thesis Chalmers University Of Technology, Publication 80:5 Göteborg, Sweden

[12] De Vekey, R.C., Page, A.W., Hedstrom, E.G. (1994), *The variability of bond wrench measurements in UK, Australia and USA*, Masonry International, Vol. 8 No. 1 pp. 21-25.

[13] Dongarra, J.J., Bunch, J.R., Moler, C.B., Stewart, G.W, (1979), LINPACK Users' Guide, SIAM, Philadelphia.

[14] Dutch Normalisation Institute NNI (1997), NEN 6790 TGB 1990, *Masonry structures, basic requirements and determination methods*, Delft

[15] European Committee for Standardisation CEN (1993), prEN 1052-2:March 1993 *Methods of test for masonry structures, Determination of flexural strength (draft)*, Brussels

[16] Ganz, H.R., Thürlimann, B. (1988), *Design of masonry walls under normal force and shear*, 8th International Brick/Block Masonry Conference, Dublin, Ireland, September, pp 1447-1457

[17] Gazzola, E.A., Drysdale R.G. and Essawy, A.S, (1985), *Bending of concrete masonry wallettes at different angles to the bed joints*, Proceedings of the 3rd North American Masonry Conference, paper 27

[18] Geel, H.J.G.M van, Pluijm, R. van der, (1994), T*he variability of tensile and flexural bond strength*, Proceedings of the 10th International Brick/Block Masonry Conference, Calgary, Canada

[19] Grandet, J.; Javelza, R.; Perrin, B.; Thenoz, B.(1972), *Rôle de l'ettringite dans la liason de type mécanique entre la terre cuite et la pâte de ciment-portland*, Revue Terre Cuite, No.53, pp. 24-34

[20] Groot, C.J.W.P. (1993), *Effects of water on mortar-brick bond*, PhD-Thesis Delft University of Technology, ISBN 90-9006569-5

[21] Haseltine, B.A.; West, H.W.H.; Tutt, J.N. (1977), *The resistance of brickwork to lateral loading 2 Design of walls to resist lateral loads*, The Structural Engineer Vol. 55 No. 10, pp. 422-429

[22] Hendry, A.W., (1981), *Structural brickwork*, MacMillan, London, 1981, 209p.

[23] Hillerborg, A.; Modeer, M.; Petersson, P.E. (1976), *Analysis of crack formation ad crack growth in concrete by means of fracture mechanics and finite elements*, Cement and Concrete Research, No. 6, pp. 773-782

[24] Hofmann, P.; Stöckl, S.; Mainz, J. (1990), *A comparative finite element evaluation of mortar joint shear tests*, Masonry International, Vol.3 No.3, pp.101-104.

[25] Hordijk, D.A.; Reinhardt, H.W. (1990), *Testing and modelling of plain concrete under mode I loading*, Micro Mechanics of failure of quasi brittle materials, Elsevier Applied Science, pp.559-568, ISBN 1-85166-511-0

[26] Hordijk, D.A, (1992), *Tensile and tensile fatigue behaviour of concrete; experiments modelling and analyses*, HERON Vol. 37 no. 1, 79 pp.

[27] Jenkins and Potter, *Laterally loaded masonry review of flexural strength data and design methods*, Technical report, Ref: 8420

[28] Lawrence, S.J. (1983), *Behaviour of brick masonry walls under lateral loading*, PhD-thesis, University of New South Wales, Australia

[29] Lawrence, S.J., (1985), *Random variations in brickwork properties*, Proceedings of the 7th International Brick/Block Masonry Conference, Melbourne, Australia, pp. 537-547.

[30] Lawrence, S.J.; Cao, H.T. (1987), *An experimental study of the interface between brick and mortar*, Proceedings of the 4th North American Masonry Conference, Los Angeles, paper 48, 14 pp.

[31] Lawrence, S.J., Cao, H.T., (1988), *Cracking of Non-loadbearing Walls Under Lateral Forces*, Proceedings of the 8th International Brick/Block Masonry Conference, Dublin, Ireland, pp. 1184-1194.

[32] Lawrence, S.J. (1991), *Stochastic analysis of masonry structures,* Proceedings of the International Symposium on Computer Methods in Structural Masonry, Swansea, 3-5 April, pp. 104-113

[33] Lawrence, S.J. (1995), *The behaviour of masonry in horizontal flexure*, Proceedings of the 7th Canadian Masonry Symposium, Hamilton, June 4-7, pp 525-536

[34] Losberg, A, Johansson, S. (1969), *Sideways pressure on masonry walls of brickwork*, CIB Symposium on Bearing Walls, Warsaw, Poland

[35] Lourenço, P.B; Rots, J.G.; Blauwendraad, J. (1994) *Implementation of an interface cap model for the analyses of masonry structures*, Proceedings of the EURO-C conference on Computational Modelling of Concrete Structures, Innsbruck, Austria

[36] Lourenço, P.B; Rots, J.G.; Blauwendraad, J. (1995), *Two approaches for the analysis of masonry structures: micro- and macro-modelling*, HERON, Vol. 40 No. 4, pp. 313-340.

[37] Lourenço, P.B. (1997), *An anisotropic macro-model for masonry plates and shells: Implementation and validation*, Technical report, Delft University of Technology, Faculty of Civil Engineering, report nr. 03.21.1.3.07

[38] Lourenço, P.B. (1996), *Computational Strategies for Masonry Structures*, PhD-Thesis, Delft University of Technology, Delft, The Netherlands, ISBN 90-407-1221-2

[39] Mann, W., H. Müller (1977), *Bruchkriterien für querbeanspruchtes Mauerwerk und ihre Anwendung auf gemauerte Windscheiben*, Bericht der Technische Hochschule Darmstadt

[40] Merchant, M.J. (1981); *Fortran F77 Language and Style*, Wadsworth Publishing Company, Belmomt, Californië, USA, isbn 0-534-00920-4

[41] Mier, J.G.M van.; Vervuurt, A; Slangen E.; (1994), *Boundary and size effects in uniaxial tensile tests: a numerical and experimental study*, Fracture and Damage in Quasibrittle Structures, E&FN, isbn 0 419 19280 8

[42] Mier, J.G.M.van; Slangen, E.; Vervuurt, A., (1996), *Tensile cracking in concrete and sandstone: Part 2 - Effect of boundary rotations*, Materials and Structures, Vol. 29, March, pp. 87-96.

[43] Mier, J.G.M. van, (1997), *Fracture processes of concrete*, CRC Press, New York, isbn 0-8493-9123-7.

[44] Mosteller, F; Rourke, R.E.K. (1973), *Sturdy statistics, nonparametrics and order statistics*, Appendix 7, Reading, Massachusetts, Addison-Weslley

[45] Page, A.W. (1982), *An experimental Investigation of the biaxial strength of Brick Masonry*, Proceedings of the 6th International Brick/Block Masonry Conference, Rome, Italy, pp 3-15

[46] Petersson, P.E. (1981), *Crack growth and development of fracture zones in plain concrete and similar materials*, Report TVBM-1007, Lund Institute of Technology, Sweden, 174 pp.

[47] Pluijm, R. van der (1992), *Material properties of masonry and its components under tension and shear*, Proceedings of the 6th Canadian Masonry Symposium, Saskatoon, Canada, pp. 675-686.

[48] Pluijm, R. van der (1992), *Micro shear tests*, technical report BI-92-104, TNO Building and Construction Research, in Dutch.

[49] Pluijm, R. van der (1993), *Shear behaviour of bed joints*, Proceedings of the 6th North American Masonry Conference, Philadelphia, USA, 6-9 June, pp.125-136.

[50] Pluijm, R. van der (1994), *Micro tests '93*, technical report 94-CON-R0801, TNO Building and Construction Research, in Dutch.

[51] Pluijm, R. van der (1994), *A simple shear test for masonry*, Technical report 94-CON-R1782, TNO Building and Construction Research

[52] Pluijm, R. van der (1994), *Influence of the angle between the bed joint and the bending axes on the flexural strength of masonry*, Proceedings of the 10th International Brick/Block Masonry Conference (Eds. N.G. Shrive, A. Huizer), Calgary, 5-7 July, pp. 579-588

[53] Pluijm, R. van der (1995), *Numerical evaluation of bond tests*, Masonry International, Vol. 9, No. 1, pp. 16-25, issn 0950-2289.

[54] Pluijm, R van der.; Rutten, H.S.; Vermeltfoort, A.Th., (1995), *Fflexural behaviour of masonry in different directions*, Proceedings of the 4th International Masonry Conference / the British Masonry Society, Masonry (7), pp.117-123

[55] Pluijm, R. van der (1995), *Measuring of bond, a comparative experimental research*, Technical report /TU/BKO/95.29, Eindhoven University of Technology

[56] Pluijm, R. van der (1996), *Bending test on masonry wallettes*, Technical report TUE/BKO/93.05, Eindhoven Unversity of Technology

[57] Pluijm, R. van der (1996), *About units, mortar and masonry, a literature review of the influence parameters on strength and stiffness*, Technical report 96-CON-R0710, TNO Building and Construction Research (in Ducth).

[58] Pluijm, R. van der (1996), *Deformation controlled tensile and flexural tests on clay brick, concrete and calcium silicate masonry*, Technical report TUE/BKO/96.2, Eindhoven University of Technology

[59] Pluijm, R. van der, (1996), *Measuring of bond, a comparative experimental research*, Proceedings of the 7th North American Masonry Conference, South Bend, Indiana, 2-5 June, edt. M.E. Baily; D.E. Sporleder, pp 267-281

[60] Pluijm, R. van der, (1997), *Non-linear behaviour of masonry under tension,* Heron, Vol. 42 No.1, issn 0046-7316, pp 25-54.

[61] Pluijm, R. van der (1998), *Deformation controlled tensile tests carried out in the period 1996-1998*, Technical report TUE/BCO/98.19, Eindhoven University of Technology

[62] Pluijm, R. van der (1998), *Overview of deformation controlled combined tensile and shear tests*, Technical report TUE/BCO/98.20, Eindhoven University of Technology

[63] Pluijm, R. van der (1999), *Panel tests*, Technical report TUE/CO/99.03, Eindhoven University of Technology

[64] Pluijm, R. van der (1999), D*eformation controlled 4-point bending tests on clay brick and calcium silicate masonry wallettes,* Technical report TUE/CO/99.16, Eindhoven University of Technology, TNO 99-CON-R3021

[65] Pluijm, R. van der (1999), *Non linear FEM meso models for masonry*, Technical report, TNO report nr. 99-CON-R3022

[66] Rots, J.G. (ed) (1997), *An experimental/numerical basis for practical design rules*, based on CUR report 171 (1994), A.A.Balkema / Rotterdam / Brookfield, ISBN 90 5410 680 8, 152 pages

[67] Rots, J.G.;Lourenço, P.B.(1993), *Fracture simulations of masonry using non-linear interface elements*, Proceedings of the 6th NAMC. Vol. 2, pp 983-993, Drexel University, Philadelphia, USA

[68] Schubert, P.(1988), The *influence of mortar on the strength of masonry*, Proceedings of the 8th International Brick/Block Masonry Conference, Trinity College, Dublin, Ireland, pp. 162-174

[69] Schubert, P. (1994), *Tensile and flexural strength of masonry: influences, test methods, test results*, Proceedings of the 10th International Brick/Block Masonry Conference, University of Calgary, Canada, pp. 895-908, 5 July 1994.

[70] Seward, D.W., (1982), *A developed elastic analyses of lightly loaded brickwork walls with lateral loading*, International Journal of Masonry Construction, Vol.2, No.3, pp. 81-84

[71] Siemes, A.J.M, (1985), *Safety of masonry structures, a probabilistic assessment,* Technical report B-85-588/60.6.2517, TNO Building and Construction Research (in Dutch).

[72] Sinha, B.P., (1978), *A simplified ultimate load analysis of lateral loaded model orthotropic brickwork panels of low tensile strength*, Structural Engineer, Vol. 56B No 4 p.81-85

[73] Slangen, E., (1993), *Experimental and numerical analysis of fracture processes in concrete*, PhD-Thesis, Delft University of Technology, ISBN 90-9006167-3

[74] Staalduinen, P. van, (1990) , *Background of windloads according to NEN 6702:1991*, Technical report B-90-483, TNO Building and Construction Research (in Dutch).

[75] Standards Association of Australia (1988), *Masonry in Buildings* (known as the SAA MASONRY CODE, AS 3700-1988, isbn 0 7262 5359 6

[76] Timoshenko, S.P.; Goodier, J.N. (1970), *Theory of elasticity*, Third edition, McGraw-Hill, ISBN 0-07-064720-8

[77] Timoshenko, S.P.; Woinowsky-Krieger, S. (1970), *Theory of plates and shells*, Second edition, McGraw-Hill, ISBN 0-07-Y85820-9

[78] Vekey, R.C. de; Page, A.W; Hedstrom, E.G., (1994), *The variability of bond wrench measurements in UK, Australia and USA*, Masonry International, Vol. 8 No. 1 pp. 21-25.

[79] Vermeltfoort, A.Th.; Pluijm, R. van der (1991), *Deformation controlled tensile and compression tests on units, mortar and masonry*, Technical report B-91-0561 /TUE/BKO/91-07, TNO Building and Construction Research/ Eindhoven University of Technology (in Dutch).

[80] Vermeltfoort, A.Th.; Pluijm, R. van der (1991), *Strength and deformation properties of masonry to be used in computer calculations*, Proceedings of the 9th International Brick/Block Masonry Conference, Berlin pp. 244-251

[81] Vermeltfoort, A.Th. (1992), *Mecahnical properties under compression of masonry and its components*, Proceedings of the 6th Canadian Masonry Symposium, Saskatoon, pp 657-662

[82] Vermeltfoort, A.Th, Pluijm, R. van der (1995), *Bond wrench testing*, Proceedings of the British Masonry Society, Masonry (7), Proceedings of the 4th International Masonry Conference, London, 23-25 October, pp.225-231.

[83] Vermeltfoort, A.Th. (1997), *ESPI for research into mechanical compressive behaviour of masonry,* Proceedings of the 11th International Brick/Block Masonry Conference, Shanghai, pp. 385-394

[84] Vermeltfoort, A.Th. (1998), *The application of electronic speckle pattern interferometry for measurements of masonry/mortar stiffness*, Proceedings of the 5th International Masonry Conference, London, pp 77-84

[85] West, H.W.W., Hodgkinson, H.R., Haseltine, B.A., Vekey, R.C. de, (1986) *The resistance of masonry to lateral loading 2 Research results on brickwork and aggregate blockwork since 1977*, Structural Engineer, Vol, 64A, Nr.11 pp.320-331

[86] Wittmann, F.H.;(1987), *Structure of concrete and crack formation*, Fracture Mechanics of Concrete, Elsevier Science Publishers B.V, Amsterdam, pp. 251-299.

[87] Zijl, G.P.A.G. van (1996), *Shear transfer across bed joints in masonry: A numerical study*, Technical report 03.21.0.22.28, Delft University of Technology

[88] Zijl, G.P.A.G. van; Lourenço, P.B.; Rots, J.G. (1997), *Non-associated plasticity formulation for masonry interface behaviour*, Proceedings of COMPLAS V, Computational Plasticity: Fundamentals and Applications, (eds. D.R.J. Owen, E. Onate and E. Hinton), Barcelona, pp. 1586-1593

[89] Zijl, G.P.A.G. van; (1999), *Numerical formulation for masonry creep, shrinkage anc cracking*, Technical report, series 11 - Engineering Mechanisms 01, Delft University of Technology, isbn 90-407-1892-x

GLOSSARY AND ABBREVIATIONS

bat	half unit, seen at head side of original unit
Bernoulli, hypothesis of	assumption in the bending theory of slender beams that plane cross-sections remain plane after bending, for thin plates extended to the assumptions that normals to the middle surface of a plate remain straight across the plate thickness and remain normal to the deflected mid-plane
block	unit with dimensions greater than bricks but not greater than approx. $500\times250\times250$ mm^3
(bond)-interface	layer between the mortar and the unit where they are bonded together with a (assumed) zero thickness at the meso level.
brick	unit with maximum dimensions of approx. $214\times102\times90$ mm^3
c:l:s	cement : lime : sand ratio by volume e.g. 1:1:6 (see also GPM)
cross joint	part of the bed joint where it is connected to the head joint
C-S hydrates	calcium silicate hydrates
CV	coefficient of variation
dw.	dead weight
element	unit with dimensions $900\times(100\text{-}300)\times600$ mm^3
EUT	Eindhoven University of Technology
fabric.year	fabrication year of specimens
FE	finite element (method)
fmGPM	factory made general purpose mortar (dense aggregate):
GPM	general purpose mortar (traditional joint thickness, dense aggregate), if laboratory made indicated with c:l:s ratio
headless masonry	masonry with unfilled head joints
interface	see bond-interface between mortar-joint and unit
joint	mortar-joint between units
lin.regr.	linear regression
LVDT	Linear Variable Differential Transducer
macro level	level at which masonry is considered as a homogeneous material
meso level	level at which masonry components units and joints are considered
MoCo	moisture content
mode I	tension
mode II	shear
normal	indication of direction perpendicular to the bed joint plane
oblique crack	crack that runs alternating through head joints and bed joints

rhs	rectangular hollow section (steel)
St.Dev	sample standard deviation
stack bonded prism	prism consisting of a number of units laid on top of each other
stretcher bond	regular geometrical arrangement of only whole units in which the overlap of units equals a bat
TLM	thin layer mortar (always factory made):
unit	general term for a masonry 'stone'
wallette	small masonry wall used in 4-point bending test arrangements

SYMBOLS AND NOTATIONS

NOTATIONS

In tables, figures between round brackets () indicate the CV in % of the given mean quantity.

Double subscripts indicating directions, are based on tensor notation. E.g. in $x_{\mathrm{index;ij}}$ the subscript i is the normal direction of the considered cross section and the second subscript is the direction of the quantity x_{index}. This double index is generally only used for tensors of the 2[nd] degree (stresses, strains etc.). In this thesis the notation is also used for scalars and vectors that can be associated with a tensor of the 2[nd] degree e.g.:

$$\sigma_{\mathrm{xy}} \rightarrow V_{\mathrm{xy}},\ \ \kappa_{\mathrm{xx}} \rightarrow \varphi_{\mathrm{xx}}$$

The second quantity is a shear force, a tensor of the first degree and only one index would be sufficient in tensor notation to indicate the normal of the plane. The last quantity is also of first order but it is associated with the curvature from which it can be derived by integrating the curvature in x-direction

Moments and curvatures may be presented by a vector with a double arrow head. The direction of the bending moment/curvature follows from right hand turning.

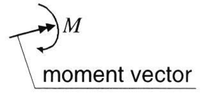

SYMBOLS

The first and second column gives the symbol, the third column the description and in the third, the dimension of the symbol, if any. The indicated dimensions are only intended for clarification. They are always presented throughout the thesis.

UPPER CASE

A		cross sectional area	[mm^2]
CV		coefficient of variation	[%]
CV		coefficient of variation	[-] or [%]
$\overline{D}$		Orthogonal flexural rigidity matrix with respect to the t-n-z co-ordinate system	-
	D_{ij}	component of $\overline{D}$	[Nmm]
D^{i}		isotropic flexural plate rigidity of masonry component i	[Nmm]
E		modulus of elasticity	[N/mm^2]
	$E^{\mathrm{hj}}_{\mathrm{reduced}}$	reduced stiffness value of head joint in analytical model after cracking of the head joints, default	

		value = 20% of original stiffness	
	E_{1st}	in flexure, through first best fit	
	E_{2nd}	in flexure, through second best fit	
	E_c	in compression, secant at $\frac{1}{3}F_u$	
	E_o	in tension, tangent of first linear part	
	E_t	in tension	
	E_u	in tension or flexure, secant at failure	
F		force	[N]
	F_{lin}	load up to which the specimen behaves linearly	
	F_n	normal (perpendicular to bed joint plane)	
	F_s	shear (parallel to bed joint plane)	
	F_u	at failure	
G		deadweight of bond wrench	[N]
G		shear modules	[N/mm^2]
	G_o	tangent of first linear part	
	G_u	secant at failure	
G_f		fracture energy per area needed to create a fully opened crack (not to be confused with the energy release rate G in linear fracture mechanics)	[N/mm]
G_{fI}		mode I fracture energy, associated with tensile cracking	
	$G_{fI;cyl}$	value determined with displacement of cylinder in small 4-point bending tests	
	$G_{fI;meas}$	theoretically measured value up to σ_{last} according to eq. (1)	
	$G_{fI;t}$	theoretical value according to eq. (1)	
	$G_{fI;mod}$	modified experimental value by extrapoltaion of tail according to eq. (1)	
	G_{fII}	mode II fracture energy, associated with shear failure	
GI_t		torsional rigidity	[Nmm^2]
I		quadratic area moment of a cross section	[mm^4]
IRA		initial rate of absorption	[kg/m^2/min]
M		bending moment	[Nmm]
	$\hat{M}_{nt}^{bj}$	additional torsion moment in the bed joint (see also ψ^{bj})	
	$\hat{M}_{nn}^{bj}$	additional bending moment in the bed joint (see also β^{bj})	
	M_u	ultimate	
SR		suction rate	[kg/m^2/min]
W_{el}		elastic section modulus	[mm^3]

Lower Case

c	cement	
c_1, c_2	dimensionless constants	
c_o	initial cohesion	[N/mm^2]

c_r		residual cohesion	[N/mm^2]
d		depth / thickness of cross-section	[mm]
e		eccentricity	[mm]
f_c		compressive strength	[N/mm^2]
	$f^{u}_{c;normalized}$	of units, normalized acc. to prEN 772-1 to a height of 100 mm	
f_{fl}		flexural strength	[N/mm^2]
	$f_{fl;bw}$	determined with the bond wrench	
	$f_{fl;hor}$	of masonry, bent around axis perpendicular to the bed plane (horizontal bending)	
	$f_{fl;ver}$	of masonry, bent around axis parallel to the bed plane (vertical bending)	
	$f_{fl;yy}$	of masonry, bent around the x-axis	
f_t		tensile strength (general)	[N/mm^2]
f_{tb}		tensile bond strength	[N/mm^2]
f_v, f_{vo}		initial cohesion (see also c_o)	[N/mm^2]
h		height	[mm]
l		length	[mm]
	l_{ch}	characteristic length, measurement for brittleness, eq. (6)	
m		moment per length	[N]
$\vec{m}$		$\vec{m} = [m_{tt}, m_{tn}, m_{nn}]^T$	
p		surface load	[N/mm^2]
	p_u	utlimate surface load	
r		roughness distance over which $\Delta\tan\psi$ reduces to zero	[mm]
r, r^2		correlation coefficient	
r_{lin}		load level expressed as a fraction of the failure load up to which a specimen behaved linearly	[-]
t		thickness	[mm]
u		displacement perpendicular to the bed plane	[mm]
	u_{last}	last measured deformation in the descending branch of a tensile test	[mm]
	u_{pl}	plastic normal displacement, developing after the top in shear test, comparable with w	[mm]
v		shear displacement	[mm]
	v_{nonlin}	shear crack displacement over which the cohesion reduces to zero	[mm]
	v_{pl}	plastic shear displacement (shear crack displacement)	
w		deflection of specimen	[mm]
w		crack width	[mm]
	w_c	crack width at which no tensile stresses are transferred any more	
	w_{last}	last measured crack width in a tensile test	

Greek symbols

β^{bj}		bending angle of bed joint in case of torsion caused by the additional bending moment (= $\hat{\kappa}_{nn}^{bj} \cdot h^{bj}$)	[rad]
Δ		incremental value	
φ		bending angle / flexural rotation	[rad]
κ		curvature	[mm^{-1}]
$\vec{\kappa}$		$\vec{\kappa} = [\kappa_{tt}, \kappa_{tn}, \kappa_{nn}]^T$	
	$\bar{\kappa}_{tn}^{u}$	average torsion in unit in *t*-direction	
	$\hat{\kappa}_{nn}^{bj}$	additional bending curvature in bed joint in case of torsion	
	κ_u	curvature at failure	
μ		dry friction coefficient	[-]
ν		Poisson's ratio	[-]
σ		stress	[N/mm^2]
	$\sigma_{dw;max}$	compressive stress due to deadweight (maximum per series)	
	σ_{fl}	flexural stress	
	σ_{last}	last measured stress in tensile test in descending branch	
θ		angle between bending axis and bed joint	[rad] [degrees]
τ		shear stress	[N/mm^2]
	τ_{fr}	in the tail of shear stress-displacement diagram occurring due to dry friction	
	τ_u	ultimate shear stress	
ψ		torsion: twist angle per length	[rad/mm]
	ψ^{bj}	of the bed joint in case of horizontal bending	
ψ		dilatancy angle	
	ψ_o	initial value ($v_{pl} = 0$)	

Superscripts

u	of unit
j	of mortar joint (when no distinction between head and bed joint is being made)
bj	of bed joint
cj	of cross joint
hj	of head joint
u+j	of masonry

Absence of suprscripts indicate macro properties.

Appendix A
MATERIALS

UNITS

In Table 32, some physical characteristics of all units are presented. The values were determined using the appropriate Dutch standards as indicated in the table. The normalised compressive strength values $f^{u}_{c;normalized}$ were calculated using the values determined according to the Dutch standards with the conversion table of prEN 772-1:1995. This conversion is intended to give a strength value for the unit with a normalised height of 100 mm.

Table 32 Overview of units and their properties

unit type	manufacturer	year(s)	code	dimensions [mm^3]	free water absorption 48h [mass-%]	mass by volume (dry) [kg/m^3]	mean compressive strength method	f^{u}_{c} [N/mm^2]	$f^{u}_{c;normalized}$ [N/mm^2]
wire cut clay brick	Joosten Kessel	90-95	wc-JO90	204×98×50	7.3	1900	NEN 2498	66	50
wire cut clay brick	Joosten Kessel	96-98	wc-JO96	204×98×50	6.5	2054	NEN 2498	72	61.4
soft mud clay brick	Vijf Eiken	90	sm-VE	208×98×50	17.4	1610	NEN 2498	33	25
soft mud clay brick	Rijswaard	95	sm-RIJ	206×96×50	15.5	1630	NEN 2498	27	20
normal density concrete brick	MBI	93	MBI93	210×100×52	-	-	NEN 7027	25 *)	19 *)
high strength wire cut clay brick	Joosten Kessel	93	hswc-JOK	206×98×50	-	-	NEN 2498 prism **)	81 69	67
calcium silicate brick	Loevestein	90, 92,95	CS-brick90	212×100×53	11.5	1880	NEN 3836	40	30
calcium silicate brick	Loevestein	93	CS-brick93	212×100×50	-	-	prism **)	28	-
calcium silicate block	Loevestein	92	CS-block92	439×100×198	-	2000	NEN 3836	25 *)	33.6 *)
calcium silicate block	Loevestein	95	CS-block95	439×100×198	12.0	2010	NEN 3836	30	41
calcium silicate block	Loevestein	96-98	CS-block96	439×100×198	-		NEN 3836	29	37
calcium silicate element	Loevestein	93	CS-el	900×100×600	-	-	NEN 3837 prism **)	15 *) 14.7	15 *) -
normal density concrete brick	MBI	95	MBI95	207×100×50	-	2370	NEN 7027	70	53

*) not tested, strength according to the manufacturer
**) prism cut out off unit 43×43×145 mm^3

Table 33 Modulus of elasticity E^{u} of units [N/mm^2]

unit	compression	tension
sm-VE brick	6050 (1990)	-
wc-JO90	16700 (1990)	16605 (1995)
wc-JO96	-	17400 (1998)
hswc-JOK	19900 (1993)	-
CS-brick	13400 (1990)	-
CS-block93	12190 (1993)	
CS-block95		12800 (1995)
MBI93	17000 (1993)	-

compression: 1990 prisms consisting of 6 to 7 units ground flat and stacked together with Bolidt (see Vermeltfoort[1992,[81]]), tested perpendicular to the bed joint
1993 prism cut out of one unit, tested parallel to the bed joint
tension: prisms cut out of one unit, tested parallel to the bed joint

Mortars

Constituents of laboratory made mortars

The grading analyses of the sands for the different mortars are presented in Figure 154. The sieve sizes are indicated along the horizontal axis.

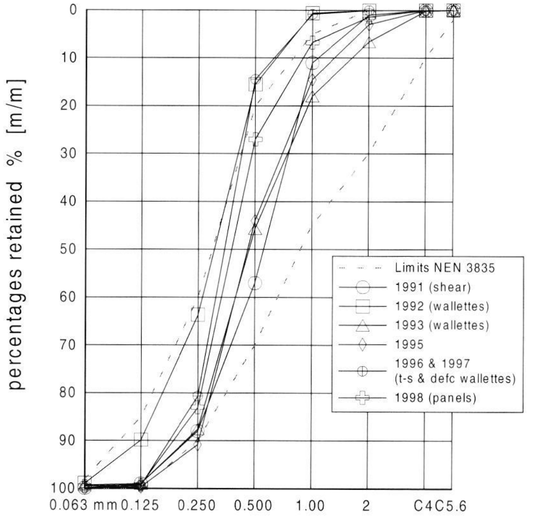

Figure 154 Grading analyses of sands

Two types of lime were used:
- hydrated shell lime
- hydrated lime with an air-entrainer (brand Mekal)

The cement used was always ordinary Portland cement type A (brand ENCI). Since 1995 this cement is sold as CEM I 32.5 R. The compressive strength of these cements is at least 32.5 N/mm^2 after 28 days according to NEN 3550:1995. It is determined with a specimen, which has the same dimensions as a mortar specimen (see section **MORTAR PROPERTIES**).

MORTAR PREPARATION

The laboratory made mortar composition was specified by volume, but weighed batches were used. The ratios by volume of the mortar were converted to ratios by mass using the following bulk densities:

cement:	1250 kg/m^3
lime:	600 kg/m^3
dry sand:	1400 kg/m^3

The amount of water was based on the workability of the mortar. The target value for the flow was 175 ± 10 mm according to NEN 3835:1991.
The dry constituents were mixed during approximately 3 minutes before the water was added. Next the mortar was mixed during 3-5 minutes before determining the flow and in case of an addition of water, mixed again during a few minutes.
Factory made mortars were prepared according to the prescriptions of the manufacturers.

MORTAR PROPERTIES

Over the years, many different mortar batches were used. The mean compressive strength value in a test series according to the Dutch standard NEN 3835:1991 is presented Table 34. The Dutch standard prescribes a prism of 40×40×160 mm^3 that is first used in a 3-point bending test. Next the compressive strength is determined on six halve prisms that remain from the flexural tests. The value obtained is comparable with a test on a 40 mm mortar cube. The Dutch test complies with the CEN test method prEN 1015-11:1995 for the determination of the flexural and compressive strength of mortar.

Table 34 Overview of the average compressive mortar strength f_c^{mortar} according to NEN 3835:1991 (at 28 days) by test-series and by unit type

fabrication year	type of test	mortar (composition by volume parts c : l : s if appropriate)	used with units	f_c^{mortar} [N/mm^2]
1990	tensile	GPM 1:1:6 (shell lime)	CS-brick90	8.2
		GPM 1:2:9 (shell lime)	wc-JO90, sm-VE, CS-brick90	3.0
		GPM 1:½:4½ (shell lime)	sm-VE, wc-JO90	17.6
1992	shear	GPM 1:2:9 (shell lime)	wc-JO90, sm-VE, CS-brick90	3.0
		GPM 1:½:4½ (shell lime)	wc-JO90, sm-VE, CS-brick90	14.4
1992-93	wall. bending	GPM 1: ½:4½ (shell lime)	wc-JO90	12.7
1994	wall. bending	GPM 1: 1: 6 (shell lime)	wc-JO90	8.2
1992-94	wall. bending	TLM (Calsifix)	CS-block92	21.9
1993	tensile, shear	fmGPM (Beamix 312)	MBI93	11.6
	shear	fmGPM (Sakrete)	CS-brick93	20.7
	tensile	TLM for clay bricks (Ytong)	hswc-JOK	32.7
1995	tensile, small bending, wall. bending, bond wrench	GPM 1:1:6 (Mekal lime)	CS-brick, wc-JO90, sm-RIJ	8.1
		TLM (Calsifix)	CS-block95	19.9
	tensile, small bending	fmGPM (Beamix C312)	MBI95	16.7
		TLM (Beamix C62)	MBI95	25.0
1996	tensile, wall. bending	GPM 1:2:9	wc-JO96	5.5
		TLM (Calsifix)	CS block 96	17.5
1997	tensile, wall. bending	GPM 1:2:12 (Mekal lime)	wc-JO96	3.0
	tensile	GPM 1:1:6 (Mekal lime)	wc-JO96	6.0
	tensile, shear	TLM (Calsifix)	CS block 96	30.0
	tensile	GPM 1:2:12 (Mekal lime)	wc-JO96	3.0
	tensile, wall. bending (70°)	GPM 1:2:9 (Mekal lime)	wc-JO96	3.1
	tensile, shear	GPM 1:1:6 (Mekal lime)	wc-JO96	5.9
1998	tensile, panel I	GPM 1:1:6 (Mekal lime)	wc-JO96	7.3
	tensile, panel II	GPM 1:1:6 (Mekal lime)	wc-JO96	8.7

Type of test:

tensile	deformation controlled tensile tests
shear	deformation controlled joint shear tests combined with normal action
small bending	deformation controlled 4-point bending test on small stack bonded piers
wall. bending	4-point bending test on wallettes
def.wall. bending	deformation controlled 4-point bending test on wallettes
panels	large masonry panels load by means of air backs.

Table 35 Overview of pre-treatments and curing conditions by year, test type and by masonry types

fabric. year	type of test	masonry	chapter	reference	pre-treatment	curing conditions
1990	tensile	CS-brick90 + GPM 1:1:6, 1:2:9	2	[79]	prewetted MoCo 6%	3 days close covering, thereafter in 20°C, 60 % RH
		wc-JO90 + GPM 1:½:4½, 1:2:9	2	[79]	prewetted SR 0.6	3 days close covering, thereafter in 20°C, 60 % RH
		sm-VE + GPM 1:1:6, 1:2:9	2	[79]	prewetted SR 1.1	3 days close covering, thereafter in 20°C, 60 % RH
1992	shear	CS-brick90 + GPM 1:½:4½,, 1:2:9	3	[48]	prewetted SR 1.1, MoCo 3.7%	3 days close covering, thereafter in 20°C, 60 % RH
		wc-JO90 + GPM 1:½:4½, 1:2:9	3	[48]	prewetted SR 1.1, MoCo 1.9%	3 days close covering, thereafter in 20°C, 60 % RH
		sm-VE + GPM 1:½:4½, 1:2:9	3	[48]	prewetted SR 2.1, MoCo 9.2%	3 days close covering, thereafter in 20°C, 60 % RH
1992	wall. bending (θ = 0,45,90°)	CS-block92 + TLM	4	[56]	bed face submerged over a depth of 1 cm in water, during a 2-3 s	no curing, 20°C, 60 % RH
1992 - 1994	wall. bending (θ = 0,30,70,90°)	wc-JO90 + GPM 1:½:4 ½, 1:1:6	4	[56]	prewetted SR 1.1	4-5 days close covering, thereafter in 20°C, 60 % RH
1993	tensile and shear	CS-brick93 + fmGPM	2, 3	[50]	prewetted MoCo 6%	7 days 20°C, 95 % RH, thereafter in 20°C, 60 % RH
		MBI93 + fmGPM	2, 3	[50]	laboratory dry condition	
	tensile	hswc-JOK + TLM	2	[50]	laboratory dry condition	
1995	tensile, small bending	CS-brick90 + GPM 1:1:6	2	[58]	prewetted to a MoCo of 6.5% (185 g water per unit added)	7 days close covering, thereafter in 20°C, 60 % RH
	tensile, small bending, wall. bending, bond wrench	wc-JO90 + GPM 1:1:6	2	[58]	laboratory dry condition (MoCo <1%)	7 days close covering, thereafter in 20°C, 60 % RH
		CS-block + TLM	2	[58]	prewetted with brush *)	no curing, after 1 week in 20°C, 60 % RH
	small bending	sm-RIJ + GPM 1:1:6	2	[58]	prewetted until SR 1.4	7 days close covering, thereafter in 20°C, 60 % RH
		MBI95 + fmGPM, fmTLM	2	[58]	laboratory dry condition	no curing, after 1 week in 20°C, 60 % RH
1996	tensile, def.wall. bending (θ = 90°)	wc-JO96 + 1:2:9	2, 4	[61], [64]	laboratory dry condition (MoCo <1%)	7 days close covering, thereafter in laboratory
		CS-block 96 + Calsifix	2, 4	[61], [64]	laboratory dry condition, prewetted with brush *)	no curing, in laboratory
1997	tensile, def.wall. bending	wc-JO96 + 1:2:12	2, 4	[61], [64]	laboratory dry condition (MoCo <1%)	7 days close covering, thereafter in laboratory
	tensile	wc-JO96 + 1:1:6	2	[61]	laboratory dry condition (MoCo <1%)	7 days close covering, thereafter in 20°C, 60 % RH
	tensile, shear	CS-block 96 + TLM	2, 3	[61], [62]	laboratory dry condition, prewetted with brush *)	no curing, in laboratory
	tensile	wc-JO96 + 1:2:12	2	[61]	laboratory dry condition (MoCo <1%)	7 days close covering, thereafter in 20°C, 60 % RH
	tensile, def.wall. bending (θ =70°)	wc-JO96 + 1:2:9	2, 4	[61], [64]	laboratory dry condition (MoCo <1%)	no curing, in laboratory
	tensile, shear	wc-JO96 + 1:1:6	2, 3	[61], [62]	laboratory dry condition (MoCo <1%)	3 days close covering, thereafter in 20°C, 60 % RH
1998	tensile, panels	wc-JO96 + 1:1:6	2, 4	[61], [63]	laboratory dry condition (MoCo <1%)	no curing, in laboratory

*) according to instructions of the Dutch calcium silicate industry
MoCo moisture content (mass-%)
SR suction rate (kg/m^2/min)
IRA initial rate of absorption (kg/m^2/min)

Appendix B
EXPERIMENTAL RESULTS

Table 36 Overview of experimental work

fabric. year	type of test	materials	purpose	reference	context
1990	tensile	units: CS-brick90, wc-JO90 sm-VE masonry: CS-brick90 + GPM, wc-JO90 + GPM sm-VE + GPM	pre- and post peak behaviour with deformation controlled tests	[79]	I, TNO
1992	shear	CS-brick90 + GPM, wc-JO90 + GPM sm-VE + GPM	pre- and post peak behaviour with deformation controlled tests	[48]	I, TNO
1992 – 1994	wall. bending (θ = 0,45,90°)	CS-block92 + TLM, wc-JO90 + GPM 1:½:4 ½, 1:1:6	influence of angle θ between bending axis and bed joint on behaviour of wallettes CS-block masonry: θ = 0,45,90° JO-brick masonry: θ = 0, 30, 70, 90°	[56]	II, EUT
1993	tensile, shear tensile shear	MBI93 + fmGPM hswc-JOK + TLM CS-brick93+ fmGPM	pre- and post peak behaviour with deformation controlled tests	[50]	I, TNO
1995	tensile, small bending	CS-brick90 + GPM 1:1:6 wc-JO90 + GPM 1:1:6 CS-block95 + TLM	pre- and post peak behaviour with deformation controlled tests under tension and mode I fracture energy with bending tests	[58]	I, EUT I, II, EUT
	small bending	sm-RIJ + GPM 1:1:6 MBI95 + fmGPM, MBI95 + fmTLM	mode I fracture energy		I, EUT
1996	tensile, def.wall. bending (θ = 90°)	wc-JO96 + 1:2:9, CS-block96 + TLM	influence of head joint, torsional shear failure of bed joint with deformation controlled wallette tests (accompanying tensile tests)	[61], [64]	II, EUT
1997	tensile, def.wall. bending (θ = 90°)	wc-JO96 + 1:2:12	influence of head joint, torsional shear failure of bed joint with deformation controlled wallette tests (accompanying tensile tests)	[61], [64]	
	tensile	wc-JO96 +1:1:6, wc-JO96 + 1:2:12	accompanying deformation controlled tensile tests for shear tests (no shear results)	[61]	
	tensile, def.wall. bending (θ =70°)	wc-JO96 + 1:2:9	oblique crack through head joints and bed joint (deformation controlled tensile and wallette tests)	[61], [64]	
	tensile, shear	wc-JO96 + 1:1:6, CS-block96 + TLM	pre- and post peak behaviour under combinations of tension and shear (deformation controlled tensile and shear tests)	[61], [62]	
1998	tensile, panels	wc-JO96 + 1:1:6	panel test result with pre- and post peak tensile properties	[61], [63]	

Type of test:

tensile	deformation controlled tensile tests
shear	deformation controlled joint shear tests combined with normal action
small bending	deformation controlled 4-point bending test on small stack bonded piers
wall. bending	4-point bending test on wallettes
def.wall. bending	deformation controlled 4-point bending test on wallettes
panels	large masonry panels load by means of air backs.

Context:

I: Dutch structural masonry research program

II: thesis-study

TENSILE TESTS

In each table, test results for one type of test and one type of unit are presented. Within a table the results are grouped by mortar batch. For each brick-mortar combination the average value is given with the coefficient of variation between brackets

The following special character is used in the tables

- uncontrolled test beyond the top, not applicable or not calculated

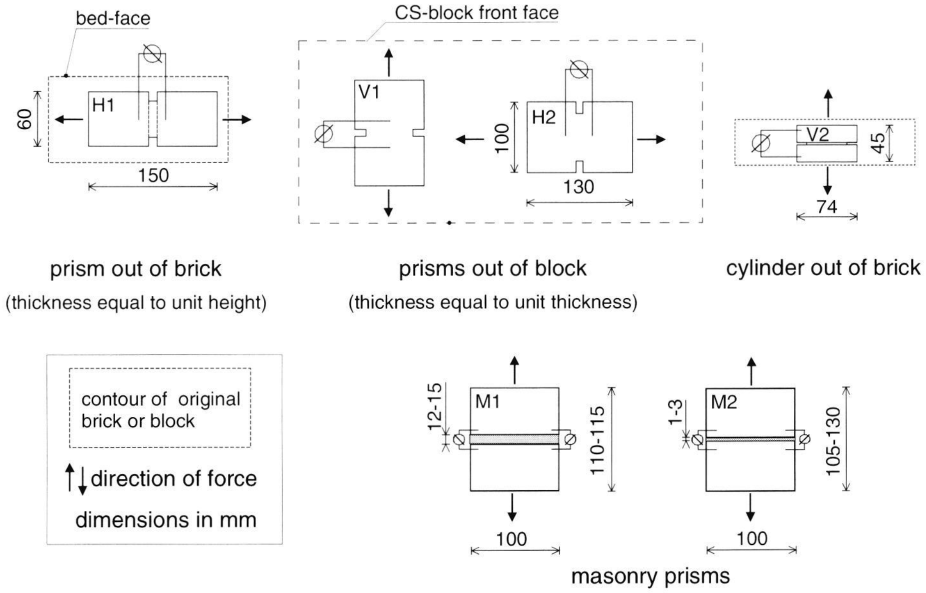

Figure 3(repeated) *Tensile specimens*

Table 37 Tensile tests with soft mud Vijf Eiken clay bricks (sm-VE) (specimens are grouped by specimen type or different mortar batches)

fabric. year	specimen type (see Figure 3)	mortar	E_o^j [N/mm^2]	E_u^j [N/mm^2]	G_{fI} [N/m]	f_t [N/mm^2]
			-	-	52	2.24
	prism H1	-	-	-	78	2.88
			-	-	54	2.29
	average (CV)				61 (24%)	2.47 (14%)
			-	-	71	1.44
	cylinder V2	-	-	-	72	1.57
			-	-	75	1.50
	average (CV)				73 (3%)	1.50 (4%)
1990			730	360	3.7	0.14
			950	501	10.4	0.37
	masonry prism M1	1:2:9	670	345	13.5	0.35
			520	320	-	0.07
			640	408	3.4	0.18
	average (CV)		700 (22%) **1)**	390 (18%)	7.8 (65%)	0.22 (60%)
			670	179	3.4	0.07
	masonry prism M1	1:½:4½	990	351	5.7	0.28
			190	52	3.4	0.04
	average (CV)		620 (65%) **2)**	194 (77%)	4.2 (32%)	0.13 (101%)

1) determined with lin. regression between 0 and $0.50f_t$ for an optimal correlation coefficient (r > 0.99)
2) determined with lin. regression between 0 and $0.63f_t$ for an optimal correlation coefficient (r > 0.99)

Table 38a Tensile tests with wire cut Joosten clay bricks (wc-JO90) (specimens are grouped by specimen type or different mortar batches)

fabric. year	specimen type (see Figure 3)	mortar	E_o^j [N/mm^2]	E_u^j [N/mm^2]	G_{fI} [N/m]	f_t [N/mm^2]
		-	-	-	-	2.01
	prism H1				98	2.47
			-	-	117	2.72
	average (CV)				117 (-)	2.36 (21%)
			-	-	129	3.48
	cylinder V2	-	-	-	131	3.43
			-	-	124	3.61
	average (CV)				128 (3%)	3.51 (3%)
			2532	592	9.8	0.24
1990	masonry prism M1	1:2:9	2887	1635	19.6	0.38
			3266	2012	5.2	0.28
	average (CV)		2895 (13%) **1)**	1413 (52%)	11.5 (64%)	0.30 (24%)
			5269	2316	8.1	0.40
		1:½:4½	6165	2994	10.8	0.52
	masonry prism M1		4384	6229	3.2	0.41
			5826	3829	5.3	0.43
		1:½:4½	8049	4686	10.4	0.77
			6316	2959	3.0	0.44
	average (CV)		6002 (20%) **2)**	3836 (37%)	6.8 (51%)	0.50 (29%)

fabric. year	specimen type (see Figure 3)	mortar	E_o^j [N/mm^2]	E_u^j [N/mm^2]	G_{fI} [N/m]	f_t [N/mm^2]
1995	masonry prism M1	1:1:6	3493	1905	3.3	0.52
			2815	728	1.7	0.27
			2143	1533	1.9	0.28
			2139	1224	3.7	0.37
		1:1:6	1942	822	9.1	0.44
			632	541	6.8	0.36
			1436	644	3.1	0.35
			2193	758	-	0.64
			1699	546	11.2	0.39
			1145	607	9.6	0.49
		1:1:6	1568	1305	2.2	0.25
			1207	643	1.8	0.24
			2717	908	3.4	0.43
			706	305	-	0.08
			1329	1096	3.2	0.45
			1052	734	2.3	0.22
		1:1:6	2630	1486	4.1	0.38
			1868	923	3.2	0.30
			2179	960	2.4	0.31
			3121	2126	-	0.57
			2711	1742	6.2	0.49
		1:1:6	3811	2464	9.1	0.44
			3192	2718	-	0.44
			5528	3229	-	0.81
			1761	830	-	0.37
			560	617	1.4	0.14
			1564	492	6.9	0.3
		1:1:6	2272	906	13.6	0.69
			4202	1417	8.5	0.56
			1519	773	2.6	0.32
			4273	1446	8.2	0.53
			1622	1127	3.7	0.23
			5986	1832	14.8	0.57
	average (CV)		2371 (55%) **3**)	1216 (57%)	5.5 (70%)	0.40 (39%)

1) determined with lin. Regression between 0 and $0.57f_t$ for an optimal correlation coefficient (r > 0.99)
2) determined with lin. Regression between 0 and $0.52f_t$ for an optimal correlation coefficient (r > 0.99)
3) determined with lin. Regression between 0 and $0.69f_t$ for an optimal correlation coefficient (r > 0.98)

Table 38b Tensile tests with wire cut Joosten clay bricks (wc-JO90)
(specimens are grouped by specimen type or different mortar batches)

fabric. year	specimen type (see Figure 3)	mortar	E^j_o [N/mm2]	E^j_u [N/mm2]	G_{fl} [N/m]	$G_{fl;mod}$ [N/m]	f_t [N/mm^2]
			-	-	35	79	1.85
			-	-	-	-	1.84
			-	-	-	-	2.06
			-	-	112	112	1.82
		-	-	-	78	78	2.34
1996	prism H1		-	-	116	116	2.67
			-	-	123	123	2.43
			-	-	-	-	1.71
			-	-	58	098	1.83
	average		-	-	87 (41)	101	2.06 (16)
			6848	5105	-	-	0.78
			10566	7375	1.5	1.5	0.57
			805	307	5.3	-	0.21
			3135	2601	3.1	6.5	0.53
			4247	3264	-	-	0.41
			1944	1681	4.2	8.5	0.22
			7518	8061	-	-	0.55
1996	masonry prsim M1	1:2:9	6506	4048	11.7	11.7	0.76
	def. wall. bending		-	-	6.1	6.1	0.50
			10594	6687	4.1	4.1	0.52
			-	-	6.3	10.3	0.79
			629	904	-	-	0.48
			6129	5814	8.0	13.3	0.58
			7745	8286	-	-	0.49
			6828	7122	-	-	0.78
	average		5653 (58) **1**)	4712 (59)	5.6 (53)	7.8 (51)	0.54 (33)
			3790	3217	6.1	12.1	0.41
			8727	7193	5.9	11.0	0.52
			5694	4700	3.5	8.9	0.36
		1:2:12	11044	1759	4.4	9.6	0.34
1997	masonry prsim M1		6507	1290	2	5.4	0.26
	def. wall. bending		3950	981	-	-	0.33
			3677	3599	3.2	6.8	0.35
	average		6198 (45) **2**)	3248 (68)	4.5 (37)	0.0090 (	0.37 (22)
			1316	1254	1.1	1.8	0.15
			942	635	-	-	0.08
			180	142	-	-	0.10
			620	86	-	-	0.10
			4324	4609	0.1	0.1	0.10
1997	masonry prsim M1	1:2:9	6327	1410	1.1	4.5	0.19
	def. wall. bending (70)		9399	5714	0.9	1.9	0.33
			2667	2739	1.0	1.7	0.17
			472	188	-	-	0.09
			1957	849	1.0	2.1	0.22
			168	59	-	-	0.07
			895	511	-	-	0.18
	average		2439 (118) **3**)	1516 (124)	0.9 (44)	2.0 (70)	0.15 (51)
			696	1352	0.9	1.9	0.17
			16004	-	1.8	1.8	0.44
1997	masonry specimen M1	1:2:12	5097	4270	1.5	2.9	0.25
	(intended for shear)		10167	5251	1.8	1.8	0.44
			-	-	1.9	3.2	0.38
			-	-	3.9	3.9	0.66
	average		7991 (83) **4**)	3624 (56)	2.0 (52)	2.6 (34)	0.39 (44)
			5317	2633	3.2	3.2	0.43
			5025	4191	12.8	12.8	0.66
1997	masonry specimen M1	1:1:6	7959	3056	1.9	1.9	0.46
	(shear trial)		5585	2980	1.2	3.4	0.39
			4786	3720	-	-	0.50
	average		5734 (22) **5**)	3316(19)	4.8 (113	5.3 (94)	0.49

fabric. year	specimen type (see Figure 3)	mortar	E_o^j [N/mm2]	E_u^j [N/mm2]	G_{fI} [N/m]	$G_{fI;mod}$ [N/m]	f_t [N/mm^2]
			-	5193	2.6	6.7	0.39
			8619	7135	2.1	3.5	0.44
1997	masonry specimen M1 (shear)		6270	2985	2.8	6.1	0.42
			1799	901	0.9	3.0	0.19
			-	8987	2.1	2.1	0.36
			-	5848	3.6	8.1	0.47
	average		5563 (62) **6)**	5175 (56)	2.4 (38)	4.9 (48)	0.38 (26)
			568	226		-	0.17
			4524	715	3.4	5.7	0.29
			9562	7840	0.7	0.7	0.36
			5018	1531	1.6	3.2	0.30
			2073	2213	0.7	1.3	0.11
			1761	1232	0.5	0.5	0.17
			3295	1655	-	-	0.27
			4462	3202	-	-	0.16
			4570	3605	1.5	2.6	0.29
1998	masonry specimen M1 (panel I)	1:1:6	7509	6594	2.1	2.1	0.36
			786	539	0.3	0.3	0.05
			3574	2240	0.0	0.1	0.07
			3453	1600	1.2	2.3	0.25
			1124	150	0.4	0.9	0.07
			1594	522	2.1	2.1	0.14
			3566	3509	1.2	2.3	0.27
			2762	2327	2.5	2.5	0.30
			7850	4533	6.5	12.7	0.70
			4259	2467	1.6	1.6	0.22
			3393	1696	1.9	3.4	0.25
	average (CV)		3785 (63) **7)**	2420 (84)	1.7 (92)	2.6 (113	0.24 (60)
			4459	4382	2.0	3.3	0.28
			179	149	0.5	0.5	0.08
			2419	1576	2.2	-	0.33
			2432	1080	2.0	2.0	0.25
			3060	1669	0.3	0.3	0.08
			10467	1910	0.4	1.3	0.16
			280	146	0.5	-	0.03
			1332	1085	0.8	0.8	0.16
1998	masonry specimen M1 (panel II)	1:1:6	1220	896	1.4		0.18
			-	504	0.8	0.8	0.11
			758	482	-	-	0.04
			1292	375	0.8	0.8	0.12
			953	248	1.0		0.08
			3009	1344	1.9	1.9	0.19
			4536	1362	0.6	1.0	0.16
			-	73	0.1	0.1	0.01
			380	379	0.3	0.3	0.07
			296	157	-	-	0.05
			473	380	0.7	1.5	0.12
	average (CV)		2208 (116)	958 (106)	1.0 (71)	1.1 (79)	0.13 (66)

1) determined with lin. regres. between 0 and 0.78ft for an optimal correlation coefficient (r > 0.96)
2) determined with lin. regres. between 0 and 0.71 ft for an optimal correlation coefficient (r > 0.98)
3) determined with lin. regres. between 0 and 0.75ft for an optimal correlation coefficient (r > 0.98)
4) determined with lin. regres. between 0 and 0.89ft for an optimal correlation coefficient (r > 0.86)
5) determined with lin. regres. between 0 and 0.62ft for an optimal correlation coefficient (r > 0.99)
6) determined with lin. regres. between 0 and 0.82ft for an optimal correlation coefficient (r > 0.89)
7) determined with lin. regres. between 0 and 0.67ft for an optimal correlation coefficient (r > 0.98)
8) determined with lin. regres. between 0 and 0.67ft for an optimal correlation coefficient (r > 0.98)

Table 39a Tensile tests with Calcium Silicate bricks, blocks and elements (CS) (specimens are grouped by specimen type or different mortar batches) upto 1995

fabric. year	specimen type (see Figure 3)	mortar	E_o^j [N/mm2]	E_u^j [N/mm2]	G_{fI} [N/m]	f_t [N/mm2]
1990 bricks	unit prism H1	-	-	-	71	2.11
			-	-	74	2.36
			-	-	56	2.56
	average (CV)				67 (17%)	2.34 (10%)
	masonry prism M1	1:2:9	4286	1274	-	0.31
			4907	1708	-	0.22
			4884	1420	-	0.47
			6360	1561	-	0.27
	average (CV)		5109 (17%) **1)**	1491 (12%)		0.32 (34%)
	masonry prism M1	1:1:6	2289	1389	-	0.18
			3299	2231	-	0.46
			2659	1983	-	0.30
			2020	1652	-	0.17
			2414	1668	-	0.55
	average (CV)		2536 (19%) **2)**	1785 (18%)		0.33 (51%)
1993	unit prism H1 (out of element 900×100×600 mm)	-	-	-	-	1.13
			-	-	-	0.69
			-	-	47	1.99
			-	-	-	0.85
	average (CV)				47 (-)	1.17(49%)
1995 blocks			E_o^{j+u} **4)**	E_u^{j+u} **4)**		
	masonry prism M2	TLMa	3874	3045	-	0.35
			5840	4902	-	0.31
			4242	2689	-	0.21
			8297	8209	-	0.29
			9433	10170	-	0.34
			5036	3876	2.0	0.35
			10827	4443	-	0.35
			2782	1528	1.6	0.18
			9911	5531	5.1	0.38
			5459	3428	-	0.38
			3793	2820	-	0.15
		TLMb	4737	3835	-	0.45
			5908	5097	-	0.28
			4256	2795	-	0.16
			7644	6004	-	0.31
			3718	2689	-	0.29
			3217	2121	-	0.21
			13171	9386	-	0.32
			5091	4152	3.4	0.28
			8314	7691	-	0.42
			4871	2985	-	0.37
		TLMc	8233	5947	-	0.44
			6573	6037	5.6	0.36
			5814	3676	2.0	0.25
			11906	9712	-	0.25
			16582	10519	2.6	0.35
			11312	9815	3.0	0.36
			8321	4122	-	0.40
			7469	6736	3.1	0.44
			12372	12995	-	0.48
			20154	11616	-	0.43
			11507	9804	4.3	0.51
			12988	11076	-	0.37
	average (CV)		7989 (54%) **3)**	6044 (53%)	3.3 (41%)	0.33 (27%)

1) determined with lin. regression between 0 and 0.50ft for an optimal correlation coefficient (r > 0.99)
2) determined with lin. regression between 0 and 0.54ft for an optimal correlation coefficient (r > 0.99)
3) determined with lin. regression between 0 and 0.82ft for an optimal correlation coefficient (r > 0.92)
4) no reliable values could be obtained for single mortar-joints (r ≈ 0.77), results over the gauge length (35 mm) are presented

Table 39b Tensile tests with Calcium Silicate bricks, blocks and elements (CS) (specimens are grouped by specimen type or different mortar batches) 1996-1998

fabric. year	specimen type (see Figure 3)	mortar	E_o^j [N/mm^2]	E_u^j [N/mm^2]	G_{fI} [N/m]	$G_{fI;mod}$ [N/m]	f_t [N/mm^2]
			-	-	37.9	37.9	1.45
			-	-	41.0	119.7	2.04
	prism H2		-	-	35.3	97.9	1.98
			-	-	42.0	42.0	1.67
		-	-	-	36.0	57.6	2.06
1996	average (CV)		-	-	38.4 (8)	71.0 (51)	1.84 (15)
			-	-	-	-	1.34
	prism V1		-	-	0.036.1	36.1	1.81
			-	-	-	-	1.67
			-	-	29.5	80.1	1.80
	average (CV)		-	-	32.8 (14)	58.1 (54)	1.66 (13)
	average prism H2 & V1		-	-	36.8 (11)	67.3 (49)	1.76 (14)
			252	285	6.8	6.8	0.30
			-	2696	10.5	10.5	0.49
1996	masonry prism M2s		340	372	8.9	8.9	0.32
	wallettes	TLM	1832	1419	11.0	11.0	0.63
			1832	-	-	-	0.76
			1832	-	14.6	14.6	0.51
			1832	-	9.0	9.0	0.52
	average (CV)		1320 (60) **1)**	1193 (94)	10.1 (26)	10.1 (26)	0.50 (32)
			592	1321	-	-	0.44
			471	287	-	-	0.42
			-	-	9.0	9.0	0.54
			-	-	-	-	0.66
			216	93	5.0	-	0.36
1997	shear	TLM	153	88	4.3	-	0.27
			687	476	2.2	2.2	0.23
			417	435	1.6	5.8	0.26
			-	-	5.3	-	0.66
			-	-	-	-	0.54
			1196	4057	-	-	0.3
			-	-	3.2	6.2	0.36
	average (CV)		533 (62) **2)**	965 (139)	4.4 (53)	7.2 (51)	0.42 (14)

1) determined with lin. regression between 0 and 0.95ft for an optimal correlation coefficient (r > 0.91)
2) determined with lin. regression between 0 and 0.79ft for an optimal correlation coefficient (r > 0.80

Table 40 Tensile tests with high strength wire cut Joosten Kessel clay bricks (hswc-JOK)

fabric. year	specimen type (see Figure 3)	mortar	E_o^j [N/mm2]	E_u^j [N/mm2]	G_{fI} [N/m]	f_t [N/mm2]
	prism 47×47×102		4455	2830	13.4	2.56
	prism 48×45×102		3354	2484	26.0	1.84
1993	prism M2	TLM	4612	1857	-	1.57
	cylinder ∅50×102		5264	4561	16.0	3.06
	cylinder ∅50×102		4326	3971	13.1	2.18
	average (CV)		4402 (16%) **1)**	3141 (35%)	17.1 (32%)	2.24 (26%)

1) determined with lin. regression between 0 and 0.85ft for an optimal correlation coefficient (r > 0.94)

Table 41 Tensile tests with normal density concrete bricks (MBI)

fabric. year	specimen type (see Figure 3)	mortar	E_o^j [N/mm^2]	E_u^j [N/mm^2]	G_{fI} [N/m]	f_t [N/mm2]
1993	masonry prism M1	fmGPM	8133	6219	-	0.82
			9616	9168	11.3	0.50
			9532	10917	-	0.84
			4497	4222	-	0.76
			8430	6838	-	0.73
	average (CV)		8042 (26%) **1)**	7473 (35%)	11.3 (-)	0.73 (19%)

1) determined with lin. regression between 0 and 0.93f_t for an optimal correlation coefficient (r > 0.92)

SMALL 4-POINT BENDING TESTS

In each table, test results for one type of test and one type of unit are presented. Within a table the results are grouped by mortar batch. For each brick-mortar combination the average value is given with the coefficient of variation between brackets
The following special character is used in the tables

- uncontrolled test beyond the top, not applicable or not calculated

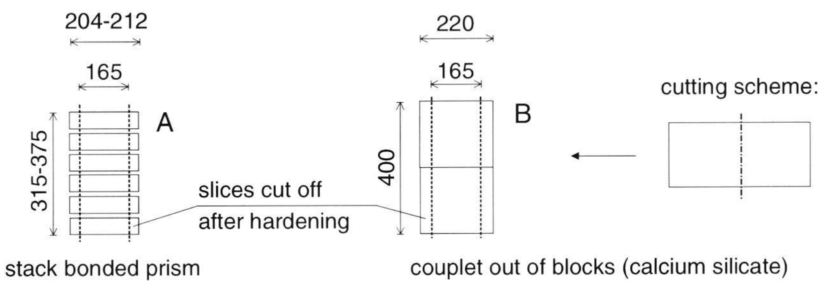

Figure 25(repeated) *Flexural Specimens*

Table 42 Flexural tests with soft mud clay bricks Rijswaard (sm-RIJ) of 1995

specimen type (see Figure 25)	mortar	f_{fl} [N/mm^2]	G_{fl} [N/m]	$G_{fl;cyl}$ [N/m]
stack bonded prism A	1:1:6	0.25	9.2	8.1
		0.26	-	-
		0.12	6.5	4.7
		0.19	11.7	12.7
average (CV)		0.19 (37%)	9.1 (41%)	8.7 (65%)

Table 43 Flexural tests with wired cut clay bricks Joosten (wc-JO90) of 1995 (specimens are grouped by mortar batch)

specimen type (see Figure 25)	mortar	f_{fl} [N/mm^2]	G_{fl} [N/m]	$G_{fl:cyl}$ [N/m]
stack bonded prism A	1:1:6	0.42	2.4	4.9
		0.72	-	5.2
	1:1:6	0.90	-	29.6
		0.34	4.0	4.7
	1:1:6	0.39	3.4	3.2
		0.39	4.4	7.3
		0.53	7.5	5.6
		0.36	-	4.5
	1:1:6	0.55	3.6	7.8
		0.40	4.2	7.3
		0.61	8.6	10.5
	1:1:6	0.50	-	18.0
		0.84	8.2	14.7
		0.65	19.3	4.3
	1:1:6	0.71	15.3	16.9
		1.00	36.8	24.9
		0.64	38.0	28.9
average (CV)		0.58 (34%)	12.0 (102%)	11.7 (77%)

Table 44 Flexural tests with Calcium Silicate bricks (CS-brick90) and blocks (CS-block95) of 1995 (specimens are grouped by unit type and mortar batch)

specimen type (see Figure 25)	mortar	f_{fl} [N/mm^2]	G_{fl} [N/m]	$G_{fl:cyl}$ [N/m]
couplet B (blocks)	TLM	0.21	10.3	2.8
		0.59	-	13.6
		0.22	4.2	6.3
	TLM	0.35	7.1	5.0
	TLM	0.48	3.7	10.0
		0.45	11.0	11.8
		0.28	-	6.1
		0.39	5.4	5.2
		0.54	7.1	6.5
average (CV)		0.39 (35%)	7.0 (52%)	7.5 (47%)
stack bonded prism A (bricks)	1:1:6	0.25	-	-
		0.16	2.4	2.8
		0.27	-	-
		0.35	5.1	5.6
		0.11	-	-
average (CV)		0.23 (41%)	3.8 (52%)	4.2 (48%)

Table 45 Flexural tests with normal density concrete bricks (MBI) of 1995 (specimens are grouped by specimen type)

specimen type (see Figure 25)	mortar	f_{fl} [N/mm^2]	G_{fl} [N/m]	$G_{fl;cyl}$ [N/m]
stack bonded prism A	fmGPM	0.52	14.5	14.5
		0.41	8.6	8.5
		0.51	19.4	16.4
		0.35	9.2	9.2
		0.50	4.2	6.7
average (CV)		0.46 (16%)	11.2 (52%)	11.1 (38%)
stack bonded prism C	TLM	0.84	24.8	26.7
		1.50	39.5	40.5
		1.29	44.8	45.9
		1.20	43.4	45.1
		1.40	-	-
		1.34	45.8	47.7
average (CV)		1.26 (18%)	39.6 (22%)	41.2 (21%)

SHEAR TESTS

In each table, test results for one type of unit are presented. Within a table the results are grouped by mortar batch. For each normal stress level average values and coefficient of variations are presented.

The following special character is used in the tables

- uncontrolled test beyond the top, not applicable or not calculated

All specimens were couplets (see Figure 42).

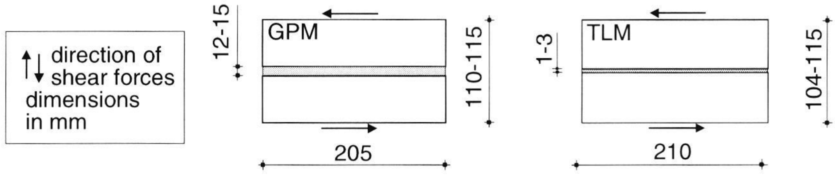

Figure 42(repeated) Shear masonry specimens made with GPM and TLM (exact dimensions depend upon unit size)

Table 46 Results of sm-VE+ GPM series of 1992 TNO shear test arrangement)

mortart		σ_u	τ_u	c_o	μ	G_o^j	G_u^j	G_{fII}	v_{nonlin}	$\tan\psi_o$
		[N/mm^2]	[N/mm^2]	[N/mm^2]	[-]	[N/mm^2]	[N/mm^2]	[N/m]	[mm]	[-]
1:2:9		-2.02	2.32	-	-	912	384	-	-	-
		-1.02	1.59	0.74	0.81	1548	577	135.8	0.479	0.27
		-0.52	0.73	0.28	0.82	812	331	43.6	0.456	0.30
		-0.52	1.06	0.56	0.93	1459	1017	47.9	0.356	0.31
		-0.52	1.19	0.66	0.76	1481	639	116.1	0.477	0.46
	average	-0.52	0.99	0.50	0.84	1250	662	69.2	0.430	0.36
	CV	0%	24%	39%	10%	30%	52%	59%	15%	25%
		-0.13	0.99	0.82	1.00	1182	773	46.3	0.219	0.91
		-0.13	0.86	0.71	0.96	1184	644	40.7	0.212	0.96
		-0.12	0.56	0.41	0.91	1117	848	21.9	0.189	1.03
		-0.12	0.92	-	-	891	418	-	-	-
	average	-0.13	0.83	0.65	0.96	1094	671	36.3	0.207	0.96
	CV	-4%	23%	33%	5%	13%	28%	35%	8%	6%
1:½:4½		-0.31	0.97	0.48	1.56	1137	742	43.0	0.327	0.50
		-0.31	1.31	-	-	1693	659	-	-	-
		-0.30	1.34	-	-	1188	543	-	-	-
		-0.29	1.29	-	-	1800	892	-	-	-
	average	-0.30	1.23			1454	709			
	CV	-2%	14%			23%	21%			
		-0.13	1.00	0.85	0.90	1427	652	26.5	0.251	1.05
		-0.11	0.85	0.68	1.12	1577	649	63.1	0.340	1.06
		-0.10	1.19	-	-	1101	974	-	-	-
	average	-0.12	1.01	0.77	1.01	1368	758	44.8	0.295	1.06
	CV	-14%	17%	16%	15%	18%	25%	58%	21%	1%

Table 47 Results of wc-JO90+ GPM series of 1992
(TNO shear test arrangement)

mortart		σ_u [N/mm^2]	τ_u [N/mm^2]	c_o [N/mm^2]	μ [-]	G_o^j [N/mm^2]	G_u^j [N/mm^2]	G_{fII} [N/m]	v_{nonlin} [mm]	$\tan\psi_o$ [-]
		-0.99	1.93	1.18	0.76	1738	584	222.0	0.549	0.38
		-0.99	1.69	0.91	0.79	1680	453	170.5	0.563	0.32
		-0.98	1.98	1.14	0.75	2071	668	226.6	0.598	0.44
	average	-0.99	1.87	1.08	0.77	1830	568	206.4	0.570	0.38
	CV	0%	8%	13%	3%	12%	19%	15%	4%	16%
		-0.50	1.34	0.95	0.77	1866	811	123.2	0.504	0.53
		-0.50	1.37	0.96	0.81	1823	692	113.8	0.440	0.55
		-0.49	1.48	1.07	0.82	2039	940	112.4	0.430	0.67
1:2:9	average	-0.50	1.39	0.99	0.80	1909	814	116.5	0.458	0.58
	CV	-1%	5%	7%	3%	6%	15%	5%	9%	13%
		-0.11	1.08	0.95	1.08	2095	976	87.1	0.396	1.13
		-0.10	0.90	0.80	1.00	1925	918	57.4	0.338	0.88
		-0.10	0.95	-	0.82	1967	1108	-	-	-
		-0.10	0.98	0.89	0.80	2128	957	56.3	0.318	1.02
	average	-0.11	0.98	0.88	0.92	2029	990	66.9	0.351	1.01
	CV	-5%	7%	9%	15%	5%	8%	26%	12%	13%
		-1.02	2.43	1.33	0.80	3084	1635	173.7	0.331	0.68
		-1.01	2.89	-	-	2657	1220	-	-	-
		-1.00	2.33	1.25	0.80	3083	2757	125.5	0.289	0.70
	average	-1.01	2.55	1.29	0.80	2941	1871	149.6	0.310	0.69
	CV	-1%	12%	4%	0%	8%	42%	23%	10%	2%
		-0.50	2.15	-	-	2633	1346	-	-	-
		-0.50	2.62	-	-	2571	1521	-	-	-
		-0.49	2.21	1.37	0.97	2642	1929	168.8	0.356	0.76
1:½:4½	average	-0.50	2.33	1.37	0.97	2615	1599	168.8	0.356	0.76
	CV	-1%	11%			1%	19%			
		-0.11	2.25	-	-	3162	2205	-	-	-
		-0.11	1.62	-	0.84	2199	1928	-	-	-
		-0.11	1.80	-	-	2728	2178	-	-	-
		-0.10	1.87	1.76	0.89	2624	2312	65.6	0.196	1.16
	average	-0.11	1.88	1.76	0.86	2679	2156	65.6	0.196	1.16
	CV	-5%	14%		4%	15%	8%			

Table 48 Results of clay brick masonry wc-JO96 + 1:1:6 of 1997 (bi-axial test arrangement of EUT)

	σ_u [N/mm²]	τ_u [N/mm²]	c_o [N/mm²]	μ [-]	G_o^j [N/mm²]	G_u^j [N/mm²]	G_{fII} [N/m]	v_{nonlin} [mm]	$\tan\psi_o$ [-]
	-1.39	2.25	-	0.74	2626	887	-	-	-
	-1.36	2.09	-	0.51	1368	1507	-	-	-
average	-1.38	2.17		0.62	1997	1197			
CV	-2%	5%		26%	45%	37%			
	-0.60	1.55	1.07	0.81	8797	2027	95.4	0.381	0.38
	-0.59	1.30	0.84	0.79	2700	1004	92.1	0.412	0.38
	-0.59	1.47	0.99	0.82	1627	2272	101.7	0.395	0.40
average	-0.59	1.44	0.97	0.81	4374	1767	96.4	0.396	0.39
CV	-1%	9%	12%	2%	88%	38%	5%	4%	4%
	-0.30	1.13	0.89	0.80	9565	3143	43.8	0.292	0.67
	-0.29	1.26	1.01	0.85	6280	2392	63.8	0.275	0.69
	-0.29	1.23	0.96	0.92	8018	2229	50.1	0.267	0.86
average	-0.29	1.21	0.95	0.86	7955	2588	52.6	0.278	0.74
CV	1%	6%	6%	7%	21%	19%	19%	5%	14%
	0.00	0.87	0.87	-	3149	2590	6.5	0.014	-
	0.00	0.97	0.97	-	3903	2662	7.5	0.025	-
	0.00	1.08		-	8264	4982		-	-
	0.01	1.03	1.03	-	13403	3888	8.0	0.029	-
average	0.00	0.99	0.96		7180	3531	7.3	0.022	
CV	113%	10%	9%		66%	32%	10%	35%	
	0.04	0.82	-	-	3840	1373	-	-	-
	0.10	0.27	-	-	6092	4515	-	-	-
	0.10	0.89	-	-	3038	1839	6.0	0.008	-
	0.10	0.87	-	-	3763	3821	3.7	0.007	-
	0.10	0.37	-	-	5074	4063	0.6	0.002	-
average	0.10	0.60			4492	3559	3.4	0.006	
CV	1%	54%			30%	33%	79%	58%	
	0.19	0.87	-	-	1762	1658	6.7	0.008	-
	0.20	0.63	-	-		-	-	-	-
	0.20	0.56	-	-	1852	1095	-	-	-
average	0.19	0.68			1807	1376			
CV	3%	24%			4%	29%			
	0.20	0.76	-	-	5536	2674	-	-	-
	0.21	0.09	-	-	-	-	-	-	-
average	0.21	0.42			5536	2674			
CV	3%	112%							
	0.34	0.10	-	-	-	-	-	-	-
	0.41	0.10	-	-	-	-	-	-	-
average	0.37	0.10							
CV	14%	0%							

Table 49 Results of hswc-JOK+ TLM series of 1993
TNO shear test arrangement

	σ_u [N/mm²]	τ_u [N/mm²]	μ [-]	G_o^j [N/mm²]	G_u^j [N/mm²]
	-1.10	6.10	0.78	806	606
	-0.99	5.65	0.78	669	483
	-0.94	6.00	0.79	606	853
average	-1.01	5.92	0.78	694	647
CV	-8%	4%	1%	15%	29%
	-0.40	5.56	1.00	679	707
	-0.39	5.93	-	406	10
	-0.39	4.55	0.89	-	1020
	-0.36	5.19	0.80	781	566
average	-0.38	5.31	0.90	466	575
CV	-4%	11%	11%	75%	73%
	-0.10	4.83	-	651	673
	-0.10	4.79	-	431	402
average	-0.10	4.81		541	537
CV	-4%	1%		29%	36%

Table 50 Results of CS-brick90 + GPM series of 1992
(TNO shear test arrangement)

mortart		σ_u [N/mm²]	τ_u [N/mm²]	c_o [N/mm²]	μ [-]	G_o^j [N/mm²]	G_u^j [N/mm²]	G_{fII} [N/m]	v_{nonlin} [mm]	$\tan\psi_o$ [-]
		-0.93	0.76	0.17	0.78	745	90	7.0	-	-
		-0.92	0.88	0.19	0.76	860	307	22.6	0.351	-
	average	-0.92	0.82	0.18	0.77	802	198	14.8		
	CV	0%	11%	8%	2%	10%	78%	75%		
		-0.53	0.49	0.13	0.70	341	269	13.6	0.234	-
		-0.50	0.53	0.16	0.74	788	225	15.6	0.296	-
		-0.49	0.36		0.71	133	20		-	-
1:2:9		-0.49	0.51	0.16	0.72	406	142	18.8	0.358	0.23
	average	-0.50	0.47	0.15	0.72	417	164	16.0	0.296	0.23
	CV	-4%	16%	13%	2%	66%	67%	16%	21%	
		-0.10	0.20	0.12	0.75	613	296	6.9	0.207	0.31
		-0.10	0.30						-	-
		-0.10	0.18	0.09	0.84	236	186	5.8	0.224	0.25
	average	-0.10	0.23	0.11	0.80	425	241	6.4	0.216	0.28
	CV	-2%	29%	16%	8%	63%	32%	12%	6%	14%
		-0.93	1.05	0.40	0.69	1576	535	42.6	0.318	0.05
		-0.93	1.24	0.54	0.75	1470	492	52.0	0.332	0.10
		-0.93	1.18	0.48	0.75	1444	509	46.2	0.295	0.14
	average	-0.93	1.16	0.48	0.73	1497	512	46.9	0.315	0.10
	CV	0%	8%	15%	5%	5%	4%	10%	6%	46%
		-0.50	0.87	0.51	0.73	1254	557	37.5	0.277	0.25
		-0.49	0.89	0.55	0.69	1489	689	42.4	0.281	0.28
1:½:4½		-0.49	0.73	0.38	0.72	1654	707	25.0	0.240	0.19
	average	-0.49	0.83	0.48	0.71	1466	651	35.0	0.266	0.24
	CV	-1%	11%	19%	3%	14%	13%	26%	8%	20%
		-0.10	0.31	0.24	0.73	675	357	10.5	0.201	0.40
		-0.10	0.38	0.30	0.73	959	650	10.6	0.186	0.49
		-0.10	0.35	0.26	0.85	558	377	12.2	0.231	0.46
	average	-0.10	0.35	0.27	0.77	731	461	11.1	0.206	0.45
	CV	-1%	10%	12%	9%	28%	36%	9%	11%	11%

Table 51 Results of CS-brik93 + fmGPM series of 1993 (TNO shear test arrangement)

	σ_u [N/mm²]	τ_u [N/mm²]	c_o [N/mm²]	μ [-]	G_o^j [N/mm²]	G_u^j [N/mm²]	G_{fII} [N/m]	v_{nonlin} [mm]	$\tan\psi_o$ [-]
	-0.96	1.42	-	0.74	4633	1853	80.9	0.554	0.21
	-0.95	1.34	-	0.75	2554	3641	-	-	-
	-0.93	1.57	0.58	0.64	2141	2315	121.9	0.983	0.35
average	-0.94	1.45		0.71	3109	2603	101.4	0.769	0.28
CV	-2%	8%		8%	43%	36%	29%	39%	35%
	-0.28	1.67	-	0.67	-	-	-	-	-
	-0.28	1.31	-	-	3450	4719	-	-	-
	-0.28	1.82	-	1.14	-	-	-	-	-
average	-0.28	1.60		0.90	3450	4719			
CV	-1%	16%		37%					

Table 52 Results of CS-block96 + TLM series of 1997 (bi-axial test arrangement of EUT)

	σ_u [N/mm²]	τ_u [N/mm²]	c_o [N/mm²]	μ [-]	G_u^j [N/mm²]	G_{fII} [N/m]	v_{nonlin} [mm]	$\tan\psi_o$ [-]
	-0.60	1.61	1.11	0.83	2929	80.4	0.301	0.34
	-0.60	1.45	1.02	0.71	1329	117.5	0.437	0.51
	-0.60	1.41	0.97	0.73	2177	112.3	0.675	0.50
average	-0.60	1.49	1.03	0.76	2145	103.4	0.471	0.45
CV	0%	7%	7%	8%	37%	19%	40%	21%
	-0.30	1.22	0.97	0.81	3196	66.5	0.262	0.70
	-0.30	1.11	0.87	0.80	1179	68.9	0.368	0.69
	-0.30	1.29	1.04	0.84	-	57.7	0.225	0.57
average	-0.30	1.21	0.96	0.82	2187	64.4	0.285	0.65
CV	0%	7%	9%	3%	65%	9%	26%	-
	0.00	1.24	1.09	-	-	17.2	0.050	-
	0.00	1.01	0.99	-	-	17.2	0.059	-
	0.00	1.17	-	-	-	-	-	-
	0.00	1.20	1.19	-	-	20.2	0.065	-
	0.00	1.22	1.21	-	-	25.4	0.073	-
	0.00	0.91	-	-	-	-	-	-
average	0.00	1.13	1.12			20.0	0.062	
CV	19%	12%	9%			19%	16%	
	0.05	1.25	1.25	-	-	12.0	0.018	-
	0.05	0.86	0.86	-	-	7.0	0.014	-
	0.05	0.98	0.98	-	-	10.0	0.020	-
	0.05	1.18	-	-	-	-	-	-
	0.05	1.06	1.06	-	-	12.5	0.028	-
	0.05	1.29	-	-	-	-	-	-
	0.05	1.17	1.17	-	-	15.7	0.023	-
average	0.05	1.11	1.06			11.4	0.021	
CV	0%	15%	15%			322%	1%	
	0.10	1.20	1.20	-	-	4.6	0.007	-
	0.10	0.86	0.86	-	-	11.7	0.017	-
	0.11	0.95	0.95	-	-	3.5	0.006	-
	0.11	0.76	0.76	-	-	4.8	0.009	-
average	0.10	0.94	0.94			6.2	0.010	
CV	7%	20%	20%			61%	55%	
	0.15	0.69	0.69	-	-	3.9	0.006	-
	0.15	1.07	1.07	-	-	2.4	0.005	-
	0.15	0.85	-	-	-	-	-	-
	0.15	0.93	0.93	-	-	1.6	0.006	-
	0.15	0.85	-	-	-	-	-	-
average	0.15	0.88	0.90			2.6	0.006	
CV	2%	16%	21%			44%	11%	

	σ_u [N/mm²]	τ_u [N/mm²]	c_o [N/mm²]	μ [-]	G_u^j [N/mm²]	G_{fII} [N/m]	v_{nonlin} [mm]	$\tan\psi_o$ [-]
	0.20	0.99	0.99	-	-	0.7	0.001	-
	0.20	1.16	1.16	-	-	1.1	0.001	-
	0.20	0.90	-	-	-	-	-	-
	0.20	0.83	-	-	-	-	-	-
average	0.20	0.97	1.08			0.9	0.001	
CV	1%	15%	11%			31%	0%	

Table 53 Results of MBI93 + fmGPM series of 1993 (TNO shear test arrangement)

	σ_u [N/mm²]	τ_u [N/mm²]	c_o [N/mm²]	μ [-]	G_u^j [N/mm²]	G_{fII} [N/m]	v_{nonlin} [mm]	$\tan\psi_o$ [-]
	-0.99	1.19	0.16	0.64	2897	224.6	0.716	0.44
	-0.97	1.79	0.83	0.58	4011	235.4	0.785	0.43
	-0.96	2.09	1.26	0.53	-	355.5	1.140	0.48
average	-0.98	1.69	0.75	0.58	3454	271.8	0.880	0.45
CV	-2%	27%	74%	9%	23%	27%	26%	6%
	-0.31	1.22	0.81	0.88	1023	172.7	0.727	0.35
	-0.30	1.48	1.02	0.96	1582	171.3	0.655	0.36
	-0.29	1.58	1.26	1.02	3618	215.9	0.664	0.44
average	-0.30	1.43	1.03	0.95	2074	186.6	0.682	0.38
CV	-3%	13%	22%	7%	66%	14%	6%	14%
	-0.10	1.34	-	-	1423	-	-	-
	-0.10	-	-	-	4559	-	-	-
average	-0.10				2991			
CV	-1%				74%			

Table 54 Overview of linear regression lines for the mode II fracture energy G_{fII} as a function of the normal stress σ of series carried out in 1992, 1993 and 1998

series	equation of linear regression line G_{fII} in N/mm, σ in N/mm²	correlation coefficient r^2
wcJO-90 + GPM	$G_{fII} = -0.13\sigma + 0.06$	0.74
wcJO-96 + 1:1:6	$G_{fII} = -0.13\sigma + 0.015$	0.96
smVE + GPM	$G_{fII} = -0.02\sigma + 0.005$	0.61
clay brick + GPM	$G_{fII} = -0.15\sigma + 0.023$	0.77
CS-brick90 + 1:2:9	$G_{fII} = -0.02\sigma + 0.005$	0.86
CS-brick90 + 1:½:4½	$G_{fII} = -0.04\sigma + 0.01$	0.90
CS-block96 + TLM	$G_{fII} = -0.14\sigma + 0.02$	0.96
MBI93 + fmGPM	$G_{fII} = -0.12\sigma + 0.15$	0.46

Table 55 Overview of linear regression lines for the dilatancy softening as a function of the normal stress σ of series carried out in 1992, 1993 and 1998

series	equation of linear regression line $\tan\psi_0$ in rad, σ in N/mm^2	correlation coefficient r^2
clay brick + GPM	$\tan\psi_0 = 0.65\sigma + 0.98$	0.55
CS-block96 + TLM	$\tan\psi_0 = 0.68\sigma + 0.86$	0.68
CS-brick90 + GPM	$\tan\psi_0 = 0.35\sigma + 0.41$	0.75

BENDING TESTS

In each table, test results for one type of unit are presented. Within a table the results are grouped by bending direction (angle between bed joint and bedning axis). For each bending direction the average value and the coefficient of variation are given.

The following special character is used in the tables:

- not applicable or not calculated

crack patterns (see also Figure 155):

s-bj straight crack through bed joints

Z-bj straight crack through several bed joints, jumping via a head joint to another row of bed joints

s-hj straigh crack through head joints and units

o oblique crack alternating through head and bed joints

mm mixed mode

In case of very irregular cracks not covered by the classification presented in Figure 155, the number of joints and units in a crack are mentioned

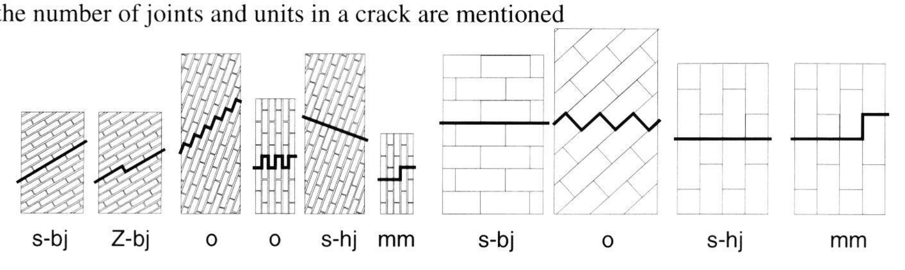

Figure 155 Crack patterns wallette tests

The specimens are presented in Figure 82 and Figure 83 (repeated from chapter 4).

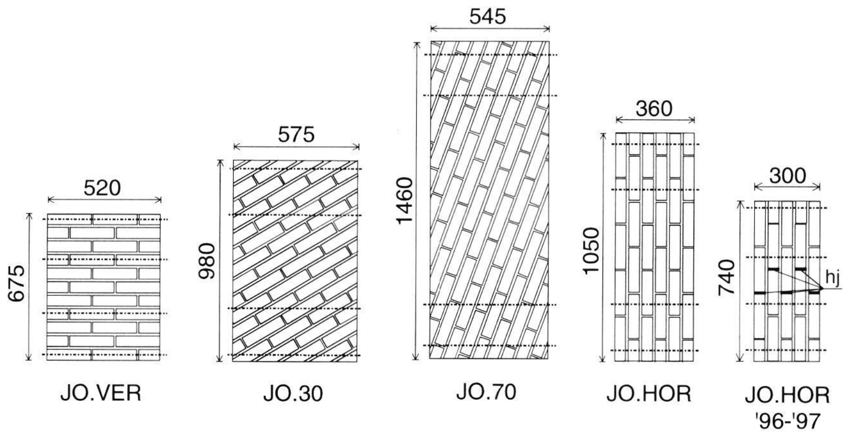

Figure 82(repeated) Wallettes of wc-JO90 & 96 + GPM series for bending in different directions (dimensions in mm)

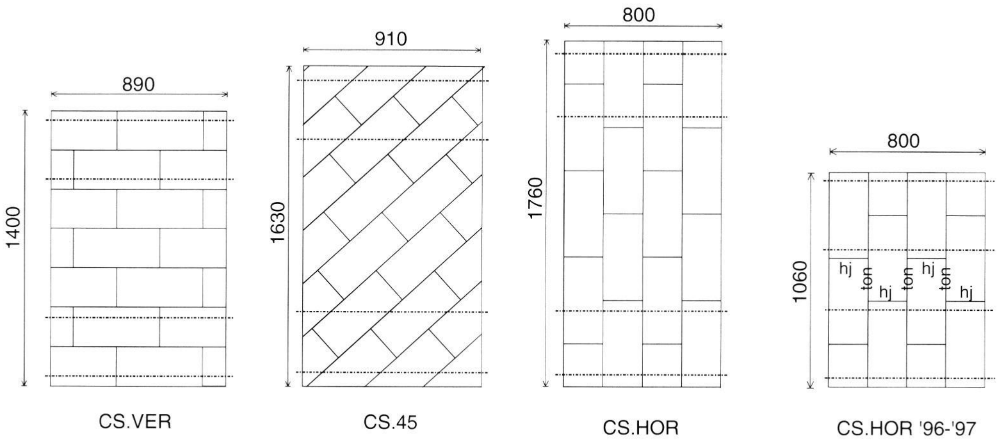

Figure 83 Wallettes of CS-block92 & 96 +TLM series for bending in different directions (dimensions in mm)

Table 56 Results of 4-point bending tests on wallettes of wc-JO90 + GPM series of 1992-1994

θ [°]	mortar	E_{1st} [N/mm^2]	r_{lin} [-]	$\kappa_{lin;yy}$ [10^{-6} mm^{-1}]	E_{2nd} [N/mm^2]	$\kappa_{u;yy}$ [10^{-6} mm^{-1}]	crack	$f_{fl;yy}$ [N/mm^2
0 VER	1:½:4½	11233	0.71	0.53	-	1.24	s-bj	0.48
		10509	0.64	0.50	-	1.95	s-bj	0.52
		8185	0.76	0.70	-	1.47	s-bj	0.53
		-	-	-	-	-	s-bj	0.55
		9510	0.79	0.51	-	1.55	s-bj	0.37
		9405	0.68	0.47	-	1.28	s-bj	0.41
		8455	0.76	0.47	-	1.39	s-bj	0.38
		8918	0.61	0.41	-	1.70	s-bj	0.39
average		9459	0.71	0.51	-	1.51		0.45
CV		12%	10%	18%	-	16%		16%
30		12235	0.39	0.52	10309	2.21	Z-bj	0.81
		10833	0.63	0.74	-	1.52	s-bj	0.7
		11848	0.54	0.69	8913	1.76	Z-bj	0.74
		11816	0.54	0.89	8387	2.70	s-bj	0.94
		10912	0.54	0.77	8847	2.00	s-bj	0.75
		12123	0.39	0.54	8513	2.36	s-bj	0.83
		11083	0.69	1.07	-	4.31	s-bj	0.84
		11910	0.61	0.74	7423	1.81	s-bj	0.73
		12082	0.49	0.48	9429	1.54	s-bj	0.66
		10589	-	-	-	1.51	s-bj	0.52
		10605	0.48	0.45	8188	1.81	s-bj	0.57
		11761	0.71	0.78	-	1.28	s-bj	0.63
average		11483	0.56	0.71	8751	2.05		0.72
CV		5%	19%	27%	10%	40%		17%
70		13380	0.45	2.24	9315	6.05	2hj+7u	2.84
		13335	0.49	1.95	-	5.07	3hj+5u	2.26
		10736	0.39	2.14	-	6.82	4hj+5u	2.47
		11579	0.4	2.02	-	6.47	3hj+5u	2.55
		11241	0.26	1.12	-	6.35	3hj+5u	2.47
		9892	0.43	1.95	8359	6.60	s-hj	2.31
average		11694	0.40	1.90	8837	6.23		2.48
CV		12%	20%	21%	8%	10%		8%
90 (HOR)		11410	0.28	0.91	-	5.26	mm	2.16
		11471	0.3	0.96	6948	5.14	s-hj	1.78
		9158	0.86	3.56	-	4.56	s-hj	1.98
		10508	0.29	1.05	7644	5.90	s-hj	1.93
		11271	0.49	1.17	7081	3.93	s-hj	1.44
		11585	0.35	1.32	8045	5.76	s-hj	2.38
		11756	0.3	1.06	7786	5.22	s-hj	2
		-	-	-	-	-	s-hj	2.36
		10797	0.34	1.27	-	5.48	s-hj	1.99
		10783	0.32	1.01	6998	5.48	s-hj	1.79
		121-20	0.26	0.68	6901	4.71	s-hj	1.76
			0.15	0.23	8078	5.59	s-hj	1.9
average		11086	0.31	0.97	7435	5.18		1.96
CV		8%	27%	33%	7%	11%		13%
70	1:1:6	10928	0.18	0.7.4	-	7.07	3hj+5u	2.34
		10052	0.24	1.21	7288	7.74	s-hj	2.52
		9982	0.26	1.24	7010	7.51	s-hj	2.4
		9401	0.21	0.99	6456	8.52	5hj+2bj+3u	2.36
		8748	0.23	0.80	4813	6.26	o	1.54
average		9822	0.22	1.00	6392	1.67		2.45 *
CV		8%	14%	23%	17%	245%		7%

* oblique crack excluded

Table 57 Results of 4-point bending tests on wallettes of wc-JO96 + GPM series of 1996-1997

θ [°]	head joints	mortar	E_{1st} [N/mm^2]	r_{lin} [-]	$\kappa_{lin;yy}$ [10^{-6} mm^{-1}]	E_{2nd} [N/mm^2]	$\kappa_{u;yy}$ [10^{-6} mm^{-1}]	crack	$f_{fl;yy}$ [N/mm^2]
90 (HOR)	filled	1:2:9	14452	0.29	0.80	9388	5.16	s-hj	1.98
			12116	0.35	0.80	6295	5.86	s-hj	1.34
			10495	0.32	1.31	5841	7.13	s-hj	2.00
			10857	0.30	0.78	6387	6.44	s-hj	1.40
	average		11980	0.32	0.92	6980	6.14		1.68
	CV		15%	8%	28%	23%	14%		21%
	unfilled		6006	0.27	1.21	-	7.54	1u, 2bj	1.35
			5835	0.35	1.77	-	6.46	2u, 1bj	1.40
			6058	0.38	1.99	-	6.57	2u, 1bj	1.56
			5249	0.25	1.52	-	7.62	2u, 1bj	1.57
			6007	0.27	1.31	-	6.86	2u, 1bj	1.41
	average		5830	0.30	1.56	-	7.01		1.46
	CV		6%	19%	21	-	8%		7%
	unfilled	1:2:12	5699	0.52	2.03	-	4.50	o (4bj)	1.13
			5333	0.58	3.84	-	7.43	o (4bj)	1.73
			5893	0.26	1.31	-	5.61	o (4bj)	1.48
			5523	0.37	1.56	-	7.32	2bj, 1u	1.15
			4984	0.34	1.89	-	6.58	o (4bj)	1.36
	average		5460	0.41	2.13	-	6.29		1.37
	CV		6%	32%	47%	-	20%		18%
70	filled	1:2:9	10101	0.42	0.69	-	2.59	o	0.80
			10075	0.56	0.70	-	1.57	o	0.62
	average		10090	0.49	0.70	-	2.08		0.71
	CV		0%	20%	1%	-	35%		18%

Table 58 Result of 4-point bending test on wallettes of the CS-block92 + TLM series of 1992-1994

θ [°]	E_{1st} [N/mm^2]	r_{lin} [-]	$\kappa_{lin;yy}$ [10^{-6} mm^{-1}]	E_{2nd} [N/mm^2]	$\kappa_{u;yy}$ [10^{-6} mm^{-1}]	crack	$f_{fl;yy}$ [N/mm^2
0 (VER)	14084	1.00	0.8.85E-07	-	0.88	s-bj	0.64
	13452	0.70	0.4.66E-07	-	0.79	s-bj	0.51
	13252	0.82	0.5.89E-07	-	0.89	s-bj	0.50
	12547	0.84	0.6.41E-07	-	0.92	s-bj	0.52
	16292	0.90	0.4.91E-07	-	0.67	s-bj	0.54
	16418	0.88	0.7.04E-07	-	0.85	s-bj	0.70
	-	-	-	-		s-bj	0.27
	14993	0.90	0.5.52E-07	-	0.70	s-bj	0.48
	12409	1.00	0.8.30E-07	-	0.83	s-bj	0.54
	11932	0.83	0.6.87E-07	-	1.08	s-bj	0.51
	13787	0.91	0.7.26E-07	-	0.86	s-bj	0.61
average	13917	0.88	0.6.57E-07		0.85		0.53
CV	11%	10%	21%		14%		21%
45	-	-	-	-	0.71	s-bj	0.52
	8587	0.95	1.21E-06	-	1.44	o	0.79
	12032	0.9	0.9.62E-07	-	1.17	s-bj	0.69
	12727	0.87	0.6.25E-07	-	0.80	s-bj	0.47
	12788	0.82	0.8.66E-07	-	1.11	s-bj	0.78
	12112	-	-	-	-	s-bj	1.26 *)
	11092	0.65	0.6.88E-07	-	1.53	s-bj	0.59
	11970	0.91	0.8.16E-07	-	0.95	s-bj	0.52
	13295	0.63	0.4.24E-07	-	0.85	s-bj	0.48
	11351	0.98	0.7.13E-07	-	0.76	s-bj	0.46
	8996	0.91	0.7.45E-07	-	0.88	s-bj	0.5
	10052	0.71	0.4.89E-07	-	0.77	s-bj	0.35
average	11364	0.833	0.7.54E-07		0.92		0.56
CV	14%	15%	30%		43%		25%
90 (HOR)	12662	0.46	0.9.19E-07	8843	2.88	s-hj	1.37
	11845	0.53	1.13E-06	9295	2.99	s-hj	1.30
	9986	0.67	1.73E-06	6394	2.95	mm	1.22
	11467	0.70	1.46E-06	4931	3.68	s-hj	1.47
	-	-	-	-	2.81	mm	1.23
	12794	0.70	1.56E-06	4333	2.79	s-hj	1.16
	13141	0.45	0.8.02E-07	9972	2.67	s-hj	1.27
	-	-	-	-	3.54	s-hj	1.18
	15128	0.35	0.6.00E-07	9243	3.35	mm	1.45
	14907	0.38	0.7.22E-07	6993	3.45	mm	1.48
	13916	0.50	1.02E-06	5853	3.56	mm	1.40
	14058	0.45	0.7.21E-07	6635	2.85	mm	1.29
average	12990	0.52	1.07E-06	7249	3.13		1.32
CV	12%	25%	37%	27%	12%		9%

*) excluded from mean

Table 59 Results of 4-point bending tests on wallettes of CS-block96 + TLM (Calsifix) series of 1996-1997 ($\theta = 90°$)

head joints	tongues, grooves	E_{1st} [N/mm^2]	r_{lin} [-]	$\kappa_{lin;yy}$ [10^{-6} mm^{-1}]	E_{2nd} [N/mm^2]	$\kappa_{u;yy}$ [10^{-6} mm^{-1}]	crack	$f_{fl;yy}$ [N/mm^2]
filled	present	11203	0.2	0.41	8915	3.06	mm	1.15
		11701	0.24	0.50	10135	3.48	s-hj	1.19
		12811	0.39	0.73	9086	2.82	s-hj	1.27
	average	11900	0.28	0.55	9379	3.12		1.20
	CV	7%	36%	30%	7%	11%		5%
	removed	11649	0.31	0.63	9236	3.24	s-hj	1.26
		13248	0.28	0.62	11561	3.14	s-hj	1.44
		15371	0.23	0.45	13835	3.44	s-hj	1.54
	average	13420	0.27	0.57	11540	3.27		1.41
	CV	14%	15%	18%	20%	5%		10%
unfilled	present	5972	0.84	2.76	6024	3.42	s-hj	1.00
		-	-	-	-	-	s-hj	1.17
		7044	0.83	2.89	5400	3.70	s-hj	1.15
	average	6510	0.84	2.82	5710	3.56		1.11
	CV	12%	1%	3%		5%		8%
	removed	9728	0.70	1.76	-	2.96	s-hj	1.20
		7666	0.79	2.35	-	3.12	s-hj	1.09
		7123	0.86	2.48	-	3.08	s-hj	1.06
	average	8170	0.78	2.20		3.05		1.12
	CV	17%	10%	17%		3%		6%

COMPARATIVE EXPERIMENTAL RESEARCH

Tensile tests results with restraints and small 4-point flexural bending tests results were also presented in Table 38 and Table 43. The number of tests for each series is presented in Table 27. Detailed results of the other test arrangements can be found in Van der Pluijm[1995,[55]].

CV's are given between round brackets.

Table 60a Comparison of mean strength values [N/mm^2] of clay brick masonry for each test method

date	mortar batch	restrained tensile test	tensile test with hinges	small 4-point bending test	normal wallettes	double width wallettes	bond wrench (piers)	bond wrench (wallettes)
4-7-95	4-7a	0.39	0.33	0.55	-	-	0.53	0.52
	4-7b	0.45	0.33	0.73	-	-	0.68	0.67
	4-7c	0.28	0.25	0.42	-	-	0.56	0.46
	4-7a+b+c	0.37	0.30	0.55	0.43	0.51	0.59	0.55
5-7-95	5-7a	0.41	0.29	0.54	-	-	0.68	0.62
	5-7b	0.42	0.53	0.66	-	-	0.76	0.75
	5-7c	0.49	0.49	0.77	-	-	0.88	0.89
	5-7a+b+c	0.44	0.47	0.66	0.71	0.60	0.77	0.75
4-7-95 + 5-7-95	overall mean strength	0.41(39)	0.38 (41)	0.60 (32)	0.57 (29)	0.56 (27)	0.68 (29)	0.66 (31)

Table 60b Comparison of mean strength values [-] of clay brick masonry relatively to the deformation controlled tensile test results for each test method

date	mortar batch	restrained tensile test	tensile test with hinges	small 4-point bending test	normal wallettes	double width wallettes	bond wrench (piers)
4-7-95	a	1.00	0.84	1.39	-	-	1.35
	b	1.00	0.74	1.63	-	-	1.52
	c	1.00	0.90	1.50	-	-	2.01
	a+b+c	1.00	0.81	1.48	1.16	1.37	1.59
5-7-95	4-7a	1.00	0.71	1.31	-	-	1.65
	4-7b	1.00	1.27	1.59	-	-	1.82
	4-7c	1.00	1.01	1.59	-	-	1.81
	a+b+c	1.00	1.07	1.49	1.61	1.36	1.75
4-7-95 + 5-7-95	overall mean relative strength	1.00	0.94	1.49	1.41	1.38	1.68

Table 61a Comparison of mean strength values [N/mm^2] of calcium silicate masonry for each test method

date	mortar batch	restrained tensile test	tensile test with hinges	small 4-point bending test	normal wallettes	double width wallettes	bond wrench
15-8-95	a	0.30	0.41	0.30	-	-	0.43
	b	0.30	0.42	0.39	-	-	0.46
16-8-95	c	0.39	0.39	0.49	-	-	0.46
15-8-95+ 16-8-95	overall mean strength	0.33 (27)	0.41 (24)	0.40 (40)	0.34 (31)	0.35 (13)	0.45 (18)

Table 61b Comparison of mean strength values [-]of calcium silicate masonry relatively to the deformation controlled tensile test results for each test method

date	mortar batch	restrained tensile test	tensile test with hinges	small 4-point bending test	normal wallettes	double width wallettes	bond wrench
15-8-95	a	1.00	1.37	1.00	-	-	1.43
	b	1.00	1.40	1.30	-	-	1.53
16-8-95	c	1.00	1.00	1.26	-	-	1.18
15-8-95+ 16-8-95	overall mean relative strength	1.00	1.24	1.22	1.03	1.06	1.36

Appendix C
MESO MODELS

ANALYTICAL MODEL – MATHEMATICAL DESCRIPTION

GENERAL

The internal linear elastic stress distribution of masonry made in stretcher bond due to bending is considered.

Assumptions and modelling aspects are outlined in chapter 5. Basic assumptions are:

- joints and units behave isotropic;
- thin plate theory is valid, because deflections w are small compared with the thickness of the masonry wall.

Thin plate theory in general is valid also for the components: units and joints, since by assuming linear distributions of displacements and stresses over the thickness of the wall, i.e. the units and joints, this thickness becomes an irrelevant parameter, and hence, may be considered small with respect to the other dimensions of the components.

For the derivation of kinematic, constitutive and equilibrium equations according to thin plate theory , the reader is referred to e.g. [77].

Equations, in general form, used in this appendix are:

Constitutive

$$m_{tt}^{i} = D^{i}(\kappa_{\mathrm{tt}}^{\mathrm{i}} + \nu\kappa_{\mathrm{nn}}^{\mathrm{i}}) \tag{40}$$

$$m_{\mathrm{nn}}^{\mathrm{i}} = D^{\mathrm{i}}(\kappa_{\mathrm{nn}}^{\mathrm{i}} + \nu^{\mathrm{i}}\kappa_{\mathrm{tt}}^{\mathrm{i}}) \tag{41}$$

$$m_{\mathrm{tn}}^{\mathrm{i}} = D^{\mathrm{i}}(1-\nu^{\mathrm{i}})\kappa_{\mathrm{tn}}^{\mathrm{i}} \tag{42}$$

with:

$$D^{\mathrm{i}} = \frac{E^{\mathrm{i}}d^{3}}{12(1-(\nu^{\mathrm{i}})^{2})}$$

Kinematic:

$$\varphi^{i} = l^{i} \cdot \kappa^{i} \tag{43}$$

HORIZONTAL BENDING

Distortion of bed joint due to bending around the n-axis

In Figure 109 (repeated below) the assumptions concerning the curvature κ_{tt}^{u} in the unit as a function of t are shown.

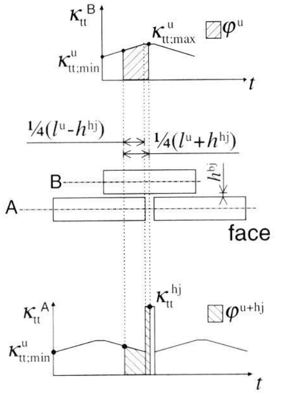

Figure 109 (repeated from page 131) Assumption of curvatures of units and head joints in t-direction

Rotations according to Figure 109 are:

$$\varphi_{\mathrm{tt}}^{\mathrm{u}} = \tfrac{1}{16}(l^{\mathrm{u}} - h^{\mathrm{hj}})\kappa_{\mathrm{tt;min}}^{\mathrm{u}} + \tfrac{1}{16}(3l^{\mathrm{u}} + h^{\mathrm{hj}})\kappa_{\mathrm{tt;max}}^{\mathrm{u}} \tag{44}$$

$$\varphi_{\mathrm{tt}}^{\mathrm{u+hj}} = \tfrac{1}{2}h^{\mathrm{hj}}\kappa_{\mathrm{tt}}^{\mathrm{hj}} + \tfrac{3}{16}(l^{\mathrm{u}} - h^{\mathrm{hj}})\kappa_{\mathrm{tt;min}}^{\mathrm{u}} + \tfrac{1}{16}(l^{\mathrm{u}} + h^{\mathrm{hj}})\kappa_{\mathrm{tt;max}}^{\mathrm{u}} \tag{45}$$

For compatibility it is necessary that (see also Figure 109):

$$\varphi_{\mathrm{tt}}^{\mathrm{u+hj}} - \varphi_{\mathrm{tt}}^{\mathrm{u}} = \psi_{\mathrm{nt}}^{\mathrm{bj}} h^{\mathrm{bj}} \tag{22}$$

Substituting eq. (44) and (45) in eq. (22) gives:

$$\psi_{\mathrm{nt}}^{\mathrm{bj}} = \frac{1}{h^{\mathrm{bj}}}\left\{\tfrac{1}{2}h^{\mathrm{hj}}\kappa_{\mathrm{tt}}^{\mathrm{hj}} + \tfrac{1}{8}(l^{\mathrm{u}} - h^{\mathrm{hj}})\kappa_{\mathrm{tt;min}}^{\mathrm{u}} - \tfrac{1}{8}(l^{\mathrm{u}} + h^{\mathrm{hj}})\kappa_{\mathrm{tt;max}}^{\mathrm{u}}\right\} \tag{46}$$

For the constitutive relation between $\hat{M}_{\mathrm{nt}}^{\mathrm{bj}}$ and $\psi_{\mathrm{nt}}^{\mathrm{bj}}$ it was assumed that $\hat{M}_{\mathrm{nt}}^{\mathrm{bj}}$ is equivalent to an equally distributed moment $\hat{m}_{\mathrm{nt}}^{\mathrm{bj}} \cdot \tfrac{1}{2}(l^{\mathrm{u}} - h^{\mathrm{hj}})$ according to thin plate theory, leading to:

$$\left.\begin{array}{l}\hat{M}_{\mathrm{nt}}^{\mathrm{bj}}=\frac{1}{2}(l^{\mathrm{u}}-h^{\mathrm{hj}})\cdot\hat{m}_{\mathrm{nt}}^{\mathrm{bj}}\\ \hat{M}_{\mathrm{nt}}^{\mathrm{bj}}=\frac{1}{2}(l^{\mathrm{u}}-h^{\mathrm{hj}})\cdot D^{\mathrm{bj}}(1-\nu^{\mathrm{bj}})\psi^{\mathrm{bj}}\\ \hat{M}_{\mathrm{nt}}^{\mathrm{bj}}=\frac{1}{6}G^{\mathrm{bj}}\frac{1}{2}(l^{\mathrm{u}}-h^{\mathrm{hj}})\cdot d^{3}\psi^{\mathrm{bj}}\\ \text{written as}\\ \hat{M}_{\mathrm{nt}}^{\mathrm{bj}}=GI_{\mathrm{t}}^{\mathrm{bj}}\psi^{\mathrm{bj}}\end{array}\right\}\tag{47}$$

An alternative for the constitutive relation according to eq. (47) could be obtained with the membrane analogy for twisted beams, resulting in a factor varying between 0.14 and 0.20 depending on the geometry of the masonry, instead of the factor $\frac{1}{6}$ used.

Equilibrium of moments acting on the units (see Figure 99 on page 122):

$$M_{\mathrm{tt;max}}^{\mathrm{u}}-2\hat{M}_{\mathrm{nt}}^{\mathrm{bj}}-M_{\mathrm{tt;min}}^{\mathrm{u}}=0\tag{48}$$

Substituting eq. (25), (47) and constitutive relations (40) in eq. (48) leads to:

$$h^{\mathrm{u}}D^{\mathrm{u}}(\kappa_{\mathrm{tt;max}}^{\mathrm{u}}+\nu^{\mathrm{u}}\kappa_{\mathrm{nn}}^{\mathrm{u}})-2GI_{\mathrm{t}}^{\mathrm{bj}}\psi_{\mathrm{nt}}^{\mathrm{bj}}-h^{\mathrm{u}}D^{\mathrm{hj}}(\kappa_{\mathrm{tt;min}}^{\mathrm{u}}+\nu^{\mathrm{hj}}\kappa_{\mathrm{nn}}^{\mathrm{u}})=0\tag{I}$$

With eq. (46), $\psi_{\mathrm{nt}}^{\mathrm{bj}}$ can be eliminated from (I).

Equilibrium in the intersecting planes between units and head joints:

$$m_{\mathrm{tt;min}}^{\mathrm{u}}=m_{\mathrm{tt}}^{\mathrm{hj}}\tag{24}$$

Substituting eq. (25) and constitutive relations (40) this becomes

$$D^{\mathrm{u}}(\kappa_{\mathrm{tt;min}}^{\mathrm{u}}+\nu^{\mathrm{u}}\kappa_{\mathrm{nn}}^{\mathrm{u}})-D^{\mathrm{hj}}(\kappa_{\mathrm{tt}}^{\mathrm{hj}}+\nu^{\mathrm{hj}}\kappa_{\mathrm{nn}}^{\mathrm{u}})=0\tag{II}$$

VERTICAL BENDING

Equilibrium between units and bed joint:

$$m_{\mathrm{nn}}^{\mathrm{bj}}=m_{\mathrm{nn}}^{\mathrm{u}}\tag{26}$$

Substitution of constitutive relation (41) in eq. (26) leads to:

$$D^{\mathrm{bj}}(\kappa_{\mathrm{nn}}^{\mathrm{bj}}+\nu^{\mathrm{bj}}\bar{\kappa}_{\mathrm{tt}}^{\mathrm{bj}})=D^{\mathrm{u}}(\kappa_{\mathrm{nn}}^{\mathrm{u}}+\nu^{\mathrm{u}}\bar{\kappa}_{\mathrm{tt}}^{\mathrm{u}})\tag{49}$$

With:

$$\bar{\kappa}_{\mathrm{tt}}^{\mathrm{bj}}=\frac{1}{2}(\kappa_{\mathrm{tt;min}}^{\mathrm{u}}+\kappa_{\mathrm{tt;max}}^{\mathrm{u}})\tag{23}$$

this becomes:

$$D^{\mathrm{bj}}(\kappa_{\mathrm{nn}}^{\mathrm{bj}}+\nu^{\mathrm{bj}}\tfrac{1}{2}(\kappa_{\mathrm{tt;min}}^{\mathrm{u}}+\kappa_{\mathrm{tt;max}}^{\mathrm{u}}))=D^{\mathrm{u}}(\kappa_{\mathrm{nn}}^{\mathrm{u}}+\nu^{\mathrm{u}}\tfrac{1}{2}(\kappa_{\mathrm{tt;min}}^{\mathrm{u}}+\kappa_{\mathrm{tt;max}}^{\mathrm{u}}))\tag{III}$$

TORSION

Additional bending of bed joint due to torsion of adjacent half units

Assuming a similar course for κ_{tn}^{u} and κ_{tn}^{hj} as for κ_{tt}^{u} and κ_{tt}^{hj} presented in Figure 109, gives:

$$\varphi_{tn}^{u} = \tfrac{1}{16}(l^{u} - h^{hj})\kappa_{tn;min}^{u} + \tfrac{1}{16}(3l^{u} + h^{hj})\kappa_{tn;max}^{u} \tag{50}$$

$$\varphi_{tn}^{u+hj} = \tfrac{1}{2}h^{hj}\kappa_{tn}^{hj} + \tfrac{3}{16}(l^{u} - h^{hj})\kappa_{tn;min}^{u} + \tfrac{1}{16}(l^{u} - h^{hj})\kappa_{tn;max}^{u} \tag{51}$$

For compatibility it is necessary that (see also Figure 109):

$$\varphi_{tn}^{u+hj} - \varphi_{tn}^{u} = \beta^{bj} \tag{27}$$

Substituting eq. (50) and (51) in eq.(27) gives:

$$\hat{\kappa}_{nn}^{bj} = \frac{\beta^{bj}}{h^{bj}} = \frac{1}{h^{bj}}\left\{\tfrac{1}{2}h^{hj}\kappa_{tn}^{hj} + \tfrac{1}{8}(l^{u} - h^{hj})\kappa_{tn;min}^{u} - \tfrac{1}{8}(l^{u} + h^{hj})\kappa_{tn;max}^{u}\right\} \tag{52}$$

Constitutive relation for the constant assumed additional bending moment acting on units over the length of the bed joints:

$$\hat{M}_{nn}^{bj} = \tfrac{1}{2}(l^{u} - h^{hj})D^{bj}\hat{\kappa}_{nn}^{bj} \tag{53}$$

The increase of the torsion moment in the unit in *t*-direction:

$$\hat{M}_{tn}^{u} = 2\hat{M}_{nn}^{bj} \tag{54}$$

The constitutive relation between the additional twist and torsion moment $\hat{M}_{tn}^{u}$ reads (according to Timoshenko et al. [76],1970, art. 109):

$$\left.\begin{array}{l} \hat{M}_{tn}^{u} = \tfrac{1}{3}G^{u}(\psi_{tn}^{u}(2a)^{3}(2b)\left(1 - \dfrac{192}{\pi^{5}}\dfrac{a}{b}\displaystyle\sum_{n=1,3,..}^{\infty}\dfrac{1}{n^{5}}\tanh(\dfrac{n\pi b}{2a})\right) \\ \text{with } 2a = h^{u},\ 2b = d \text{ and } \psi_{tn}^{u} = \kappa_{tn;max}^{u} - \kappa_{tn;min}^{u} \\ \text{written as} \\ \hat{M}_{tn}^{u} = GI_{t}^{u}(\kappa_{tn;max}^{u} - \kappa_{tn;min}^{u}) \end{array}\right\} \tag{55}$$

Substituting eq. (42), (53) and (55) in eq. (54) leads to:

$$GI_{t}^{u}(\kappa_{tn;max}^{u} - \kappa_{tn;min}^{u}) - 2\cdot\tfrac{1}{2}(l^{u} - h^{hj})D^{bj}\hat{\kappa}_{nn}^{bj} = 0 \tag{56}$$

With eq. (52) $\hat{\kappa}_{nn}^{bj}$ can be eliminated leading to:

$$(\tfrac{1}{8}\frac{D^{bj}}{h^{bj}}(l^{u} - h^{hj})(l^{u} + h^{hj}) + GI_{t}^{u})\kappa_{tn;max}^{u} - (\tfrac{1}{8}\frac{D^{bj}}{h^{bj}}(l^{u} - h^{hj})^{2} + GI_{t}^{u})\kappa_{tn;min}^{u} - \tfrac{1}{2}\frac{D^{bj}}{h^{bj}}h^{hj}(l^{u} - h^{hj})\kappa_{tn}^{hj} = 0 \tag{IV}$$

Equilibrium between the equivalent shear forces at the intersection between unit, head joint and bed joint

$$2m^{\mathrm{u}}_{\mathrm{tn;min}} = m^{\mathrm{hj}}_{\mathrm{tn}} + m^{\mathrm{bj}}_{\mathrm{nt}} \tag{29)a}$$

With eq. (42) this becomes:

$$2D^{\mathrm{u}}(1-\nu^{\mathrm{uj}})\kappa^{\mathrm{u}}_{\mathrm{tn;min}} D^{\mathrm{hj}}(1-\nu^{\mathrm{hj}})\kappa^{\mathrm{hj}}_{\mathrm{tn}} + D^{\mathrm{bj}}(1-\nu^{\mathrm{bj}})\kappa^{\mathrm{bj}}_{\mathrm{nt}} \tag{V}$$

Torsion of unit

From the linear change of $\kappa^{\mathrm{u}}_{\mathrm{tn}}$ as a function of t, it can be derived that:

$$\bar{\kappa}^{\mathrm{u}}_{\mathrm{tn}} = \tfrac{1}{2}\frac{l^{\mathrm{u}} - h^{\mathrm{hj}}}{l^{\mathrm{u}}}\kappa^{\mathrm{u}}_{\mathrm{tn;min}} + \tfrac{1}{2}\frac{l^{\mathrm{u}} + h^{\mathrm{hj}}}{l^{\mathrm{u}}}\kappa^{\mathrm{u}}_{\mathrm{tn;max}} \tag{57}$$

In n-direction the torsion of the units was taken equal to the actual value of the torsion in t-direction.:

$$\kappa^{\mathrm{u}}_{\mathrm{nt}}(t) = \kappa^{\mathrm{u}}_{\mathrm{tn}}(t) \tag{58}$$

COMPATIBILITY BETWEEN MESO AND MACRO CURVATURES

HORIZONTAL BENDING

Along the centre line through units and head joints parallel to the t-axis compatibility demands (see also Figure 112):

$$\varphi_{\mathrm{tt}} = \varphi^{\mathrm{u}}_{\mathrm{tt}} + \varphi^{\mathrm{hj}}_{\mathrm{tt}} \tag{30}$$

On the basis of Figure 109, the average curvature $\bar{\kappa}^{\mathrm{u}}_{\mathrm{tt}}$ in the unit equals:

$$\bar{\kappa}^{\mathrm{u}}_{\mathrm{tt}} = \tfrac{1}{2}\frac{l^{\mathrm{u}} - h^{\mathrm{hj}}}{l^{\mathrm{u}}}\kappa^{\mathrm{u}}_{\mathrm{tt;min}} + \tfrac{1}{2}\frac{l^{\mathrm{u}} + h^{\mathrm{hj}}}{l^{\mathrm{u}}}\kappa^{\mathrm{u}}_{\mathrm{tt;max}} \tag{59}$$

Substituting eq. (59) and other kinematic equations (see eq. (43)) in eq. (30) gives:

$$\kappa_{\mathrm{tt}}(l^{\mathrm{u}} + h^{\mathrm{hj}}) = \kappa^{\mathrm{hj}}_{\mathrm{tt}}h^{\mathrm{hj}} + \tfrac{1}{2}(l^{\mathrm{u}} - h^{\mathrm{hj}})\kappa^{\mathrm{u}}_{\mathrm{tt;min}} + \tfrac{1}{2}(l^{\mathrm{u}} + h^{\mathrm{hj}})\kappa^{\mathrm{u}}_{\mathrm{tt;max}} \tag{VI}$$

VERTICAL BENDING

$$\varphi_{\mathrm{nn}} = \varphi^{\mathrm{u}}_{\mathrm{nn}} + \varphi^{\mathrm{bj}}_{\mathrm{nn}} \tag{31}$$

Substitution of eq. (43) in eq. (31) leads to:

$$\kappa_{\mathrm{nn}}(h^{\mathrm{u}} + h^{\mathrm{bj}}) = \kappa^{\mathrm{u}}_{\mathrm{nn}}h^{\mathrm{u}} + \kappa^{\mathrm{bj}}_{\mathrm{nn}}h^{\mathrm{bj}} \tag{VII}$$

Torsion

t-direction:

$$\varphi_{\mathrm{tn}} = \varphi_{\mathrm{tn}}^{\mathrm{u}} + \varphi_{\mathrm{tn}}^{\mathrm{hj}} \qquad (33)$$

Substituting eq. (43) and eq. (57) in eq. (33) leads to:

$$\kappa_{\mathrm{tn}}(l^{\mathrm{u}} + h^{\mathrm{hj}}) = \kappa_{\mathrm{tn}}^{\mathrm{hj}} h^{\mathrm{hj}} + \tfrac{1}{2}(l^{\mathrm{u}} - h^{\mathrm{hj}})\kappa_{\mathrm{tn;min}}^{\mathrm{u}} + \tfrac{1}{2}(l^{\mathrm{u}} + h^{\mathrm{hj}})\kappa_{\mathrm{tn;max}}^{\mathrm{u}} \qquad \text{(VIII)}$$

n-direction (parallel to line *s* in Figure 112):

$$\varphi_{\mathrm{nt}} = \varphi_{\mathrm{nt}}^{\mathrm{u}} + \varphi_{\mathrm{nt}}^{\mathrm{bj}} \qquad (34)$$

Substituting eq. (43) and eq. (58) in eq. (34) results in:

$$\kappa_{\mathrm{nt}}(h^{\mathrm{u}} + h^{\mathrm{bj}}) = \tfrac{1}{2}(\kappa_{\mathrm{tn;min}}^{\mathrm{u}} + \kappa_{\mathrm{tn;max}}^{\mathrm{u}})h^{\mathrm{u}} + \kappa_{\mathrm{nt}}^{\mathrm{bj}} h^{\mathrm{bj}} \qquad \text{(IX)}$$

Deformation equations

In the previous part nine equations indicated with Roman numbers have been derived with nine component (meso) curvatures. The nine equations are repeated below:

$$\begin{aligned}&\kappa_{\mathrm{tt;max}}^{\mathrm{u}}\left(h^{\mathrm{u}} D^{\mathrm{u}} + \tfrac{1}{4} GI_{\mathrm{t}}^{\mathrm{bj}} \frac{l^{\mathrm{u}} + h^{\mathrm{hj}}}{h^{\mathrm{bj}}}\right) - \kappa_{\mathrm{tt;min}}^{\mathrm{u}} \cdot \tfrac{1}{4} GI_{\mathrm{t}}^{\mathrm{bj}} \frac{l^{\mathrm{u}} - h^{\mathrm{hj}}}{h^{\mathrm{bj}}} + \\ &+ \kappa_{\mathrm{nn}}^{\mathrm{u}} \cdot h^{\mathrm{u}}(\nu^{\mathrm{u}} D^{\mathrm{u}} - \nu^{\mathrm{hj}} D^{\mathrm{hj}}) - \kappa_{\mathrm{tt}}^{\mathrm{hj}}\left(GI_{\mathrm{t}}^{\mathrm{bj}} \frac{h^{\mathrm{hj}}}{h^{\mathrm{bj}}} + h^{\mathrm{u}} D^{\mathrm{hj}}\right) = 0\end{aligned} \qquad \text{(I)}$$

$$D^{\mathrm{u}}(\kappa_{\mathrm{tt;min}}^{\mathrm{u}} + \nu^{\mathrm{u}} \kappa_{\mathrm{nn}}^{\mathrm{u}}) - D^{\mathrm{hj}}(\kappa_{\mathrm{tt}}^{\mathrm{hj}} + \nu^{\mathrm{hj}} \kappa_{\mathrm{nn}}^{\mathrm{u}}) = 0 \qquad \text{(II)}$$

$$D^{\mathrm{bj}}(\kappa_{\mathrm{nn}}^{\mathrm{bj}} + \nu^{\mathrm{bj}} \tfrac{1}{2}(\kappa_{\mathrm{tt;min}}^{\mathrm{u}} + \kappa_{\mathrm{tt;max}}^{\mathrm{u}})) = D^{\mathrm{u}}(\kappa_{\mathrm{nn}}^{\mathrm{u}} + \nu^{\mathrm{u}} \tfrac{1}{2}(\kappa_{\mathrm{tt;min}}^{\mathrm{u}} + \kappa_{\mathrm{tt;max}}^{\mathrm{u}})) \qquad \text{(III)}$$

$$\begin{aligned}&\left(\tfrac{1}{8}\frac{D^{\mathrm{bj}}}{h^{\mathrm{bj}}}(l^{\mathrm{u}} - h^{\mathrm{hj}})(l^{\mathrm{u}} + h^{\mathrm{hj}}) + GI_{\mathrm{t}}^{\mathrm{u}}\right)\kappa_{\mathrm{tn;max}}^{\mathrm{u}} + \\ &- \left(\tfrac{1}{8}\frac{D^{\mathrm{bj}}}{h^{\mathrm{bj}}}(l^{\mathrm{u}} - h^{\mathrm{hj}})^2 + GI_{\mathrm{t}}^{\mathrm{u}}\right)\kappa_{\mathrm{tn;min}}^{\mathrm{u}} - \tfrac{1}{2}\frac{D^{\mathrm{bj}}}{h^{\mathrm{bj}}} h^{\mathrm{hj}}(l^{\mathrm{u}} - h^{\mathrm{hj}})\kappa_{\mathrm{tn}}^{\mathrm{hj}} = 0\end{aligned} \qquad \text{(IV)}$$

$$2D^{\mathrm{u}}(1 - \nu^{\mathrm{uj}})\kappa_{\mathrm{tn;min}}^{\mathrm{u}} = D^{\mathrm{hj}}(1 - \nu^{\mathrm{hj}})\kappa_{\mathrm{tn}}^{\mathrm{hj}} + D^{\mathrm{bj}}(1 - \nu^{\mathrm{bj}})\kappa_{\mathrm{nt}}^{\mathrm{bj}} \qquad \text{(V)}$$

$$\kappa_{\mathrm{tt}}(l^{\mathrm{u}} + h^{\mathrm{hj}}) = \kappa_{\mathrm{tt}}^{\mathrm{hj}} h^{\mathrm{hj}} + \tfrac{1}{2}(l^{\mathrm{u}} - h^{\mathrm{hj}})\kappa_{\mathrm{tt;min}}^{\mathrm{u}} + \tfrac{1}{2}(l^{\mathrm{u}} + h^{\mathrm{hj}})\kappa_{\mathrm{tt;max}}^{\mathrm{u}} \qquad \text{(VI)}$$

$$\kappa_{\mathrm{nn}}(h^{\mathrm{u}} + h^{\mathrm{bj}}) = \kappa_{\mathrm{nn}}^{\mathrm{u}} h^{\mathrm{u}} + \kappa_{\mathrm{nn}}^{\mathrm{bj}} h^{\mathrm{bj}} \qquad \text{(VII)}$$

$$\kappa_{\mathrm{tn}}(l^{\mathrm{u}} + h^{\mathrm{hj}}) = \kappa_{\mathrm{tn}}^{\mathrm{hj}} h^{\mathrm{hj}} + \tfrac{1}{2}(l^{\mathrm{u}} - h^{\mathrm{hj}})\kappa_{\mathrm{tn;min}}^{\mathrm{u}} + \tfrac{1}{2}(l^{\mathrm{u}} + h^{\mathrm{hj}})\kappa_{\mathrm{tn;max}}^{\mathrm{u}} \qquad \text{(VIII)}$$

$$\kappa_{\mathrm{nt}}(h^{\mathrm{u}} + h^{\mathrm{bj}}) = \tfrac{1}{2}(\kappa_{\mathrm{tn;min}}^{\mathrm{u}} + \kappa_{\mathrm{tn;max}}^{\mathrm{u}})h^{\mathrm{u}} + \kappa_{\mathrm{nt}}^{\mathrm{bj}} h^{\mathrm{bj}} \qquad \text{(IX)}$$

Of course a further reduction of the number of variables is possible, but it does not make the set of equations more transparent. With the last 3 equations for example, the curvatures in the joints could be eliminated, and with eq. (58) it is possible to reduce the equations to a set of 5 from which 5 unknown curvatures of the unit can be solved. The equations were solved with a Fortran program using the LINPACK library (see Dongarra et al.[1979,[13]] for a complete overview of the library).

MACRO MOMENTS AND MACRO STIFFNESSES

Macro moments were derived by averaging meso moments.

$$m_{\mathrm{tt}} = \frac{m^{\mathrm{u}}_{\mathrm{tt;max}} \cdot \frac{1}{2} h^{\mathrm{u}} + m^{\mathrm{bj}}_{\mathrm{tt}} \cdot h^{\mathrm{bj}} + m^{\mathrm{hj}}_{\mathrm{tt}} \cdot \frac{1}{2} h^{\mathrm{u}}}{h^{\mathrm{u}} + h^{\mathrm{bj}}} \tag{60}$$

$$m_{\mathrm{nn}} = \frac{m^{\mathrm{hj}}_{\mathrm{nn}} \cdot \frac{1}{2} h^{\mathrm{hj}} + m^{\mathrm{u}}_{\mathrm{nn}} \cdot \frac{1}{2} l^{\mathrm{u}}}{\frac{1}{2} h^{\mathrm{hj}} + \frac{1}{2} l^{\mathrm{u}}} \tag{61}$$

The averaging of the torsion moments needs special consideration. In the unit an additional torsion moment $\hat{M}^{\mathrm{u}}_{\mathrm{tn}}$ with round running shear stresses is present in cross sections prependicular to the *t*-axos. On the boundary parallel to the *t*-axis, only the horizontal shear stresses of that moment have an influence on the average torsion moment, hence:

$$m_{\mathrm{nt}} = \frac{m^{\mathrm{u}}_{\mathrm{tn;min}} \cdot l^{\mathrm{u}} + \frac{1}{4} \frac{\hat{M}^{u}_{tn}}{h^{\mathrm{u}}} \cdot l^{\mathrm{u}} + m^{\mathrm{hj}}_{\mathrm{tn}} \cdot h^{\mathrm{hj}}}{l^{\mathrm{u}} + h^{\mathrm{hj}}} \tag{62}$$

In the other direction:

$$m_{\mathrm{tn}} = \frac{m^{\mathrm{u}}_{\mathrm{tn;min}} \cdot h^{\mathrm{u}} + \hat{M}^{\mathrm{u}}_{\mathrm{tn}} + 2m^{\mathrm{bj}}_{\mathrm{nt}} \cdot h^{\mathrm{bj}} + m^{\mathrm{hj}}_{\mathrm{tn}} \cdot h^{\mathrm{u}}}{2(h^{\mathrm{u}} + h^{\mathrm{bj}})} \tag{63}$$

Macro flexural rigidities follow from (with i and j equal to *n* or *t*):

$$D_{\mathrm{ij}} = \frac{m_{\mathrm{ij}}}{\kappa_{\mathrm{ij}}} \tag{64}$$

CALCULATION RESULTS OF THE ANALYTICAL MODEL

For each calculation discussed in chapter 5, detailed results (calculated meso curvatures, moments and the resulting stiffness matrix) are presented on the following pages

Results of Analytical Model - Uniform Stiffness

```
INPUT
Geometry
         d         lu         hu        hbj        hhj
     100.0      204.0       50.0       12.5        8.0

Materials
        Eu        Ehj        Ebj        nuu       nuhj       nubj
   10000.0    10000.0    10000.0       0.20       0.20       0.20

OUTPUT

Ktt = 1.0e-6

Curvatures
     knnbj       knnu    kttumin    kttumax     psiben      ktthj    ktnumin    ktnumax      ktnhj      kntbj   knnbjadd
 0.000E+00  0.000E+00  0.968E-06  0.103E-05  0.203E-07  0.968E-06  0.000E+00  0.000E+00  0.000E+00  0.000E+00  0.000E+00
Moments
   mttumin    mttumax      mtthj      mttbj       mnnu      mnnbj      mnnhj    mtbjadd   mnnbjadd    mtnumin      Mutor       mntu      mtnhj      mntbj
 0.840E+03  0.896E+03  0.840E+03  0.868E+03  0.174E+03  0.174E+03  0.168E+03  0.141E+02  0.000E+00  0.000E+00  0.000E+00  0.000E+00  0.000E+00  0.000E+00

Knn = 1.0e-6

Curvatures
     knnbj       knnu    kttumin    kttumax     psiben      ktthj    ktnumin    ktnumax      ktnhj      kntbj   knnbjadd
 0.100E-05  0.100E-05  0.000E+00  0.000E+00  0.000E+00  0.000E+00  0.000E+00  0.000E+00  0.000E+00  0.000E+00  0.000E+00
Moments
   mttumin    mttumax      mtthj      mttbj       mnnu      mnnbj      mnnhj    mtbjadd   mnnbjadd    mtnumin      Mutor       mntu      mtnhj      mntbj
 0.174E+03  0.174E+03  0.174E+03  0.174E+03  0.868E+03  0.868E+03  0.868E+03  0.000E+00  0.000E+00  0.000E+00  0.000E+00  0.000E+00  0.000E+00  0.000E+00

knt = 1.0e-6

Curvatures
     knnbj       knnu    kttumin    kttumax     psiben      ktthj    ktnumin    ktnumax      ktnhj      kntbj   knnbjadd
 0.000E+00  0.000E+00  0.000E+00  0.000E+00  0.000E+00  0.000E+00  0.968E-06  0.103E-05  0.940E-06  0.996E-06  0.467E-08
Moments
   mttumin    mttumax      mtthj      mttbj       mnnu      mnnbj      mnnhj    mtbjadd   mnnbjadd    mtnumin      Mutor       mntu      mtnhj      mntbj
 0.000E+00  0.000E+00  0.000E+00  0.000E+00  0.000E+00  0.000E+00  0.000E+00  0.000E+00  0.405E+01  0.672E+03  0.794E+03  0.676E+03  0.653E+03  0.692E+03

Matrix

   10416.7        0.0     2083.3
       0.0  8101.6/8094.1    0.0
    2080.8        0.0    10416.7
```

RESULTS OF ANALYTICAL MODEL - E^u/E^j = 10

```
INPUT
Geometry
         d          lu          hu         hbj         hhj
     100.0       204.0        50.0        12.5         8.0

Materials
        Eu         Ehj         Ebj         nuu        nuhj        nubj
   10000.0      1000.0      1000.0        0.15        0.25        0.25

OUTPUT

Ktt = 1.0e-6

Curvatures
     knnbj        knnu     kttumin     kttumax      psiben       ktthj     ktnumin     ktnumax       ktnhj       kntbj    knnbjadd
 0.279E-06  -0.699E-07   0.631E-06   0.967E-06   0.110E-05   0.597E-05   0.000E+00   0.000E+00   0.000E+00   0.000E+00   0.000E+00
Moments
   mttumin     mttumax       mtthj       mttbj        mnnu       mnnbj       mnnhj     mtbjadd    mnnbjadd     mtnumin       Mutor        mntu       mtnhj       mntbj
 0.529E+03   0.815E+03   0.529E+03   0.772E+02   0.426E+02   0.426E+02   0.126E+03   0.731E+02   0.000E+00   0.000E+00   0.000E+00   0.000E+00   0.000E+00   0.000E+00

Knn = 1.0e-6

Curvatures
     knnbj        knnu     kttumin     kttumax      psiben       ktthj     ktnumin     ktnumax       ktnhj       kntbj    knnbjadd
 0.352E-05   0.369E-06  -0.185E-07  -0.251E-08   0.523E-07   0.260E-06   0.000E+00   0.000E+00   0.000E+00   0.000E+00   0.000E+00
Moments
   mttumin     mttumax       mtthj       mttbj        mnnu       mnnbj       mnnhj     mtbjadd    mnnbjadd     mtnumin       Mutor        mntu       mtnhj       mntbj
 0.314E+02   0.450E+02   0.314E+02   0.774E+02   0.313E+03   0.313E+03   0.386E+02   0.349E+01   0.000E+00   0.000E+00   0.000E+00   0.000E+00   0.000E+00   0.000E+00

knt = 1.0e-6

Curvatures
     knnbj        knnu     kttumin     kttumax      psiben       ktthj     ktnumin     ktnumax       ktnhj       kntbj    knnbjadd
 0.000E+00   0.000E+00   0.000E+00   0.000E+00   0.000E+00   0.000E+00   0.397E-06   0.113E-05   0.668E-05   0.195E-05   0.522E-06
Moments
   mttumin     mttumax       mtthj       mttbj        mnnu       mnnbj       mnnhj     mtbjadd    mnnbjadd     mtnumin       Mutor        mntu       mtnhj       mntbj
 0.000E+00   0.000E+00   0.000E+00   0.000E+00   0.000E+00   0.000E+00   0.000E+00   0.000E+00   0.464E+02   0.288E+03   0.910E+04   0.333E+03   0.445E+03   0.130E+03

Matrix

    6636.0         0.0       552.3
       0.0    4048.5 4392.2      0.0
     548.9         0.0      3570.5
```

RESULTS OF ANALYTICAL MODEL - $E^{u}/E^{bj} = 10$, $E^{hj}=0$

```
INPUT
Geometry
        d          lu         hu        hbj        hhj
    100.0       204.0       50.0       12.5        8.0

Materials
       Eu         Ehj        Ebj        nuu       nuhj       nubj
  10000.0         0.0     1000.0       0.15       0.25       0.25

OUTPUT

Ktt = 1.0e-6

Curvatures
      knnbj        knnu     kttumin     kttumax      psiben       ktthj     ktnumin     ktnumax       ktnhj       kntbj    knnbjadd
  0.155E-06  -0.388E-07   0.582E-08   0.882E-06   0.286E-05   0.147E-04   0.000E+00   0.000E+00   0.000E+00   0.000E+00   0.000E+00
Moments
    mttumin     mttumax      mtthj       mttbj        mnnu       mnnbj       mnnhj     mtbjadd    mnnbjadd     mtnumin       Mutor        mntu       mtnhj       mntbj
 -0.533E-04   0.747E+03   0.000E+00   0.429E+02   0.237E+02   0.237E+02   0.000E+00   0.191E+03   0.000E+00   0.000E+00   0.000E+00   0.000E+00   0.000E+00   0.000E+00

Knn = 1.0e-6

Curvatures
      knnbj        knnu     kttumin     kttumax      psiben       ktthj     ktnumin     ktnumax       ktnhj       kntbj    knnbjadd
  0.352E-05   0.371E-06  -0.556E-07  -0.752E-08   0.157E-06   0.781E-06   0.000E+00   0.000E+00   0.000E+00   0.000E+00   0.000E+00
Moments
    mttumin     mttumax      mtthj       mttbj        mnnu       mnnbj       mnnhj     mtbjadd    mnnbjadd     mtnumin       Mutor        mntu       mtnhj       mntbj
  0.672E-06   0.410E+02   0.000E+00   0.754E+02   0.312E+03   0.312E+03   0.000E+00   0.105E+02   0.000E+00   0.000E+00   0.000E+00   0.000E+00   0.000E+00   0.000E+00

knt = 1.0e-6

Curvatures
      knnbj        knnu     kttumin     kttumax      psiben       ktthj     ktnumin     ktnumax       ktnhj       kntbj    knnbjadd
  0.000E+00   0.000E+00   0.000E+00   0.000E+00   0.000E+00   0.000E+00   0.208E-06   0.116E-05   0.855E-05   0.226E-05   0.681E-06
Moments
    mttumin     mttumax      mtthj       mttbj        mnnu       mnnbj       mnnhj     mtbjadd    mnnbjadd     mtnumin       Mutor        mntu       mtnhj       mntbj
  0.000E+00   0.000E+00   0.000E+00   0.000E+00   0.000E+00   0.000E+00   0.000E+00   0.000E+00   0.605E+02   0.151E+03   0.119E+05   0.210E+03   0.000E+00   0.151E+03

Matrix

     3688.7         0.0      377.6
        0.0  2424.8 / 2224.0   0.0
      273.3         0.0     3531.6
```

FE MODEL

MACRO BEHAVIOUR OF THE FE MODEL

The average macro moments were derived from the support reactions of the nodes laying in two perpendicular boundary planes using the following equations with *t, n and z* being the co-ordinates of the considered nodes.

Moments at the boundary plane perpendicular to *t*-axis:

$$M_{\mathrm{tt}} = \sum F_{\mathrm{tt}} \cdot z \tag{65}$$

$$M_{\mathrm{tn}} = \sum F_{\mathrm{tn}} \cdot z - \sum F_{\mathrm{tz}} \cdot (n - n_{\mathrm{max}}) \tag{66}$$

Moments at the boundary plane perpendicular to *n*-axis:

$$M_{\mathrm{nn}} = \sum F_{\mathrm{nn}} \cdot z \tag{67}$$

$$M_{\mathrm{nt}} = \sum F_{\mathrm{nt}} \cdot z - \sum F_{\mathrm{nz}} \cdot (t - t_{\mathrm{max}}) \tag{68}$$

Flexural rigidities follow from (with i and j equal to *n* or *t*):

$$D_{\mathrm{ij}} = \frac{M_{\mathrm{ij}}}{l^{\mathrm{i}}} \frac{1}{\kappa_{\mathrm{ij}}} \tag{69}$$

with l^{i} being de length of the considered boundary plane

SAMENVATTING

Het gedrag van metselwerk onder buiging uit het vlak, wordt beheerst door een complexe interactie tussen stenen en voegen. Het begrijpen van deze interactie was het hoofdonderwerp van dit proefschrift. Het probleem is op meso-niveau onderzocht. Op dit niveau werden stenen en voegen separaat beschouwd als homogene isotrope materialen met ieder hun eigen eigenschappen.

Hoofdstuk 2 beschrijft het gedrag van stenen, voegen en hechtvlak onder trek, dat werd bepaald met behulp van experimenten. De gebruikte experimentele techniek en methode van analyseren waren reeds beschikbaar. De niet-lineaire breukmechanica voor quasi brosse materialen kon ook worden gebruikt voor het beschrijven van het gedrag van de metselwerkcomponenten.
Hoofdstuk 3 gaat in op het afschuifgedrag en -sterkte van de voeg en het hechtvlak. Twee opstellingen werden ontwikkeld om het gedrag zowel voor, als na de piek in het kracht-verplaatsingsdiagram vast te stellen. Dit gebeurde onder belastingscombinaties van afschuiving en druk loodrecht op de lintvoeg en van afschuiving en trek loodecht op de lintvoeg. Vanuit de literatuur was reeds bekend dat de afschuifsterkte onder afschuiving en druk kan worden beschreven op basis van het wrijvingscriterium van Coulomb. Dit werd bevestigd door de uitgevoerde experimenten. Het onderzoek ging een stap verder door ook de invloed van normaal-trekspanningen op de afschuifsterkte vast te stellen. Het na-de-top gedrag onder afschuiving vertoonde een grote overeenkomst met het gedrag onder trek en overeenkomstige formuleringen als bij trek konden worden gebruikt om de dalende tak te beschrijven. Belangrijke verschillen tussen één-assige trek en afschuiving zijn de invloed van de normaalspanningen op het gedrag en de verplaatsing loodrecht op de lintvoeg bij afschuiving in dit vlak. Formuleringen om deze fenomenen te beschrijven, zijn opgenomen in dit proefschrift.
Buigproeven op mestelwerk zijn beschreven in hoofdstuk 4. De proeven waren vooral gericht op de invloed van de hoek tussen de buigings-as en de lintvoeg. Ondanks dat de proeven één-assig werden uitgevoerd, zijn de spanningen die ontstaan in het metselwerk ook representatief voor twee-assige buiging, zodra de hoek tussen de buigings-as en de lintvoeg anders is dan 0° of 90°. Het gedrag en de sterke werden geanalyseerd. Tezamen met de resultaten van de trek en afschuifproeven die in hoofdstuk 2 en 3 zijn beschreven, vormen de resultaten van de buigproeven een unieke data set, die het mogelijk maken om op buiging belast metselwerk niet-lineair te modelleren en te verifiëren.

Het buiggedrag van metselwerk is in hoofdstuk 5 theoretisch geanalyseerd. Aan de hand van drie onderscheiden buigvervormingen: horizontale buiging, verticale buiging en torsie, is een beschrijving gegeven van de fenomenen die op meso-niveau optreden. Overeenkomstig de verrwringing van lintvoegen in de overlap tussen stenen bij horizontale buiging, werd een 'extra' buigvervorming in de voegen in de overlap in het geval van torsie vastgesteld.
Een analytisch en een eindig elementenmethode(EEM)model zijn ontwikkeld om het gedrag lineair elastisch vast te stellen. Deze modellen hadden betrekking op een kleine 'basis-bouwsteen' waarin alle meso-vervormingen zonder belemmering kunnen optreden. De orthogonale stijfheden (evenwijdig aan en loodrecht op de lintvoeg) die met deze modellen werden afgeleid, kwamen goed overeen met de experimentele resultaten. Deze stijfheden konden ook worden voorspeld met een simpele aanpak gebaseerd op serie- en parallelsystemen. Een rationele benadering gebaseerd op het analytische model, waarbij verschillende scheuren kunnen ontstaan (Multiple Crack Pattern of MCP benadering), gaf inzicht in de buigtreksterkte van metselwerk Het model gebruikt de buigtreksterkte in de twee orthogonale richtingen om de sterkte in een willekeurige richting te berekenen. Het kan ook worden toegepast om de sterkte onder invloed van twee-assige buiging te berekenen.

In hoofdstuk 1 werd gesteld dat het onderzoek was geïnitieerd om "een wetenschappelijk acceptabele beschrijving van de relatie tussen de mechanische eigenschappen van metselwerk op meso- en op macro-niveau te vinden" en dat het uit te voeren werk "gebruikers en ontwikkelaars van (niet-lineaire) EEM-modellen moet voorzien van een basis waarmee zij op buiging belast metselwerk op macro-niveau kunnen modelleren op basis van enkele mechanische grootheden die algemeen bekend zijn". In principe is het mogelijk om op basis van de verkregen onderzoeksresultaten metselwerk op het meso-niveau compleet niet-lineair te modelleren. Het is nog niet gelukt om macro-eigenschappen op basis van het gebruikte EEM model via de gevolgde 'bottom-up' benadering vast te stellen. Daarvoor is nog een aanvullende onderzoeksinspanning vereist.
Ingenieursmodellen waarin de buigtreksterkte voor de dimensionering wordt gebruikt, kunnen de MCP-benadering gebruiken om de buigtreksterkte in een willekeurige richting te bepalen. Doordat in de MCP-aanpak de krachtsverdeling lineair elastisch wordt berekend, heeft deze aanpak zijn beperkingen. Een toekomstige niet-lineaire verificatie met een EEM-model kan de MCP-aanpak van een meer fundamentele basis voorzien.

CURRICULUM VITAE

7 juni 1959	Geboren te Almelo
1978	VWO diploma R.S.G. Gouda
1987	Diploma TU Delft, faculteit der Civiele Techniek Constructieleer - betonconstructies
1987 - heden	Wetenschappelijk medewerker TNO Bouw
1991 - 1994	AIO bij de TU Eindhoven, vakgroep BKO
1994 - 1998	Toegevoegd onderzoeker bij de TU Eindhoven, vakgroep BKO voor een onderzoek van de Stichting Technische Wetenschappen

21 april 1989	Getrouwd met Irene de Haan
21 april 1990	Geboorte Suzan
25 oktober 1993	Geboorte Bas